**Title**
Genetic Analyses of the Development and Function of Sensory Neurons

**Permalink**
https://escholarship.org/uc/item/9ff1276t

**Author**
Bogert, Brigitte

**Publication Date**
2007-12-21

Peer reviewed|Thesis/dissertation

Genetic analyses of the Development and Function of Sensory Neurons

by

Brigitte Anne Grace Bogert

DISSERTATION

Submitted in partial satisfaction of the requirements for the degree of

DOCTOR OF PHILOSOPHY

in

Neuroscience

in the

GRADUATE DIVISION

of the

UNIVERSITY OF CALIFORNIA, SAN FRANCISCO

## Dedication and Acknowledgements

First and foremost, I am absolutely indebted to Dr. Louis Reichardt. His advice, guidance, support and caring has been absolutely essential to the completion of my graduate degree. He has been an incredible mentor scientifically, professionally, and personally. He truly takes his responsibilities as both a thesis committee member and the Neuroscience program chair to the utmost.

I would like to thank Dr. Fen-Biao Gao for his support and guidance; in particular, I would like to thank him for his input in my thesis. I would like to also thank him for the opportunities he gave me during my early graduate years.

I would also like to acknowledge the faculty members who have helped me to grow as a scientist. My qualifying exam committee, including Dr. Cori Bargmann and Dr. Barbara Panning, taught me a tremendous amount about rigorous scientific analysis. I greatly enjoyed the challenge of my thesis committee meetings with my thesis committee, including Dr. Louis Reichardt, Dr. Cynthia Kenyon and Dr. Wallace Marshall. I would also like to thank Dr. David Copenhagen for his kindness and support during various points in my graduate career.

I would also like to thank the many lab members who have helped me throughout graduate school. Members of the Gao lab first introduced me to science and to many basic techniques. In addition, members of the Ashrafi lab were always supportive and really pushed my scientific thinking. I owe much of my scientific development to them. In particular, I'd like to acknowledge Amanda Kahn-Kirby, who really took an interest in me both scientifically and personally. Supriya Srinivasan has also given me wonderful

advice at various points during my project. I would also like to thank Jason Liu for all of his assistance.

Undoubtedly, I owe a tremendous amount to the friends and family that have stood by me throughout my graduate career. I am blessed to have a wonderful mother who is also my best friend. My mother's strength and independence are inspiring, and she has been my biggest role model. I must also thank my fiancé Hemang, who has been there for me through the last three years of graduate school. His unwavering, tireless support gave me strength through some of the most difficult parts of my graduate career. I would like to thank my friends who have provided immeasurable support. Karen Menuz has been an incredible friend from the very beginning when we first rotated in the same lab. She has always been available and ready to help me through the ups and downs of graduate school. She's also dragged me away from the lab bench and out into the wilderness from time to time! Ritu Kapur and Sean Pintchovski have also been wonderful people in my life who have made my time at UCSF very special.

# Statement of Contribution

This dissertation is a joint dissertation based on research performed in the laboratories of Dr. Fen-Biao Gao and Dr. Kaveh Ashrafi and supervised by Dr. Fen-Biao Gao and Dr. Kaveh Ashrafi.

Chapter One is an adaptation of a review that was largely written by Dr. Fen-Biao Gao, with some contributions from Brigitte Bogert. The review was published as a paper:

> Gao, F. B. & Bogert, B. A. (2003). Genetic control of dendritic morphogenesis in *Drosophila. Trends in Neurosciences*, 26(5): 262-268.

Permission has been given by Elsevier to reprint copyrighted material from this article in this thesis. The format and much of the original text from the review remains the same in Chapter One. In addition, Chapter One includes many updates and discussions of recent studies in the field of *Drosophila* dendritogenesis.

Part One of Chapter Two represents a collaboration between Brigitte Bogert and several other members of the Gao laboratory. Part of this work was published in a paper that was originally conceived by Dr. Fen-Biao Gao and Dr. Kanyan Xu:

> Xu, K., Bogert, B. A., Li, W., Su, K. S., Lee, A. & Gao, F.B. (2004). The *fragile X-related* gene affects the crawling behavior of *Drosophila* larvae by regulating the mRNA level of the DEG/ENaC protein Pickpocket1. *Current Biology*, 14: 1025-1034.

Permission has been given by Cell Press to reprint copyrighted material from this article in this thesis.

The *Ago2^{51B}* mutant was created with the help of Dr. Fen-Biao Gao and Alan Lee. Real-Time PCR analyses were performed by Dr. Kanyan Xu.
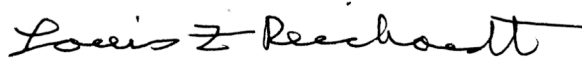
UAS-Ago2 transgenic flies were created with Dr. Li-Ping Chang and Michael Kim.

In Chapter Four, two of the double mutants were created with the help of Jason Liu of the Ashrafi laboratory.

# Genetic Analyses of the Development and Function of Sensory Neurons

by

**Brigitte Anne Grace Bogert**

*[signature]*

**Dr. Louis Reichardt**

**Thesis Committee Chair**

## Abstract

The coordination of behavior and physiology by the nervous system is complex, requiring the integration of inputs from the environment. Sensory neurons, as the detectors of external stimuli, have the important role of detecting and relaying this information to the rest of the nervous system. Proper formation, connectivity, and function of dendrites and cilia in sensory neurons are essential for the detection of stimuli. In this thesis, I use the power of invertebrate genetic systems to explore the development and function of these neuronal structures.

In the first part of my thesis, I use the *Drosophila melanogaster* larval PNS to explore the role of three different genes in dendritic morphology and neuronal function. The dendritic arborization (DA) neurons are sensory neurons that elaborate complex and

diverse dendritic morphologies beneath the epidermis. I find that Argonaute 1 (Ago1), an important part of the microRNA pathway, and Argonaute 2 (Ago2), an essential component RNAi pathway, do not have a role in dendrite patterning. However, Ago2 does regulate expression of *pickpocket1* mRNA, a channel that regulates larval locomotion. Additionally, I find that mutations in the BTB-POZ domain transcription factor *longitudinals lacking* reduce dendrite elaboration.

In the second half of my thesis, I use *Caenorhabditis elegans* as a model organism to examine the role of the Bardet-Biedl Syndrome genes, required for intraflagellar transport in cilia, in metabolic homeostasis. *bbs* mutant worms display increased lipid accumulation, as revealed by the lipophilic dye Nile Red. Surprisingly, in a comprehensive analysis of cilia mutants, mutations in only some intraflagellar transport components alter fat content, suggesting that generally interfering with cilia formation and signaling does not affect lipid levels. A series of epistasis experiments reveal that these IFT genes participate in the *bbs* pathway to regulate intestinal lipid accumulation. Intriguingly, the heterotrimeric kinesin-II *kap-1* functions downstream of *bbs*. I then use candidate gene approaches and RNAi screens to seek an understanding of how *bbs* genes regulate fat stores. Taken together, these studies provide insight into the formation and function of sensory neuronal processes.

# Table of Contents

# List of Tables

# List of Figures

**Chapter One**


**Genetic control of dendritic morphogenesis in *Drosophila melanogaster***

Describing the beauty of neuronal dendrites in many species a century ago, Santiago Ramón y Cajal remarked: 'One cannot help being astounded by the complex dendritic arborizations of such cells' (Ramón y Cajal, 1911). Accumulating evidence indicates that these diverse dendritic branching patterns are essential for neuronal function. For instance, elaborate dendritic arbors allow the computation of local dendritic signals and affect the input-output relationships of neurons (Hausser et al., 2000; Single and Borst, 1998). However, we still do not fully understand the genetic programs that specify dendritic morphologies of different neuronal subtypes. Several reviews have discussed various aspects of this issue in different experimental systems (Chen and Ghosh, 2005; Cline, 2001; Gao, 2007; Goldberg, 2004; Grueber and Jan, 2004; Kim and Chiba, 2004; Lohmann and Wong, 2005; McAllister, 2000; Parrish et al., 2007b; Scott and Luo, 2001; Tada and Sheng, 2006; Van Aelst and Cline, 2004). Here, we focus on the progress made during the last few years on dendritic development using genetic approaches in Drosophila.

**Dendrites in flies**

Unlike the majority of mammalian neurons, most insect neurons are unipolar. A single process extends from the cell body and further differentiates into dendritic branches and more distal axonal arbors (Ramón y Cajal, 1911; Shankland and Goodman, 1982; Strausfeld and Campos-Ortega, 1973). In the PNS of Drosophila embryos and larvae, however, many neurons have multipolar morphologies, similar to CNS neurons in mammals (Bodmer, 1987). Neuronal polarity of Drosophila neurons can be further demonstrated by the selective localization of fusion proteins consisting of

$\beta$ galactosidase and either microtubule plus-end-directed or minus-end-directed motor proteins to axons or dendrites, respectively (Clark et al., 1997).

Modern genetic tools in Drosophila allow direct visualization and characterization of neuronal dendrites in living embryos or larvae. For instance, dendrites of all or of a subset of neurons can be labeled by green fluorescent protein (GFP) using the UAS–Gal4 system (Brand and Perrimon, 1993; Gao et al., 1999; Sun et al., 1999). In addition, single neurons can be labeled with the 'mosaic analysis with a repressible cell marker' (MARCM) technique (Lee and Luo, 1999). This elegant technique allows GFP labeling of either wild-type or mutant single cells or clones, in larvae or adult flies. Using the MARCM approach, it was shown that $\gamma$, $\alpha'/\beta'$ and $\alpha/\beta$ neurons in the Drosophila mushroom bodies are generated at different developmental stages but acquire similar unipolar morphologies in adults (Lee et al., 1999). Dendrites and axons of projection neurons in the antennal lobe of the olfactory system also differentiate from the same process extended from the cell body (Jefferis et al., 2001). Application of the MARCM technique to the Drosophila PNS revealed that single PNS neurons have defined dendritic fields and morphological polarity similar to mammalian neurons (Grueber et al., 2002; Sweeney et al., 2002), consistent with the previous characterization using antibody staining (Bodmer, 1987). For instance, external sensory (ES) neurons have single unbranched dendrites extending in the direction opposite to axonal growth (Figure 1-1B &E). Individual dendritic arborization (DA) neurons, a subgroup of multiple dendritic (MD) neurons, elaborate stereotypic and highly branched dendritic trees and extend a single axon directly from the cell body (Figure 1-1 C,D,&E).

**Genetic analysis of dendritic outgrowth and branching**

The in vivo GFP-labeling of neurons as described above has enabled the use of

systematic genetic approaches to study dendritic morphogenesis. Three such genetic

screens have identified several genes essential for normal dendritic growth, branching

and guidance (Gao et al., 1999; Reuter et al., 2003; Medina et al., 2006). The first screen

used the UAS–Gal4 system specifically to label MD neurons only in homozygous mutant

embryos, and isolated 25 lethal mutations in 12 different complementation groups from

>3000 mutant lines (Gao et al., 1999). The second screen utilized the MARCM

technique to reveal mutations on the second chromosome that affected the morphogenesis

of mushroom body neurons. Approximately 4600 mutant lines were examined at the

third-instar larvae stage; eight alleles in five different complementation groups were

reported (Reuter et al., 2003). A third more recent screen utilized actin::GFP to examine

F-actin-rich dendritic filopodia and dendritic spines in sensory neurons. Of >4000

mutant lines, 13 mutations in 11 complementation groups were identified (Medina et al.,

2006). In addition to genetic screens, candidate gene approaches have also uncovered

several molecules that play important roles in dendritic morphogenesis in Drosophila.

These molecules are summarized in Table 1-1. Some of them will be discussed here in

greater detail.

*Cytoskeleton-associated proteins*

The growth and branching of dendrites depend on the proper formation of

cytoskeletal structures. Recent studies indicate that Short stop (Shot)/Kakapo plays an

important role in this process. *shot* was first identified in genetic screens for mutations

that affected axon development of motor and sensory neurons in Drosophila embryos

(Kolodziej et al., 1995; Vactor et al., 1993). Subsequent molecular analysis revealed that

*shot* is allelic to *kakapo* (Lee et al., 2000), which encodes a large intracellular protein

containing sequences homologous to vertebrate cytoskeleton-associated proteins, such as

plakin, dystrophin and Gas2 (Gregory and Brown, 1998; Strumpf and Volk, 1998). The

subcellular localization of Shot/Kakapo in epidermal muscle attachment cells raises the

possibility that this protein links actin and microtubules (Gregory and Brown, 1998;

Strumpf and Volk, 1998; Roper and Brown, 2003). Indeed, Shot/Kakapo binds the

EB1/APC1 microtubule-binding complex through its association with EB1via its

C-terminal EF-hands and Gas2-containing domains. The absence of Shot/Kakapo activity

in tendon cells causes dissociation of EB1/APC1 from the muscle-tendon junction and

lengthening of the microtubule array (Subramanian et al., 2003). A role for *shot*/*kakapo*

in dendrite development was suggested by defects in *kakapo* mutant embryos, in which

the dendritic branching of RP3 motor neurons (Prokop et al., 1998) or DA sensory

neurons (Gao et al., 1999) was greatly reduced. Taken together, these findings raise the

possibility that Shot/Kakapo-mediated coupling of actin and microtubules is essential for

the dendritic branching process. Further studies will clarify the exact function of

Shot/Kakapo in dendrite development.

Another class of proteins that control dendritic development seems to affect

microtubule-based transport. Recent studies demonstrate that mutations in the

Drosophila dynein complex, including the cytoplasmic dynein heavy chain (*Dhc64*), the

dynein light chain (*roadblock*) and dynein-associated *Lis1*, all reduce the extension and

branching of mushroom body neurons (Liu et al., 2000; Reuter et al., 2003). The

mechanism by which the dynein complex affects dendrite morphogenesis is unknown.

Additionally, proteins that modulate actin and cytoskeleton stability have been demonstrated to regulate dendritic morphology. Abelson (Abl), a non-receptor tyrosine kinase, and Enabled (Ena), the substrate of Abl, have opposite roles in actin dynamics and the formation of axonal filopodia (Bashaw et al., 2000; Gertler et al., 1995; Wills et al., 1999). Similarly, Ena is required for the formation of dendritic branches and spine-like protrusions of DA neurons while Abl limits dendritic branching (Li et al., 2005). Interestingly, p120catenin (p120ctn), involved in cell adhesion by stabilizing cadherins (Xiao et al., 2007) suppresses the increase in spine-like protrusions caused by overexpression of Ena (Li et al., 2005). Similarly, loss of function of p120 catenin in mammalian hippocampal neurons causes a reduction in spine density and maturation via altered cadherin levels and Rho-family GTPase signaling (Elia et al., 2006). Another actin-stabilizing protein, tropomyosin II, is required to limit the extension of dorsal and lateral dendrites, and interacts genetically with *flamingo*, a gene encoding a transmembrane protein that regulates dendrite development (Li and Gao, 2003; Sweeney et al., 2002). Taken together, these findings highlight importance of actin and microtubule dynamics in controlling dendritic outgrowth.

*Receptor-like molecules*

As in mammals, extracellular cues affect dendritic morphogenesis in *Drosophila* (McAllister, 2000; Wong and Ghosh, 2002). Roundabout (Robo) is a transmembrane protein that contains immunoglobulin-like and fibronectin-type-III domains and plays a pivotal role in axon growth and guidance (Kidd et al., 1998). Overexpression of Robo, but not Robo2 or Robo3, in tergotrochanteral motor neurons resulted in dramatic dendritic repulsion from the CNS midline (Godenschwege et al., 2002). Loss of function

mutations in *robo* cause misguidance of motoneuron dendrites at the midline of the central nervous system (CNS; Furrer et al., 2003; Furrer et al., 2007). Accordingly, Slit, a diffusible signaling molecule that acts through Robo, promotes dendritic outgrowth; the CNS motoneuron aCC fails to elaborate dendrites in *slit/slit* mutants (Furrer et al., 2007). In addition, studies in mammalian systems have provided strong evidence that the Robo pathway is involved in dendrite development (Whitford et al., 2002). Netrin, another conserved diffusible signaling molecule, and its receptor Frazzled, known in vertebrates as deleted in colorectal cancer (DCC), also control dendritic guidance of motoneurons at the CNS midline (Furrer et al., 2003).

The transmembrane protein Flamingo contains nine cadherin motifs, four epidermal growth factor (EGF) domains, two laminin-A globular domains and a G-protein-coupled-receptor-like transmembrane domain (Chae et al., 1999; Usui et al., 1999). Dorsal dendrites of DA neurons overextend toward the dorsal midline in *flamingo* mutant embryos (Gao et al., 1999; Kimura et al., 2006) and even invade the contralateral dorsal cluster in mutant larvae (Gao et al., 2000a; Kimura et al., 2006). A similar dendritic overextension phenotype was also observed in mushroom body neurons (Reuter et al., 2003). Although Flamingo is expressed in embryos in both PNS neurons and the adjacent epithelial cells (Gao et al., 2000a), it has a cell-autonomous function in dendritic growth. Single *flamingo* mutant neurons labeled by the MARCM technique exhibit a dorsal dendrite overextension phenotype (Grueber et al., 2002; Sweeney et al., 2002). Furthermore, dendritic defects in mutant embryos or mushroom body neuroblast clones can be partially rescued by expression of *flamingo* transgenes in neurons only (Gao et al., 2000a; Reuter et al., 2003). Because Flamingo expressed in precursor cells affects

asymmetric division (Lu et al., 1999) and dorsal dendrites are initiated precociously in mutant embryos (Sweeney et al., 2002), it seems that *flamingo* mutations affect early differentiation of postmitotic neurons.  The mammalian Flamingo homolog Celsr2 also participates in dendritic arborization but in a different manner; Celsr2 is required for the maintenance of dendritic branches (Shima et al., 2004).  At the mechanistic level, it remains to be determined which other proteins also function in the Flamingo pathway and how the signaling mediated by Flamingo leads to changes in the cytoskeleton during dendritic development.

**Transcriptional control of dendritic morphogenesis**

Recently, several transcription factors have been shown to control dendritic morphogenesis in Drosophila.  Prospero is a homeodomain transcription factor involved in axonal growth and guidance of PNS sensory neurons without affecting cell fate determination (Chu-Lagraff et al., 1991; Vaessin et al., 1991).  In *prospero* mutant embryos, dendritic guidance of dorsal cluster DA neurons is disrupted. The anterior and posterior dorsal dendrites fail to extend in parallel towards the dorsal midline and instead make dramatic turns and occasionally crisscross each other (Gao et al., 1999).  Another transcription factor that affects dendritic development without changing cell fate is Regulatory factor X (RFX; Dubruille et al., 2002).  RFX contains a 76 amino acid DNA-binding domain with a winged-helix structure (Gajiwala et al., 2000) and controls cilium differentiation of sensory neurons (Dubruille et al., 2002).  In the Drosophila PNS, Prospero is expressed in neuronal precursors and glial cells but only transiently in postmitotic neurons (Vaessin et al., 1991).  RFX is also expressed in PNS precursor cells but later its expression is restricted to type-I sensory neurons, with transient expression in

glial cells (Vandaele et al., 2001). It is likely that both Prospero and RFX regulate a transcriptional program in neurons to control dendritic morphogenesis.

Several transcription factors are expressed in specific DA neurons, in which they regulate dendritic complexity independently of neuronal identity. The stereotyped dendritic trees of the DA neurons in *Drosophila* are classified into four classes (class I, II, III, and IV) of increasing arbor complexity (Grueber et al., 2002). Two transcription factors, Abrupt and Cut, are expressed in complementary sets of DA neurons, and are essential in determining dendritic complexity. Abrupt, a BTB-POZ domain transcription factor, is expressed in the simple class I neurons ddaE and ddaF (Li et al., 2004; Sugimura et al., 2004), whereas Cut, a homeodomain transcription factor, is expressed at high levels in the class III and IV neurons, which have complex dendritic trees, and is nondetectable in class I neurons (Grueber et al., 2003a). Abrupt is required to limit the dendritic branching in class I neurons; when ectopically expressed in higher-order neurons, Abrupt reduces the number of terminal ends (Li et al., 2004; Sugimura et al., 2004). In contrast, loss of *cut* reduces dendrite growth and terminal branching of class II, III and IV neurons, and overexpression of Cut increases the number of terminal ends (Grueber et al., 2003a). Spineless (Ss), is another transcription factor with a more complex role in regulating the complexity of dendritic arbors; loss of *ss* in class I and II neurons increases arbor complexity, whereas loss of *ss* in class III and IV neurons decreases dendrite elaboration (Kim et al., 2006).

Dendritic morphology, as an important aspect of neuronal identity, is also regulated by factors that control neuronal cell fates. Sequoia is such a transcription factor that has a dual function in both processes. The *sequoia* gene was identified from a

genetic screen for dendrite mutants (Gao et al., 1999) and encodes a Tramtrack-related novel zinc-finger protein that is exclusively expressed in the developing nervous system (Brenman et al., 2001). In *sequoia* mutant embryos, ES neurons are transformed into DA neurons, as judged by neuronal subtype-specific markers. Expressed in postmitotic DA neurons in addition to ES neurons and glial cells, Sequoia also has a role in controlling dendritic growth (Brenman et al., 2001). In *sequoia* mutant embryos, DA neurons that are generated either through normal lineages or through ES neuron transformation exhibit defects in dendritic morphology. For instance, the dorsal dendrites of ddaE neurons in sequoia mutant embryos overextend toward the dorsal midline (Brenman et al., 2001). Sequoia is a nuclear zinc-finger protein and is expressed in DA neuron precursors as early as stage 10 (Brenman et al., 2001). It remains to be determined whether Sequoia functions directly in postmitotic DA neurons or whether it functions in precursor cells, to alter the expression of downstream transcription factors or other proteins that, in turn, control dendritic growth.

Hamlet, another transcription factor identified from a genetic screen for dendrite mutants (Gao et al., 1999), is a nuclear protein that contains zinc-finger motifs and plays an important role in specifying dendritic morphology (Moore et al., 2002). Interestingly, the mechanism of Hamlet function seems quite different from that of Sequoia. Unlike Sequoia, which controls the morphology of most, if not all, neurons in the developing nervous system of Drosophila embryos, Hamlet has a very restricted role. It is expressed only in the IIIB precursor cells that give rise to ES neurons and their sibling glial cells. In addition, Hamlet is transiently expressed in postmitotic ES neurons during dendritic extension, with no expression in DA neurons or the CNS. In the IIIB lineage in *hamlet*

mutant embryos, the ES neuron is transformed into a DA neuron, and the sibling glial cell is transformed into an external cell (trichogen), as judged using cell-type-specific markers (Figure 1-2). Amazingly, the transformed neurons exhibit similar dendritic branching patterns to the normal DA neurons, which are generated from the IIB precursors that also give rise to the IIIB lineage. Taken together, these findings suggest that Hamlet functions in IIIB precursor cells to initiate a transcription program that promotes multiple aspects of ES neuronal fate, including single-dendrite morphology. This notion is further supported by overexpression studies. When Hamlet was ectopically expressed in postmitotic DA neurons, which do not normally express Hamlet, the dendritic branching process was dramatically inhibited (Moore et al., 2002). The next step is to understand how the Hamlet-expressing IIIB precursors give rise to ES neurons with single dendrites, and how IIB precursors give rise to a subtype of DA neurons with lineage-specific dendritic branching pattern in the absence of inhibition by Hamlet.

Other transcription factors that regulate dendritic complexity are likely to emerge through screens as well as candidate-gene approaches. A recent RNA interference screen used double stranded RNAs targeting 730 known and putative transcription factors to identify 76 genes that affect dendritic branching of the simple class I neurons (Parrish et al., 2006). These genes were categorized according to three groups: factors that determine the size of the dendritic field, genes that coordinate primary dendrite extension with lateral branch growth, and factors that control the orientation of the dendritic field of the neurons (Parrish et al., 2006). The challenges in the future will be not only to identify the functions of these genes but also to understand how these genes interact to elicit a

precise transcriptional program that regulates the development of dendrites in the DA neurons.

**Dendritic tiling in the *Drosophila* PNS**

Dendritic tiling, a complete but non-overlapping coverage of a receptive field by dendrites of functionally homologous neurons, was first described in the mammalian retina (Wassle et al., 1981). For instance, dendrites of $\alpha$ and $\beta$ ganglion cells overlap extensively; however, dendrites of the same subtype of ganglion cell cover the whole retina with minimal overlap. Direct dendro–dendritic contacts (Lohmann and Wong, 2001) might mediate the repulsive interaction that limits the size of dendritic fields of homologous neurons (Perry and Linden, 1982). Dendritic tiling plays an important role in the organization of a functional neural circuit that contains a large number of neurons with diverse morphologies (Masland, 2001).

Dendritic tiling occurs in the *Drosophila* PNS, which affords a unique opportunity to apply genetic approaches to dissect the molecular basis of tiling. In each hemisegment of Drosophila third-instar larvae, individual DA sensory neurons that are derived from different lineage (Orgogozo et al., 2001; Vervoort et al., 1997) have distinct dendritic fields as revealed by MARCM analysis (Grueber et al., 2002; Sweeney et al., 2002). For instance, in the dorsal cluster, there are six DA neurons, ddaA to ddaF. The dendrites of ddaC neurons extend to both anterior and posterior segment boundaries and from the dorsal midline to the lateral cluster, whereas ddaE neurons send out dendrites only towards the posterior segment boundary (Grueber et al., 2002; Sweeney et al., 2002). Several observations suggest that dendritic tiling between neighboring neurons (heteroneuronal) plays a role in defining the dendritic fields of class III and IV DA

neurons (Figure 1-3). First, dendrites of homologous neurons in contralateral dorsal clusters meet at the dorsal midline and often make dramatic turns to avoid each other (Gao et al., 2000a). Second, when single class IV neurons in one cluster are ablated with a laser beam, the dendrites of homologous neurons in the contralateral cluster and adjacent clusters overextend across the midline and segments boundaries, respectively (Gao et al., 2000a; Grueber et al., 2003b). Third, the dendrites of classes III and IV DA neurons separately cover the whole epidermis in each segment in a class-specific manner (Grueber et al., 2002). However, in contrast to class III and IV neurons, class I and II neurons do not clearly exhibit heteroneuronal dendritic repulsion. Supernumerary class I and II neurons overlap extensively with the same class neuron (Grueber et al., 2003b). Taken together, these findings indicate that neuronal subtype-specific dendritic tiling occurs in flies as well as in mammals.

Recent studies of tiling in DA neurons have made significant headway in elucidating the underlying molecular mechanisms that mediate repulsive interactions. In *flamingo* mutant larvae, dorsal dendrites overextend and cross the dorsal midline (Gao et al., 2000a). The apparent absence of dendritic repulsion near the dorsal midline could be due to the robust overextension of a few dorsal dendrites and/or the lack of repulsive interactions caused by the *flamingo* mutations. Because Flamingo is expressed in all DA neurons, other factors must be also involved in the neuronal subtype-specific dendritic repulsion.

Another genetic pathway that regulates tiling is the NDR family kinases Tricornered (Trc), its activator Furry (Fry), and the upstream Ste-20 family kinase Hippo (Hpo; Emoto et al., 2004; Emoto et al., 2006). The DA neurons of *trc* and *fry* mutants

exhibit supernumerary branches and defective dendritic tiling. The dendritic fields of three class IV neurons in each abdominal hemisegment, ddaC, v'ada, and vdaB, usually extend across the epidermis with minimal overlap. However, mutations in *fry* and *trc* result in a partial overlap of the v'ada and vdaB dendritic field (Figure 1-3; Emoto et al., 2004). The upstream kinase Hpo interacts with Trc and is also required for heteroneuronal dendrite avoidance (Emoto et al., 2006), thus defining a series of molecular interactions that control dendritic arborization.

An equally intriguing and related observation is that dendritic processes of the same DA neuron (isoneuronal) do not overlap (Grueber et al., 2002; Sweeney et al., 2002), which suggests a 'self-avoidance' mechanism, as has been proposed for axonal branches of the equivalent sensory neuron in leech (Kramer and Stent, 1985). Self-avoidance participates in shaping the dendritic arbors of all classes of MD neurons. Isoneuronal dendritic tiling ensures that the dendrites of a single neuron innervate the entire receptive field equally. Mutations in *trc* and *fry* also affect tiling of terminal dendritic branches of the same neuron resulting in a substantial increase in the number of terminal branches that overlap each other (Emoto et al., 2004).

Recently, three exciting studies have uncovered a significant role for the Down's syndrome Cell Adhesion Molecule (Dscam), a type I membrane protein of the immunoglobulin superfamily encoding for 38,016 splice variants (Hughes et al., 2007; Matthews et al., 2007; Soba et al., 2007). Strong homophilic interactions occur only between the same isoforms of Dscam (Wojtowicz et al., 2004), giving rise to the hypothesis that isoform-specific interactions contribute to patterning within the nervous system (Zinn, 2007). Accordingly, the authors of these studies found an important role

for Dscam in mediating isoneuronal, but not heteroneuronal, tiling.  Sister dendrite

branches in *Dscam* null mutants fail to avoid each other, and these self-avoidance defects

can be rescued both by expressing Dscam, and by expressing any one of a number of

Dscam isoforms (Hughes et al., 2007; Matthews et al., 2007; Soba et al., 2007Shi, 2007

#274).  Furthermore, different classes of DA neurons can overlap with each other because

they do not express the same Dscam isoforms.  Ectopically expressing one Dscam

isoform in neurons of different classes causes abnormal repulsion between their dendritic

branches (Hughes et al., 2007; Matthews et al., 2007; Soba et al., 2007).  These results

lend to the conclusion that a different set of Dscam isoforms expressed in each neuron

drives self-repulsion of its own dendritic branches but not the branches of other neurons

(Zinn, 2007).  Further molecular dissection of these interesting processes promises a

deeper understanding of dendritic field formation.

**Dendritic targeting in the olfactory system**

In Drosophila, ~1300–1500 olfactory receptor neurons (ORNs) are dispersed in

the olfactory sensory organs (the antennae and the maxillary palps; Vosshall, 2000).

Each ORN expresses one, or a small number of, odor receptors and sends its axon to one

of the 40–50 glomeruli in the antennal lobe of the brain (Vosshall, 2000).  Projection

neurons relay olfactory information by sending their dendrites to these glomeruli to make

synaptic connections with ORN axons and by projecting their axons to higher olfactory

centers (Gao et al., 2000b; Jefferis et al., 2001). The correct targeting of dendrites of each

projection neuron to a specific glomerulus is essential for the proper wiring of the

olfactory system; however, the underlying cellular and molecular mechanisms have not

been addressed until very recently.

Using the MARCM technique, Jefferis and colleagues determined the neuronal

lineage and dendritic projection patterns of individual projection neurons (Jefferis et al.,

2001). Several interesting observations emerged from this analysis. First, at least 50% of

the projection neurons were derived from three neuroblasts: an anterodorsal, a lateral and

a ventral neuroblast. Subsequent analyses focused on anterodorsal and lateral projection

neurons because most of these target their dendrites to a single glomerulus. Second,

projection neurons derived from the anterodorsal and lateral neuroblasts innervated

separate and non-overlapping sets of glomeruli, suggesting that dendritic targeting is

lineage dependent. Third, within a neuroblast lineage, the birth-time of a specific

projection neuron correlated with the glomerulus to which the neuron sent its dendrites.

Because projection neurons are generated before the arrival of ORN axons in the antennal

lobe, these findings suggest that dendritic targeting of projection neurons to specific

glomeruli is genetically determined, independently of presynaptic inputs (Jefferis et al.,

2001; Jefferis et al., 2004). Further studies indicate that projection neurons that send

dendrites to the same glomerulus exhibit spatially similar axonal branching patterns in

higher olfactory centers (Marin et al., 2002; Wong et al., 2002), suggesting that dendritic

targeting and axonal projection of these neurons are coordinately controlled.

**Molecular control of dendritic targeting**

Transcriptional control plays a pivotal role in regulating dendritic targeting in the

antennal lobe (Komiyama et al., 2003). The *abnormal chemosensory jump 6* (*acj6*) gene

encodes a POU-domain transcription factor that is expressed in all ORNs (Clyne et al.,

1999). Drifter is another POU-domain transcription factor in Drosophila that is required

for the proper development of multiple tissues (Anderson et al., 1995). Interestingly,

Acj6 and Drifter are expressed in anterodorsal and lateral projection neurons (adPNs and lPNs), respectively. MARCM analyses indicate that *acj6* or *drifter* loss-of-function mutations lead to less specific dendritic targeting of either adPNs or lPNs in the antennal lobe. Similarly, four other transcription factors—*islet*, *cut*, *squeeze*, and *lim1*—have been identified thus far to cooperate with *acj6* and *drifter* to regulate dendritic targeting of specific subsets of *Drosophila* olfactory projection neuron (PN) in a combinatorial manner (Komiyama and Luo, 2007). Identification of the other transcription factors required to specify dendritic targeting and the direct downstream targets that are regulated by these transcription factors will be interesting.

Cell-surface molecules are probably among the most interesting candidates that control dendritic targeting in the olfactory system. The transmembrane protein Semaphorin-1a (Sema-1a) works cell-autonomously to guide PN dendritic targeting in the antennal lobe along the dorsolateral-to-ventromedial axis. Expressed at different levels in distinct PNs, Sema-1a directs coarse dendritic targeting, which is later refined through cell-cell interactions (Komiyama et al., 2007). Another cell-surface molecule, Dscam, regulates the axonal targeting of a subset of ORNs (Hummel et al., 2003), and the dendritic targeting of projection neurons to glomeruli (Zhu et al., 2006). Overexpression of Dscam in projection neurons causes a shift in the projection neuron dendrites to a different glomerulus and a corresponding shift in its partner ORN axons, thus preserving connection specificity independently of glomerular positioning (Zhu et al., 2006). Identification of the molecular components that mediate recognition between ORN axons and projection neuron dendrites is of great interest.

**Concluding remarks**

17

Significant headway has been made in identifying some of the molecules that regulate dendritic morphology.  A large number of molecules regulate dendritogenesis, including transcription factors, cytoskeleton-associated proteins, receptor-like molecules, transmembrane factors, and secretory pathway molecules.  However, much remains to be uncovered.  Identification of the targets of the transcription factors will advance our understanding of the transcriptional regulatory network that controls dendritic morphogenesis.  Similarly, further elucidation of the signaling pathways that coordinate responses to extracellular signals and organization of the cytoskeleton is required.  Additionally, forward genetic screens have only focused on part of the *Drosophila* genome; it is likely that screens targeting the rest of the genome will unearth a significant number of new molecules that govern dendritic morphology. Finally, identification of the pathways that are conserved in mammals and examination of the role of dendritic development in disease are of great interest.  Although these questions are large, they are answerable with many of the available techniques.  Undoubtedly, an exciting future awaits the field of dendritic morphogenesis.

**Table 1-1. Genes that regulate dendritic morphology in *Drosophila*.**

| Proteins | Major structural domains or Orthologs | References | Functions in dendritic morphogenesis | References |
|---|---|---|---|---|
| **Cytoskeleton-associated** | | | | |
| Kakapo | Actin-and microtubule-binding domain | (Gregory and Brown, 1998; Lee and Kolodziej, 2002; Strumpf and Volk, 1998) | Affects dendritic branching patterns of DA neurons and motor neurons | (Gao et al., 1999; Prokop et al., 1998) |
| Enabled | Proline-rich motifs | (Gertler et al., 1995) | Promotes formation of dendritic branches and actin-rich protrusions in DA neurons | (Gao et al., 1999; Li et al., 2005) |
| Futsch | MAP2B-like protein | (Hummel et al., 2000; Roos et al., 2000) | Required for proper development of chordotonal neuron dendrites | (Hummel et al., 2000) |
| Dhc64 | Cytoplasmic dynein heavy chain | (Liu et al., 2000) | Required for dendritic growth and branching of MB neurons | (Liu et al., 2000) |
| Lis1 | Coiled-coil domain and WD-40 repeats | (Neer et al., 1994) | Required for dendritic growth and branching of MB neurons | (Liu et al., 2000) |
| Roadblock | Dynein light chain | (Reuter et al., 2003) | Reduces dendritic complexity of MB neurons | (Reuter et al., 2003) |
| Tropomyosin | Actin-binding | (Araya et al., 2002) | Required to restrict dendritic field of DA neurons | (Li and Gao, 2003) |
| **Small GTPases** | | | | |
| RhoA | GTP-binding protein | (Hall, 1998) | LOF results in dendritic overextension of MB neurons | (Lee and Luo, 1999) |
| Cdc42 and Rac1 | GTP-binding protein | (Hall, 1998) | Affects dendritic growth and branching of ES and DA neurons | (Gao et al., 1999; Lee et al., 2003; Luo et al., 1994) |
| **Transmembrane proteins** | | | | |
| Flamingo | Cadherin and GPCR-like transmembrane domains | (Chae et al., 1999; Usui et al., 1999) | Controls dendritic extension of DA and MB neurons | (Gao et al., 1999; Gao et al., 2000a; Kimura et al., 2006; Reuter et al., 2003; Sweeney et al., 2002) |

| | | | | |
|---|---|---|---|---|
| Roundabout | Ig-and FN-like repeats | (Kidd et al., 1998) | LOF in RP2, RP3, and aCC causes dendrite misguidance at CNS midline | (Furrer et al., 2003; Furrer et al., 2007) |
| Frazzled | Ig- and FN-like repeats | (Kolodziej et al., 1996) | LOF in RP3 and aCC causes dendrite misguidance at CNS midline | (Furrer et al., 2003) |
| DScam | Ig-domains and FN type III repeats | (Hughes et al., 2007; Matthews et al., 2007; Soba et al., 2007) | Mediates self-avoidance of DA dendrites | (Hughes et al., 2007; Matthews et al., 2007; Soba et al., 2007) |
| Semaphorin-1A | Sema and plexin-semaphorin-integrin domain | (Yazdani and Terman, 2006) | Graded expression directs targeting of PN neurons | (Komiyama et al., 2007) |
| N-cadherin | Cadherin ,EGF-like, and laminin globular-like domains | (Takeichi, 2007) | Required for PNs to restrict their dendrites to single glomerulus | (Zhu and Luo, 2004) |
| **Kinases** | | | | |
| Tricornered and Furry | NDR family | (Cong et al., 2001; Tamaskovic et al., 2003) | Required for heteroneuronal and isoneuronal tiling | (Emoto et al., 2004) |
| Warts | NDR family | (Justice et al., 1995) | Required for maintenance of dendritic branches | (Emoto et al., 2006) |
| Hippo | Ste-20 family | (Harvey et al., 2003) | Required for tiling and maintenance of dendrites | (Emoto et al., 2006) |
| CaMKII | Serine/threonine kinase | (Joiner Ml and Griffith, 1997) | Alters dendritic filopodia stability | (Andersen et al., 2005) |
| **Transcription factors** | | | | |
| Prospero | Homeodomain | (Chu-Lagraff et al., 1991; Vaessin et al., 1991) | LOF results in the misrouting of DA neuron dendrites | (Gao et al., 1999; Prokop et al., 1998) |
| Sequoia | Two zinc-finger motifs | (Brenman et al., 2001) | LOF causes abnormal dendritic morphology of most PNS neurons | (Brenman et al., 2001; Gao et al., 1999) |
| Hamlet | Nine zinc-finger motifs | (Moore et al., 2002) | GOF in DA neurons reduces branching complexity | (Moore et al., 2002) |
| Regulatory factor X | Winged-helix DNA-binding domain | (Gajiwala et al., 2000) | Required for dendritic cilium differentiation of type I sensory neurons | (Dubruille et al., 2002) |
| Acj6 and Drifter | POU domain | (Anderson et al., 1995; Clyne et al., 1999)} | Control dendritic targeting in the olfactory system | (Komiyama et al., 2003) |

| | | | | |
|---|---|---|---|---|
| Abrupt | BTB-POZ domain | (Hu et al., 1995) | Restricts dendritic branching of class I neurons | (Li et al., 2004; Sugimura et al., 2004) |
| Cut | Homeodomain | (Blochlinger et al., 1991; Bodmer, 1987) | LOF in many DA neurons reduces branching complexity | (Grueber et al., 2003a) |
| Islet and Lim1 | LIM-homeodomain | (Komiyama and Luo, 2007) | Controls dendritic targeting in the olfactory system | (Komiyama and Luo, 2007) |
| Squeeze | Zinc-finger | (Komiyama and Luo, 2007) | Controls dendritic targeting in the olfactory system | (Komiyama and Luo, 2007) |
| Spineless | bHLH-PAS domain | (Duncan et al., 1998) | Required for dendritic diversity of DA neurons | (Kim et al., 2006) |
| Pc, extra sex combs, Enhancer of zeste | Polycomb genes | (Jones et al., 1998; Muller et al., 2002) | Required for maintenance of class IV dendrites | (Parrish et al., 2007a; Parrish et al., 2006) |
| Longitudinals lacking | BTB-POZ domain | (Giniger et al., 1994) | LOF causes dendrite wiring defects in the olfactory system | (Spletter et al., 2007) |
| **Translation** | | | | |
| Nanos and Pumilio | mRNA binding | (Macdonald, 1992; Wang and Lehmann, 1991) | Required for elaboration of class III and IV not class I and II DA neurons | (Ye et al., 2004) |
| Glycyl-tRNA synthetase | Aminoacylation | (Antonellis et al., 2003) | Affects terminal arborization of MB dendrites | (Chihara et al., 2007) |
| Fragile X Mental Retardation Protein 1 | N-terminal, K homology, and RGG box RNA binding domains | (Ashley et al., 1993; Siomi et al., 1993) | LOF causes overgrowth and overbranching of DA and MB neurons | (Lee et al., 2003; Pan et al., 2004) |
| **Vesicular pathways** | | | | |
| Shrub | Snf7/VPS32 | (Sweeney et al., 2006) | LOF in DA neurons increases number of dendrites and reduces dendritic field | (Sweeney et al., 2006) |
| Dar2, Dar3, Dar6 | Sec23, Sar1, Rab1 | (Ye et al., 2007) | LOF reduces dendrite elongation and branching | (Ye et al., 2007) |
| **Protein Degradation** | | | | |
| UbcD1 | E2 ubiquitin conjugating | (Kuo et al., 2006) | Required for dendritic pruning of class IV DA neurons | (Kuo et al., 2006) |
| Dronc | Caspase | (Kuo et al., 2006; Williams et al., 2006) | Required for dendritic pruning of class IV DA neurons | (Kuo et al., 2006; Williams et al., 2006) |

| Proteins in support cells | | | | |
|---|---|---|---|---|
| NompA | ZP domain and several PAN modules | (Chung et al., 2001) | Dendrites of adult type I sensory neurons fail to reach the bristle bases | (Chung et al., 2001) |
| Glial cells missing | Glial cells missing motif | (Hosoya et al., 1995; Jones et al., 1995) | Dendrites of BD neurons fail to form in the absence of glial cells | (Hosoya et al., 1995; Jones et al., 1995) |
| Neuroglian | Ig- and fibronectin-domains | (Bieber et al., 1989) | Limits branching of class I DA neurons | (Yamamoto et al., 2006) |

LOF = loss of function; GOF = gain of function; DA = dendritic arborization neurons of PNS; MB = Mushroom Body; PN = Projection neurons; RP2, RP3, aCC = motor neurons; BD = Bipolar dendritic neuron of PNS

**Figure 1-1**
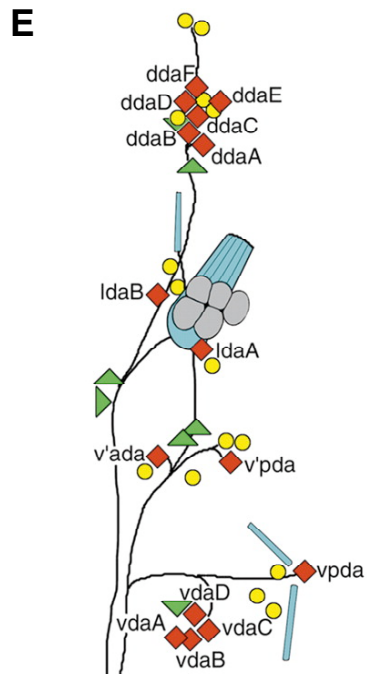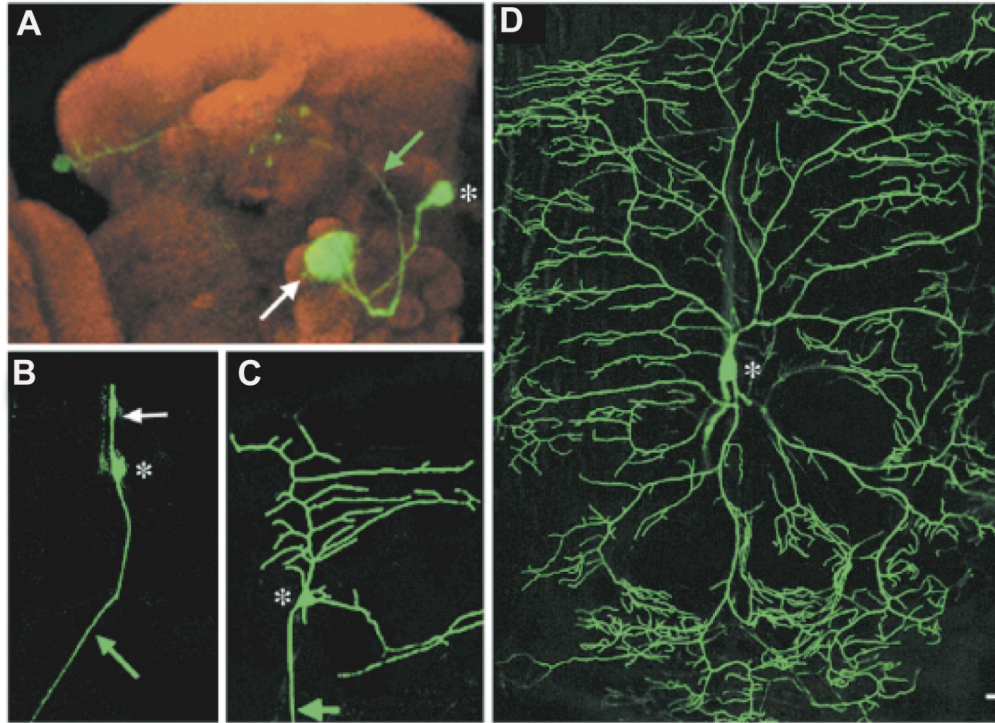
**Figure 1-1. Various dendritic morphologies in *Drosophila*.**

(A) A projection neuron in the antennal lobe extends its dendrites (indicated by the white arrow) to the glomerulus and its axon (indicated by the green arrow) to the higher olfactory centers. Reprinted by permission from Macmillan Publishers Ltd: Nature, (Jefferis et al., 2001) © 2001.

(B) An external sensory neuron sends its axon (green arrow) to the ventral nerve cord and its dendrite (white arrow) dorsally.

(C) Most ddaE neuron dendrites extend in the posterior direction whereas the axon (indicated by the green arrow) extends ventrally to the CNS.

(D) The dendrites of a ddaC neuron cover the whole hemisegment, from the anterior to the posterior segment boundaries and from the dorsal midline to lateral cluster neurons. The white asterisks indicate the cell bodies of individual neurons. Scale bar, 40 $\mu$m for (B-D). (B-D) reprinted from (Sweeney et al., 2002) ©2002 with permission from Elsevier.

(E) Schematic of the *Drosophila* abdominal PNS. DA neurons = red diamonds; yellow circles = external sensory neurons; green triangles = other multidendritic neurons; blue rectangles = chordotonal organs. Reprinted from (Grueber et al., 2002) with permission from Company of Biologists.

**Figure 1-2**
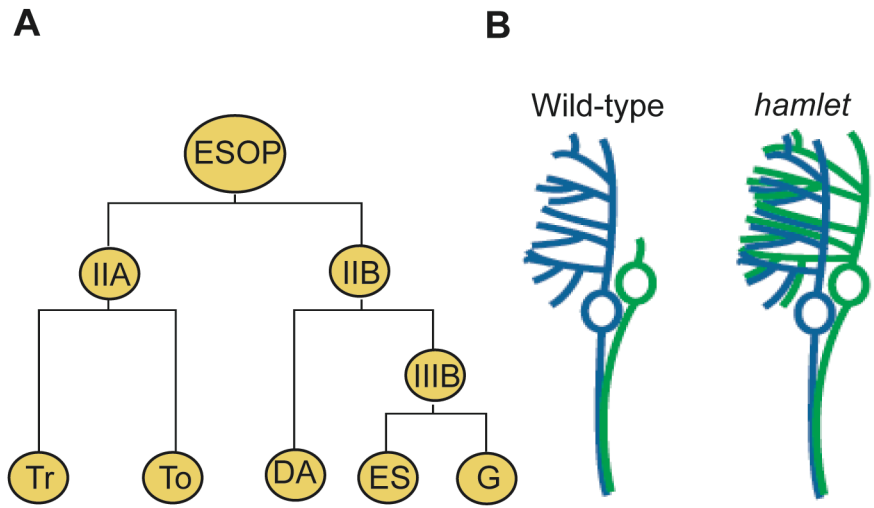
**Figure 1-2. The external sensory organ precursor (ESOP) lineage and the transformation of external sensory (ES) neurons into dendritic arborization (DA) neurons in *hamlet* mutants.**

(A) Schematic representation of the ESOP lineage. Abbreviations: G, glial cell; Tr, trichogen cell; To, tormagen cell.

(B) An illustration of a DA (blue) and an ES (green) neuron in a wild-type third-instar larva. Note that the single dendrite of the ES neuron extends dorsally.

(C) Schematic representation of the DA neurons that are generated from the IIB precursor (blue) and from the transformed ES neuron (green) in *hamlet* mutant flies. The dendritic branching patterns of the two DA neurons are similar to each other. This figure is based on the data in (Moore et al., 2002).

**Figure 1-3**
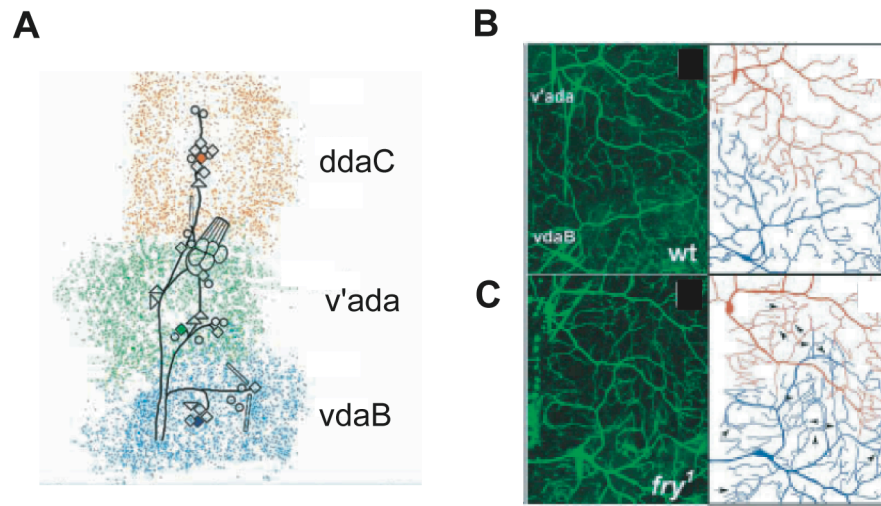
**Figure 1-3. Tiling of the class IV DA neurons.**

(A) An illustration of the dendritic fields of the different class IV neurons ddaC, v'ada and vdaB in an abdominal hemisegment. Reproduced from (Grueber et al., 2003b)with permission of the Company of Biologists.

(B) An example of non-overlapping boundaries between the dendrites of v'ada and vdaB.

(C) An example of the dendritic fields of the tiling defective mutant $fry^1$. Dendrites between v'ada and vdaB overlap extensively.

Dendrites in (B) and (C) are color-coded in the tracing to the right to indicate individual branches of each neuron. (B and C) reprinted from (Emoto et al., 2004) © 2004 with permission from Elsevier.

# Chapter Two


# Genetic analyses of PNS dendrites in *Drosophila melanogaster*

Correct dendritic patterning is essential for the connectivity and functioning of the nervous system. Dendrites navigate a complex environment to synapse with their correct targets. To appropriately innervate a receptive field, a neuron must elaborate a sufficient number of dendrites of proper length and orientation. Several different factors regulate dendritic morphology, such as neuronal activity, genetic factors and extracellular guidance cues.

The larval peripheral nervous system (PNS) of *Drosophila melanogaster* provides a useful model system to study genes that govern dendritic patterning. The fly PNS contains 44 neurons in each abdominal hemisegment that can be grouped into the ventral, lateral and dorsal clusters. Each cluster contains external sensory, chordotonal, and multiple dendritic (MD) neurons (Bodmer et al., 1989; Orgogozo et al., 2001; Vervoort et al., 1997). A subtype of the MD neurons, the dendritic arborization (DA) neurons, are multipolar sensory neurons that develop complex dendrites just beneath the larval epidermis (Bodmer, 1987; Gao et al., 1999), where they receive sensory inputs from the cuticle. The DA neurons have a variety of sensory functions, including nociception and mechanosensation (Ainsley et al., 2003; Tracey et al., 2003). Different classes of MD neurons elaborate stereotyped dendritic arbors that range from very simple structures to complex trees with higher-order branches (Bodmer, 1987; Grueber et al., 2002; Sweeney et al., 2002). Visualization of these neurons in vivo by green fluorescent protein (GFP) using the UAS-GAL4 system (Brand and Perrimon, 1993) has provided the basis for a powerful genetic system to analyze the function of different genes in the development of these neurons (Gao et al., 1999; Gao et al., 2000a).

Here, I use the *Drosophila* PNS model to study the role of two different genetic pathways in dendritic development. In Part One, I investigate the role of *argonaute 1* and *argonaute 2*, two genes that function in the RNA interference (RNAi) and microRNA (miRNA) pathways, in dendritic development and function. In Part Two, I examine the role of *longitudinals lacking* in dendritic branching.

**Part One: The role of the *argonautes* in sensory neuron function and development**

The discovery of novel post-transcriptional forms of regulation, including the RNA interference and miRNA pathways has sparked intense, exciting research in this novel area of biology and unleashed powerful molecular tools for studying genes. These pathways utilize small RNAs of 21 to 24 nucleotides to target cognate mRNAs for translational inhibition or degradation. Since the discovery of small RNAs, significant advances have been made in elucidating their functions, regulatory mechanisms, and their production machinery.

The miRNA and RNAi pathways regulate genes post-transcriptionally using similar molecular machinery but different mechanisms to process their targets. In *Drosophila,* the miRNA pathway begins with the nuclear processing and exporting of a miRNA hairpin precursor (Bohnsack et al., 2004; Denli et al., 2004), which is then cleaved by Dicer-1 in the cytoplasm (Lee et al., 2004). The resulting 21-24 nucleotide miRNA duplex is incorporated into an RNA-induced silencing complex (RISC), whose major component is the miRNA binding protein Argonaute 1 (Ago1; Okamura et al., 2004), and guides the RISC to the target cognate mRNA for translational inhibition or degradation (Pillai et al., 2007). Similarly, in the RNAi pathway, long double-stranded RNA molecules are cleaved by Dicer-2 into 21-24 nt small-interfering RNAs (siRNA;

Lee et al., 2004), and incorporated into a RISC complex containing Argonaute 2 (Ago2). These siRNAs (or, in some cases, miRNAs) guide the RISC complex to the cognate target mRNA for cleavage by Ago2 (Hammond et al., 2000; Martinez et al., 2002). Complementarity between the miRNA and the target mRNA determines the mode of silencing. A target mRNA that is perfectly complementary to its miRNA will be cleaved by the Ago2-RISC; conversely, Ago1 mediates translation inhibition of an mRNA that has central mismatches in its miRNA-binding sites (Forstemann et al., 2007; Okamura et al., 2004).

Thus far, these small RNAs have been found to have a variety of functions. siRNAs have been suggested to have a role in viral protection, transposon silencing, and chromatin-based silencing (Almeida and Allshire, 2005; Andino, 2003; Sijen and Plasterk, 2003; Tabara et al., 1999; van Rij et al., 2006). In addition, thousands of miRNAs have been discovered with diverse roles ranging from energy metabolism to muscle differentiation; the function of most of these miRNAs has not been identified yet (Aravin et al., 2003; Dostie et al., 2003; Jaubert et al., 2007; Lagos-Quintana et al., 2001; Lagos-Quintana et al., 2003; Lagos-Quintana et al., 2002; Lim et al., 2003a; Lim et al., 2003b; Mourelatos et al., 2002; Teleman et al., 2006). Many of these miRNAs are expressed in the nervous system and participate in development (Kapsimali et al., 2007; Kosik, 2006; Zhao and Srivastava, 2007). For example, *Drosophila* miR-9a specifies the number of neuronal precursors cells during development (Li et al., 2006). A major quest is currently underway to identify and understand the functions of these small RNA pathways in the nervous system.

Intriguingly, two independent studies found that two components of the RNAi pathway, Dicer and Ago2, interact with the *Drosophila* homolog of Fragile X Mental Retardation protein (DFMR1) in *Drosophila* Schneider 2 cells (Caudy et al., 2002; Ishizuka et al., 2002). The FMR protein (FMRP) was previously shown to be a negative regulator of translation (Laggerbauer et al., 2001; Li et al., 2001; Mazroui et al., 2002). Although DFMR1 is not required for efficient RNAi (Caudy et al., 2002), the interaction between DFMR1 and RNAi proteins suggested that FMR regulates target mRNAs via a miRNA or an RNAi-related mechanism (Jin et al., 2004; Plante and Provost, 2006; Schaeffer et al., 2003).

Fragile X syndrome is associated with cognitive, behavioral, and sensory deficits: patients present with hyperactivity, hypersensitivity to sensory stimuli, impaired motor coordination, and deficits in attention span (Penagarikano et al., 2007). Similarly, *Drosophila dfmr1* mutants display locomotory defects, such as impaired adult flight (Zhang et al., 2001) and altered larval crawling (Xu et al., 2004), and deficits in complex behaviors, including courtship ritual and altered circadian rhythm (Dockendorff et al., 2002; Inoue et al., 2002; McBride et al., 2005; Morales et al., 2002). Some of the DFMR1-regulated molecular targets that mediate these behaviors have been identified. For example, DFMR1 modulates larval locomotion by negatively regulating the mRNA *pickpocket1* (*ppk1*), a degenerin/epithelial sodium channel family (DEG/ENaC) member expressed in a subset of MD neurons (Xu et al., 2004).

Furthermore, several reports have found dendritic abnormalities in Fragile X patients and animal models. In Fragile X patients (Hinton et al., 1991; Irwin et al., 2001; Rudelli et al., 1985; Wisniewski et al., 1991) and *Fmr1* knockout mice (Comery et al.,

1997; Galvez et al., 2003; Galvez and Greenough, 2005; Nimchinsky et al., 2001), the cortex presents with a significantly higher density of long, thin dendritic spines, typical of immature spines, rather than the stubby, mushroom-shaped spines characteristic of normal development. Similarly, both mushroom body and DA neurons in *Drosophila dfmr1* mutants exhibit overgrowth and excessive branching (Lee et al., 2003; Pan et al., 2004). Ultrastructural analysis of *dfmr1* mutant mushroom body neurons has revealed an overaccumulation of synaptic vesicles in the enlarged and irregularly shaped synaptic boutons (Pan et al., 2004). DFMR1 affects dendritic branching by negatively regulating the mRNA of the *Drosophila* homolog *profilin* (Reeve et al., 2005) and the Rho GTPase *Rac1* (Lee et al., 2003), which regulate actin dynamics.

Given that components of the miRNA and RNAi pathways interact with DFMR1 in *Drosophila*, these components may also perform similar functions, including regulating some of the same targets as DFMR1 and regulating dendritic branching. Here, we show that Ago2 controls expression of the DFMR1 target gene *ppk1*. However, we fail to find an effect of Ago1 or Ago2 on dendritic branching.

**Results**

**dFMR and Ago2 act in the same genetic pathway to regulate *ppk1***

The physical interaction between DFMR1 and Ago2 suggests that they may regulate some of the same targets. We previously found that FMR controls the mRNA levels of the DEG/ENAC channel *ppk1* (Xu et al., 2004). To examine whether Ago2 also regulates *ppk1*, we created an *ago2* deletion mutant using the P-element fly line EP(3)3417, which contains a P-element insertion in the first exon of *ago2*. By imprecise excision of the P-element, we generated a 628-bp deletion in the first and second exons of

34

*ago2* (*ago2⁵¹ᴮ*), which we identified by PCR analysis with primers flanking the deletion (Figure 2-1 A & B). The *ago2* locus produces two transcripts that differ in the first exon; the deletion in *ago2⁵¹ᴮ* eliminates the ATG-initiation codon in both transcripts. Therefore, *ago2⁵¹ᴮ* is a null mutant. Real-Time PCR confirmed that almost no *ago2* transcript is produced (Figure 2-1 C). *Ago2* mutant flies are viable and do not have gross morphological defects.

Ago2 is required for efficient RNAi in S2 cells. To confirm that Ago2 is also needed for RNAi in vivo, we expressed a *ppk1* dsRNA construct in MD neurons of *ago2* mutants. As expected, RNAi-induced inhibition of target-gene expression was significantly reduced in *ago2* mutants (Figure 2-1 D).

We then investigated whether Ago2 regulates *ppk1* mRNA. We measured the endogenous levels of *ppk1* mRNA and found that it is elevated in *ago2* mutants (Figure 2-2). This result suggests that *ago2* and *dfmr1* may function in the same genetic pathway to control the level of *ppk1* mRNA. To further test this hypothesis, we created heterozygous and homozygous *ago2* and *dfmr1* mutants. The level of *ppk1* mRNA in double-heterozygous *ago2⁵¹ᴮ/+*, *dfmr1⁴/+* mutant larvae is similar to wild-type or single-heterozygous larvae (data not shown). If two genes work in the same genetic pathway, reducing the dosage of *dfmr1* will not affect the phenotype of the homozygous null *ago2* mutant. Indeed, we found that the level of *ppk1* mRNA is increased by a similar amount in *ago2⁵¹ᴮ* homozygous null mutants as in *ago2⁵¹ᴮ, dfmr⁴* double mutants or *ago2⁵¹ᴮ/ ago2⁵¹ᴮ, dfmr⁴ /+* mutant larvae (Figure 2-2). Similarly, the level of *ppk1* mRNA is not affected by reducing the dosage of *ago2* in *dfmr⁴* homozygous null mutants. Furthermore, overexpression of *dfmr1* causes a significant decrease in *ppk1* mRNA

levels, which can be partially rescued by reducing the dosage of *Ago2* (Figure 2-2). Taken together, these data suggest that *dfmr* and *ago2* work in the same genetic pathway to regulate *ppk1* mRNA levels.

***ago2* does not regulate dendritic morphology of PNS neurons**

Given that mutations in *dfmr1* cause an increase in dendritic branches (Lee et al., 2003), I hypothesized that *ago2* also has a role dendritic development. To visualize dendritic processes, I used the MD subtype-specific *Gal4$^{221}$* to drive expression of UAS-mCD8::GFP, which targets to the cell membrane, in the simple class I neurons ddaE and vpda. Overexpression of Ago2 has no effect on the number of dendritic ends in the dorsal neuron ddaE nor in the ventral neuron vpda (Figure 2-3). Although the number of dendritic ends was not precisely quantitated, overexpressing UAS-Ago2 in the class IV ddaC neuron with highly complex dendrites using the MD-subtype-specific *Gal4$^{477}$* failed to produce an obvious effect on the number of dendritic ends (data not shown). However, a major issue is that overexpression of Ago2 may not be sufficiently high enough compared to levels of the endogenous protein to have an effect on dendritic branching. Thus, these results suggest that *ago2* has a minimal role or no role in regulating dendritic branching, but further experiments are required to confirm these findings.

***ago1* does not regulate dendritic morphology of PNS neurons**

I sought to determine whether the microRNA pathway is important in the development of dendrites in the PNS. Ago1, strongly expressed in the nervous system (Williams and Rubin, 2002), has an essential role in the biogenesis of miRNAs (Pillai et al., 2007). I examined the dendritic morphologies of *ago1* mutants to determine whether

*ago1* functions in dendrite development. The *ago1^{k08121}* allele creates an insertion near the start site of the two *ago1* isoforms, and was previously shown to be a strong allele (Kataoka et al., 2001). I used 'mosaic analysis with a repressible cell marker' (MARCM) technique (Lee and Luo, 1999), which generates a single GFP-labeled, mutant neuron in a wild-type background, to examine the role of *ago1* in dendritic branching in third-instar larvae. I found no difference in dendritic branching patterns of the dorsal class I neurons, ddaE and ddaF, in *ago1^{k08121}* mutant neurons (Figure 2-4). Although not precisely quantitated, I also failed to find a difference in dendritic branching of the dorsal class IV complex neurons ddaC. However, a major issue with MARCM is perdurance of the wild-type protein or mRNA. Additionally, more subtle effects in higher-order branches are possible. Therefore, these results suggest that *ago1* does not participate in regulation of dendritic arbors, but further investigation is needed.

**Figure 2-1**
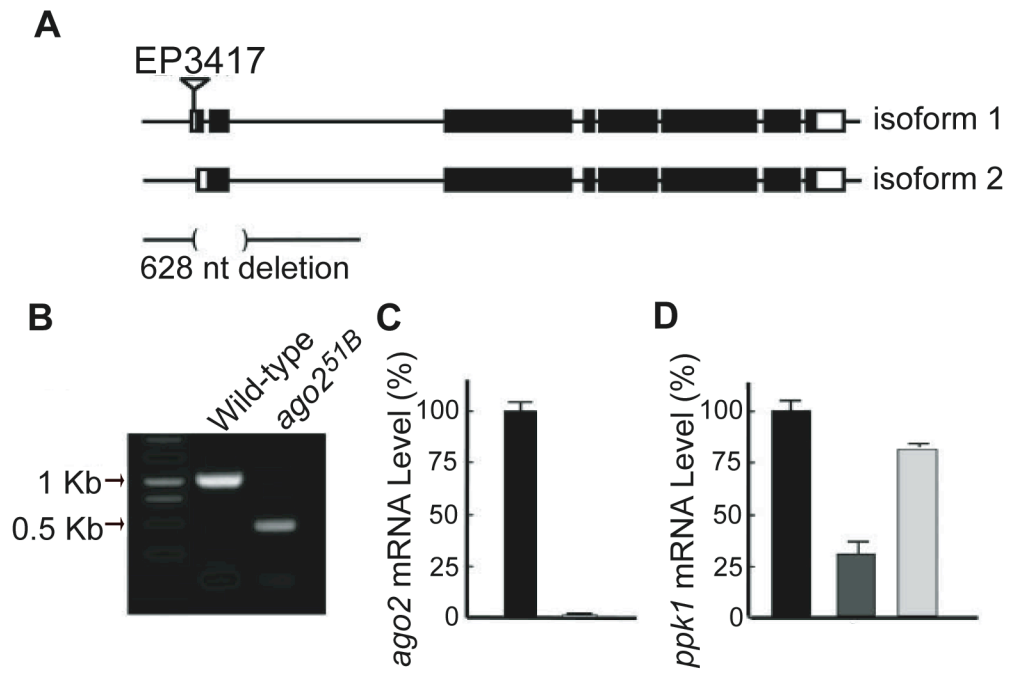
**Figure 2-1.  Generation of *ago2* mutant flies.**

(A) Genomic organization of the *ago2* locus.  The *ago2* gene produces two isoforms that share six common exons.  The boxes indicate the exons, and the black area indicates the coding region. The first six amino acids of isoform 1 are different from the first nine amino acids of isoform 2.  The P-element (*EP(3)3417*) is inserted in the first exon of isoform 1 and 65 nt away from the ATG start codon. The 628 nt deletion generated by imprecise excision covers the first and second exons of isoform 1 and first exon of isoform 2.

(B) PCR analysis of the deletion site in *ago2$^{51B}$*.  Two primers flanking the site of deletion were used for PCR analysis of genomic DNA isolated from either wild-type or *ago2$^{51B}$* mutant larvae.  The PCR products are 1.1 kb and 0.48 kb for wild-type and mutant larvae, respectively.

(C) Real-time PCR analysis of *ago2* mRNA level in control and *ago2$^{51B}$* mutant larvae. Control larvae were derived from precise excision of the P-element.

(D) Inhibition of *ppk1* gene expression by RNAi in vivo is greatly reduced in *ago2* mutants.
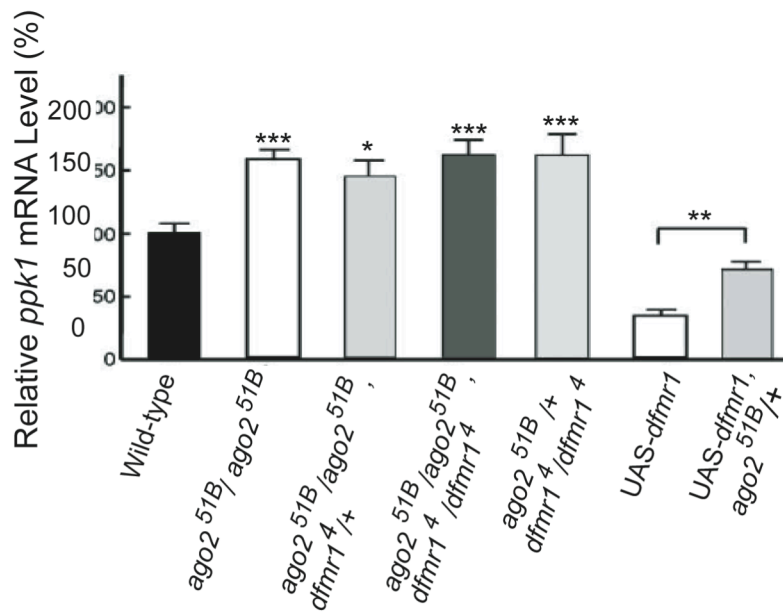
**Figure 2-2**

**Figure 2-2. Ago2 controls the level of *ppk1* mRNA in vivo.**

(A) Ago2 also controls the level of *ppk1* mRNA in vivo. The relative levels of *ppk1* mRNA in control larvae, *ago2$^{51B}$* homozygous mutants, and larvae with different genotypes were measured by real-time PCR. Flies generated from precise excision of *EP(3)3417* were used as controls. Real-time PCR analyses were performed multiple times. Compared to control larvae, the levels of *ppk1* mRNA are increased in *ago2$^{51B}$* homozygous larvae similar to *ago2$^{51B}$, dfmr1$^4$* double homozygous larvae, and *ago2$^{51B}$/+, dfmr1$^4$/dfmr1$^4$* larvae. For DFMR1 overexpression, the UAS-*dfmr1* transgene is located on the second chromosome. In each experiment, five larvae were used for RNA extraction.

*p<0.05, **p<0.01; ***p<0.001, by the Student's t test.

Figure 2-3

**A** Wild-type UAS-Ago2

**B** Number of dendritic ends — Wild-type, UAS-Ago2

**C** Wild-type UAS-Ago2

**D** Number of dendritic ends — Wild-type, UAS-Ago2
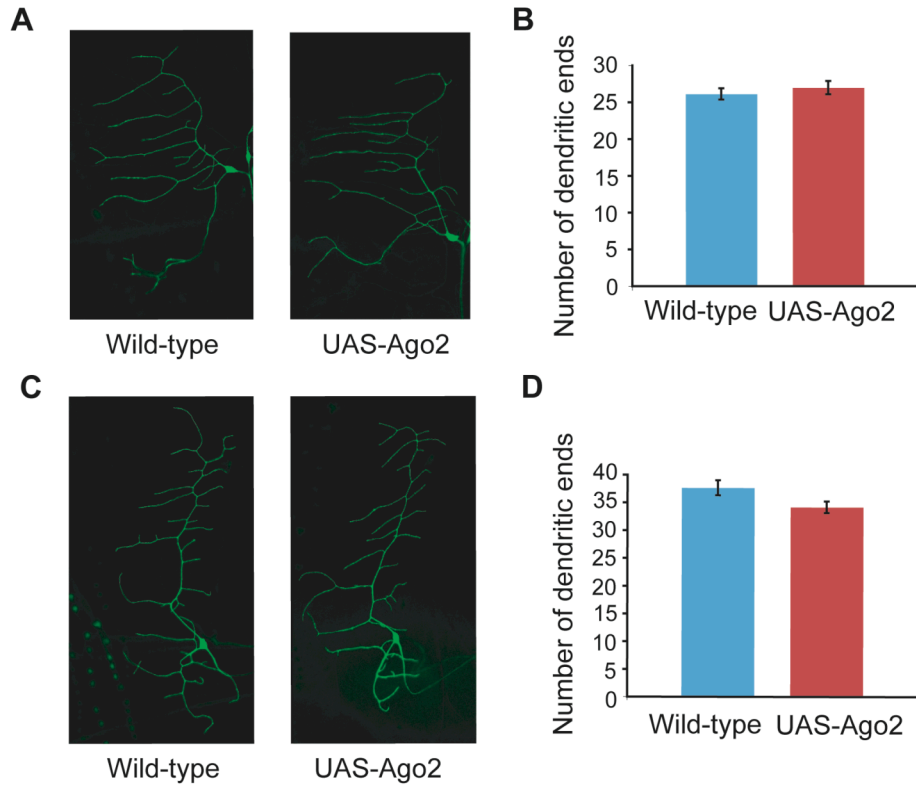
**Figure 2-3.  *ago2* does not have a role in dendrite morphogenesis.**

(A) Wild-type ddaE neurons and ddaE neurons overexpressing Ago2 have similar numbers of dendritic terminals.

(B) Quantitation of the number of dendritic ends in wild-type ddaE neurons (*n*=12) and in ddaE neurons overexpressing Ago2 (*n*=15) reveals that overexpression of Ago2 has no effect on the number of dendritic ends.

(C) Wild-type vpda neurons and vpda neurons overexpressing Ago2 have similar numbers of dendritic ends.

 (D) Quantitation of the number of dendritic ends in wild-type vpda neurons (*n*=12) and in vpda neurons overexpressing Ago2 (*n*=15) reveals that overexpression of Ago2 has no effect on the number of dendritic ends.

ddaE and vpda neurons were labeled by UAS-mCD8::GFP using *Gal4[221]* in third-instar larvae. No differences were statistically significant.

**Figure 2-4**

A



Wild-type      *ago1$^{k08121}$*

B



C



Wild-type      *ago1$^{k08121}$*

D
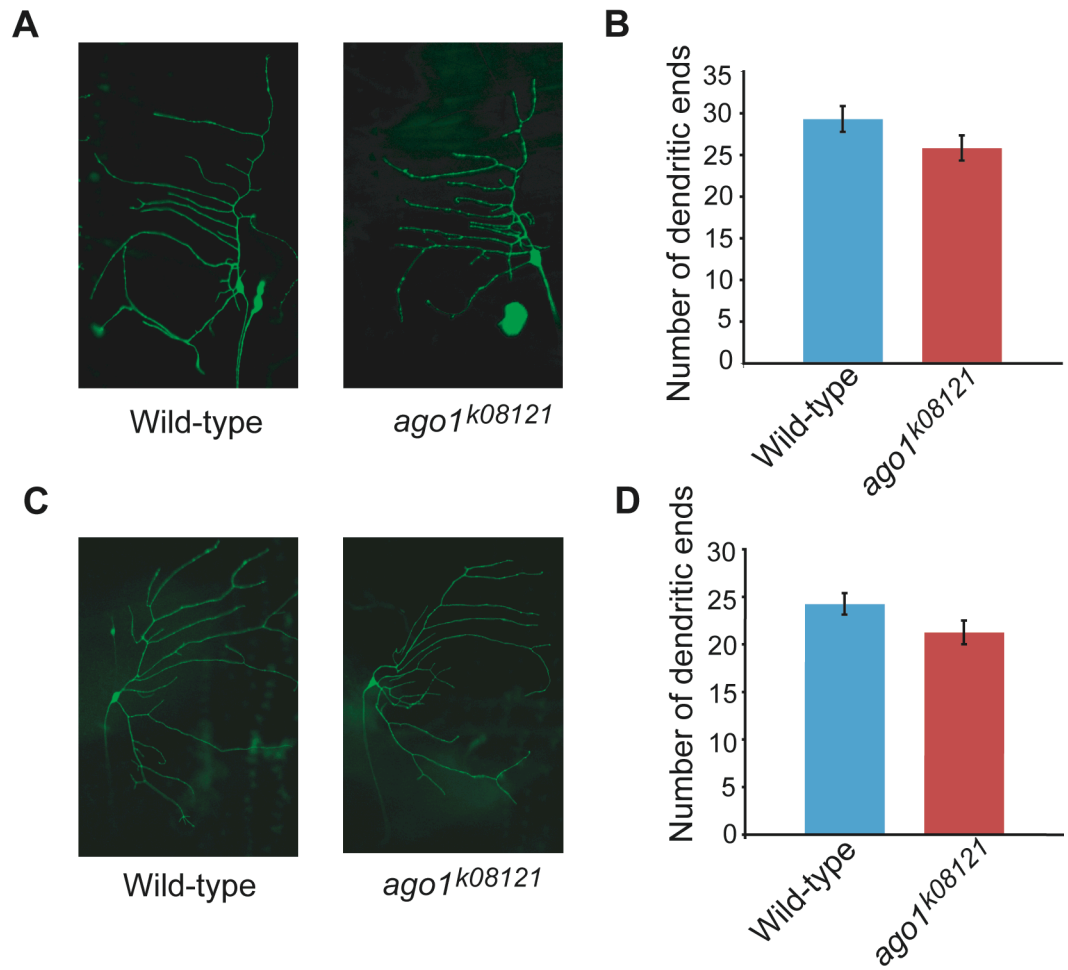
**Figure 2-4. *ago1* has little or no role in dendrite morphogenesis as revealed by MARCM.**

(A) *ago1 $^{k08121}$* mutant ddaE neurons have a similar number of dendritic terminals as wild-type ddaE neurons.

(B) Quantitation of the number of dendritic ends in ddaE neurons in *ago1 $^{k08121}$* mutants (*n*=10) and wild-type (*n*=11) third-instar larvae.

(C) *ago1 $^{k08121}$* mutant ddaF neurons have a similar number of dendritic terminals as wild-type ddaF neurons.

 (D) Quantitation of the number of dendritic ends of ddaF neurons in *ago1 $^{k08121}$* mutants (*n*=9) and wild-type (*n*=18)  third-instar larvae.

ddaE and ddaF neurons were labeled with UAS-mCD8::GFP using the MARCM technique, which labels single mutant neurons in a wild-type background. None of the decreases were statistically significant.

**Part Two: The role of *longitudinals lacking* in dendrite development**

A single gene may perform multiple functions within the developing nervous system. *Longitudinals lacking* (*lola*) achieves its functional diversity and specificity through the generation of at least 20 alternative splice isoforms (Horiuchi et al., 2003; Ohsako et al., 2003). A large, complex locus, *lola* extends over 60 kb and consists of 32 exons. *lola* harbors a BTB (Broad complex, Tramtrack, Bric à brac) or POZ (poxyvirus and Zn-finger) dimerization domain at the amino terminus and a pair of zinc fingers at the carboxy terminus (Goeke et al., 2003; Horiuchi et al., 2003; Ohsako et al., 2003). Although variable at both the 5' and 3' ends, the isoforms all share a common region that includes the BTB domain and append unique carboxy terminal exons via *trans*- and/or *cis*-pre-mRNA splicing. Seventeen of the 20 isoforms contain zinc-finger motifs (Goeke et al., 2003; Horiuchi et al., 2003; Ohsako et al., 2003). In addition, four different promoters contribute to variability in the N-terminus (Ohsako et al., 2003).

Mutations in *lola* are associated with CNS and PNS defects, and various isoforms of Lola are differentially expressed in the nervous system (Goeke et al., 2003). Lola promotes the longitudinal extension of CNS axons and inhibits midline crossing (Crowner et al., 2002; Giniger et al., 1994). Additionally, Lola is required for the orientation of lateral chordotonal neurons as well as pathfinding and target innervation by the axon of the peripheral $ISN_b$ (intersegmental nerve) motor neuron (Giniger et al., 1994; Goeke et al., 2003; Madden et al., 1999). A recent study found that Lola is essential for proper axon and dendrite connectivity and for specification of the neuronal identity of olfactory projection neurons (PN; Spletter et al., 2007). Most Lola isoforms are expressed in the PNs, and expression of specific isoforms in the PNs failed to rescue

the dendrite growth defects, suggesting that the diversity of *lola* isoforms is important (Spletter et al., 2007).   Lola may exert its effects by the regulation of guidance factors and interacts genetically with *slit* and *robo* (Crowner et al., 2002).  Furthermore, different *lola* isoforms have distinct functions: mutations in isoform K block targeting of $ISN_b$ motor neurons while mutations in L disrupt muscle innervation and CNS development (Goeke et al., 2003).

I was interested in the role of *lola* in dendritic morphogenesis of the DA neurons for two reasons.  First, Lola was found to interact with the BTB-POZ domain transcription factor Abrupt in a yeast-two-hybrid screen for targets that interact with Abrupt  (E. Giniger, personal communication).  Expressed solely in the class I PNS neurons, Abrupt, another BTB-POZ domain transcription factor, limits dendritic branching of class I neurons ddaE and ddaF (Li et al., 2004; Sugimura et al., 2004).  These findings raise the possibility that *lola* and *abrupt* may act in the same pathway to regulate dendrite morphology.  Second, as illustrated in the example above, different *lola* isoforms have unique roles in the nervous system.  Similarly, specific Lola isoforms may perform distinct functions in regulating dendritic elaboration in different DA neuron classes. Thus, to determine whether Lola regulates dendritic morphology, I examined the effect of *lola* null mutations on dendritic branching in *Drosophila* larval DA neurons.  I found that dendritic branching in *lola* mutants was greatly reduced in all types of neurons examined.  This result provides a foundation for further investigation of the function of *lola* in controlling dendrite morphology.

**Results**

**_lola_ is required for dendritic elaboration**

The diverse functions of Lola suggested that it may also regulate dendritic morphology in the DA neurons of the PNS. I examined the function of _lola_ mutations in regulating dendritic arbors using the MARCM technique. No phenotypic difference between the two different _lola_ null alleles, _lola_$^{ORE76}$ and _lola_$^{5D2}$, was observed; therefore, analyses from these two different mutants were combined. I found that _lola_ mutations reduced the number of dendritic ends of the simple class I neurons ddaE and ddaF (Figure 2-5 A-D). Because some genes only regulate the dendritic morphology of one neuronal class, I examined whether _lola_ also controls dendritic branching in the complex class IV neuron ddaC. _lola_ mutations decrease the dendritic branches in the complex neuron ddaC (Figure 2-5 E & F), but the basic neuronal structure remains intact. In addition, the dendritic morphology of a few neurons (not included in analysis) were so severely altered that the identity of the neurons was unrecognizable. Therefore, _lola_ is essential for establishing dendritic branching patterns.

**Figure 2-5**
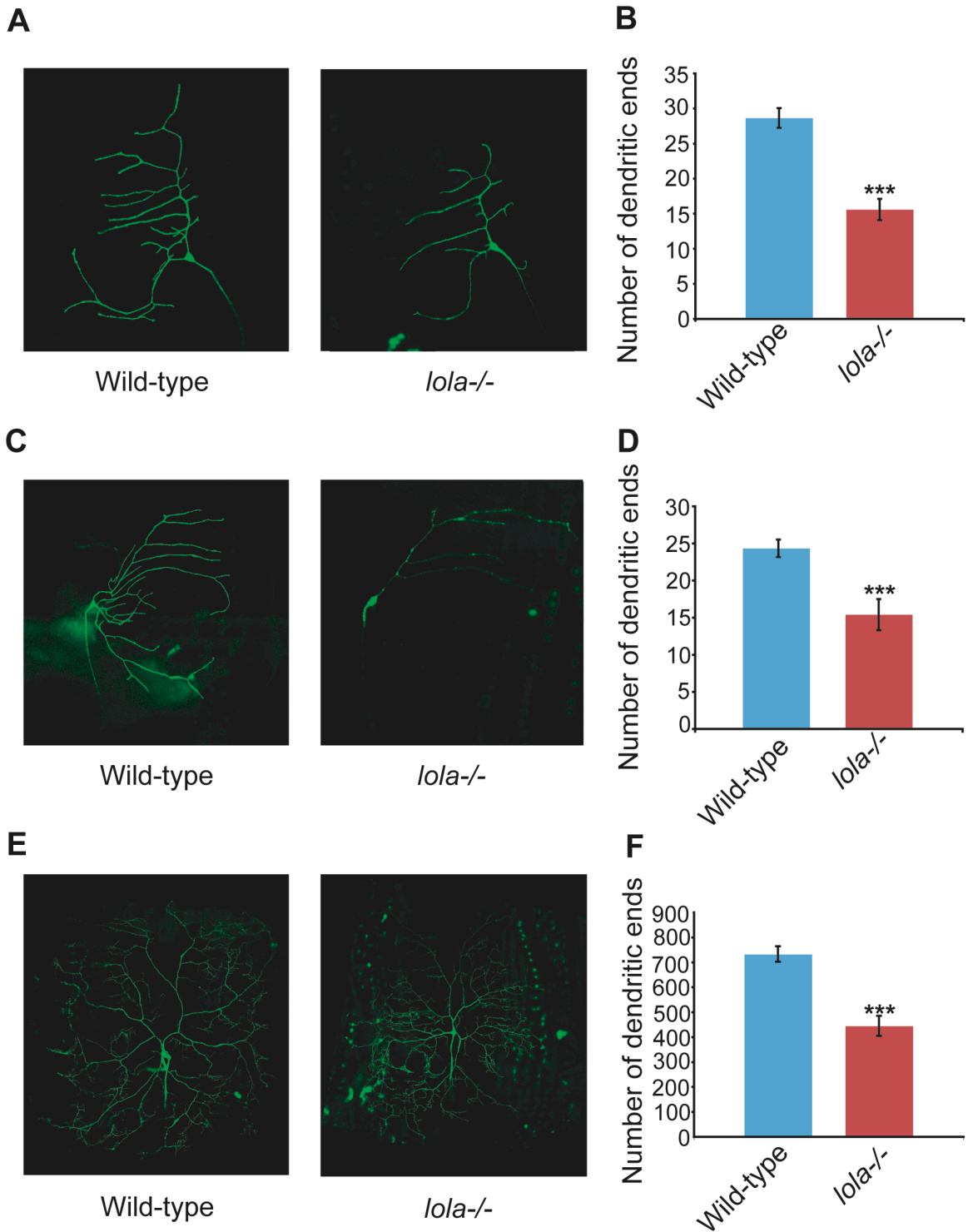
**Figure 2-5. Loss of function mutations in *lola* significantly decrease the number of dendritic terminal ends as revealed by MARCM.**

(A) *lola* mutant ddaE neurons exhibit a reduced number of dendritic terminals compared to wild-type ddaE neurons.

(B) Quantitation of the number of dendritic ends in ddaE neurons in *lola* mutants (*n*=10) and wild-type (*n*=13) third-instar larvae.

(C) The number of dendritic branches in *lola* mutant ddaF neurons is reduced compared to wild-type ddaF neurons.

(D) Quantitation of the number of dendritic ends in ddaF neurons in *lola* mutants (*n*=8) and wild-type (*n*=10) third-instar larvae.

(E) *lola* mutant ddaC neurons display a reduction in the number of dendritic terminals compared to wild-type ddaC neurons.

(F) Quantitation of the number of dendritic ends in ddaC neurons in *lola* mutants (*n*=13) and wild-type (*n*=10) third-instar larvae.

Images and data were obtained from two null alleles of *lola*, *lola$^{ORE76}$* and *lola$^{5D2}$*. The data from the two alleles was compiled since no difference in dendritic phenotype between the two alleles was observed.

Neurons were labeled with UAS-mCD8::GFP using the MARCM technique, which labels single mutant neurons in a wild-type background.

\*\*\* p<0.001

**Discussion**

Here I present an analysis of two different groups of genes in dendritic morphogenesis. The preliminary findings that overexpression of Ago2 and loss of function mutations in *ago1* have little to no effect on dendrite number in ddaE, ddaF, and vpda neurons suggests that these two genes do not have a role in dendrite morphology in post-mitotic neurons. However, two caveats with the techniques used in these experiments deserve consideration. First, Ago2 may not be expressed at high enough levels in comparison to the endogenous protein to affect dendritic elaboration. Quantitative Western analyses would reveal levels of Ago2 expression. Second, a potential limitation of MARCM is perdurance of the wild-type Ago1 protein or mRNA in the mutant neurons. In MARCM, heterozygous cells only become homozygous for a mutation following mitotic recombination; thus, MARCM would not reveal a role for Ago1 in dendritogenesis if it is required early in development or if its protein or mRNA are very stable.

Additionally, several other experiments are needed to further confirm the result that Ago2 and Ago1 are not required for dendritic morphogenesis. The dendritic ends of the spiny class III neurons and complex class IV in *ago1* and *ago2* mutant neurons should be carefully quantitated to ensure that they do not have subtle defects. Additionally, because *ago1$^{k08121}$/ ago1$^{k08121}$* homozygous mutants are embryonic lethal, the mutant is maintained as a heterozygote raising the possibility of perdurance of the maternally produced protein in embryos. Maternal contribution of *ago1* can be eliminated by a genetic technique that uses a dominant sterile female mutation, *ovo$^{D1}$*, to create mutant germ-line clones (Chou et al., 1993); dendritic morphology of *ago1* mutant neurons can

then be examined in embryos. Finally, examination of *ago1/ago1, ago2/ago2* double homozygous mutant neurons may reveal additional defects that are not apparent in single mutants. However, the possibility of functional redundancy is unlikely because biochemical analysis of the two proteins have revealed that Ago1 and Ago2 are functionally specialized in their silencing of target mRNAs (Forstemann et al., 2007). Taken together, these experiments will confirm whether *ago1* and *ago2* have a role in determining dendritic morphology.

Interestingly, *ago2* and *dfmr1* participate in the same genetic pathway to regulate the levels of *ppk1*, an MD-specific DEG/ENaC channel (Ainsley et al., 2003). How does *ago2* regulate *ppk1* mRNA, and does it regulate other mRNAs? One possibility is that *ago2* regulates *ppk1* levels via *dfmr1*. Alternatively, *ago2* may regulate *ppk1* mRNA via a miRNA with perfect complementarity to *ppk1*; if so, identification of the miRNA is of great interest. Furthermore, as *dfmr1* and *ago1* have recently been found to cooperate with each other in miRNA-mediated translational repression (Jin et al., 2004; Plante and Provost, 2006), *ago1* may also regulate *ppk1* mRNA levels together with *dfmr1* and *ago2*.

Similar to *dfmr1*, *ago2* may also control locomotion through the regulation of *ppk1*. Because overexpression of PPK1 has no effect on larval movement (Xu et al., 2004), loss of *ago2* function may have no effect. However, overexpressing Ago2 should reduce PPK1 levels, resulting in altered locomotion. Thus, further exploration of the *argonautes* in relationship to *ppk1* may uncover new functions for the *argonautes* in behavior.

In contrast to *ago1* and *ago2*, examination of the BTB transcription factor *lola* revealed that it does have a function in regulating dendritic branching. In addition to

dendritic outgrowth and elaboration, *lola* regulates axonal outgrowth.  As both axons and dendrites are shortened in *lola* mutants, a common process may underlie the function of *lola* in axon and dendritic outgrowth and guidance. In most cases, the basic dendrite structure is still intact in *lola* mutants, but the number of terminal ends is reduced.  The effect of *lola* in all of the DA neuronal classes deserves exploration as *lola* may have unique functions in neurons with distinct dendritic complexity.  Furthermore, careful quantification of the effects of *lola* mutations on higher-order dendrites versus primary branches that arise from the cell body may provide further insight into the *lola* phenotype.

Different *lola* isoforms have distinct functions in the developing nervous system. For example, distinct isoforms of *lola* have unique contributions to $ISN_b$ innervation of target muscles (Goeke et al., 2003).  Similarly, specific *lola* isoforms may participate in regulating dendritic elaboration in different MD neurons. *In situ* hybridization using isoform-specific probes may reveal whether different *lola* isoforms are expressed in specific MD neurons.  If this is the case, then MARCM analysis using isoform-specific mutations may reveal unique functions for individual isoforms.

*lola* may also interact with other genes that regulate dendritic morphology.  The BTB-POZ domain transcription factor Abrupt is required to limit the dendritic branching of the simple class I neurons (Li et al., 2004; Sugimura et al., 2004).  A yeast-two-hybrid screen for targets that interact with Abrupt revealed that Abrupt interacts with Lola (E. Giniger, personal communication).  Such an interaction is not surprising because both Abrupt and Lola contain BTB-POZ domains, which participate in protein-protein interactions (Bardwell and Treisman, 1994); other BTB-POZ domain proteins interact

with each other via their BTB-POZ domains (Collins et al., 2001). These findings raise the possibility that *lola* and *abrupt* may act in the same pathway to regulate dendrite morphology. Several experiments may provide insight into this hypothesis. Immunoprecipitation experiments would determine whether Abrupt and Lola interact in vivo. Additionally, genetic experiments would reveal whether they participate in the same genetic pathway to regulate dendritic morphology. If *lola* and *abrupt* work in the same genetic pathway, then one might expect that *lola/lola, abrupt/abrupt* double mutant neurons may either exhibit increased dendritic branching similar to *abrupt* single mutants or decreased dendritic branching comparable to *lola* single mutants. Furthermore, as transcription factors, *lola* and *abrupt* may regulate each other to affect arborization. Immunohistochemistry in DA neurons, real-time PCR, or Western analyses may shed light on this question. Such an interaction between *lola* and *abrupt* would unveil components of a transcriptional program that regulates dendritic morphogenesis of the DA neurons.

In conclusion, I have presented preliminary analyses of the role of two different groups of genes in DA dendritic patterning and RNA regulation. Although I failed to find a role for *ago1* and *ago2* in dendritic morphogenesis, *ago2* does regulate *ppk1*, which has been implicated in larval locomotion, thus suggesting that *ago2* may also have a function in movement. Additionally, the promising finding that *lola* mutant neurons have reduced dendritic trees opens the door for many interesting studies about its function in dendritogenesis. Thus, these studies take a step forward in our understanding of the development and function of the DA sensory neurons in *Drosophila*.

## Materials and Methods

**Fly lines**

Flies were maintained at 25°C and fed standard fly-food. The following stocks were used in this study: (1) EP(3)3417 (Szeged Stock Center, Hungary) used to generate an null mutant, $ago2^{51B}$; (2) $y^1w^{67c23}$; P[lacW]AGO1$^{k08121}$/Cyo (Bloomington Stock Center), referred to as $ago1^{k08121}$, is a strong null allele (Williams and Rubin, 2002); (3) $lola^{ORE76}$ contains early stop codon in the BTB domain and is predicted to be null for all *lola* isoforms (kindly provided by Edward Giniger); (4) $lola^{5D2}$ contains a transposon insertion and is a null for all isoforms (kindly provided by Edward Giniger); (5) $Gal4^{C155}$, *UAS-mCD8::GFP*, *hs-FLP1* which expresses GFP at a high level in all neurons but is also detectable in epithelial cells in larvae; (6) *tubP-Gal80, FRT$^{G13}$/Cyo*; (7) $GAL4^{221}$, UAS-*mCD8::GFP/Cyo* which labels ddaE, ddaF, and vpda neurons in each segment; (8) UAS-*ppk1-RNAi/Gal4 109(2)80*, which is expressed in all MD neurons and less than one hundred central neurons (Gao et al., 1999).

**Generation of *Ago2* deletion mutant**

The P-element line EP(3)3417 was crossed to flies containing the transposase Δ2-3 to isolate 200 lines of flies in which the P-element had hopped out. The deletion mutations were screened by polymerase chain reaction (PCR) with primers specific to the flanking region of the P element. A single mutant, $ago2^{51B}$, was identified with a 628 bp deletion that included the first exon and part of the second exon.

**RNA Interference**

A 350-bp DNA fragment corresponding to part of the *ppk1* cDNA coding sequence was amplified using primers containing restriction sites and cloned in the pUAST vector

between EcoRI and XbaI sites. The same fragment in reverse orientation was cloned into the same vector between XbaI and XhoI sites. The RNAi construct was used to make transgenic flies.

**RNAi Isolation and Quantitative Real-Time PCR**

Total RNAs were extracted with Trizol, treated with DNase to eliminate genomic DNA, and purified with the RNeasy Mini Kit (Qiagen). Total RNA ($1\mu g$) was used for the reverse transcriptase reaction (Taqman Kit, Applied Biosystems). For each reaction, 0.5% of cDNAs were used for analysis by quantitative Real-Time PCR. PPK1 PCR products were detected with SYBR Green using the ABI PRISM 7700 Sequence Detection System. Data were analyzed with Sequence Detector software (v1.7a). $\alpha$-tubulin-specific primers were used as internal control for the quantification of gene expression. Multiple independent real-time PCR analyses were carried out to reliably detect the low abundance of *ppk1* mRNA.

**Imaging and quantitation of dorsal cluster DA neuron dendrites**

*GAL4$^{221}$*, UAS-*mCD8::GFP/Cyo* was used to image dorsal ddaE and ddaF neurons and ventral vpda neurons. Wild-type and mutant embryos were collected on grape agar plates and grown for three-four days at 25°C to the third-instar larval stage. The dendrites of GFP-labeled dorsal and ventral DA neurons was imaged by Nikon D-Eclipse C1 confocal microscope and the number of dendritic ends was counted.

**MARCM**

MARCM was carried out as described (Li and Gao, 2003). *ago1$^{k08121}$* mutations were recombined onto the same chromosome containing *FRT$^{G13}$*. *ago1$^{k08121}$*, *FRT$^{G13}$/CyO* male flies were crossed with *Gal4$^{C155}$*, *UAS-mCD8::GFP*, *hs-FLP1/FM7* virgin flies.

Then, $Gal4^{C155}$, $UAS$-$mCD8$::$GFP$, $hs$-$FLP1$; $ago1^{k08121}$, $FRT^{G13}$/+ male flies were crossed with $Gal4^{C155}$, $UAS$-$mCD8$::$GFP$, $hs$-$FLP1$;$tubP$-$Gal80$, $FRT^{G13}$/$Cyo$ virgin flies. Embryos were collected on grape agar plates for 3 hours and allowed to grow for another 3 hours at 25°. Embryos were then heat-shocked in a 37° water bath for 40 minutes to induce mitotic recombination. Three or four days after egg-laying, third-instar larvae were collected, and those containing single GFP-labeled dorsal cluster PNS neurons were selected for imaging. A Nikon D-Eclipse C1 confocal microscope was used to capture images of single neurons. To quantify the number of dendritic ends, the total numbers of dendritic ends of different DA neurons were counted.

*lola* mutations were also recombined onto chromosome containing $FRT^{G13}$. MARCM was carried out as described above. Because no clear difference between the null alleles of *lola* were observed, these data together were compiled together.

# References

Ainsley, J.A., J.M. Pettus, D. Bosenko, C.E. Gerstein, N. Zinkevich, M.G. Anderson, C.M. Adams, M.J. Welsh, and W.A. Johnson. 2003. Enhanced locomotion caused by loss of the Drosophila DEG/ENaC protein Pickpocket1. *Curr Biol*. 13:1557-63.

Almeida, R., and R.C. Allshire. 2005. RNA silencing and genome regulation. *Trends Cell Biol*. 15:251-8.

Andersen, R., Y. Li, M. Resseguie, and J.E. Brenman. 2005. Calcium/calmodulin-dependent protein kinase II alters structural plasticity and cytoskeletal dynamics in Drosophila. *J Neurosci*. 25:8878-88.

Anderson, M.G., G.L. Perkins, P. Chittick, R.J. Shrigley, and W.A. Johnson. 1995. drifter, a Drosophila POU-domain transcription factor, is required for correct differentiation and migration of tracheal cells and midline glia. *Genes Dev*. 9:123-37.

Andino, R. 2003. RNAi puts a lid on virus replication. *Nat Biotechnol*. 21:629-30.

Antonellis, A., R.E. Ellsworth, N. Sambuughin, I. Puls, A. Abel, S.Q. Lee-Lin, A. Jordanova, I. Kremensky, K. Christodoulou, L.T. Middleton, K. Sivakumar, V. Ionasescu, B. Funalot, J.M. Vance, L.G. Goldfarb, K.H. Fischbeck, and E.D. Green. 2003. Glycyl tRNA synthetase mutations in Charcot-Marie-Tooth disease type 2D and distal spinal muscular atrophy type V. *Am J Hum Genet*. 72:1293-9.

Aravin, A.A., M. Lagos-Quintana, A. Yalcin, M. Zavolan, D. Marks, B. Snyder, T. Gaasterland, J. Meyer, and T. Tuschl. 2003. The small RNA profile during Drosophila melanogaster development. *Dev Cell*. 5:337-50.

Araya, E., C. Berthier, E. Kim, T. Yeung, X. Wang, and D.M. Helfman. 2002. Regulation of coiled-coil assembly in tropomyosins. *J Struct Biol*. 137:176-83.

Ashley, C.T., Jr., K.D. Wilkinson, D. Reines, and S.T. Warren. 1993. FMR1 protein: conserved RNP family domains and selective RNA binding. *Science*. 262:563-6.

Bardwell, V.J., and R. Treisman. 1994. The POZ domain: a conserved protein-protein interaction motif. *Genes Dev*. 8:1664-77.

Bashaw, G.J., T. Kidd, D. Murray, T. Pawson, and C.S. Goodman. 2000. Repulsive axon guidance: Abelson and Enabled play opposing roles downstream of the roundabout receptor. *Cell*. 101:703-15.

Bieber, A.J., P.M. Snow, M. Hortsch, N.H. Patel, J.R. Jacobs, Z.R. Traquina, J. Schilling, and C.S. Goodman. 1989. Drosophila neuroglian: a member of the immunoglobulin superfamily with extensive homology to the vertebrate neural adhesion molecule L1. *Cell*. 59:447-60.

Blochlinger, K., L.Y. Jan, and Y.N. Jan. 1991. Transformation of sensory organ identity by ectopic expression of Cut in Drosophila. *Genes Dev*. 5:1124-35.

Bodmer, R., and Jan, Y.N. 1987. Morphological differentiation of the embryonic peripheral neurons in Drosophila. *Roux's Archives of Developmental Biology*. 196:69-77.

Bodmer, R., R. Carretto, and Y.N. Jan. 1989. Neurogenesis of the peripheral nervous system in Drosophila embryos: DNA replication patterns and cell lineages. *Neuron*. 3:21-32.

Bohnsack, M.T., K. Czaplinski, and D. Gorlich. 2004. Exportin 5 is a RanGTP-dependent dsRNA-binding protein that mediates nuclear export of pre-miRNAs. *Rna*. 10:185-91.

Brand, A.H., and N. Perrimon. 1993. Targeted gene expression as a means of altering cell fates and generating dominant phenotypes. *Development*. 118:401-15.

Brenman, J.E., F.B. Gao, L.Y. Jan, and Y.N. Jan. 2001. Sequoia, a tramtrack-related zinc finger protein, functions as a pan-neural regulator for dendrite and axon morphogenesis in Drosophila. *Dev Cell*. 1:667-77.

Caudy, A.A., M. Myers, G.J. Hannon, and S.M. Hammond. 2002. Fragile X-related protein and VIG associate with the RNA interference machinery. *Genes Dev*. 16:2491-6.

Chae, J., M.J. Kim, J.H. Goo, S. Collier, D. Gubb, J. Charlton, P.N. Adler, and W.J. Park. 1999. The Drosophila tissue polarity gene starry night encodes a member of the protocadherin family. *Development*. 126:5421-9.

Chen, Y., and A. Ghosh. 2005. Regulation of dendritic development by neuronal activity. *J Neurobiol*. 64:4-10.

Chihara, T., D. Luginbuhl, and L. Luo. 2007. Cytoplasmic and mitochondrial protein translation in axonal and dendritic terminal arborization. *Nat Neurosci*. 10:828-37.

Chou, T.B., E. Noll, and N. Perrimon. 1993. Autosomal P[ovoD1] dominant female-sterile insertions in Drosophila and their use in generating germ-line chimeras. *Development*. 119:1359-69.

Chu-Lagraff, Q., D.M. Wright, L.K. McNeil, and C.Q. Doe. 1991. The prospero gene encodes a divergent homeodomain protein that controls neuronal identity in Drosophila. *Development*. Suppl 2:79-85.

Chung, Y.D., J. Zhu, Y. Han, and M.J. Kernan. 2001. nompA encodes a PNS-specific, ZP domain protein required to connect mechanosensory dendrites to sensory structures. *Neuron*. 29:415-28.

Clark, I.E., L.Y. Jan, and Y.N. Jan. 1997. Reciprocal localization of Nod and kinesin fusion proteins indicates microtubule polarity in the Drosophila oocyte, epithelium, neuron and muscle. *Development*. 124:461-70.

Cline, H.T. 2001. Dendritic arbor development and synaptogenesis. *Curr Opin Neurobiol*. 11:118-26.

Clyne, P.J., S.J. Certel, M. de Bruyne, L. Zaslavsky, W.A. Johnson, and J.R. Carlson. 1999. The odor specificities of a subset of olfactory receptor neurons are governed by Acj6, a POU-domain transcription factor. *Neuron*. 22:339-47.

Collins, T., J.R. Stone, and A.J. Williams. 2001. All in the family: the BTB/POZ, KRAB, and SCAN domains. *Mol Cell Biol*. 21:3609-15.

Comery, T.A., J.B. Harris, P.J. Willems, B.A. Oostra, S.A. Irwin, I.J. Weiler, and W.T. Greenough. 1997. Abnormal dendritic spines in fragile X knockout mice: maturation and pruning deficits. *Proc Natl Acad Sci U S A*. 94:5401-4.

Cong, J., W. Geng, B. He, J. Liu, J. Charlton, and P.N. Adler. 2001. The furry gene of Drosophila is important for maintaining the integrity of cellular extensions during morphogenesis. *Development*. 128:2793-802.

Crowner, D., K. Madden, S. Goeke, and E. Giniger. 2002. Lola regulates midline crossing of CNS axons in Drosophila. *Development*. 129:1317-25.

Denli, A.M., B.B. Tops, R.H. Plasterk, R.F. Ketting, and G.J. Hannon. 2004. Processing of primary microRNAs by the Microprocessor complex. *Nature*. 432:231-5.

Dockendorff, T.C., H.S. Su, S.M. McBride, Z. Yang, C.H. Choi, K.K. Siwicki, A. Sehgal, and T.A. Jongens. 2002. Drosophila lacking dfmr1 activity show defects in circadian output and fail to maintain courtship interest. *Neuron*. 34:973-84.

Dostie, J., Z. Mourelatos, M. Yang, A. Sharma, and G. Dreyfuss. 2003. Numerous microRNPs in neuronal cells containing novel microRNAs. *Rna*. 9:180-6.

Dubruille, R., A. Laurencon, C. Vandaele, E. Shishido, M. Coulon-Bublex, P. Swoboda, P. Couble, M. Kernan, and B. Durand. 2002. Drosophila regulatory factor X is necessary for ciliated sensory neuron differentiation. *Development*. 129:5487-98.

Duncan, D.M., E.A. Burgess, and I. Duncan. 1998. Control of distal antennal identity and tarsal development in Drosophila by spineless-aristapedia, a homolog of the mammalian dioxin receptor. *Genes Dev*. 12:1290-303.

Elia, L.P., M. Yamamoto, K. Zang, and L.F. Reichardt. 2006. p120 catenin regulates dendritic spine and synapse development through Rho-family GTPases and cadherins. *Neuron*. 51:43-56.

Emoto, K., Y. He, B. Ye, W.B. Grueber, P.N. Adler, L.Y. Jan, and Y.N. Jan. 2004. Control of dendritic branching and tiling by the Tricornered-kinase/Furry signaling pathway in Drosophila sensory neurons. *Cell*. 119:245-56.

Emoto, K., J.Z. Parrish, L.Y. Jan, and Y.N. Jan. 2006. The tumour suppressor Hippo acts with the NDR kinases in dendritic tiling and maintenance. *Nature*. 443:210-3.

Forstemann, K., M.D. Horwich, L. Wee, Y. Tomari, and P.D. Zamore. 2007. Drosophila microRNAs are sorted into functionally distinct argonaute complexes after production by dicer-1. *Cell*. 130:287-97.

Furrer, M.P., S. Kim, B. Wolf, and A. Chiba. 2003. Robo and Frazzled/DCC mediate dendritic guidance at the CNS midline. *Nat Neurosci*. 6:223-30.

Furrer, M.P., I. Vasenkova, D. Kamiyama, Y. Rosado, and A. Chiba. 2007. Slit and Robo control the development of dendrites in Drosophila CNS. *Development*. 134:3795-804.

Gajiwala, K.S., H. Chen, F. Cornille, B.P. Roques, W. Reith, B. Mach, and S.K. Burley. 2000. Structure of the winged-helix protein hRFX1 reveals a new mode of DNA binding. *Nature*. 403:916-21.

Galvez, R., A.R. Gopal, and W.T. Greenough. 2003. Somatosensory cortical barrel dendritic abnormalities in a mouse model of the fragile X mental retardation syndrome. *Brain Res*. 971:83-9.

Galvez, R., and W.T. Greenough. 2005. Sequence of abnormal dendritic spine development in primary somatosensory cortex of a mouse model of the fragile X mental retardation syndrome. *Am J Med Genet A*. 135:155-60.

Gao, F.B. 2007. Molecular and cellular mechanisms of dendritic morphogenesis. *Curr Opin Neurobiol*.

Gao, F.B., J.E. Brenman, L.Y. Jan, and Y.N. Jan. 1999. Genes regulating dendritic outgrowth, branching, and routing in Drosophila. *Genes Dev*. 13:2549-61.

Gao, F.B., M. Kohwi, J.E. Brenman, L.Y. Jan, and Y.N. Jan. 2000a. Control of dendritic field formation in Drosophila: the roles of flamingo and competition between homologous neurons. *Neuron*. 28:91-101.

Gao, Q., B. Yuan, and A. Chess. 2000b. Convergent projections of Drosophila olfactory neurons to specific glomeruli in the antennal lobe. *Nat Neurosci*. 3:780-5.

Gertler, F.B., A.R. Comer, J.L. Juang, S.M. Ahern, M.J. Clark, E.C. Liebl, and F.M. Hoffmann. 1995. enabled, a dosage-sensitive suppressor of mutations in the Drosophila Abl tyrosine kinase, encodes an Abl substrate with SH3 domain-binding properties. *Genes Dev*. 9:521-33.

Giniger, E., K. Tietje, L.Y. Jan, and Y.N. Jan. 1994. lola encodes a putative transcription factor required for axon growth and guidance in Drosophila. *Development*. 120:1385-98.

Godenschwege, T.A., J.H. Simpson, X. Shan, G.J. Bashaw, C.S. Goodman, and R.K. Murphey. 2002. Ectopic expression in the giant fiber system of Drosophila reveals distinct roles for roundabout (Robo), Robo2, and Robo3 in dendritic guidance and synaptic connectivity. *J Neurosci*. 22:3117-29.

Goeke, S., E.A. Greene, P.K. Grant, M.A. Gates, D. Crowner, T. Aigaki, and E. Giniger. 2003. Alternative splicing of lola generates 19 transcription factors controlling axon guidance in Drosophila. *Nat Neurosci*. 6:917-24.

Goldberg, J.L. 2004. Intrinsic neuronal regulation of axon and dendrite growth. *Curr Opin Neurobiol*. 14:551-7.

Gregory, S.L., and N.H. Brown. 1998. kakapo, a gene required for adhesion between and within cell layers in Drosophila, encodes a large cytoskeletal linker protein related to plectin and dystrophin. *J Cell Biol*. 143:1271-82.

Grueber, W.B., L.Y. Jan, and Y.N. Jan. 2002. Tiling of the Drosophila epidermis by multidendritic sensory neurons. *Development*. 129:2867-78.

Grueber, W.B., L.Y. Jan, and Y.N. Jan. 2003a. Different levels of the homeodomain protein cut regulate distinct dendrite branching patterns of Drosophila multidendritic neurons. *Cell*. 112:805-18.

Grueber, W.B., and Y.N. Jan. 2004. Dendritic development: lessons from Drosophila and related branches. *Curr Opin Neurobiol*. 14:74-82.

Grueber, W.B., B. Ye, A.W. Moore, L.Y. Jan, and Y.N. Jan. 2003b. Dendrites of distinct classes of Drosophila sensory neurons show different capacities for homotypic repulsion. *Curr Biol*. 13:618-26.

Hall, A. 1998. G proteins and small GTPases: distant relatives keep in touch. *Science*. 280:2074-5.

Hammond, S.M., E. Bernstein, D. Beach, and G.J. Hannon. 2000. An RNA-directed nuclease mediates post-transcriptional gene silencing in Drosophila cells. *Nature*. 404:293-6.

Harvey, K.F., C.M. Pfleger, and I.K. Hariharan. 2003. The Drosophila Mst ortholog, hippo, restricts growth and cell proliferation and promotes apoptosis. *Cell*. 114:457-67.

Hausser, M., N. Spruston, and G.J. Stuart. 2000. Diversity and dynamics of dendritic signaling. *Science*. 290:739-44.

Hinton, V.J., W.T. Brown, K. Wisniewski, and R.D. Rudelli. 1991. Analysis of neocortex in three males with the fragile X syndrome. *Am J Med Genet*. 41:289-94.

Horiuchi, T., E. Giniger, and T. Aigaki. 2003. Alternative trans-splicing of constant and variable exons of a Drosophila axon guidance gene, lola. *Genes Dev*. 17:2496-501.

Hosoya, T., K. Takizawa, K. Nitta, and Y. Hotta. 1995. glial cells missing: a binary switch between neuronal and glial determination in Drosophila. *Cell*. 82:1025-36.

Hu, S., D. Fambrough, J.R. Atashi, C.S. Goodman, and S.T. Crews. 1995. The Drosophila abrupt gene encodes a BTB-zinc finger regulatory protein that controls the specificity of neuromuscular connections. *Genes Dev*. 9:2936-48.

Hughes, M.E., R. Bortnick, A. Tsubouchi, P. Baumer, M. Kondo, T. Uemura, and D. Schmucker. 2007. Homophilic Dscam interactions control complex dendrite morphogenesis. *Neuron*. 54:417-27.

Hummel, T., K. Krukkert, J. Roos, G. Davis, and C. Klambt. 2000. Drosophila Futsch/22C10 is a MAP1B-like protein required for dendritic and axonal development. *Neuron*. 26:357-70.

Hummel, T., M.L. Vasconcelos, J.C. Clemens, Y. Fishilevich, L.B. Vosshall, and S.L. Zipursky. 2003. Axonal targeting of olfactory receptor neurons in Drosophila is controlled by Dscam. *Neuron*. 37:221-31.

Inoue, S., M. Shimoda, I. Nishinokubi, M.C. Siomi, M. Okamura, A. Nakamura, S. Kobayashi, N. Ishida, and H. Siomi. 2002. A role for the Drosophila fragile X-related gene in circadian output. *Curr Biol*. 12:1331-5.

Irwin, S.A., B. Patel, M. Idupulapati, J.B. Harris, R.A. Crisostomo, B.P. Larsen, F. Kooy, P.J. Willems, P. Cras, P.B. Kozlowski, R.A. Swain, I.J. Weiler, and W.T. Greenough. 2001. Abnormal dendritic spine characteristics in the temporal and visual cortices of patients with fragile-X syndrome: a quantitative examination. *Am J Med Genet*. 98:161-7.

Ishizuka, A., M.C. Siomi, and H. Siomi. 2002. A Drosophila fragile X protein interacts with components of RNAi and ribosomal proteins. *Genes Dev*. 16:2497-508.

Jaubert, S., A. Mereau, C. Antoniewski, and D. Tagu. 2007. MicroRNAs in Drosophila: The magic wand to enter the Chamber of Secrets? *Biochimie*. 89:1211-20.

Jefferis, G.S., E.C. Marin, R.F. Stocker, and L. Luo. 2001. Target neuron prespecification in the olfactory map of Drosophila. *Nature*. 414:204-8.

Jefferis, G.S., R.M. Vyas, D. Berdnik, A. Ramaekers, R.F. Stocker, N.K. Tanaka, K. Ito, and L. Luo. 2004. Developmental origin of wiring specificity in the olfactory system of Drosophila. *Development*. 131:117-30.

Jin, P., D.C. Zarnescu, S. Ceman, M. Nakamoto, J. Mowrey, T.A. Jongens, D.L. Nelson, K. Moses, and S.T. Warren. 2004. Biochemical and genetic interaction between the fragile X mental retardation protein and the microRNA pathway. *Nat Neurosci*. 7:113-7.

Joiner Ml, A., and L.C. Griffith. 1997. CaM kinase II and visual input modulate memory formation in the neuronal circuit controlling courtship conditioning. *J Neurosci*. 17:9384-91.

Jones, B.W., R.D. Fetter, G. Tear, and C.S. Goodman. 1995. glial cells missing: a genetic switch that controls glial versus neuronal fate. *Cell*. 82:1013-23.

Jones, C.A., J. Ng, A.J. Peterson, K. Morgan, J. Simon, and R.S. Jones. 1998. The Drosophila esc and E(z) proteins are direct partners in polycomb group-mediated repression. *Mol Cell Biol*. 18:2825-34.

Justice, R.W., O. Zilian, D.F. Woods, M. Noll, and P.J. Bryant. 1995. The Drosophila tumor suppressor gene warts encodes a homolog of human myotonic dystrophy

kinase and is required for the control of cell shape and proliferation. *Genes Dev*. 9:534-46.

Kapsimali, M., W.P. Kloosterman, E. de Bruijn, F. Rosa, R.H. Plasterk, and S.W. Wilson. 2007. MicroRNAs show a wide diversity of expression profiles in the developing and mature central nervous system. *Genome Biol*. 8:R173.

Kataoka, Y., M. Takeichi, and T. Uemura. 2001. Developmental roles and molecular characterization of a Drosophila homologue of Arabidopsis Argonaute1, the founder of a novel gene superfamily. *Genes Cells*. 6:313-25.

Kidd, T., K. Brose, K.J. Mitchell, R.D. Fetter, M. Tessier-Lavigne, C.S. Goodman, and G. Tear. 1998. Roundabout controls axon crossing of the CNS midline and defines a novel subfamily of evolutionarily conserved guidance receptors. *Cell*. 92:205-15.

Kim, M.D., L.Y. Jan, and Y.N. Jan. 2006. The bHLH-PAS protein Spineless is necessary for the diversification of dendrite morphology of Drosophila dendritic arborization neurons. *Genes Dev*. 20:2806-19.

Kim, S., and A. Chiba. 2004. Dendritic guidance. *Trends Neurosci*. 27:194-202.

Kimura, H., T. Usui, A. Tsubouchi, and T. Uemura. 2006. Potential dual molecular interaction of the Drosophila 7-pass transmembrane cadherin Flamingo in dendritic morphogenesis. *J Cell Sci*. 119:1118-29.

Kolodziej, P.A., L.Y. Jan, and Y.N. Jan. 1995. Mutations that affect the length, fasciculation, or ventral orientation of specific sensory axons in the Drosophila embryo. *Neuron*. 15:273-86.

Kolodziej, P.A., L.C. Timpe, K.J. Mitchell, S.R. Fried, C.S. Goodman, L.Y. Jan, and Y.N. Jan. 1996. frazzled encodes a Drosophila member of the DCC immunoglobulin subfamily and is required for CNS and motor axon guidance. *Cell*. 87:197-204.

Komiyama, T., W.A. Johnson, L. Luo, and G.S. Jefferis. 2003. From lineage to wiring specificity. POU domain transcription factors control precise connections of Drosophila olfactory projection neurons. *Cell*. 112:157-67.

Komiyama, T., and L. Luo. 2007. Intrinsic control of precise dendritic targeting by an ensemble of transcription factors. *Curr Biol*. 17:278-85.

Komiyama, T., L.B. Sweeney, O. Schuldiner, K.C. Garcia, and L. Luo. 2007. Graded expression of semaphorin-1a cell-autonomously directs dendritic targeting of olfactory projection neurons. *Cell*. 128:399-410.

Kosik, K.S. 2006. The neuronal microRNA system. *Nat Rev Neurosci*. 7:911-20.

Kramer, A.P., and G.S. Stent. 1985. Developmental arborization of sensory neurons in the leech Haementeria ghilianii. II. Experimentally induced variations in the branching pattern. *J Neurosci*. 5:768-75.

Kuo, C.T., S. Zhu, S. Younger, L.Y. Jan, and Y.N. Jan. 2006. Identification of E2/E3 ubiquitinating enzymes and caspase activity regulating Drosophila sensory neuron dendrite pruning. *Neuron*. 51:283-90.

Laggerbauer, B., D. Ostareck, E.M. Keidel, A. Ostareck-Lederer, and U. Fischer. 2001. Evidence that fragile X mental retardation protein is a negative regulator of translation. *Hum Mol Genet*. 10:329-38.

Lagos-Quintana, M., R. Rauhut, W. Lendeckel, and T. Tuschl. 2001. Identification of novel genes coding for small expressed RNAs. *Science*. 294:853-8.

Lagos-Quintana, M., R. Rauhut, J. Meyer, A. Borkhardt, and T. Tuschl. 2003. New microRNAs from mouse and human. *Rna*. 9:175-9.

Lagos-Quintana, M., R. Rauhut, A. Yalcin, J. Meyer, W. Lendeckel, and T. Tuschl. 2002. Identification of tissue-specific microRNAs from mouse. *Curr Biol*. 12:735-9.

Lee, A., W. Li, K. Xu, B.A. Bogert, K. Su, and F.B. Gao. 2003. Control of dendritic development by the Drosophila fragile X-related gene involves the small GTPase Rac1. *Development*. 130:5543-52.

Lee, S., K.L. Harris, P.M. Whitington, and P.A. Kolodziej. 2000. short stop is allelic to kakapo, and encodes rod-like cytoskeletal-associated proteins required for axon extension. *J Neurosci*. 20:1096-108.

Lee, S., and P.A. Kolodziej. 2002. Short Stop provides an essential link between F-actin and microtubules during axon extension. *Development*. 129:1195-204.

Lee, T., A. Lee, and L. Luo. 1999. Development of the Drosophila mushroom bodies: sequential generation of three distinct types of neurons from a neuroblast. *Development*. 126:4065-76.

Lee, T., and L. Luo. 1999. Mosaic analysis with a repressible cell marker for studies of gene function in neuronal morphogenesis. *Neuron*. 22:451-61.

Lee, Y.S., K. Nakahara, J.W. Pham, K. Kim, Z. He, E.J. Sontheimer, and R.W. Carthew. 2004. Distinct roles for Drosophila Dicer-1 and Dicer-2 in the siRNA/miRNA silencing pathways. *Cell*. 117:69-81.

Li, W., and F.B. Gao. 2003. Actin filament-stabilizing protein tropomyosin regulates the size of dendritic fields. *J Neurosci*. 23:6171-5.

Li, W., Y. Li, and F.B. Gao. 2005. Abelson, enabled, and p120 catenin exert distinct effects on dendritic morphogenesis in Drosophila. *Dev Dyn*. 234:512-22.

Li, W., F. Wang, L. Menut, and F.B. Gao. 2004. BTB/POZ-zinc finger protein abrupt suppresses dendritic branching in a neuronal subtype-specific and dosage-dependent manner. *Neuron*. 43:823-34.

Li, Y., F. Wang, J.A. Lee, and F.B. Gao. 2006. MicroRNA-9a ensures the precise specification of sensory organ precursors in Drosophila. *Genes Dev*. 20:2793-805.

Li, Z., Y. Zhang, L. Ku, K.D. Wilkinson, S.T. Warren, and Y. Feng. 2001. The fragile X mental retardation protein inhibits translation via interacting with mRNA. *Nucleic Acids Res*. 29:2276-83.

Lim, L.P., M.E. Glasner, S. Yekta, C.B. Burge, and D.P. Bartel. 2003a. Vertebrate microRNA genes. *Science*. 299:1540.

Lim, L.P., N.C. Lau, E.G. Weinstein, A. Abdelhakim, S. Yekta, M.W. Rhoades, C.B. Burge, and D.P. Bartel. 2003b. The microRNAs of Caenorhabditis elegans. *Genes Dev*. 17:991-1008.

Liu, Z., R. Steward, and L. Luo. 2000. Drosophila Lis1 is required for neuroblast proliferation, dendritic elaboration and axonal transport. *Nat Cell Biol*. 2:776-83.

Lohmann, C., and R.O. Wong. 2001. Cell-type specific dendritic contacts between retinal ganglion cells during development. *J Neurobiol*. 48:150-62.

Lohmann, C., and R.O. Wong. 2005. Regulation of dendritic growth and plasticity by local and global calcium dynamics. *Cell Calcium*. 37:403-9.

Lu, B., T. Usui, T. Uemura, L. Jan, and Y.N. Jan. 1999. Flamingo controls the planar polarity of sensory bristles and asymmetric division of sensory organ precursors in Drosophila. *Curr Biol*. 9:1247-50.

Luo, L., Y.J. Liao, L.Y. Jan, and Y.N. Jan. 1994. Distinct morphogenetic functions of similar small GTPases: Drosophila Drac1 is involved in axonal outgrowth and myoblast fusion. *Genes Dev*. 8:1787-802.

Macdonald, P.M. 1992. The Drosophila pumilio gene: an unusually long transcription unit and an unusual protein. *Development*. 114:221-32.

Madden, K., D. Crowner, and E. Giniger. 1999. LOLA has the properties of a master regulator of axon-target interaction for SNb motor axons of Drosophila. *Dev Biol*. 213:301-13.

Marin, E.C., G.S. Jefferis, T. Komiyama, H. Zhu, and L. Luo. 2002. Representation of the glomerular olfactory map in the Drosophila brain. *Cell*. 109:243-55.

Martinez, J., A. Patkaniowska, H. Urlaub, R. Luhrmann, and T. Tuschl. 2002. Single-stranded antisense siRNAs guide target RNA cleavage in RNAi. *Cell*. 110:563-74.

Masland, R.H. 2001. Neuronal diversity in the retina. *Curr Opin Neurobiol*. 11:431-6.

Matthews, B.J., M.E. Kim, J.J. Flanagan, D. Hattori, J.C. Clemens, S.L. Zipursky, and W.B. Grueber. 2007. Dendrite self-avoidance is controlled by Dscam. *Cell*. 129:593-604.

Mazroui, R., M.E. Huot, S. Tremblay, C. Filion, Y. Labelle, and E.W. Khandjian. 2002. Trapping of messenger RNA by Fragile X Mental Retardation protein into cytoplasmic granules induces translation repression. *Hum Mol Genet*. 11:3007-17.

McAllister, A.K. 2000. Cellular and molecular mechanisms of dendrite growth. *Cereb Cortex*. 10:963-73.

McBride, S.M., C.H. Choi, Y. Wang, D. Liebelt, E. Braunstein, D. Ferreiro, A. Sehgal, K.K. Siwicki, T.C. Dockendorff, H.T. Nguyen, T.V. McDonald, and T.A. Jongens. 2005. Pharmacological rescue of synaptic plasticity, courtship behavior, and mushroom body defects in a Drosophila model of fragile X syndrome. *Neuron*. 45:753-64.

Medina, P.M., L.L. Swick, R. Andersen, Z. Blalock, and J.E. Brenman. 2006. A novel forward genetic screen for identifying mutations affecting larval neuronal dendrite development in Drosophila melanogaster. *Genetics*. 172:2325-35.

Moore, A.W., L.Y. Jan, and Y.N. Jan. 2002. hamlet, a binary genetic switch between single- and multiple- dendrite neuron morphology. *Science*. 297:1355-8.

Morales, J., P.R. Hiesinger, A.J. Schroeder, K. Kume, P. Verstreken, F.R. Jackson, D.L. Nelson, and B.A. Hassan. 2002. Drosophila fragile X protein, DFXR, regulates neuronal morphology and function in the brain. *Neuron*. 34:961-72.

Mourelatos, Z., J. Dostie, S. Paushkin, A. Sharma, B. Charroux, L. Abel, J. Rappsilber, M. Mann, and G. Dreyfuss. 2002. miRNPs: a novel class of ribonucleoproteins containing numerous microRNAs. *Genes Dev*. 16:720-8.

Muller, J., C.M. Hart, N.J. Francis, M.L. Vargas, A. Sengupta, B. Wild, E.L. Miller, M.B. O'Connor, R.E. Kingston, and J.A. Simon. 2002. Histone methyltransferase activity of a Drosophila Polycomb group repressor complex. *Cell*. 111:197-208.

Neer, E.J., C.J. Schmidt, R. Nambudripad, and T.F. Smith. 1994. The ancient regulatory-protein family of WD-repeat proteins. *Nature*. 371:297-300.

Nimchinsky, E.A., A.M. Oberlander, and K. Svoboda. 2001. Abnormal development of dendritic spines in FMR1 knock-out mice. *J Neurosci*. 21:5139-46.

Ohsako, T., T. Horiuchi, T. Matsuo, S. Komaya, and T. Aigaki. 2003. Drosophila lola encodes a family of BTB-transcription regulators with highly variable C-terminal domains containing zinc finger motifs. *Gene*. 311:59-69.

Okamura, K., A. Ishizuka, H. Siomi, and M.C. Siomi. 2004. Distinct roles for Argonaute proteins in small RNA-directed RNA cleavage pathways. *Genes Dev*. 18:1655-66.

Orgogozo, V., F. Schweisguth, and Y. Bellaiche. 2001. Lineage, cell polarity and inscuteable function in the peripheral nervous system of the Drosophila embryo. *Development*. 128:631-43.

Pan, L., Y.Q. Zhang, E. Woodruff, and K. Broadie. 2004. The Drosophila fragile X gene negatively regulates neuronal elaboration and synaptic differentiation. *Curr Biol*. 14:1863-70.

Parrish, J.Z., K. Emoto, L.Y. Jan, and Y.N. Jan. 2007a. Polycomb genes interact with the tumor suppressor genes hippo and warts in the maintenance of Drosophila sensory neuron dendrites. *Genes Dev*. 21:956-72.

Parrish, J.Z., K. Emoto, M.D. Kim, and Y.N. Jan. 2007b. Mechanisms that regulate establishment, maintenance, and remodeling of dendritic fields. *Annu Rev Neurosci*. 30:399-423.

Parrish, J.Z., M.D. Kim, L.Y. Jan, and Y.N. Jan. 2006. Genome-wide analyses identify transcription factors required for proper morphogenesis of Drosophila sensory neuron dendrites. *Genes Dev*. 20:820-35.

Penagarikano, O., J.G. Mulle, and S.T. Warren. 2007. The pathophysiology of fragile x syndrome. *Annu Rev Genomics Hum Genet*. 8:109-29.

Perry, V.H., and R. Linden. 1982. Evidence for dendritic competition in the developing retina. *Nature*. 297:683-5.

Pillai, R.S., S.N. Bhattacharyya, and W. Filipowicz. 2007. Repression of protein synthesis by miRNAs: how many mechanisms? *Trends Cell Biol*. 17:118-26.

Plante, I., and P. Provost. 2006. Hypothesis: A Role for Fragile X Mental Retardation Protein in Mediating and Relieving MicroRNA-Guided Translational Repression? *J Biomed Biotechnol*. 2006:16806.

Prokop, A., J. Uhler, J. Roote, and M. Bate. 1998. The kakapo mutation affects terminal arborization and central dendritic sprouting of Drosophila motorneurons. *J Cell Biol*. 143:1283-94.

Ramón y Cajal, S. 1911. Histology of the Nervous System of Man and Vertebrates. Oxford University Press.

Reeve, S.P., L. Bassetto, G.K. Genova, Y. Kleyner, M. Leyssen, F.R. Jackson, and B.A. Hassan. 2005. The Drosophila fragile X mental retardation protein controls actin dynamics by directly regulating profilin in the brain. *Curr Biol*. 15:1156-63.

Reuter, J.E., T.M. Nardine, A. Penton, P. Billuart, E.K. Scott, T. Usui, T. Uemura, and L. Luo. 2003. A mosaic genetic screen for genes necessary for Drosophila mushroom body neuronal morphogenesis. *Development*. 130:1203-13.

Roos, J., T. Hummel, N. Ng, C. Klambt, and G.W. Davis. 2000. Drosophila Futsch regulates synaptic microtubule organization and is necessary for synaptic growth. *Neuron*. 26:371-82.

Roper, K., and N.H. Brown. 2003. Maintaining epithelial integrity: a function for gigantic spectraplakin isoforms in adherens junctions. *J Cell Biol*. 162:1305-15.

Rudelli, R.D., W.T. Brown, K. Wisniewski, E.C. Jenkins, M. Laure-Kamionowska, F. Connell, and H.M. Wisniewski. 1985. Adult fragile X syndrome. Clinico-neuropathologic findings. *Acta Neuropathol (Berl)*. 67:289-95.

Schaeffer, C., M. Beaulande, C. Ehresmann, B. Ehresmann, and H. Moine. 2003. The RNA binding protein FMRP: new connections and missing links. *Biol Cell*. 95:221-8.

Scott, E.K., and L. Luo. 2001. How do dendrites take their shape? *Nat Neurosci*. 4:359-65.

Shankland, M., and C.S. Goodman. 1982. Development of the dendritic branching pattern of the medial giant interneuron in the grasshopper embryo. *Dev Biol*. 92:489-506.

Shima, Y., M. Kengaku, T. Hirano, M. Takeichi, and T. Uemura. 2004. Regulation of dendritic maintenance and growth by a mammalian 7-pass transmembrane cadherin. *Dev Cell*. 7:205-16.

Sijen, T., and R.H. Plasterk. 2003. Transposon silencing in the Caenorhabditis elegans germ line by natural RNAi. *Nature*. 426:310-4.

Single, S., and A. Borst. 1998. Dendritic integration and its role in computing image velocity. *Science*. 281:1848-50.

Siomi, H., M.C. Siomi, R.L. Nussbaum, and G. Dreyfuss. 1993. The protein product of the fragile X gene, FMR1, has characteristics of an RNA-binding protein. *Cell*. 74:291-8.

Soba, P., S. Zhu, K. Emoto, S. Younger, S.J. Yang, H.H. Yu, T. Lee, L.Y. Jan, and Y.N. Jan. 2007. Drosophila sensory neurons require Dscam for dendritic self-avoidance and proper dendritic field organization. *Neuron*. 54:403-16.

Spletter, M.L., J. Liu, J. Liu, H. Su, E. Giniger, T. Komiyama, S. Quake, and L. Luo. 2007. Lola regulates Drosophila olfactory projection neuron identity and targeting specificity. *Neural Develop*. 2:14.

Strausfeld, N.J., and J.A. Campos-Ortega. 1973. The L4 monopolar neurone: a substrate for lateral interaction in the visual system of the fly Musca domestica (L.). *Brain Res*. 59:97-117.

Strumpf, D., and T. Volk. 1998. Kakapo, a novel cytoskeletal-associated protein is essential for the restricted localization of the neuregulin-like factor, vein, at the muscle-tendon junction site. *J Cell Biol*. 143:1259-70.

Subramanian, A., A. Prokop, M. Yamamoto, K. Sugimura, T. Uemura, J. Betschinger, J.A. Knoblich, and T. Volk. 2003. Shortstop recruits EB1/APC1 and promotes microtubule assembly at the muscle-tendon junction. *Curr Biol*. 13:1086-95.

Sugimura, K., D. Satoh, P. Estes, S. Crews, and T. Uemura. 2004. Development of morphological diversity of dendrites in Drosophila by the BTB-zinc finger protein abrupt. *Neuron*. 43:809-22.

Sun, B., P. Xu, and P.M. Salvaterra. 1999. Dynamic visualization of nervous system in live Drosophila. *Proc Natl Acad Sci U S A*. 96:10438-43.

Sweeney, N.T., J.E. Brenman, Y.N. Jan, and F.B. Gao. 2006. The coiled-coil protein shrub controls neuronal morphogenesis in Drosophila. *Curr Biol*. 16:1006-11.

Sweeney, N.T., W. Li, and F.B. Gao. 2002. Genetic manipulation of single neurons in vivo reveals specific roles of flamingo in neuronal morphogenesis. *Dev Biol*. 247:76-88.

Tabara, H., M. Sarkissian, W.G. Kelly, J. Fleenor, A. Grishok, L. Timmons, A. Fire, and C.C. Mello. 1999. The rde-1 gene, RNA interference, and transposon silencing in C. elegans. *Cell*. 99:123-32.

Tada, T., and M. Sheng. 2006. Molecular mechanisms of dendritic spine morphogenesis. *Curr Opin Neurobiol*. 16:95-101.

Takeichi, M. 2007. The cadherin superfamily in neuronal connections and interactions. *Nat Rev Neurosci*. 8:11-20.

Tamaskovic, R., S.J. Bichsel, H. Rogniaux, M.R. Stegert, and B.A. Hemmings. 2003. Mechanism of Ca2+-mediated regulation of NDR protein kinase through autophosphorylation and phosphorylation by an upstream kinase. *J Biol Chem*. 278:6710-8.

Teleman, A.A., S. Maitra, and S.M. Cohen. 2006. Drosophila lacking microRNA miR-278 are defective in energy homeostasis. *Genes Dev*. 20:417-22.

Tracey, W.D., Jr., R.I. Wilson, G. Laurent, and S. Benzer. 2003. painless, a Drosophila gene essential for nociception. *Cell*. 113:261-73.

Usui, T., Y. Shima, Y. Shimada, S. Hirano, R.W. Burgess, T.L. Schwarz, M. Takeichi, and T. Uemura. 1999. Flamingo, a seven-pass transmembrane cadherin, regulates planar cell polarity under the control of Frizzled. *Cell*. 98:585-95.

Vactor, D.V., H. Sink, D. Fambrough, R. Tsoo, and C.S. Goodman. 1993. Genes that control neuromuscular specificity in Drosophila. *Cell*. 73:1137-53.

Vaessin, H., E. Grell, E. Wolff, E. Bier, L.Y. Jan, and Y.N. Jan. 1991. prospero is expressed in neuronal precursors and encodes a nuclear protein that is involved in the control of axonal outgrowth in Drosophila. *Cell*. 67:941-53.

Van Aelst, L., and H.T. Cline. 2004. Rho GTPases and activity-dependent dendrite development. *Curr Opin Neurobiol*. 14:297-304.

van Rij, R.P., M.C. Saleh, B. Berry, C. Foo, A. Houk, C. Antoniewski, and R. Andino. 2006. The RNA silencing endonuclease Argonaute 2 mediates specific antiviral immunity in Drosophila melanogaster. *Genes Dev*. 20:2985-95.

Vandaele, C., M. Coulon-Bublex, P. Couble, and B. Durand. 2001. Drosophila regulatory factor X is an embryonic type I sensory neuron marker also expressed in spermatids and in the brain of Drosophila. *Mech Dev*. 103:159-62.

Vervoort, M., D.J. Merritt, A. Ghysen, and C. Dambly-Chaudiere. 1997. Genetic basis of the formation and identity of type I and type II neurons in Drosophila embryos. *Development*. 124:2819-28.

Vosshall, L.B. 2000. Olfaction in Drosophila. *Curr Opin Neurobiol*. 10:498-503.

Wang, C., and R. Lehmann. 1991. Nanos is the localized posterior determinant in Drosophila. *Cell*. 66:637-47.

Wassle, H., L. Peichl, and B.B. Boycott. 1981. Dendritic territories of cat retinal ganglion cells. *Nature*. 292:344-5.

Whitford, K.L., V. Marillat, E. Stein, C.S. Goodman, M. Tessier-Lavigne, A. Chedotal, and A. Ghosh. 2002. Regulation of cortical dendrite development by Slit-Robo interactions. *Neuron*. 33:47-61.

Williams, D.W., S. Kondo, A. Krzyzanowska, Y. Hiromi, and J.W. Truman. 2006. Local caspase activity directs engulfment of dendrites during pruning. *Nat Neurosci*. 9:1234-6.

Williams, R.W., and G.M. Rubin. 2002. ARGONAUTE1 is required for efficient RNA interference in Drosophila embryos. *Proc Natl Acad Sci U S A*. 99:6889-94.

Wills, Z., L. Marr, K. Zinn, C.S. Goodman, and D. Van Vactor. 1999. Profilin and the Abl tyrosine kinase are required for motor axon outgrowth in the Drosophila embryo. *Neuron*. 22:291-9.

Wisniewski, K.E., S.M. Segan, C.M. Miezejeski, E.A. Sersen, and R.D. Rudelli. 1991. The Fra(X) syndrome: neurological, electrophysiological, and neuropathological abnormalities. *Am J Med Genet*. 38:476-80.

Wojtowicz, W.M., J.J. Flanagan, S.S. Millard, S.L. Zipursky, and J.C. Clemens. 2004. Alternative splicing of Drosophila Dscam generates axon guidance receptors that exhibit isoform-specific homophilic binding. *Cell*. 118:619-33.

Wong, A.M., J.W. Wang, and R. Axel. 2002. Spatial representation of the glomerular map in the Drosophila protocerebrum. *Cell*. 109:229-41.

Wong, R.O., and A. Ghosh. 2002. Activity-dependent regulation of dendritic growth and patterning. *Nat Rev Neurosci*. 3:803-12.

Xiao, K., R.G. Oas, C.M. Chiasson, and A.P. Kowalczyk. 2007. Role of p120-catenin in cadherin trafficking. *Biochim Biophys Acta*. 1773:8-16.

Xu, K., B.A. Bogert, W. Li, K. Su, A. Lee, and F.B. Gao. 2004. The fragile X-related gene affects the crawling behavior of Drosophila larvae by regulating the mRNA level of the DEG/ENaC protein pickpocket1. *Curr Biol*. 14:1025-34.

Yamamoto, M., R. Ueda, K. Takahashi, K. Saigo, and T. Uemura. 2006. Control of axonal sprouting and dendrite branching by the Nrg-Ank complex at the neuron-glia interface. *Curr Biol*. 16:1678-83.

Yazdani, U., and J.R. Terman. 2006. The semaphorins. *Genome Biol*. 7:211.

Ye, B., C. Petritsch, I.E. Clark, E.R. Gavis, L.Y. Jan, and Y.N. Jan. 2004. Nanos and Pumilio are essential for dendrite morphogenesis in Drosophila peripheral neurons. *Curr Biol*. 14:314-21.

Ye, B., Y. Zhang, W. Song, S.H. Younger, L.Y. Jan, and Y.N. Jan. 2007. Growing dendrites and axons differ in their reliance on the secretory pathway. *Cell*. 130:717-29.

Zhang, Y.Q., A.M. Bailey, H.J. Matthies, R.B. Renden, M.A. Smith, S.D. Speese, G.M. Rubin, and K. Broadie. 2001. Drosophila fragile X-related gene regulates the MAP1B homolog Futsch to control synaptic structure and function. *Cell*. 107:591-603.

Zhao, Y., and D. Srivastava. 2007. A developmental view of microRNA function. *Trends Biochem Sci*. 32:189-97.

Zhu, H., T. Hummel, J.C. Clemens, D. Berdnik, S.L. Zipursky, and L. Luo. 2006. Dendritic patterning by Dscam and synaptic partner matching in the Drosophila antennal lobe. *Nat Neurosci*. 9:349-55.

Zhu, H., and L. Luo. 2004. Diverse functions of N-cadherin in dendritic and axonal terminal arborization of olfactory projection neurons. *Neuron*. 42:63-75.

Zinn, K. 2007. Dscam and neuronal uniqueness. *Cell*. 129:455-6.

# Chapter Three


## Ciliated neurons in *Caenorhabditis elegans*

Cilia—thin , microtubule-based structures that protrude from cells—are present on most eukaryotic cells and in most tissues of vertebrates. Biologists have long recognized the importance of motile cilia in propelling movement, but primary cilia were largely thought to be vestigial (Davenport and Yoder, 2005). Only recently has the field started to understand and appreciate the complexity of these multi-functional organelles. This burgeoning field has been stimulated by the discoveries that several human diseases are due to dysfunction in cilia. Many of the significant advances in the cilia field have been made in non-vertebrate model organisms. Here, I present a review of the current understanding of cilia structure and function, with a focus on *Caenorhabditis elegans.*

**The ciliated neurons of *C. elegans***

*C. elegans* consists of 959 somatic cells, of which 302 are neurons. Sixty of these neurons have primary, nonmotile cilia and comprise the only ciliated cells in the worm (Figure 3-1A & B). The major function of these ciliated neurons is sensory; *C. elegans* do not have motile cilia.

The ciliated neurons of *C. elegans* fall into several classes. The amphid sensilla in the head contain 12 bilateral pairs of neurons whose ciliated dendrites are encased in support cells, the sheath and socket cells (Figure 3-1C; Perkins et al., 1986; Ward et al., 1975; Ware, 1975). The cilia of eight pairs of neurons (ADF, ADL, ASE, ASG, ASH, ASI, ASJ, and ASK) extend through a channel formed by the sheath and socket cells that terminates in a pore that has contact with the external environment. Three other neurons (AWA, AWB, and AWC), called winged cells because of the shape of their cilia (Figure 3-1 C), individually extend into the lumen of the sheath cell. The twelfth neuron pair, AFD or the finger cell, has a rudimentary cilium that expands into approximately 50

microvilli within the sheath cell (Perkins et al., 1986; Ward et al., 1975; Ware, 1975). The phasmids in the tail (PHA and PHB) are also encased in a sheath and socket cell and have contact with the external environment (Figure 3-1C; Hall and Russell, 1991; Perkins et al., 1986).

In addition to the amphids, the head has several other types of ciliated neurons. Four classes of cuticular sensilla also reside in the head and have sheath and socket cells that encase the cilia. The six pairs of inner labials neurons (IL1 and IL2) are found on the inner lips of the mouth, and two pairs of cephalic neurons (CEP), two pairs of outer labial quadrant neurons (OLQ) and one pair of outer labial lateral neurons (OLL) reside in the outer lips of the head (Figure 3-1C). The IL1, OLL, and OLQ cilia are embedded in the subcuticle while the IL2 cilia have access to the external environment through pores in the cuticle (Figure 3-1C; Perkins et al., 1986; Ward et al., 1975; Ware, 1975).

The ciliated neurons include several other classes of neurons. The deirids, or cervical sensory organs, contain two pairs of lateral neurons, ADE and PDE neurons with cilia structure that is very similar to the CEP cilia (Figure 3-1C). Together with the CEP neurons, the ADE and PDE neurons comprise the only dopaminergic neurons of the worm (Sulston et al., 1975; Ward et al., 1975; Ware, 1975). The cilia of the ADE and PDE neurons reside in a channel comprising a sheath and socket cell and terminate in the subcuticle (Ward et al., 1975; Ware, 1975). The BAG and FLP ciliated neurons have cilia that terminate in bag and flap-shaped sheets, respectively, in the outer, lateral lips of the mouth of the worm (Perkins et al., 1986). Finally, AQR and PQR, have cell bodies that reside near the pharynx and posterior to the phasmids, respectively; these ciliated neurons

are unique in that their cilia come into contact with the pseudocoelomic fluid (White, 1986).

Males have 52 additional ciliated neurons. These neurons are also mostly sensory, and the majority of them reside in the tail ray/hooks (Peden and Barr, 2005; Sulston et al., 1980).

**Architecture of cilia**

Of all the ciliated sensory neurons (CSN) in *C. elegans,* the structures of amphid cilia have been best characterized.  The other ciliated neurons contain the same structures but often reduced in size (Perkins et al., 1986).   Cilia nucleate from the basal body, a modified pair of centrioles.  In *C. elegans*, the basal body was renamed "transition zone" because it is degenerate compared to the basal bodies of other organisms (Perkins et al., 1986).  The transition zone, or proximal segment, consists of nine doublet-microtubules that contact the membrane through Y-shaped links (Figure 3-1D), in contrast to the nine triplet-microtubules in the basal body of other organisms (Inglis, 2006; Perkins et al., 1986).  In some neurons the transition zone is even more degenerate, reduced to 5-7 doublet microtubules in IL cilia, or 6-8 doublet microtubules in CEP neurons.  Arising from the transition zone, the middle segment consists of nine doublet microtubules, the A and B subfibers, and inner singlet microtubules (Figure 3-1D). The distal segment contains the A subfiber of the doublet microtubules and the inner singlet microtubules (Figure 3-1D).  The typical length of an amphid channel cilia is 7.5 μm, while the length of AFD cilia is 2μm (Perkins et al., 1986).

**Constructing the cilium**

*Regulation of the development of the cilium*

The RFX transcription factor *daf-19* regulates the expression of many ciliogenic genes to control the development of cilia. DAF-19 binds an X-box motif that is present in the promoters of many cilia genes, such as the IFT complexes, to control their expression. Accordingly, *daf-19* mutants fail to form cilia at all (Swoboda et al., 2000). Thus far, three splice isoforms of *daf-19* have been identified, only one of which is expressed solely in ciliated neurons (Gahmon, 2006).

*Constructing the cilium by Intraflagellar Transport*

Kozminski et al. (1993) first discovered particles moving bidirectionally along the flagellar axoneme of *Chlamydomonas reinhardtii* and defined the process as intraflagellar transport (IFT; Kozminski et al., 1993). IFT also has been observed in *C. elegans* and the mouse (Cole et al., 1998; Murcia et al., 2000; Pazour et al., 2000), and many of the core IFT components are conserved in species as diverse as *Chlamydomonas reinhardtii* and humans.

IFT is a complex process required to transport proteins synthesized in the cell body to the cilium (Figure 3-2). The IFT machinery and cargo machinery assemble at the basal body where they associate with the transitional fibers (Deane et al., 2001). They are sorted and loaded onto the axoneme by a poorly understood process, and then shuttled by heterotrimeric kinesin II along the axoneme in the anterograde direction towards the tip of the cilium (Iomini et al., 2001; Scholey, 2003). More than 17 IFT components form "IFT rafts" that associate with kinesin; these components can be biochemically fractionated into IFT complex A and B (Cole et al., 1998; Lucker et al., 2005; Piperno et al., 1998). Mutations in these IFT complex proteins result in trafficking defects and improper formation of the cilia, suggesting that they are necessary for building the cilia

and for IFT (Collet et al., 1998; Fujiwara et al., 1999; Haycraft et al., 2003; Haycraft et al., 2001; Perkins et al., 1986; Snow et al., 2004). At the cilium tip, the IFT particles are remodeled, cargo is unloaded and turnover products are loaded (Iomini et al., 2001; Piperno et al., 1998). Relatively little is known about the mechanisms that mediate this process, but the complex B component IFT172 has been implicated in turnover at the cilium tip (Pedersen et al., 2005). Dynein is activated and carries kinesin, which is now cargo, together with the smaller IFT particles in the retrograde direction toward the cell body (Figure 2; Pazour et al., 1998; Porter et al., 1999; Scholey, 2003; Signor et al., 1999a).

*Constructing the cilium by IFT: the motors*

In *C. elegans*, the transport motors are conserved. Similar to other organisms, the dynein heavy chain 1b ortholog CHE-3 and dynein light chain XBX-1 traffic back towards the cell body in the retrograde direction (Schafer et al., 2003; Signor et al., 1999a). However, cilia in the worm do have notable differences in anterograde transport. In addition to the heterotrimeric kinesin II complex, comprising KAP-1, KLP-11, and KLP-20, *C. elegans* express another kinesin, the OSM-3 homodimeric kinesin, in a subset of ciliated neurons, including the amphid neurons (Evans et al., 2006; Signor et al., 1999b; Snow et al., 2004; Tabish et al., 1995). The current model of IFT in *C. elegans* proposes that OSM-3 and heterotrimeric kinesin II function redundantly to build the middle segment of the cilium (Figure 3-2). However, OSM-3 alone traffics within the distal segment (Shakir et al., 1993; Snow et al., 2004; Tabish et al., 1995). Mutants in the heterotrimeric kinesin have relatively normal cilia, suggesting that OSM-3 alone is capable of constructing the cilium. In contrast, in *osm-3* mutants, the distal segments of

the cilia are truncated, consistent with the essential function of OSM-3 in the distal segment (Snow et al., 2004). In the absence of both motors, as in *osm-3*; *kap-1* mutants, IFT ceases and cilia completely fail to form (Snow et al., 2004).

OSM-3 and the heterotrimeric kinesin-II are proposed to move at different rates. Trafficking assays have revealed that the independent rate of the OSM-3 kinesin (1.3 $\mu m/s^{-1}$) is much faster than that of the heterotrimeric kinesin complex (0.5 $\mu m/s^{-1}$). In the middle segment, the two kinesins appear to move together at an intermediate rate (0.7 $\mu m/s^{-1}$); however, OSM-3 moves independently at its characteristic faster rate in the distal segment to the cilium tip (Ou et al., 2005; Snow et al., 2004).

How are these two motors stabilized? The Bardet-Biedl Syndrome (BBS) proteins, BBS-1, BBS -2, BBS -5, BBS -7, BBS -8, and BBS-9, stabilize the two kinesin motors and their associated IFT complexes together (Figure 3-3; Ou et al., 2005; Ou et al., 2007; Pan et al., 2006). This hypothesis is largely based on observation of cilia transport in *bbs* mutants. In the absence of one of the BBS proteins, IFT-A complex proteins move at the slow rate of the linked heterotrimeric kinesin-II (0.5 $\mu m/s^{-1}$), and IFT-B complex proteins are shuttled at the faster rate of the coupled OSM-3 kinesin (1.3 $\mu m/s^{-1}$; Ou et al., 2005; Ou et al., 2007; Pan et al., 2006). Therefore, because the BBS complex acts as a physical link between the two motors and their associated IFT particles, the heterotrimeric kinesin-II exerts a mechanical drag on the faster OSM-3 (Pan et al., 2006). In the absence of both BBS and the heterotrimeric kinesin-II, OSM-3 kinesin transports both IFT-A and IFT-B at its fast rate along the length of the cilium; the IFT-A and IFT-B complexes remain attached because the heterotrimeric kinesin no longer exerts a pull on the IFT-A particle. Similarly, in *bbs* and *osm-3* double mutants,

the heterotrimeric kinesin shuttles both IFT-A and IFT-B at its slow rate along the remaining middle segment (Pan et al., 2006). The functional significance of the coupling of these two motors is unknown.

*Constructing the cilium by IFT*: *Components that modify motor activity*

Two components that may modify motor activity in the cilia have been identified. The novel conserved protein DYF-1 may interact with OSM-3 homodimeric kinesin (Figure 3-3). One study suggested that DYF-1 is needed to activate and dock OSM-3 to IFT-B. In the absence of DYF-1, OSM-3 fails to move, and heterotrimeric kinesin transports the IFT-A and B complexes along the axoneme at the slow rate characteristic of the heterotrimeric kinesin (Ou et al., 2005). However, a separate study failed to detect a physical interaction between OSM-3 and DYF-1, and DYF-1 failed to directly activate OSM-3 in a single-molecular motility assay (Imanishi et al., 2006). The authors conclude that additional proteins or posttranslational modifications of the DYF-1 regulatory machinery may be required. Therefore, how DYF-1 controls OSM-3 motility still remains unresolved.

*dyf-5,* another recently identified cilia gene, has several different functions in kinesin motility (Figure 3-3). DYF-5 has been hypothesized to restrict heterotrimeric kinesin II to the middle segment; in the absence of DYF-5, the heterotrimeric kinesin is found throughout the cilium. All of the IFT particles in a *dyf-5* mutant move at the slow rate of the heterotrimeric kinesin II, implying that DYF-5 is required for OSM-3 to associate with the other IFT complex proteins and heterotrimeric kinesin II. OSM-3 moves independently at a much slower speed than normal, though not as slowly as the heterotrimeric kinesin; this finding suggests that DYF-5 is needed for OSM-3 to travel at

its characteristic fast rate (Burghoorn et al., 2007). Interestingly, defects in DYF-5 result in cilia that are much longer than wild-type (Burghoorn et al., 2007).

*Constructing the cilium by IFT*: *IFT complexes and other cilia machinery*

Although homologues of some *Chlamydomonas* IFT complex proteins have not been identified yet in *C. elegans,* many have clear orthologs in the worm. The IFT-A complex includes DAF-10/OSM-4/IFT122 and CHE-11/IFT140 (Bell et al., 2006; Inglis, 2006; Scholey et al., 2004). The core IFT-B complex comprises OSM-5/IFT88, OSM-6/IFT52, F32A6.2/IFT81, and C18H9.8/ IFT(74/72) (Blacque et al., 2005; Chen et al., 2006; Collet et al., 1998; Haycraft et al., 2001; Inglis, 2006; Kobayashi et al., 2007; Ou et al., 2007; Qin et al., 2001), while the peripheral IFT-B complex contains OSM-1/IFT172, CHE-2/IFT80, CHE-13/IFT57 (Figure 3-3; Bell et al., 2006; Fujiwara et al., 1999; Haycraft et al., 2003; Inglis, 2006).

Converging evidence in *C. elegans* and *Chlamydomonas* suggests that the IFT complex A and B have different roles in transport. *C. elegans* with mutations in IFT-A complex proteins have slightly truncated, swollen cilia, and contain accumulated electron-dense material along the cilia, a phenotype one might expect if retrograde transport is disrupted. Indeed, little retrograde transport is observed in IFT-A particle mutants, but anterograde IFT is relatively normal. Thus, IFT-A particles function in retrograde transport (Piperno et al., 1998; Rosenbaum and Witman, 2002; Scholey, 2003). Conversely, in IFT-B complex mutants, cilia are truncated, and many cilia proteins fail to enter the cilia. (Fujiwara et al., 1999; Haycraft et al., 2003; Haycraft et al., 2001; Perkins et al., 1986; Qin et al., 2001). Therefore, IFT-B complex proteins have a key role in anterograde transport. IFT-B complex proteins may also have a role in

retrograde transport given that two recent studies have found that IFT-B particles may associate with dynein heavy chain (Efimenko et al., 2006; Pedersen et al., 2006).

In addition to the core IFT particles, other proteins that participate in IFT continue to emerge. Mutant phenotypes and transport profiles of candidate cilia components reveal possible functions of these novel cilia genes. IFTA-1 is another component likely to be closely associated with the IFT-A complex based on its behavior in IFT motility assays and its ciliary mutant phenotype; in addition, mutations in the IFT-A particle *che-11* prevent IFTA-1 from entering the cilium (Blacque et al., 2006). Comparison of IFTA-1 with previously identified *Chlamydomonas* IFT-A subcomplex proteins implies that IFTA-1 may be the ortholog of IFT122B (Blacque et al., 2006). Another cilia component, DYF-3/Qilin, undergoes IFT (Ou et al., 2005; Ou et al., 2007). DYF-3 is likely to function as an accessory to the IFT-B complex based on its mutant ciliary phenotype and its IFT motility (Murayama et al., 2005; Ou et al., 2007). Interestingly, the *C. elegans* interactome project identified an interaction between DYF-3 and BBS-7 (Li et al., 2004b) although the DYF-3 ortholog did not co-sediment with the IFT particle complexes in *Chlamydomonas*, suggesting that it might be only loosely associated with IFT complexes (Cole et al., 1998; Ou et al., 2007). Similarly, DYF-13 may be associated with the IFT-B complex: DYF-13 is also needed to build the distal segment and moves at the same rate as OSM-3 in a *bbs-7* mutant (Ou et al., 2005; Ou et al., 2007). DYF-3 and DYF-13 have been proposed to comprise part of an accessory module used to help OSM-3 to build the distal part of the cilium (Figure 3-3;(Ou et al., 2005; Ou et al., 2007). As more cilia genes are identified, classification based on their transport profiles and their

mutant cilia phenotypes will help to reveal their function. However, additional analyses will be needed to elucidate their precise functions in IFT.

Knowledge of IFT in *C. elegans* comes from mostly from studies of the amphids and phasmids; by contrast, relatively little is known about trafficking and structure of the cilia of other ciliated neurons, such as the deirids. IFT particles and/or motors in different ciliated neurons are likely to have variations in function. A recent study found that OSM-3 is dispensable for constructing the AWB wing cilium, but not for building the ASH and ASI channel cilia (Mukhopadhyay et al., 2007b). In addition, some of the IFT components needed for IFT in the amphids and phasmids are not expressed in all other ciliated neurons. For example, *osm-3, dyf-2* and *dyf-3* are only expressed in subsets of ciliated neurons (Efimenko et al., 2006; Mukhopadhyay et al., 2007b; Murayama et al., 2005; Tabish et al., 1995), suggesting variations in IFT in different ciliated neuron types.

Notably, although the working model detailed above is intriguing, additional analyses in *C. elegans* are essential. Biochemical fractionation experiments originally identified the different IFT complexes in *Chlamydomonas*, and some of these have been further substantiated by genetic analyses in *Chlamydomonas* (Cole et al., 1998; Piperno et al., 1998; Rosenbaum, 2002; Scholey, 2003). Subsequently, the *C. elegans* homologs were found to localize to cilia and undergo IFT; these genes were also established to be necessary for ciliary assembly (Bell et al., 2006; Blacque et al., 2005; Collet et al., 1998; Fujiwara et al., 1999; Haycraft et al., 2001; Inglis, 2006; Qin et al., 2001; Scholey et al., 2004). Based on homology to *Chlamydomonas* genes and different transport profiles of these components, different functions for the *C. elegans* IFT components have been assigned. However, significant differences between IFT in *Chlamydomonas* flagella and

in *C. elegans* CSNs are likely to exist. For example, unlike in *C. elegans*, heterotrimeric kinesin-II is the main workhorse of anterograde transport in *Chlamydomonas*; the ortholog of homodimeric kinesin OSM-3 is not needed (Rosenbaum, 2002; Scholey, 2003). This alone suggests that BBS is not needed in IFT in *Chlamydomonas*; indeed, most BBS genes are absent from the flagellar proteome (Pazour et al., 2005; Stolc et al., 2005). Other differences between *Chlamydomonas* and *C. elegans* are likely to be revealed in the future. Thus, extrapolating from *Chlamydomonas* data should be done with caution. Furthermore, the majority of the above model is based on the observations of trafficking of GFP-tagged IFT-A and IFT-B particles in various worm mutant backgrounds. The assumption that the IFT-A and IFT-B complexes traffic together in worms is based on the observation that they move at the same rate and that these particles move together in *Chlamydomonas*; however, biochemical evidence in *C. elegans* is lacking. Thus, although the model nicely fits the existing data, it should be verified by further analyses.

Many open questions and uncharacterized cilia mutants remain. What is the functional significance of having two motors that operate at different speeds? How are cargo loaded at the basal body and unloaded at the cilium tip? How are particles recycled? What are the roles of all of the different IFT components? A combination of biochemical analyses, IFT transport assays, and studies of cilia mutants will provide further insight into some of these questions. However, the complex phenotypes of mutants such as *dyf-5* suggest that much remains to be discovered.

**Approaches for the identification of cilia genes**

*C. elegans mutagenesis screens*

A series of mutagenesis screens have provided a wealth of *C. elegans* cilia mutants that have been instrumental in identifying and understanding the function of key cilia components. Here, I briefly highlight some of the original screens.

Screens for sensory behaviors were the first to uncover many cilia mutants that have been cloned and characterized in the subsequent three decades; these also highlight the importance of intact cilia for sensation in *C. elegans*. Many of the mutations found in these screens turned out to cause defects in key IFT components. Osmotic avoidance abnormal (*osm*) mutants were originally identified in a screen for animals defective in an avoidance response to solutions of high concentration of fructose and NaCl (Culotti and Russell, 1978). Two screens for worms that fail to chemotax towards Na$^+$ or Cl$^-$ ions isolated chemotaxis abnormal (*che*) mutants (Dusenbery et al., 1975; Lewis and Hodgkin, 1977). A screen for touch-defective mechanosensory abnormal (*mec)* mutants identified at least two more cilia structural mutants (Chalfie and Sulston, 1981; Perkins et al., 1986). A worm strain lacking AFD cilia emerged from a search for mutants with defects in thermotaxis (*ttx*; Hedgecock and Russell, 1975; Perkins et al., 1986). Odorant-defective mutants (*odr*) have defects in the detection of odorants, tastants, and other substances, as a consequence of either cilia structural aberrations or loss of signal transduction components needed to detect the stimulus (Bargmann, 2006; Bargmann et al., 1993). Finally, ciliated sensory neurons regulate the formation of dauer larvae, an alternative development hibernation state, and accordingly, several cilia mutants have also emerged from dauer mutant screens (Albert et al., 1981; Perkins et al., 1986).

Searching for cilia mutants has also been facilitated by a simple assay for structural defects. When exposed to DiI or FITC, six pairs of amphid neurons (ADL,

82

ASH, ASI, ASJ, ASK, AWB) and the two pairs of phasmid neurons (PHA and PHB) fill

with dye via the cilia's contact with the external environment. <u>Dy</u>e-<u>f</u>illing (*dyf*) mutants

whose cilia do not uptake dye have defects in the cilia or supporting sheath and socket

cells (Perkins et al., 1986). Dye-filling serves as a quick, easy method to determine

whether a strain has defects in cilia structure and thus has been used to identify many

novel cilia defects (Perkins et al., 1986; Starich et al., 1995). More recently, studies have

used a combination of these approaches, such as chemotaxis and dye-filling, together

with IFT motility assays to discover novel cilia mutants (Ou et al., 2007).

*Bioinformatic, genomic and proteomic approaches to identifying cilia components*

Numerous bioinformatic, comparative genomic and proteomic approaches have

helped to identify additional conserved ciliary and flagellar genes. In *C. elegans* one

approach to discover novel cilia genes has relied on the common *daf-19* regulatory

motif—the X-box—in the promoter of many cilia genes. Several studies performed a

genome-wide search for genes with the X-box-consensus motif in the promoter region.

Such an approach successfully identified known IFT-related genes, including *osm*, *che*,

and *bbs* genes. Based on the rationale that true X-box elements would be conserved in

the closely related species *C. briggsae*, Efimenko et al., identified approximately 758

genes in *C. elegans* that contained the X-box motif within 1,000 bp of the start codon

(Efimenko et al., 2005). Using more stringent criteria, Blacque et al., identified

approximately 293 genes with X-boxes within 250 bp of the start codon. They refined

this list to 46 genes by comparison with ciliated-neuron specific genes identified using

SAGE analysis (Serial Analysis of Gene Expression) on ciliated and non-ciliated cells

(Blacque et al., 2005). A third study searched for X-box motifs that are conserved in *C.*

*elegans*, *C. briggsae* and *C. remanei,* based on the assumptions that X-box motifs are also used to control expression of ciliary genes in these related nematode species and that transcriptionally significant X-box motifs would be conserved. In this study, they identified 93 genes regulated by X-box genes (Chen et al., 2006). Comparative genomic approaches can uncover cell or basal body genes that participate in cilia function but are not exclusively localized to cilia. However, this approach may miss cilia genes because they are too divergent, belong to multigene families, or do not contain sufficient sequence information to be identified (Inglis et al., 2006).

Expression analysis of ciliated neurons has also proved a fruitful, complementary method for finding candidate genes specific to ciliated neurons. Kunitomo et al., expressed Poly-A Binding Protein (PABP) under the control of the *che-2* promoter to bind and extract RNAs expressed specifically in ciliated cells; microarray analysis was then used to uncover genes enriched in ciliated neurons (Kunitomo et al., 2005). Colosimo et al., generated embryonic cultures from two *C. elegans* ciliated neuron types, AFD and AWB, and used microarrays to isolate genes that were differentially expressed in these two cell types compared to other cells (Colosimo et al., 2004). The benefit of microarrays and expression studies is that they can reveal any gene required for cilia function or formation, but a major disadvantage is the high false-positive and false-negative rate.

In addition to studies in the nematode, significant advances in the identification of cilia-specific genes have been made using proteomic and genomic approaches in other organisms. Comparative genomic studies subtracted the genome of nonciliated organisms from the genetic set of ciliated organisms based on the rationalization that the

remaining overlapping genes were likely to represent genes specific to cilia assembly and

function (Avidor-Reiss et al., 2004; Li et al., 2004a). Li et al. utilized this approach to

define a flagellar apparatus-basal body (FABB) proteome consisting of 688 proteins (Li

et al., 2004a). Various proteomic methods have uncovered flagellar and cilia-specific

proteins in isolated *Chlamydomonas* flagella, *Tetrahymena thermophila* ciliary

axonemes, and cilia of human bronchial epithelial tissue culture (Ostrowski et al., 2002;

Pazour et al., 2005; Smith et al., 2005). Additionally, microarrays in *Chlamydomonas*

have been used to identify flagellar-specific genes upregulated during flagellar

regeneration (Stolc et al., 2005).

Taken together, the combination of proteomic methods, cross-species

comparisons, and expression analyses has led to a rich cilia data set. The identification of

a comprehensive ciliary proteome inspired the name "ciliomics" (Inglis et al., 2006).

Future analyses of individual genes identified in these studies will help to spur the cilia

field forward in elucidating the functions of these genes.

**Function of ciliated sensory neurons**

Generally, non-motile, primary cilia in many organisms perform sensory

functions. In *C. elegans*, CSNs detect a broad range of stimuli, including chemicals,

odors, mechanosensory stimuli, and oxygen levels. These sensory signals govern many

behaviors.

The amphids and phasmids detect a variety of attractants and repellents, including

water-soluble and volatile odorants. Attractants include NaCl, ions, cAMP, cGMP,

lysine, alcohols, ketones, esters, and aldehydes. Acid pH, copper ions, octanol, and high

osmolarity are among the repellents (Bargmann et al., 1993; Bargmann and Horvitz,

1991a; Bargmann, 1997; Dusenbery, 1974; Ward, 1973).  Laser ablation experiments have revealed that different ciliated neurons detect specific chemosensory stimuli.  For example, ASE responds to many attractants, including NaCl, cAMP, and lysine while AWB detects volatile repellents (Bargmann and Horvitz, 1991a; Troemel et al., 1997).  While any single stimulus may be detected by several neurons, no two neurons detect exactly the same set of stimuli.  Furthermore, each sensory neuron is hard-wired such that the response to an odorant is determined by the cells that express its receptor, not by the odorant itself.  For example, ODR-10, the receptor for the attractive odorant diacetyl is expressed exclusively in AWA.  When ODR-10 is misexpressed in AWB, animals are repulsed by diacetyl (Troemel et al., 1997).

In addition to chemosensory signals, worms also sense mechanosensory and thermosensory stimuli. When worms collide with something in their environment, they respond by reversing and moving in a different direction.  Three ciliated neurons ASH, FLP, and OLQ detect mechanosensory stimuli to the nose; ablation of these neurons eliminates worms' response to nose-touch (Hart et al., 1995; Kaplan and Horvitz, 1993).  Many cilia mutants, such as *osm-3, osm-6, che-2, che-3,* and *che-13,* are also defective in their response to light-nose touch (Kaplan and Horvitz, 1993).  The dopaminergic ciliated neurons, CEP, ADE, and PDE, mediate mechanosensation of bacteria.  Accordingly, ablation of these neurons causes an attenuation of the basal slowing response, a characteristic deceleration in locomotion upon encountering food (Sawin et al., 2000).  Additionally, ciliated neuron AFD, with a cilium that terminates with approximately 50 microvilli, responds to temperature (Mori, 1999; Perkins et al., 1986).  The thermotaxis

mutant *ttx-1* lacks AFD microvilli suggesting that proper elaboration of the cilium is need for temperature sensation (Mori, 1999; Perkins et al., 1986).

Ciliated neurons also detect oxygen levels—a critical ability for an animal that spends much of its life buried in the soil. *C. elegans* typically prefers 5-12% $O_2$. Avoidance of non-optimal oxygen conditions is dependent upon the ciliated neurons AQR and PQR and the non-ciliated neuron URX, which contact the pseudocoelomic fluid (Gray et al., 2004).

CSNs participate in the regulation of lifespan and the development of the dauer state. *daf-19* worms, which completely lack cilia, enter the dauer stage constitutively, while other cilia mutants, such as *daf-6* and *daf-10,* are unable to enter dauer state (Albert et al., 1981; Perkins et al., 1986). Accordingly, four amphid neurons--ADF, ASG, ASI, and ASJ—have been implicated in the regulation of dauer entry and exit (Bargmann and Horvitz, 1991b). In addition, cilia regulate lifespan: mutations in cilia and ablation of specific ciliated neurons increase lifespan (Apfeld and Kenyon, 1999; Alcedo and Kenyon, 2004).

Intact cilia are also important for several steps of male mating behavior. IFT occurs in several male-specific ciliated neurons. Males detect the presence of hermaphrodites through a diffusible, chemosensory cue; consequently, *daf-10, osm-5, osm-6,* and *che-3* mutants fail to find mates effectively (Barr et al., 2001; Barr and Sternberg, 1999; Simon and Sternberg, 2002).

CSNs have also been implicated in the regulation of metabolism. This will be discussed in much greater detail in Chapters Four and Five.

In sum, CSNs have been implicated in many different behaviors that are essential for the organism's survival. The next challenge is to identify CSN-specific signaling pathways that participate in these behaviors.

*Cilia participate in signaling*

Converging evidence suggests that the cilium participates in signal transduction. Localization of signaling molecules and receptors to the cilium is needed for appropriate responses to stimuli; expression of such signaling molecules in the dendrites or elsewhere within the neuron is not sufficient. Cilia localization is essential for signal transduction by the TRPV family genes *osm-9* and *ocr-2*, involved in the detection of several chemosensory and mechanosensory cues. OSM-9 and OCR-2 are mutually dependent upon each other for their cilia localization (Tobin et al., 2002). Similarly, *odr-4* and *odr-8*, identified in screens for odorant mutants, are required for proper localization of chemoreceptors such as the diacetyl receptor ODR-10*,* to the cilium. Localization of different receptors and channels is likely to be somewhat specialized, as *odr-4* is not needed for proper localization of other channels and receptors (Dwyer et al., 1998).

In addition to targeting proteins to the ciliary membrane, an exciting recent study in *Chlamydomonas* demonstrated that transport within the cilium may actually participate in signaling (Wang et al., 2006). The authors took advantage of a temperature-sensitive mutant in the heterotrimeric kinesin *fla10*. At the permissive temperature, *fla10-1* cells assemble flagella normally; when switched to the restrictive temperature, anterograde IFT stops, but the flagellum remains intact for a while. Mating in *Chlamydomonas* occurs via flagellar adhesion, which initiates a signaling pathway involving cGMP-dependent protein kinase (PKG) that activates gametes. PKG is dependent upon IFT to

associate with a new flagellar subcompartment containing IFT particles. In the absence of intact IFT, as in *fla-10-1* mutants, PKG no longer associates with this subcompartment and signaling is blocked even though flagellar adhesion occurs normally (Wang et al., 2006). These data suggest that signaling through the PKG pathway requires intact IFT. The temperature-sensitive *fla10-1* mutant is the only model system in which IFT can be dissected independently of cilium structure; however, IFT is likely to participate in signaling in many different types of ciliated cells.

**Disease and cilia**

The discovery that many diseases are a consequence of cilia or basal body dysfunction has sparked a great interest in these organelles. Many of these disease genes are conserved in *C. elegans*.

Several kidney diseases are caused by defects in the non-motile primary cilia of kidney epithelial cells, which project into the lumen of the ducts and tubules of the nephrons (Pazour and Rosenbaum, 2002; Badano et al., 2006; Qamar et al., 2007). The first insight into the importance of cilia in kidney disease arose from studies of mice with a hypomorphic mutation in *Tg737*. *Tg737^{orpk}* mice have abnormal kidney cilia and develop cystic kidneys similar to human patients with Polycystic Kidney Disease (PKD; Moyer et al., 1994). Additional evidence that *Tg737* has a role in cilia comes from the finding that complete knockout of *Tg737* prevents ciliary assembly in the embryonic node and causes prenatal lethality (Murcia et al., 2000). *Tg737* is the ortholog of *osm-5* in *C. elegans* and IFT88 in *Chlamydomonas,* a key IFT-B complex component, as described above (Haycraft et al., 2001; Pazour et al., 2000; Qin et al., 2001). Further support for a connection between cilia and cyst formation comes from the finding that

mutations in *Kif3a*, the heterotrimeric kinesin, are associated with a loss of cilia and cystic lesions in the mouse kidney (Lin et al., 2003).

Autosomal dominant polycystic kidney disease (ADPKD) is caused by mutations in polycystins *PKD1* and *PKD2*. These TRPP $Ca^{2+}$ channels are essential for the increase in intracellular $Ca^{2+}$ produced by fluid-flow deflection of the cilia axoneme (Davenport and Yoder, 2005; Nauli et al., 2003). Polycystin defects cause overproliferative kidney cells that fail to differentiate and form cysts by a poorly understood mechanism (Qamar et al., 2007). The *C. elegans* homologs of *PKD1* and *PKD2*, *lov-1* and *pkd-2*, localize to the cilia in male-specific tail sensory neurons. Although *lov-1* and *pkd-2* are not needed for the formation of cilia, mutations cause abnormal male-mating behavior likely due to mechanosensory defects (Barr et al., 2001; Hu and Barr, 2005).

Nephronophthisis (NPH) is another cystic kidney disease that may also arise from defects in the cilia. In mammals, nephrocystin-1 and nephrocystin-4 localize to primary cilia and basal bodies and associate with β-tubulin, the central component of the cilium axoneme (Fliegauf et al., 2006; Mollet et al., 2005). Similarly, in *C. elegans*, NPH-1 and NPH-4, orthologs of mouse *NPHP1* and *NPHP4*, concentrate at the transition zone and are regulated by *daf-19*. Mutations in *nph-1* and *nph-4* cause phenotypes similar to other cilia mutants, including chemotaxis defects and extended lifespan. However, *nph-1* and *nph-4* mutants have normal cilia, suggesting that *nph-1* and *nph-4* are not necessary for the development of cilia (Winkelbauer et al., 2005).

Several cilia diseases, such as Bardet-Biedl Syndrome, nephronophthisis, and murine models of PKD, including *Tg737 $^{orpk}$*, are also associated with retinal disorders. Accordingly, IFT has an important role in the formation and maintenance of

photoreceptors.  The outer segment (OS) of the photoreceptor, a highly modified primary

cilium, is attached to the inner segment (IS) by a connecting cilium and is dependent

upon IFT for continuous regeneration (Davenport and Yoder, 2005).  Interfering with IFT

by mutations *Kif3a* or *Tg737* causes accumulation of pigments in the IS followed by

degeneration of the OS (Marszalek et al., 2000; Murcia et al., 2000).  Thus, IFT is

essential for the maintenance of the photoreceptor, and diseases that perturb IFT often

cause retinal degeneration or retinopathy.

Several other diseases with a ciliary origin have been identified.  Meckel-Gruber

syndrome (MKS) is a several fetal disease characterized by neural tube defects, kidney

dysplasia and polydactyly (Kyttala et al., 2006; Smith et al., 2006).  The *C. elegans*

homologs of MKS the genes, *MKS1* and *MKS3* (Kyttala et al., 2006; Smith et al., 2006),

are expressed in ciliated sensory neurons (Blacque et al., 2005; Efimenko et al., 2005)

although their function is still unknown.  Kartagener's syndrome, is associated with

recurrent respiratory infections, male infertility, and situs inversus, a reversal of the left-

right asymmetry of visceral organs due to dysfunction of the embryonic node cilia

(Guichard et al., 2001; Olbrich et al., 2002; Pennarun et al., 2000).  The disease is a

consequence of mutations in ciliary intermediate and heavy chain dyneins (Guichard et

al., 2001; Olbrich et al., 2002; Pennarun et al., 2000).

Examining the functions of these disease genes in animal models, including *C.*

*elegans,* will provide further insight into the underlying mechanisms of these diseases.

The pleiotropic symptoms associated with cilia diseases highlight the many functions of

cilia.  Bardet-Biedl Syndrome, another disease associated with cilia dysfunction, is

characterized by many of the same symptoms as other cilia diseases.  In Chapter Four, I

will discuss extensive evidence that defects in BBS genes give rise to cilia-associated

pleiotropies.

# Figure 3-1
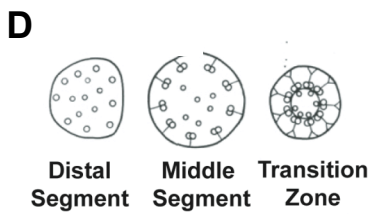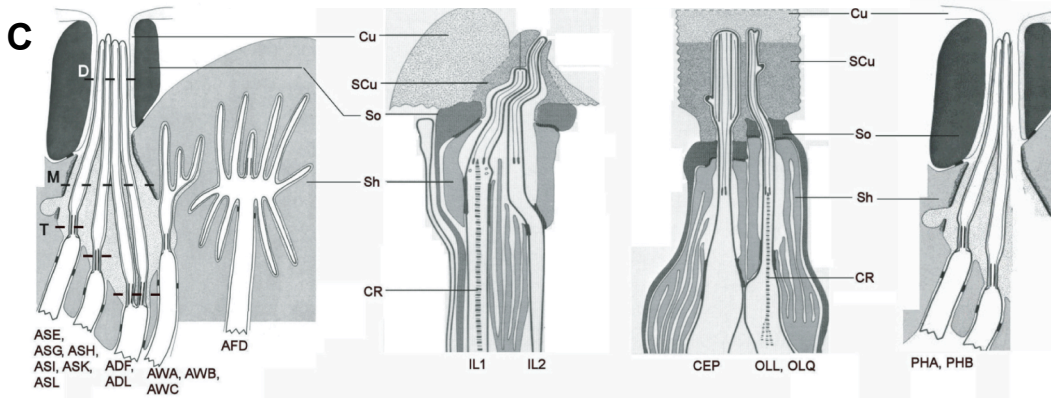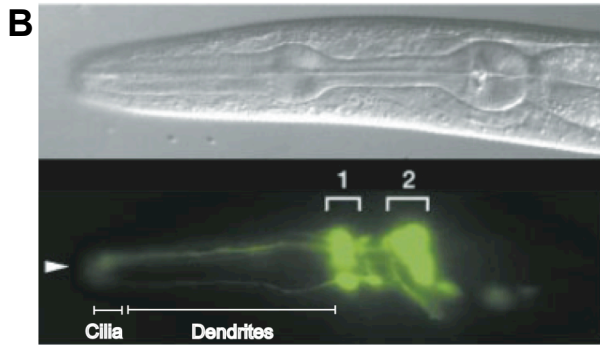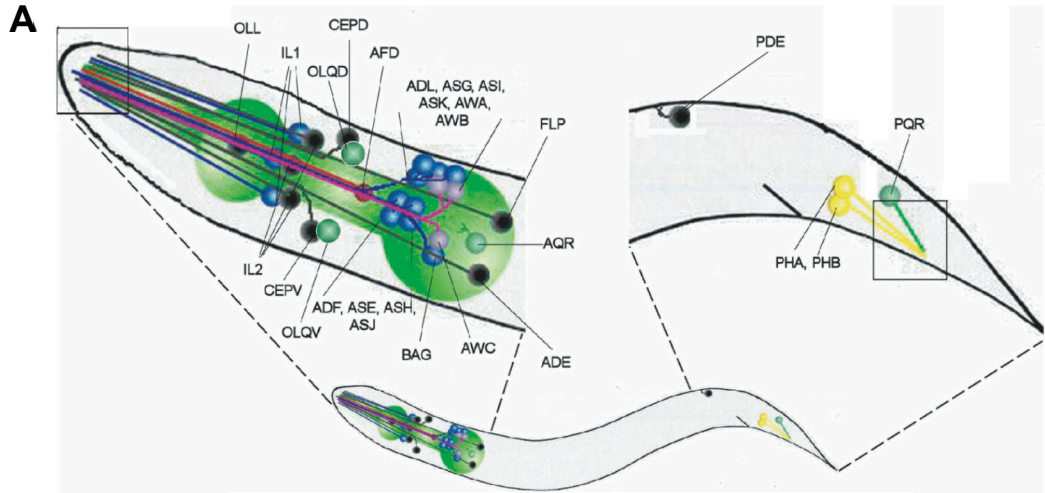
**Figure 3-1. Ciliated sensory neurons in *C. elegans***

(A) Schematic of the position of the cell bodies of the ciliated neurons in the worm. Anterior is to the left. The green shaded area represents the pharynx. The ciliated neurons located in the head send long dendrites towards the tip of the nose that terminate in cilia. Similarly, the ciliated neurons in the tail send ciliated dendrites posteriorly.

(B) GFP-labeled ciliated neurons in *C. elegans.* The amphids send long dendrites towards the tip of the nose (indicated by white arrow) that terminate in cilia. 1 = labial neuron cell bodies; 2 = the amphid neuron cell bodies. Reprinted by permission from Macmillan Publishers Ltd: Nature, (Ansley et al., 2003) © 2003.

(C) Schematic of longitudinal section through the amphids, inner labials, outer labials, cephalic neurons, and phasmids. The cilia of the amphids, inner and outer labials, cephalic neurons, and phasmids are housed in a sheath and socket cell. The dendrites of the winged cells AWA, AWB, AWC separate from the other amphid dendrites and terminate in the sheath. AFD dendrite is separate from the other amphid dendrites, and its rudimentary cilium elaborates into 50 microvilli in the sheath. The inner labial, outer labial and CEP neurons their cilia terminate in the cuticle. The eight channel amphids, the phasmids and IL2 gain access to the external environment through a n the cuticle pores. Sh: sheath, So: socket, Cu: cuticle; CR: cilia rootlet

(D) Transection through the distal and middle segments and the transition zone of an amphid cilium. The transverse cuts are shown in (C). Each circle represents a microtubule. The transition zone contains an outer ring of nine doublet microtubules that contact the cell membrane through Y-shaped links and inner single microtubules. The outer ring of doublet microtubules and the inner singlet microtubules are continuous

through the middle segment. The distal segment contains an outer ring of nine singlet

microtubules and inner microtubules. (A), (C), (D) adapted from (Inglis); amphids and

phasmids illustrations reprinted originally from originally from (Perkins et al., 1986) with

permission from Elsevier. Labial and cephalic neurons reprinted from (Ward et al., 1975)

by permission from John Wiley & Sons, Inc.

**Figure 3-2**



0.7 µm/sec   1.3 µm/sec

TZ   Middle Segment   Distal Segment

Heterotrimeric kinesin-II
OSM-3 kinesin
CHE-3 dynein
IFT-A
IFT-B
BBS
IFT-A cargo
IFT-B cargo
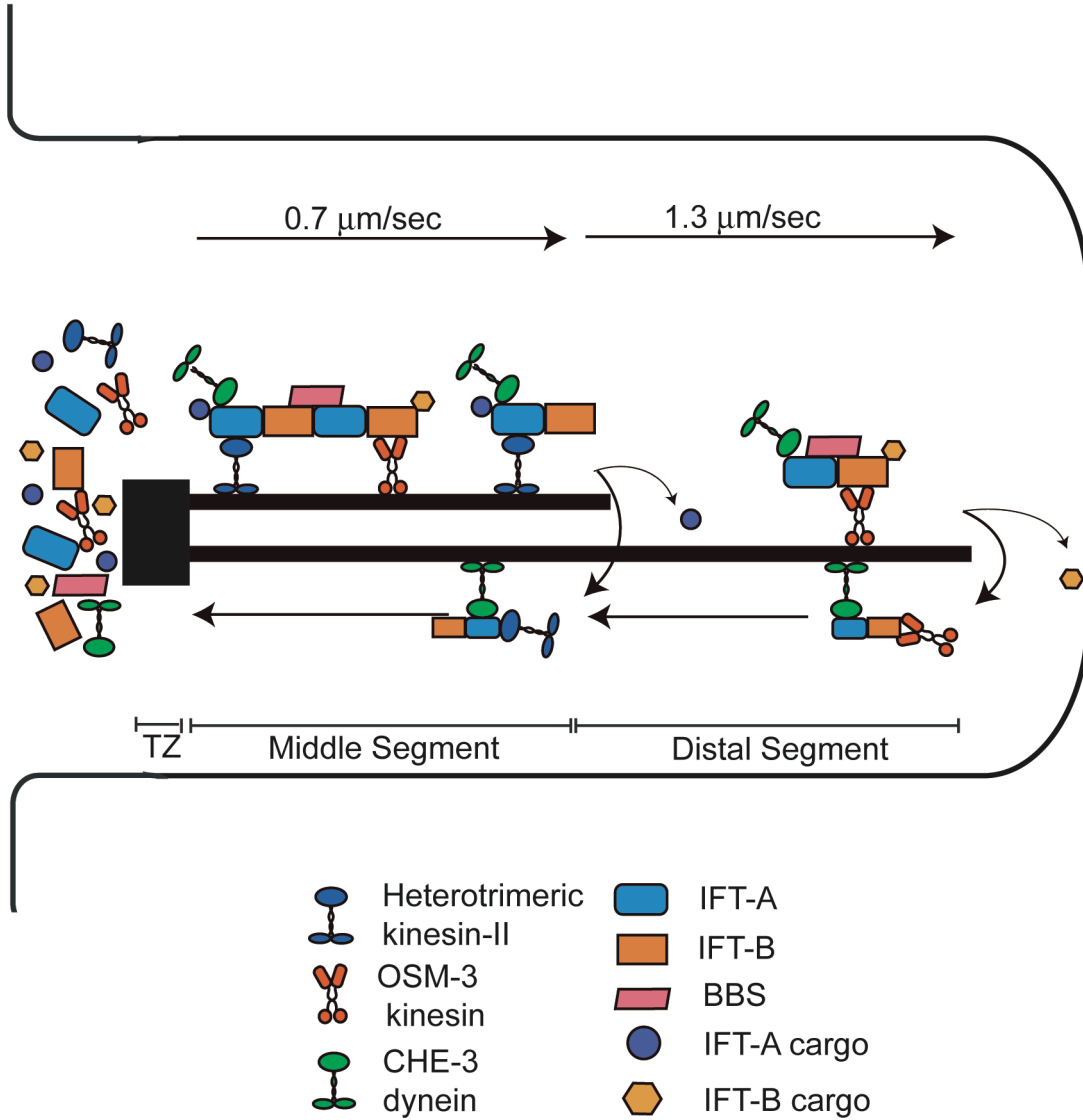
**Figure 3-2. Intraflagellar transport in *C. elegans*.**

Motors, IFT particles, and cargo are assembled and loaded at the transition zone (TZ).

The heterotrimeric kinesin-II and homodimeric OSM-3 kinesin transport cargo, including

dynein, in the anterograde direction towards the cilium tip at an intermediate rate (0.7

μm/sec).  At the end of the middle segment, the heterotrimeric kinesin-II turns around,

becomes cargo, and is carried by dynein back to the basal body.  The OSM-3 kinesin

continues to carry its cargo along the distal segment at a faster rate (1.3 μm/sec).  At the

cilium tip, OSM-3 releases its cargo, turns around and is also transported by dynein back

to the basal body. Based on model from (Ou et al., 2007).

**Figure 3-3**
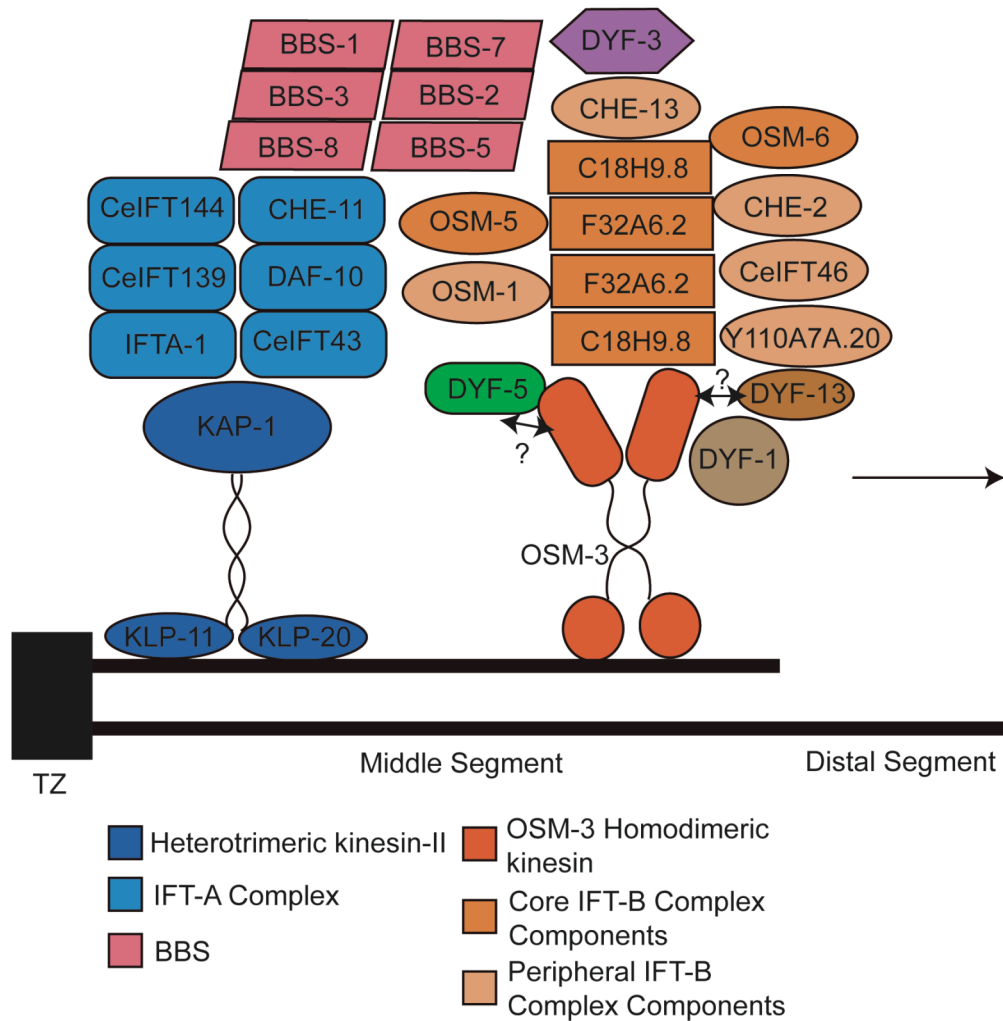
**Figure 3-3.  Illustration of the known IFT components in *C. elegans.***

Anterograde transport is mediated by two kinesins, the homodimeric OSM-3 and the heterotrimeric kinesin, in the middle segment, and by OSM-3 alone in the distal segment. IFT complexes A and B associate with heterotrimeric kinesin-II and OSM-3, respectively.  The BBS complex stabilizes the kinesins and their linked IFT complexes in the middle segment.

F32A6.2/IFT81 and C18H9.8/IFT(74/72) in *Chlamydomonas* have been shown to form a tetrameric complex that has been suggested to form a scaffold for the IFT-B complex (Lucker et al., 2005).  IFT-B consists of both core complex components (in dark orange) and peripheral components (in lighter orange).  DYF-5 has a role in OSM-3 motility and helps OSM-3 to associate with the rest of the IFT complex (Burghoorn et al., 2007); the position of DYF-5 with respect to the core IFT machinery is still unknown.

The arrangement of different IFT components within the IFT-A and IFT-B complexes has not yet been determined.  The classification of different components into IFT-A or IFT-B complexes is based on homology to *Chlamydomonas* IFT particles. *Chlamydomonas* homologs are as follows: CHE-11 = IFT140; DAF-10 = IFT122; IFTA-1 = IFT122B; OSM-5 = IFT88 ; OSM-6 = IFT52; CHE-2 = IFT80; OSM-1 = IFT172;  C18H9.8 = IFT(74/72); F32A6.2 = IFT81; CeIFT144, CeIFT139, CeIFT43, CeIFT46 are unknown in *C. elegans*.  Adapted from (Ou et al., 2007).

**Chapter Four**


**The role of Bardet-Biedl Syndrome and cilia genes in fat storage**

In Chapter Four, I provide extensive background of Bardet-Biedl Syndrome. I describe the animal models of the disease and explore current hypotheses about the molecular causes of the disease. In the second half of this chapter, as part of my own work, I examine the role of BBS in metabolism in *C. elegans.*

**Bardet-Biedl Syndrome**

Laurence & Moon reported the first case of Bardet-Biedl Syndrome (BBS) in 1865—a young obese girl with visual impairment and mental disabilities. Bardet & Biedl, for whom the disease was named, further characterized the disease in 1920, with reports of additional symptoms, including polydactyly and hypogenitalism (Beales, 2005; Tobin and Beales, 2007). Currently, primary clinical features of BBS have been expanded to include renal abnormalities, polydactyly, male hypogonadism, learning disabilities, rod-cone dystrophy, and obesity. Secondary features include developmental and speech delay, behavioral abnormalities, diabetes, hearing loss, anosmia, situs inversus, cardiac defects, and altered facial features (Beales et al., 1999). Many of these symptoms are not detectable at birth, but develop during childhood or later (Tobin and Beales, 2007). Polycystic kidneys and complications from obesity are the most frequent causes of premature death of BBS patients (Beales et al., 1999; Beales et al., 1997; Blacque and Leroux, 2006; Croft et al., 1995).

BBS is a rare disorder with a prevalence of ~1:120,000 in Europe and North America (Beales et al., 1997; Blacque and Leroux, 2006; Croft et al., 1995). However, some populations, such the Bedouin tribes of Kuwait and Saudia Arabia, have a much higher prevalence of Bardet-Biedl Syndrome ranging from approximately 1:13,000-17,000 (Farag and Teebi, 1988; Farag and Teebi, 1989).

Thus far, twelve *BBS* genes have been identified through a combination of approaches, including both traditional positional cloning and linkage analysis, as well as SNP arrays and cross-species comparisons (Ansley et al., 2003; Badano et al., 2003; Chiang et al., 2004; Fan et al., 2004; Katsanis et al., 2000; Li et al., 2004a; Mykytyn et al., 2001; Mykytyn et al., 2002; Nishimura et al., 2001; Nishimura et al., 2005; Slavotinek et al., 2000; Stoetzel et al., 2006; Stoetzel et al., 2007).  BBS1 and BBS10 are most commonly mutated in BBS patients (Beales et al., 2003; Blacque and Leroux, 2006; Mykytyn et al., 2003; Stoetzel et al., 2006).  Although Bardet-Biedl Syndrome was previously considered an autosomal recessive disorder, recently several studies have found that some patients have a much more complex oligogenic inheritance (Beales et al., 2003; Katsanis et al., 2001).

Although Bardet-Biedl Syndrome is a rare disorder, recent advances in our understanding of the disease pathology have sparked much enthusiasm.  With the discovery in 2003 that cilia dysfunction is the root of many BBS symptoms (Ansley et al., 2003), BBS joins the growing number of diseases attributed to defective cilia.  As described below, *BBS* genes are highly conserved, and murine, zebrafish, and *C. elegans* models of the disease have provided insight into the molecular and cellular pathology of BBS.

**Animal studies of BBS highlight a function in cilia**

All twelve of the identified *BBS* genes are conserved in rodents.  Thus far, knockout mice models for *BBS1, BBS2, BBS4, BBS6* have been created (Fath et al., 2005; Kulaga et al., 2004; Mykytyn et al., 2004; Nishimura et al., 2004; Ross et al., 2005).  Murine *Bbs* null mice demonstrate many phenotypic similarities to BBS patients.

Although slightly small and underweight at birth, *Bbs2-/-*, *Bbs4-/-*, and *Bbs6-/-* mice develop age-dependent obesity (Fath et al., 2005; Mykytyn et al., 2004; Nishimura et al., 2004). *Bbs2-/-* animals also develop renal cysts (Nishimura et al., 2004), and both male *BBS* patients and male *Bbs* null mice are infertile (Fath et al., 2005; Mykytyn et al., 2004; Nishimura et al., 2004). Furthermore, like BBS patients, mice also exhibit behavioral and sensory abnormalities, including progressive retinal degeneration, hearing loss, and anosmia (Fath et al., 2005; Mykytyn et al., 2004; Nishimura et al., 2004). However, unlike humans, mice fail to develop polydactyly or situs inversus (Beales, 2005; Mykytyn et al., 2004; Nishimura et al., 2004).

The pleiotropic symptoms of BBS remained unexplained until a highlight study in 2003, which was the first to attribute a role for *BBS* in cilia (Ansley et al., 2003). The cloning of *BBS8* provided the first hint that the etiology of BBS was related to the cilium. *BBS8* contains tetratricopeptide repeat (TPR) domains that are similar to the prokaryotic domain *pilF*, involved in pilus assembly and twitching. A second clue was a BBS patient who presented with situs inversus, a reversal in left-right asymmetry caused by a defect in nodal cilia (Ansley et al., 2003). Localization experiments in this study as well as later studies supported these authors' ciliary hypothesis. BBS proteins localize to the basal bodies of cilia and centrosomes and are expressed in ciliated tissues, including the connecting cilium of the retina, bronchial epithelial cells, the telencephalon, and the olfactory epithelium (Ansley et al., 2003; Mykytyn et al., 2004; Nishimura et al., 2004). Finally, BBS proteins, which are conserved in *C. elegans*, are expressed solely in 60 ciliated neurons, the only ciliated cells of the worm (Ansley et al., 2003; Fan et al., 2004; Li et al., 2004a).

Examination of ciliated tissue in *Bbs* null mice revealed additional defects that are consistent with a BBS function in cilia. Retinal degeneration in *Bbs* mice and BBS patients has been attributed to deficient intracellular transport and intraflagellar transport (IFT) needed for maintenance of the outer segments of photoreceptors (Mykytyn et al., 2004; Nishimura et al., 2004). Furthermore, anosmia in *Bbs1-/-*, *Bbs2-/-*, and *Bbs4-/-* null mice and BBS patients (Kulaga et al., 2004; Mykytyn et al., 2004; Nishimura et al., 2004) is a consequence of a mislocalization of cilia-enriched olfactory proteins due to defects in trafficking (Kulaga et al., 2004). Infertility in BBS patients and *Bbs* mutant mice is due to the essential role of BBS in flagella formation; *Bbs2-/-*, *Bbs4-/-*, and *Bbs6-/-* spermatozoa lack flagella (Fath et al., 2005; Mykytyn et al., 2004; Nishimura et al., 2004). Studies in zebrafish also support a role for BBS in cilia maintenance or transport: reduction of zebrafish *BBS* homologs results in altered organ left-right asymmetry by causing a progressive loss of cilia in Kupffer's Vesicle, a spherical organ that appears transiently at the end of gastrulation and determines laterality (Chiang et al., 2006; Yen et al., 2006).

However, aside from the flagella of spermatozoa, BBS is not needed for the general formation of motile or primary cilia in other tissues. *Bbs2-/-*, *Bbs4-/-*, and *Bbs6-/-* mice have tracheal and renal cilia that appear relatively normal by size, number, and structure, indicating that BBS function is not needed for the development of cilia (Fath et al., 2005; Mykytyn et al., 2004; Nishimura et al., 2004). Also, photoreceptors and cilia of the retina are initially intact and later degenerate, suggesting that BBS is not needed for formation of the cilia in photoreceptors (Mykytyn et al., 2004; Nishimura et

al., 2004).  Thus, BBS proteins are needed for transport within cilia or maintenance of cilia but not for the initial formation of cilia.

Our understanding of the role of BBS in intraflagellar transport (IFT) has been enhanced by studies of *bbs* in *C. elegans*.  All of the BBS proteins examined in *C. elegans* undergo transport within the cilium (Fan et al., 2004; Ou et al., 2005; Ou et al., 2007).  Trafficking assays have revealed an essential function for BBS in anterograde IFT (Figure 3-3).  OSM-3 homodimeric kinesin and the heterotrimeric kinesin-II, comprising KAP-1, KLP-11, and KLP-20, shuttle cargo together along the middle segment, but in the distal segment, OSM-3 alone transports cargo.  OSM-3 and the heterotrimeric kinesin-II are associated with IFT complex B and IFT complex A, respectively (Ou et al., 2005; Ou et al., 2007).  The BBS complex stabilizes the OSM-3 kinesin and the IFT-B complex together with the heterotrimeric kinesin-II and the IFT-A complex (Figure 3-3).  The independent rate of the OSM-3 kinesin is much faster than that of the heterotrimeric kinesin complex; however, because the BBS complex couples together these two motors in the middle segment, these two kinesins move together at an intermediate rate (Ou et al., 2005; Ou et al., 2007).  In the absence of any one of the BBS complex proteins, which includes BBS-1, BBS-2, BBS-3, BBS-5, BBS-7, and BBS-8, the motors move independently at their own rates (Ou et al., 2005; Ou et al., 2007).  Whether BBS similarly stabilizes IFT components in other organisms, or whether this function is specific to *C. elegans,* remains to be seen.

A recent study by Nachury and colleagues also provided further insight into how BBS may function in transport.  Their study was the first to demonstrate that BBS moves within mammalian cilia at rates similar to normal intraflagellar transport (IFT; Nachury et

al., 2007).  In an elegant series of biochemical experiments, they found that BBS proteins associate with the ciliary membrane and interact with Rabin8 to activate Rab8.  Activated Rab8 leads to vesicle docking and fusion to the base of the cilium as well as the entry of transmembrane proteins into the cilium; in addition, it allows the entry of BBS into the cilium and thus promotes ciliation (Leroux, 2007; Nachury et al., 2007).

Besides a role in cilia transport, BBS may have additional functions in intracellular transport.  Evidence for this hypothesis comes mostly from studies using a model for retrograde transport in zebrafish (Yen et al., 2006).  Zebrafish can control their skin pigmentation by regulating the distribution of melanosomes within their melanophores; kinesin mediates melanosome dispersal to the cell periphery while dynein shuttles melanosomes back to the perinuclear region.  Knocking down any of the *bbs* genes examined thus far, including *bbs2*, *bbs4*, *bbs5*, *bbs6*, *bbs7*, *bbs8*, and *bbs11*, results in significant delay of retrograde melanosome transport but has no detectable effect on anterograde transport (Chiang et al., 2006; Yen et al., 2006).  Further examination of BBS in other transport models should reveal whether BBS functions more generally in cellular transport.

**A role for BBS in cell cycle regulation?**

Cilium formation and the cell cycle are intimately related processes. The anchor of the cilium to the cell membrane, the basal body, develops from the mother centriole of the centrosome.  The cilium and basal body are disassembled when cells enter the cell cycle, thereby allowing the centriole to organize the mitotic spindle; once the cell cycle ends, the mother centriole forms the basal body, and the cilium is re-assembled (Michaud and Yoder, 2006; Quarmby and Parker, 2005).  Several IFT components have been

implicated in cell cycle regulation consistent with the idea that the development of cilia and regulation of the cell cycle are interrelated processes. For example, loss of IFT88/polaris/*osm-5*, a key IFT-B complex protein, induces cell cycle progression (Robert et al., 2007); conversely, depletion of IFT27 results in multinucleate cells and a lengthening of the cell cycle (Qin et al., 2007).

Some studies have suggested that in addition to a cilia function, BBS proteins may also be involved in cell division. Localization and loss-of-function studies similarly implicate BBS proteins in cell cycle regulation. In HeLa cells, BBS4 recruits pericentriolar material 1 protein (PCM1) to centriolar satellites—poorly characterized, PCM1-containing, electron-dense granules surrounding centrosomes (Kubo and Tsukita, 2003)—and is required for the establishment of the microtubule organizing center; BBS6 in COS-7 cells has also been found to localize to centrosomes (Kim et al., 2004; Kim et al., 2005). Furthermore, *BBS4*-depleted HeLa cells and *BBS6*-depleted COS cells fail to undergo cell division and often contain more than one nucleus and centrosome (Kim et al., 2004). Thus, these studies in cultures of non-ciliated cells suggest that BBS has a role in cell cycle.

However, another study proposes a different model. In retinal pigmented epithelial (RPE) cells, BBS4 localizes to the centriolar satellites in non-ciliated cells but is found predominantly in the cilium in ciliated cells (Nachury et al., 2007). Additional analyses revealed that BBS4 only transiently interacts with PCM1, and that depleting *BBS1* or *BBS5* does not affect several markers of centrosome function. Depletion of *BBS1* also failed to have an effect on cell cycle exit (Nachury et al., 2007). These results suggest that the centriolar satellites transport BBS proteins to the base of the cilium

where BBS proteins disassociate and carry out their functions at the basal body or in the cilia (Nachury et al., 2007).  Differences in the findings between the studies may be a consequence of the cell type or the BBS gene that is depleted.  Certainly, these results merit further study into the role of BBS in the cell cycle.

**Table 4-1.  Currently known *BBS* genes**

| Gene | Domain | Function | References | *C. elegans BLAST homology e-value* |
|------|--------|----------|------------|-------------------------------------|
| *BBS1* | None | Cilia Function | (Kulaga et al., 2004; Nachury et al., 2007) | 7e-70 |
| *BBS2* | None | Cilia Function/ Flagellum Formation | (Nishimura et al., 2004) | 2e-94 |
| *BBS3/ ARL6* | GTP-binding | Vesicle trafficking | (Fan et al., 2004) | 3e-42 |
| *BBS4* | TPR /PilF | Microtubule transport | (Kim et al., 2004) | 9e-56 |
| *BBS5* | DM16 DUF1448 | Cilia function/ Flagellum formation | (Li et al., 2004a) | 1e-87 |
| *BBS6* | Type II Chaperonin | Cilia function/ Flagellum formation | (Fath et al., 2005; Kim et al., 2005) | None |
| *BBS7* | TPR/PilF | IFT particle assembly | (Blacque et al., 2004) | 7e-112 |
| *BBS8* | TPR/PilF | IFT particle assembly | (Blacque et al., 2004) | 9e-118 |
| *BBS9* | C0G1361 membrane biogenesis | Unknown | (Nishimura et al., 2005) | 2e-25 |
| *BBS10* | Type II Chaperonin | Unknown | (Stoetzel et al., 2006) | None |
| *BBS11/ TRIM32* | RING WD40 NHL Bamotin B-Box | E3 Ubiquitin Ligase | (Chiang et al., 2006) | None |
| *BBS12* | Type II Chaperonin | Unknown | (Stoetzel et al., 2007) | None |

Abbreviations: TPR: Tetratricopeptide Repeats; PilF: Tfp pilus assembly protein (cell motility/ intracellular trafficking); DM16: Repeat domains; Adapted from Tobin & Beales (2007)

**Table 4-1.  Currently known *BBS* genes**
Genes were originally identified in humans.  Evidence for function comes from studies in mice, zebrafish, and *C. elegans.*  Very little is known about the functions of the more recently identified *BBS9-BBS12*.   The *H. sapiens* BBS protein was used to determine the *C. elegans* BLAST homology e-value.

**Functional categorization of BBS genes**

Several studies of BBS highlight a categorization of BBS genes based on function and the degree of conservation of the BBS genes (Nachury et al., 2007; Stoetzel et al., 2006; Stoetzel et al., 2007; Tobin and Beales, 2007). Biochemical characterization by Nachury and colleagues suggests that a core group of the most highly conserved BBS genes function together as a complex in transport, while BBS3 modifies their activity (Nachury et al., 2007). The chaperonins (BBS6, BBS10, BBS12), a class of chaperones, comprise a separate, more recently evolved collection of BBS genes (Stoetzel et al., 2006; Stoetzel et al., 2007).

*The most highly conserved BBS genes*

Nachury and colleagues found that seven BBS proteins co-fractionate together in stoichiometric proportions, consist with the formation of a stable heptameric complex that they termed the "BBSome" (Nachury et al., 2007). These seven BBS proteins are amongst the eight most conserved BBS proteins, including BBS1, BBS2, BBS4, BBS5, BBS7, BBS8, and BBS9. BBS9 strongly interacts with BBS8 and moderately interacts with BBS1, BBS2, BBS4, and BBS5, indicating that BBS9 may be the central organizing subunit of the BBSome (Nachury et al., 2007). In worms, based on IFT assays, BBS proteins have also been proposed to act as a complex: a defect in one of the BBS proteins prevents the other BBS proteins from properly assembling a complex and entering the cilium (Nachury et al., 2007; Ou et al., 2007). Phenotypic analysis supports the idea that BBS proteins act in a complex. Single, double and triple *bbs* mutants have similar defects in trafficking and similarly shortened cilia. In addition, mutations in *bbs-7* or -*bbs-8* results in similar chemotaxis defects (Mak et al., 2006; Ou et al., 2005; Ou et al.,

2007).  Finally, the fact that diverse mutations in *BBS* genes in humans cause the same pleiotropic symptoms is also consistent with a function for different BBS proteins in the same process.

BBS3, the eighth conserved BBS gene, encodes for ADP-ribosylation factor-like 6 (ARL6; Chiang et al., 2004).  ARL6, which is clearly separated from the BBSome in co-fractionation experiments, may modify the activity of the BBSome (Nachury et al., 2007).  ARL6 is expressed in ciliated neurons in *C. elegans* and also undergoes IFT (Fan et al., 2004).

*Vertebrate-conserved BBS genes*

Three *BBS* genes *BBS6*, *BBS10*, and *BBS12* belong to the type II chaperonin family; taken together, mutations in these three genes account for approximately one-third of the mutational load of BBS patients (Stoetzel et al., 2007).  Similar to *Bbs2-/-* and *Bbs4-/-* mice, *Bbs6-/-* mutant mice develop obesity and retinal degeneration, and sperm fail to form flagella (Fath et al., 2005).  Unlike the other *BBS* genes, the chaperonins form a vertebrate-specific branch of BBS (or possibly chordate-specific for BBS6) and are rapidly evolving (Kim et al., 2005; Stoetzel et al., 2007).  The BBS chaperonins are likely to perform redundant functions.  Injection of morpholinos (MOs) against *bbs6*, *bbs10* or *bbs12* in zebrafish embryos resulted in subtle phenotypes in less than 20 percent of embryos that include shortened body axis, broadened somites, kinked notochord and dorsal thinning.  Injection of morpholinos against two or three of the *bbs* chaperonins caused a substantial increase in the proportion of affected embryos.  Coinjection of all three MOs resulted in an extremely severe phenotype in which more than 90 percent of embryos were affected (Stoetzel et al., 2006; Stoetzel et al., 2007).

BBS11, also vertebrate-specific, encodes for Tripartite Motif-Containing Protein (TRIM) 32 E3 ubiquitin ligase and is the only BBS to be implicated in the ubiquitination/proteasome system (Chiang et al., 2006).

**BBS and energy metabolism**

Of the many BBS symptoms detailed above, the experiments in my thesis focus on obesity and altered metabolism. Truncal obesity is one of the defining features of BBS and causes complications such as diabetes and hypertension (Beales et al., 1999; Tobin and Beales, 2007). Although birth weight is usually normal, weight gain often begins in childhood; hyperphagia rather than a reduction in metabolic activity is likely to contribute to obesity (Grace et al., 2003). Murine BBS models recapitulate the obesity phenotype: they are born underweight but by 8-12 weeks are of similar weight to their wild-type littermates and continue to gain weight (Fath et al., 2005; Mykytyn et al., 2004; Nishimura et al., 2004). The weight gain, associated with increased centrally deposited adipose tissue, is a consequence of hyperphagia (Fath et al., 2005; Mykytyn et al., 2004; Nishimura et al., 2004). In addition, the lower activity level of *Bbs6-/-* mice likely contributes to excess energy storage. These mutant mice display physiological changes associated with weight gain, including elevated leptin levels and blood pressure (Fath et al., 2005; Mykytyn et al., 2004; Nishimura et al., 2004). *BBS* also plays a role energy metabolism in other organisms. In *C. elegans, bbs-1* mutations cause a modest increase in fat stores and interact genetically with *kat-1*, an intestinal thiolase involved in the breakdown of fats, to cause an aggravated increase in fat. Altered fat storage in *bbs-1* mutants has been proposed to be a consequence of a general defect in cilia (Mak et al., 2006).

In the second half of this chapter, I explore energy metabolism in *bbs* mutant worms. The examined *bbs* mutations function in the same pathway to increase fat stores, supporting the notion that BBS proteins in the worm function in a complex. I also seek to determine whether changes in fat content in *bbs* mutants can be explained by changes in various measures of energy intake and expenditure. Finally, I examine whether the increase in fat seen in *bbs* mutants can be attributed to a general cilia defect. Surprisingly, many cilia mutants do not display a similar change in fat levels. I further explore this finding through a series of genetic experiments and find that *bbs* cooperates with other IFT genes to regulate lipid accumulation.

**Results**

Here, I examine the role of *bbs* and other cilia genes in intestinal fat storage in *C. elegans.* Eight of the *bbs* genes are highly conserved in *C. elegans* (see Table 4-1). Although worms do not have adipose tissue, fat is stored predominantly in the intestine and the hypodermis. In these studies, I relied on the lipophilic dye Nile Red that the worms ingest together with their bacterial food source. The dye fluoresces only in a hydrophobic environment, and thus provides a sensitive assay *in vivo* for the detection of intestinal lipids (Ashrafi et al., 2003).

### *bbs* **genes act in the same genetic pathway to regulate fat content**

To determine whether *bbs* genes have a conserved role in fat storage in *C. elegans*, I used Nile Red to examine the fat content of *bbs* mutants. Single mutations in *bbs-1, bbs-7, bbs-8*, and *bbs-9* genes increase fat to a similar extent (30-40% greater than wild-type; Figure 4-1A & B; data not shown; Mak et al., 2006). Given that BBS proteins function in a single complex consisting of BBS-1, BBS-2, BBS-3, BBS-5, BBS-7 & BBS-8 (Ou et al., 2007), I hypothesized that *bbs* genes act in the same pathway to affect fat. As expected, double and triple *bbs* mutants show an increase in fat content similar to single *bbs* mutants (Figure 4-1A & B). Unexpectedly, triple mutants are slightly smaller and more developmentally delayed than the single and double mutants. Thus, *bbs-1, bbs-7,* and *bbs-8* act in the same genetic pathway to affect intestinal fat storage in the worm. [1]

### **Physiology of *bbs* mutants**

---

[1]Because thus far the *bbs* genes have only been shown to act in a complex in *C. elegans* and no difference in function has yet been assigned to the different *bbs* genes, rather than referring to a specific *bbs* gene, I refer to the group of *bbs* genes as a single entity, except when talking explicitly about an experiment.

*Energy intake and energy expenditure*

To better understand whether behavioral defects may provide an obvious explanation for increased metabolic storage in these mutants, I analyzed two aspects of energy intake and expenditure. *C. elegans* feeds constitutively by pumping its muscular pharynx. Feeding rate can be assayed by counting contractions of the pharynx. The pumping rates of *bbs-7* & *bbs-8* mutants are similar to that of wild-type worms (Figure 4-1C); similarly, another study also reported wild-type feeding rates for *bbs-1* mutants (Mak et al., 2006).

Energetically expensive, egg production is one of the main ways that organisms expend energy. In worms, egg-laying is modulated by a variety of environmental and sensory cues, such as the abundance of food (Schafer, 2005). Increased fat storage in *bbs* mutants, which have sensory defects, may be a consequence of decreased energy utilization due to changes in egg-laying. Thus, I also examined egg-laying in *bbs-7* mutants and found that they laid similar numbers of eggs to wild-type worms over a period of five days (Figure 4-1D; data not shown).

*Transcriptional levels of metabolic genes*

A shift in metabolism may occur as a result of changes in activity levels or food intake, changes in signaling molecules that regulate energy levels, or changes in activity of core metabolic enzymes. One way to alter the activity of core metabolic enzymes is to change their expression. Changes in fat content in some mutants have been linked to altered transcriptional levels of metabolic genes (Van Gilst et al., 2005a; Van Gilst et al., 2005b). For example, mutations in *nhr-49*, the homolog of mammalian hepatocyte nuclear factor 4, cause increased lipid storage due to reduced expression of β-oxidation genes that

break down fat.  Similarly, increased fat content in *bbs* mutant worms may be a consequence of increased expression of fatty acid synthesis genes or decreased expression of fatty-acid β-oxidation genes. Van Gilst developed a real-time PCR assay, which detects expression levels of 150 genes that include core components of gluconeogenesis, glycolysis, glucose transport, the glyoxylate pathway, fatty acid synthesis, desaturation and elongation, beta oxidation and fatty acid binding and transport (Van Gilst et al., 2005a; Van Gilst et al., 2005b).  I examined *bbs-7*, *bbs-8* single mutant worms and *bbs-1; bbs-7; bbs-8* triple mutant worms at the L4 stage and found no changes in gene expression that were above threshold (2-fold; see Appendix Table 2-1 for identities of genes examined).

However, because the increase in fat content in *bbs-7* mutants is much greater on the first day of adulthood (72 hours), transcriptional changes may only appear in adulthood. Extracting RNA from adult hermaphrodites is confounded by the presence of embryonic RNA.  To avoid RNA contamination from embryos, I crossed *bbs-7(n1606)* into a temperature-sensitive sterile strain *glp-4(bn2)* and examined the double mutant at 80 hours, when *bbs-7(n1606)* mutants display a robust increase in fat.  As expected, at the restrictive temperature, the *glp-4(bn2); bbs-7(n1606)* double mutant displayed an increase in fat compared to *glp-4(bn2)* single mutants.  However, again I found no difference in transcription of genes involved in metabolism.  Therefore, the fat phenotype of *bbs* mutants cannot be explained by large transcriptional changes in any single metabolic gene. However, this does not rule out the possibility of post-transcriptional changes, small changes below the level of detection, or small, cumulative changes over time in a gene's transcription that may affect fat storage.

**The role of other cilia components in fat storage**

The BBS proteins are essential components of the IFT machinery, and *bbs* defects

cause improperly formed cilia. Therefore, increased fat storage is likely a consequence

of a general cilia defect, as suggested by Mak and colleagues (Mak et al., 2006). To test

this hypothesis, I took advantage of a plethora of worm cilia mutants that have cilia

defects, including aberrations in core components of the IFT machinery such as the

motors and IFT complexes. These mutants have been identified through screens for

behaviors that are dependent on intact cilia, such as *che* (abnormal <u>che</u>motaxis), *osm*

(abnormal <u>osm</u>otic avoidance) and *odr* (abnormal <u>od</u>orant <u>r</u>esponse) mutants (Bargmann

et al., 1993; Culotti and Russell, 1978; Dusenbery et al., 1975). Other *dyf* (<u>dy</u>e-<u>f</u>illing

defective) mutants have been identified in screens for abnormal cilia formation (Starich et

al., 1995).

I examined several mutants in core cilia motor components, including the

heterotrimeric kinesin-II, OSM-3 homodimeric kinesin, and dynein. Surprisingly, none

of the mutants displayed the robust increase in fat observed in *bbs* mutants. *osm-3(p802)*

mutants, which have stumpy cilia, have mildly increased fat (Figure 4-3A & B; Table

4-2); this phenotype is variable. In contrast, mutants in the heterotrimeric motor,

*klp-11(tm324)* and *kap-1(ok676)*, and dynein *che-3(e1124),* have a wild-type fat

phenotype (Figure 4-2 and 4-3). This suggests that altering IFT does not affect fat

content.

I also examined the fat phenotypes of mutants with defects in the IFT machinery.

Again, only a few mutants exhibited notable fat phenotypes. Mutations in *dyf-5(mn400)*,

a kinase that participates in regulation of the anterograde motors (Burghoorn et al., 2007),

cause a robust increase in fat stores, similar to *bbs* mutants (Figure 4-4). *che-2(e1033)*

mutants, possessing a defect in the core IFT-B component IFT80, also presented with a mild to moderate increase in fat storage from 15 to 30% increase (compare Figure 4-2 and Figure 4-4 A & B). In contrast, *osm-6(p811)*, a mutant in the core IFT-B component IFT52, consistently had wild-type levels of fat similar to *osm-1(p808)*, another IFT-B mutant with a defect in IFT172 (Figure 4-2). Alterations in the IFT-A component CHE-11/IFT140 were also associated with wild-type levels of fat (Figure 4-2). However, *daf-10(p821)* and *daf-10(e1387)* mutants, with defects in the IFT-A component IFT122, have lower fat content (Appendix Figure 2-1). Of note, *bbs* and *dyf-5* Nile Red phenotypes were rarely very variable, but the degree of increase of Nile Red staining in *che-2(e1033)* and *osm-3(p802)* varied between independent experimental trials from a subtle increase in fluorescence to increases similar to that observed in *bbs* mutants. However, within a single trial, the phenotype was reasonably consistent. This variability may be a consequence of sensory deficits in cilia mutants that increases their sensitivity to unidentified environmental factors.

In addition to mutants in core cilia machinery, I analyzed the fat phenotype of other mutants with a defect in cilia structure or function. These include other mutants identified in *che, osm, odr,* and *dyf* screens. A few mutants have defects in the amphid sheath needed for the development and maintenance of cilia. Some have mutations in receptors, channels, and signaling proteins needed for the function of ciliated neurons. For others, the ciliary function of the mutated gene is still undefined. The majority of these mutants demonstrate wild-type fat levels (Table 4-2; Figure 4-6). Taken together, these results suggest that altered fat storage in *bbs* mutants is not simply a consequence of ciliary dysfunction.

**Table 4-2. Fat phenotypes of cilia mutants**

| Gene | Description | Fat phenotype | Gene | Description | Fat phenotype |
|---|---|---|---|---|---|
| **WT** | | 0 | **Amphid sheath** | | |
| **Anterograde Transport Motors** | | | che-12 | uncloned | 0 |
| osm-3 | homodimeric kinesin | + | daf-6 | Patched-related protein | +/- |
| kap-1 | heterotrimeric kinesin | 0 | **Other cilia genes** | | |
| klp-11 | heterotrimeric kinesin | 0 | unc-101 | AP-1 complex subunit mu-1 | 0 |
| dyf-1 | Activates osm-3 | 0 | dyf-4 | uncloned | 0 |
| **Retrograde Transport Motors** | | | dyf-7 | uncloned | 0 |
| che-3 | dynein heavy chain 1b | 0 | dyf-8 | uncharacterized | 0 |
| xbx-1 | dynein light chain | 0 | dyf-9 | uncloned | 0 |
| xbx-2 | dynein light chain | 0 | dyf-10 | uncloned | 0 |
| **IFT-A** | | | dyf-12 | uncloned | 0 |
| che-11 | IFT140 | 0 | odr-2 | Ly6 | 0 |
| daf-10/ osm-4 | IFT122 | - | odr-5 | uncloned | 0 |
| **IFT-B** | | | odr-6 | uncloned | 0 |
| che-2 | IFT80 | + | che-5 | uncloned | 0 |
| che-13/ che-9 | IFT57/Hippi | 0 | che-7 | uncloned | 0 |
| osm-1 | IFT172 | 0 | che-10 | uncloned | 0 |
| osm-5 | IFT88 | 0 | xbx-3 | uncharacterized | 0 |
| osm-6 | IFT52 | 0 | xbx-4 | | 0 |
| dyf-3 | Qilin | 0 | xbx-7 | Meckel syndrome type protein | 0 |
| F32A6.2 | IFT81 | + | osm-10 | novel | 0 |
| **IFT components** | | | nph-1 | Nephrocystin-1 | 0 |
| dyf-2 | WDR19 | 0 | nph-4 | Nephrocystin-4 | 0 |
| dyf-5 | kinase | ++ | odr-8 | uncloned | 0 |
| dyf-6 | uncharacterized | 0 | **Channels/receptors** | | |
| dyf-13 | uncharacterized | 0 | osm-9 | TRPV channel | 0 |
| bbs-1 | BBS | ++ | odr-1 | Guanylyl cyclase | 0 |
| bbs-5 | BBS | ++ | odr-3 | Gα protein | 0 |
| bbs-7 | BBS | ++ | odr-7 | Nuclear receptor | 0 |
| bbs-8 | BBS | ++ | odr-10 | 7TM receptor | 0 |
| bbs-9 | BBS | ++ | ocr-1 | TRPV channel | 0 |
| **Transcription Factors** | | | ocr-2 | TRPV channel | 0 |
| che-1 | C2H2-type Zn finger transcription factor | 0 | tax-2 | cGMP channel | 0 |
| alr-1 | homeodomain transcription factor | + | tax-4 | cGMP channel | 0 |
| ttx-1 | homeodomain transcription factor | 0 | str-182 | 7TM receptor | 0 |

0 = wild-type Nile Red fluorescence, + = 0-30% increase in Nile Red staining, ++ = 30-50% increase in Nile Red staining; uncharacterized = gene is cloned, but function/homologs are undefined. TRP = Transient Receptor Potential Vanilloid channel; TM = TransMembrane; AP = Adaptor Protein complex

**Interactions between *bbs* and other IFT components**

Do *bbs* genes act in the same genetic pathway as other IFT components to affect fat? I examined the phenotypes of double mutants with defects in *bbs* and in the core cilia machinery. If *bbs* works independently of cilia transport, then double mutants will exhibit an increase in fat that is greater than single mutants.[2] Because the fat phenotypes of *bbs-7(n1606)* and *bbs-8(nx77)* are similar and the two genes are thought to function together in a complex, I used *bbs-7(n1606)* and *bbs-8(nx77)* interchangeably in these experiments.

I first examined the effects of double mutations in *bbs* and various motor components. Mutations in the homodimeric kinesin *osm-3*, needed for transport within the entire cilium, cause a mild to moderate increase in fat. *bbs-8(nx77); osm-3(p802)* double mutants have excessive fat stores similar to that of single *bbs-8* mutants (Figure 4-4 A & B). I also examined the interaction between *bbs* and mutants in the heterotrimeric kinesin II complex, including *kap-1(ok676)* and *klp-11(tm324)*, which have wild-type fat stores. In *kap-1(ok676)* and *klp-11(tm324)* single and double mutants, anterograde transport remains relatively unaffected, and the length of cilia is wild-type. Fat content in the *bbs-7(n1606); klp-11(tm324)* double mutant is similar to that in *bbs-7(n1606)*, suggesting that *klp-11* is dispensable for altered fat content in *bbs-7* mutants (Figure 4-4 C & D).

By contrast, the *kap-1(ok676); bbs-8(nx77)* double mutant unexpectedly was lower in fat content than wild-type and *kap-1(ok676)* mutant worms (Figure 3A and B).

---

[2] *bbs* mutants display only a moderate increase in fat. Several mutants have been isolated that exhibit much greater Nile Red staining (Ashrafi lab, unpublished data). Thus, Nile Red fluorescence of *bbs-7* mutants is within the dynamic range of detection, and observation of an enhancement of Nile Red in *bbs* mutants is possible.

Also, although these worms were relatively normal in terms of development and size, they moved very slowly and intermittently, and their sinusoidal posture was flattened.  It is unlikely that these movement defects can explain the low-fat phenotype; examination of fat content of mutants with altered movement, such as <u>uncoordinated</u> (*unc*) mutants, has revealed that there is no correlation between movement and fat storage in worms (Ashrafi lab, unpublished data).  Although additional analyses are warranted to ensure that these animals do not display reduced fat content due to general malaise, this data suggests that the *kap-1* functions downstream of *bbs-8* to regulate fat content

To further determine whether *bbs* act in the same pathway as other cilia mutants to affect fat, I examined the effect of double mutations between *bbs* and two cilia mutants that have fat phenotypes.  *dyf-5(mn400)* mutants also have a moderate increase in fat similar to *bbs-8(nx77)* worms.   DYF-5 is required for intact motility of OSM-3 kinesin and for OSM-3 to associate with other IFT components (Burghoorn et al., 2007).  In *dyf-5* and *bbs-8* mutants, the IFT machinery is no longer intact and the motors no longer travel at wild-type speeds.  These aberrations may contribute to the increased fat storage phenotype.  Although the animals are extremely small, *dyf-5(mn400)*; *bbs-8(nx77)* double mutants have similar fat content to single mutants, thus suggesting that these *dyf-5* and *bbs-8* act in the same genetic pathway to regulate fat storage (Figure 4-4A & B).

Mutations in *che-2*, which encodes the peripheral IFT-B complex particle IFT-80, causes a mild increase in fat.  Similarly, fat storage in *che-2(e1033); bbs-8(nx77)* double mutants is similar to *bbs-8(nx77)* worms but is slightly more variable (Figure 4-4A & B).  Thus, these experiments suggest that *bbs*-8 acts in the same genetic pathway as *che-2* and *dyf-5* to affect fat.

**Mutations in the ciliogenic transcription factor *daf-19* cause increased fat content**

To further test the hypothesis that abrogation of cilia function causes increased fat storage, I examined a mutant that has no cilia. The *daf-19* regulatory transcription factor (RFX) regulates the expression of genes that control ciliogenesis, and accordingly, the cilia of *daf-19* mutants do not extend beyond the transition zone (Swoboda et al., 2000). Studying the effects of *daf-19* mutations is complicated by the fact that *daf-19* mutants are constitutive dauers, an alternative larval state characterized by morphological changes such as increased fat stores. However, mutations in *daf-12*, a steroid hormone receptor downstream of dauer regulatory pathways, completely suppress the dauer phenotype and have no effect on fat storage. I analyzed fat levels in *daf-19(m86); daf-12(sa204)* using Sudan Black[3] and found that *daf-19(m86); daf-12(sa204)* have much higher fat content than wild-type animals (Figure 4-5). Therefore, this result suggests that complete disruption of cilia causes increased fat storage.

However, an alternative possibility is that a defect in *daf-19* causes increased fat through its interaction with the dauer pathway. Dauers store additional fat to survive periods of starvation, and many constitutive dauer mutants retain excess fat. For example, Sudan Black staining of *daf-2* insulin receptor mutants and *daf-7* TGF-β mutants reveals a similar, robust increase in fat (Ashrafi et al., 2003; Kimura et al., 1997; Ogg et al., 1997). Four CSNs (ADF, ASG, ASI, ASJ) regulate dauer development (Bargmann and Horvitz, 1991b); the *daf-19* constitutive dauer phenotype is likely due to morphological defects in the cilia of these CSNs (Swoboda et al., 2000). Thus, daf-*19;*

---

[3] Fat storage cannot be assayed by Nile Red in *daf-19* mutants, as in many other constitutive dauer mutants, likely due to an uptake defect of the dye (Ashrafi, K. 2007) ; instead, fat storage can be assayed by a method involving fixation and staining with the fat-soluble dye Sudan Black, which stains lipids blue-black.

*daf-12* mutants may store greater amounts of fat due to the effects of *daf-19* on dauer pathways. It may be possible to separate the effects of *daf-19* on anatomy and signaling by rescuing *daf-19* in the four CSNs that control dauer development and assaying fat in rescued mutants. Therefore, whether *daf-19; daf-12* mutants have increased fat levels because a core cilia process has been affected or because of effects on the dauer pathway is unclear.

**Discussion**

As in mammals, mutations in *bbs* in *C. elegans* cause excess fat storage. The result that single, double and triple *bbs* mutants showed similar increases in lipid content suggests that *C. elegans bbs* genes act in the same pathway to affect fat. This is consistent with the finding in *C. elegans* and mammals that BBS proteins act in a single complex (Nachury et al., 2007; Ou et al., 2007), and that diverse *BBS* mutations in other organisms cause similar phenotypes, including obesity. These changes in fat storage cannot be explained by changes in pharyngeal pumping rate or egg-laying. In addition, large gene expression changes in any of the examined metabolic genes cannot account for the fat phenotype of *bbs* mutants.

Much further exploration of metabolism in *bbs* is warranted. Pumping rates are similar to wild-type; because pumping correlates with intestinal filling in wild-type worms (Avery and Horvitz, 1990), this suggests that *bbs* mutants consume a similar quantity of food to wild-type worms. However, it is formally possible that *bbs* mutants may consume more food. This hypothesis can be tested in a food-consumption assay, in which the amount of time required for a specified quantity of food to be eaten is measured. Similarly, assaying defecation rates would reveal whether *bbs* mutant worms

retain food excessively. Food consumption and elimination rates could also be determined by measuring the amount of time it takes for the intestine to fill with and expel fluorescently labeled bacteria. Additionally, although the real-time PCR assay failed to reveal changes in expression levels of genes that regulate fatty acid synthesis, fatty acid synthesis in *bbs* mutants may be increased through non-transcriptional means. A recently developed approach employs mass spectrometry in combination with $^{13}$C-labeled bacteria to detect the quantity of dietary and *de novo* synthesized fatty acids in worm lipids. The approach has revealed a substantial increase in *de novo* fatty acid synthesis in *daf-2* mutants, which have increased fat stores (Perez and Van Gilst, 2007). Similarly, *de novo* fatty acid synthesis may be increased in *bbs* mutants worms. Finally, oxygen consumption assays, a measure of metabolic rate, may reveal energy utilization defects in *bbs* mutants worms.

A simple explanation for the excess lipid accumulation in *bbs* mutants is that the effects of *bbs* are a consequence of a general defect in cilia. Contrary to this hypothesis, I found that the increased fat storage in *bbs* mutants is not common to all cilia mutants. In a comprehensive examination of mutants with defects in IFT motors, IFT complex components, other cilia structural aberrations, and alterations in receptors and channels in ciliated neurons, I found that only a few had notably altered fat stores (Table 4-2; Figure 4-2 and 4-6). Many of the mutants used in this study are well-characterized mutants that have been reported to have cilia structural defects or defects in sensory behaviors dependent on intact cilia (e.g. Collet et al., 1998; Haycraft et al., 2003; Perkins et al., 1986; Signor et al., 1999b).

Examination of the fat phenotypes of *osm-3* and *IFT-B* mutants uncovered an interesting pattern of phenotypes. OSM-3, which mediates anterograde transport in the middle and distal segments, and the IFT-B complex are required for normal anterograde motility and for building the distal segment. Defects in homodimeric OSM-3 kinesin and the peripheral IFT-B component CHE-2 cause a mild increase in fat. However, interestingly, aberrations in other IFT-B components, such as OSM-1, OSM-5 or OSM-6, that are also required to build the distal segment, failed to alter lipid content. This suggests that the fat phenotypes of *che-2* or *osm-3* mutants are not simply due to the lack of a distal segment or the absence of an intact IFT-B particle. Moreover, no further fat increase was observed in *osm-3; bbs-8* and *bbs-8; che-2* double mutants, indicating *bbs* works in the same pathway as *osm-3* and *che-2* to regulate fat (Figure 4-3 and 4-6).

Does this suggest that IFT-B complex and OSM-3 have a specific role in the regulation of fat possibly through their effects on BBS? Several experiments may shed light on this hypothesis. The absence of CHE-2, a peripheral IFT-B protein, or OSM-3 may affect the ability of BBS to associate with the IFT particles and motors; how BBS proteins attach to the IFT complexes is completely unknown. Examination of the localization and transport of BBS in *che-2* and *osm-3* mutants would reveal the relationship between BBS and these two IFT components. Furthermore, epistasis analyses between *bbs* and other *IFT-B* mutants that have a wild-type fat phenotype, such as *osm-6,* may provide further insight into how BBS affects lipid stores through IFT. For example, if *osm-6* suppresses the fat increase in *bbs* mutants, then *bbs* may be dependent upon signaling through the IFT-B complex to regulate metabolic homeostasis.

Analysis of the heterotrimeric kinesin-II and IFT-A complex revealed further interesting phenotypes. Aberrations in heterotrimeric kinesin-II, which cooperates with OSM-3 to build the middle segment, and the IFT-A subcomplex have only subtle effects on anterograde trafficking, and do not affect cilium length. Mutations in the heterotrimeric kinesin-II components KAP-1 and KLP-11 and the IFT-A component CHE-11 do not affect fat. By contrast, the IFT-A complex mutant *daf-10* has reduced fat. Moreover, the most surprising result was the reduced lipid content of *kap-1*; *bbs-8* mutants, indicating that *kap-1* functions downstream of *bbs* (Figure 4-3 and 4-6). Do these findings indicate that an intact KAP-1/IFT-A complex is needed for the transport or assembly of fat stimulatory signals? This hypothesis could be tested by examining the fat phenotype of *bbs-8; daf-10* double mutants; I predict that these mutants would decrease fat storage, similar to *daf-10* mutants due to the absence of an intact IFT-A particle. Similarly, double mutants between *daf-10* and other IFT-B components would also have reduced lipid content.

Another possibility is that the differences in phenotypes between *che-11* and *daf-10* mutants may be explained by different roles of these components in IFT-A assembly. In *kap-1;bbs-8* worms, GFP-tagged CHE-11 and GFP-tagged CHE-2, markers of IFT-A and IFT-B, respectively, are transported by OSM-3 (Pan et al., 2006), implying that the IFT-A complex is still being trafficked in these mutants. However, much further work is needed to confirm this notion. Whether the IFT-A complex assembles and traffics in the absence of DAF-10 or CHE-11 has not been tested. Analysis of the localization and movement of other IFT-A and IFT-B particles in *daf-10* or *che-11* mutants would clarify our understanding of how DAF-10 and CHE-11 participate in the assembly of the IFT machinery and also in the regulation of fat content. The localization and trafficking of

DAF-10 in a *bbs* mutant is also unknown. In *bbs* mutants, a different IFT-A particle, CHE-11, is proposed to be shuttled by the heterotrimeric kinesin-II based on the transport rates of GFP-tagged CHE-11 (Ou et al., 2005); whether DAF-10 is also shuttled by kinesin-II in *bbs* mutants awaits confirmation.

Retrograde transport, which is dependent upon the IFT-A complex (Piperno et al., 1998; Rosenbaum and Witman, 2002; Scholey, 2003), may be perturbed in *daf-10* mutants, consequently interrupting the recycling of proteins at the cilia tip. However, the reduction of lipids in *daf-10* mutants is unlikely to be due solely to its role in retrograde transport. Defects in CHE-3 (dynein heavy chain 1b) and XBX-1 (dynein light chain), which are required for retrograde transport in cilia do not affect fat (Figure 4-2 and 4-6; Table 4-2). Analysis of lipid content in *che-3*; *bbs-8* double mutants would provide further insight into the role of retrograde transport in altered fat content in *bbs* mutants.

Redundancy may partially explain the differences in phenotypes between different IFT-A and IFT-B mutants. The robust fat increase in *daf-19* mutants, which completely lack cilia, may be due to the effect of knocking out several IFT components (barring the caveat that *daf-19* has a role in the dauer pathway, as discussed above). It would be interesting to examine the fat content of IFT-A or IFT-B double or triple mutants. For example, a result that *osm-5*; *osm-6*; *osm-1* IFT-B triple mutants display increased fat levels similar to *bbs* mutants would suggest that redundancy plays a role in the absence of fat phenotypes in many of the cilia mutants.

*dyf-5* and *bbs* mutants have the most robust and consistent fat phenotypes of all of the cilia mutants. DYF-5 and BBS proteins coordinate the heterotrimeric kinesin-II and OSM-3 motors and their associated IFT particles to form a single cohesive IFT machine in

the middle segment; by stabilizing this machine, DYF-5 and BBS also regulate its speed (Burghoorn et al., 2007; Ou et al., 2005). In the absence of either BBS or DYF-5, the machine is no longer intact, and the motors do not operate as part of the same unit nor traffic at the appropriate speed. It is likely that this has diverse effects on the trafficking of various cilia structural components and signaling molecules. Thus, the robustness of the phenotype in *bbs* and *dyf-5* mutants may be a function of pleiotropic effects on the trafficking machinery.

My findings contrast those of Mak and colleagues who proposed that all cilia mutants have a fat storage defect, and changes in fat storage in *bbs* mutants is a consequence of a general cilia defect (Mak et al., 2006). However, Mak and colleagues only analyzed five cilia mutant strains: *che-2, osm-5, daf-6, tax-2,* and *tax-4*. Furthermore, in contrast to Mak et al. (Mak et al., 2006), I failed to find increased fat storage in *osm-5(p813)*, *tax-2(p691)*, and *tax-4(p678)* mutants (data not shown); *daf-6(e1377)* mutants were extremely variable, with individual worms showing either increased, wild-type, or decreased fat (data not shown).

Intriguingly, *kap-1; bbs-8* mutants have a unique slow movement phenotype. A wild-type hermaphrodite worm explores most of the plate and crawls in a sinusoidal pattern at an intermediate rate with occasional reversals. Although they move relatively normally, many cilia mutants exhibit a defect in exploratory behavior, and only move in one area of the plate. Casual observation revealed that the movement phenotype that characterizes *kap-1; bbs-8* double mutants is very distinct from that of other cilia mutants and wild-type worms. These worms crawl infrequently and very slowly with a flattened sinusoidal pattern. Quantitative analyses and controls, such as rescuing *kap-1* in the *kap-1*; *bbs-8*

double mutant, should be performed to ensure that this defect is not due to a background effect. However, it is tempting to speculate that movement defects may be an example of coordinate regulation of energy: *kap-1*; *bbs-8* have very low fat stores and may conserve energy by minimizing energy expenditure through movement. Measuring metabolic rate by oxygen consumption experiments and analyzing expression levels of metabolic genes by real-time PCR may provide further insight into how metabolism is altered in these mutants.

Notably, *bbs* is needed only in a subset of ciliated sensory neurons for its function in regulating fat levels. Expressing *bbs-1* in 15 of the 60 ciliated neurons using the *tax-4* promoter is sufficient to rescue the fat phenotype of *bbs-1(mg409)* mutants (Mak et al., 2006). BBS may participate in specific signaling pathways within these neurons via its role in IFT. Other cilia defects in cilia components, such as CHE-2 or DYF-5, may alter fat by affecting BBS or IFT pathways in these same neurons.

Finally, in light of recent studies implicating BBS in vesicular transport (Nachury et al., 2007), it is tempting to speculate that BBS affects the transport of specific vesicles or other signaling molecules that are involved in metabolic regulation. Analyses of *bbs* and genes involved in vesicular transport may provide further insight into this hypothesis. Hints may come from the finding that BBS-5, which contains a PH-like domain, binds phosphoinositidyl 3-phosphate, which has been linked to the endosomal trafficking pathway (Leroux, 2007; Nachury et al., 2007; Takai et al., 2001). The future challenge will be to identify which vesicular pathways are affected.

These data demonstrate that the fat phenotype of *bbs* mutants is not a consequence of interference with general cilia signaling. Rather, a more specific pathway involving BBS and other IFT components regulates lipid storage. Further experiments

may illuminate how BBS functions through IFT to regulate fat content.  Identifying

signaling molecules that participate in this pathway is of great interest.  In the next

chapter, I will attempt to identify interaction between *bbs* and other fat regulatory

pathways as well as ciliated-neuron specific molecules that interact with *bbs.*

**Figure 4-1**
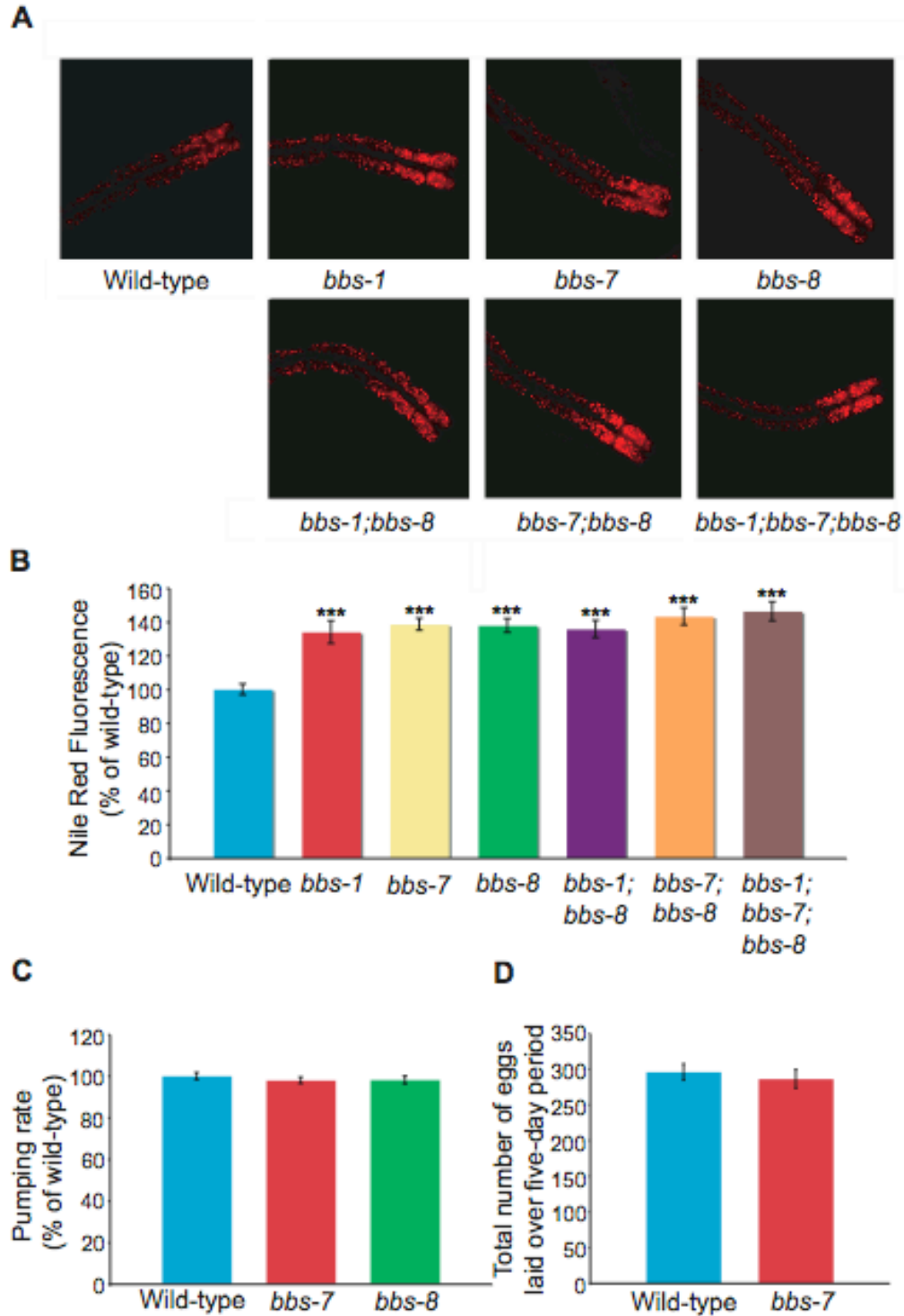
**Figure 4-1.** *bbs* **genes act in the same genetic pathway to increase fat content.**

(A) Single *bbs-1(ok1111)*, *bbs-7(n1606)*, and *bbs-8(nx77)* mutants, double

*bbs-1(ok1111)*; *bbs-8(nx77)* and *bbs-7(n1606)*; *bbs-8(nx77)* mutants, and triple

*bbs-1(ok1111)*; *bbs-7(n1606)*; *bbs-8(nx77)* mutants demonstrate a similar increase in fat.

(B) Quantitation of Nile Red fluorescence of *bbs* mutants. All comparisons are between

mutant and wild-type worms. None of the differences between the *bbs* mutants was

significant. *n*=12-19 worms for each genotype.

(C) *bbs-7* and *bbs-8* mutants exhibit wild-type pumping rates. *n*=11-15 worms for each

genotype. At least three trials for each genotype was conducted on separate days.

(D) *bbs-7* mutants (*n*=11) lay a wild-type (*n*=12) number of eggs.

*** $p < 0.01$ by t-test. Errors bars indicate Standard Error of the Mean.

# Figure 4-2



A

Wild-type    *bbs-7*    *osm-1*    *osm-6*

*che-2*    *che-3*    *che-11*

B

Nile Red Fluorescence (% of wild-type)

Wild-type   *bbs-7*   *che-2*   *che-3*   *osm-1*   *osm-6*   *che-11*
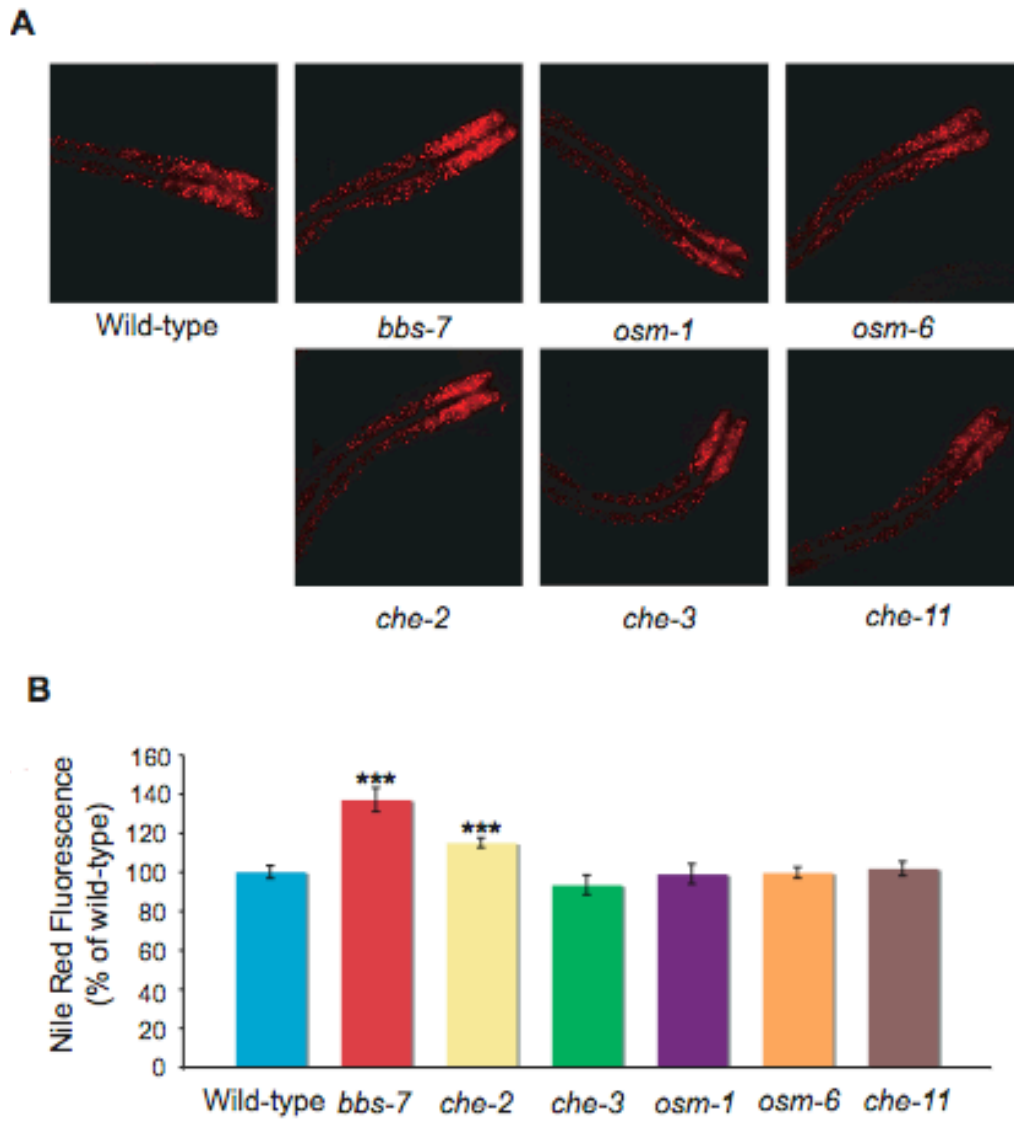
**Figure 4-2. Some cilia mutants have altered fat content.**

(A) The IFT-B mutant *che-2(e1033)* has increased fat content. In contrast, the dynein mutant *che-3(e1124)*, IFT-A complex mutant *che-11(e1810)*, and IFT-B mutants, *osm-1(p808)* and *osm-6(p811),* have wild-type levels of fat.

(B) Quantitation of cilia mutants. *n*=12-14 worms for each genotype. All comparisons are between mutant and wild-type worms.

* p<0.05 and *** p<0.01 by t-test. Errors bars indicate Standard Error of the Mean.

# Figure 4-3



**A**

Wild-type  osm-3  kap-1

bbs-8  osm-3;bbs-8  kap-1;bbs-8

**B**

Nile Red Fluorescence (% of wild-type)

Wild-type, bbs-8, osm-3, osm-3;bbs-8, kap-1, kap-1;bbs-8

**C**

Wild-type  klp-11

bbs-7  bbs-7;klp-11

**D**

Nile Red Fluorescence (% of wild-type)

Wild-type, klp-11, bbs-7, bbs-7;klp-11
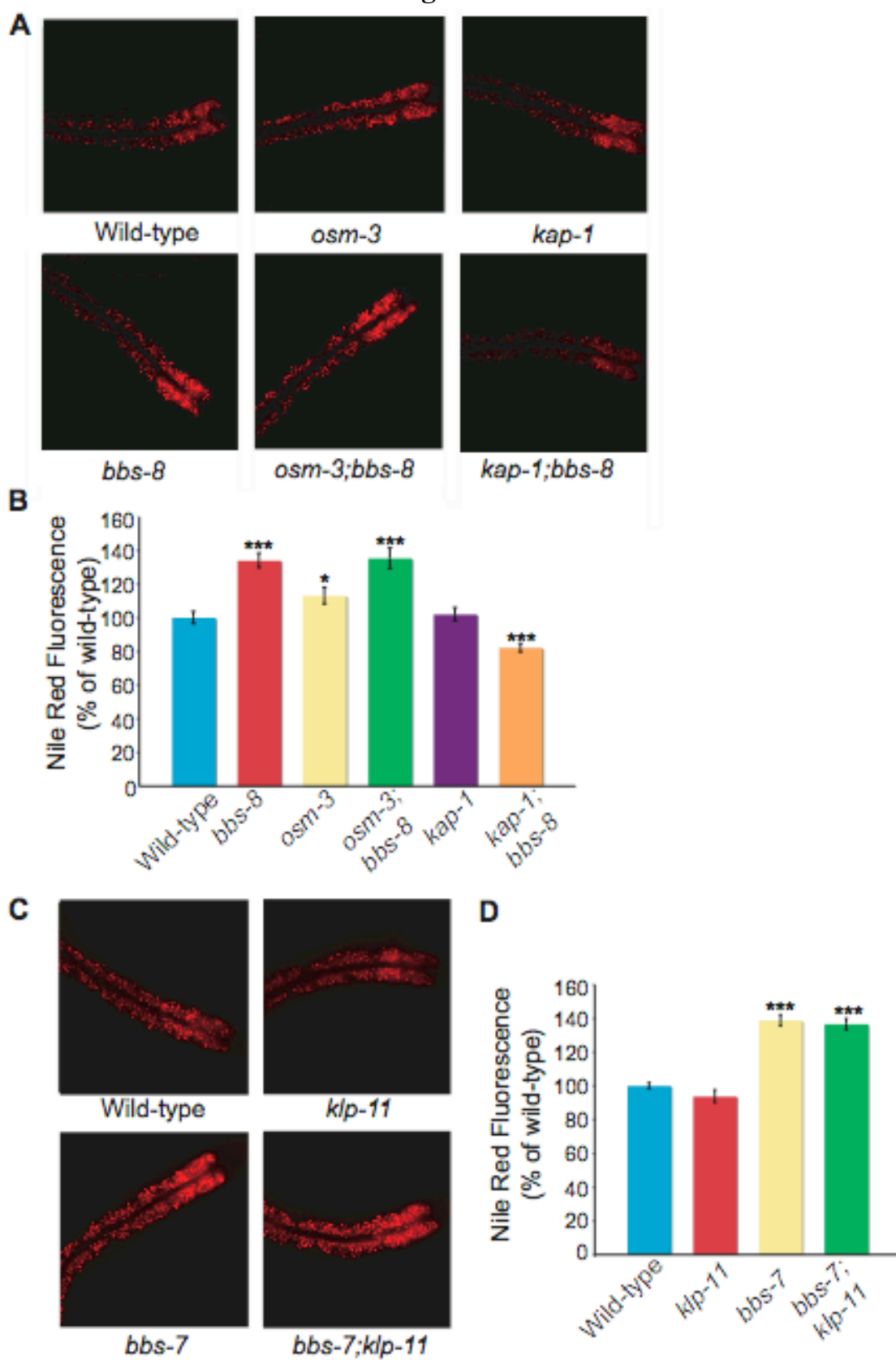
**Figure 4-3. Mutations in cilia motors interact with *bbs* to regulate fat content.**

(A) *osm-3(p802)*, a homodimeric kinesin motor mutant, has mildly increased fat content, and *kap-1(ok676),* a heterotrimeric kinesin mutant, has wild-type fat levels. The *osm-3(p802); bbs-8(nx77)* double mutant has high fat content , similar to that of *bbs-8(nx77)* mutants. *kap-1(ok676)*; *bbs-8(nx77)* mutants have reduced fat levels compared to wild-type, *bbs-8(nx77)* or *kap-1(ok676)* mutant worms.

(B) Quantitation of Nile Red fluorescence in *osm-3(p802); bbs-8(nx77)* and *kap-1(ok676)*; *bbs-8(nx77)*.  *n*=11-18 worms for each genotype.

(C) *bbs-7(n1606)* affects fat independently of *klp-11(tm324)*.  *klp-11(tm324)*, a heterotrimeric kinesin mutant, has wild-type fat content while fat content of *bbs-7(n1606); klp-11(tm324)* double mutants is similar to *bbs-7(n1606).*

 (D) Quantitation of Nile Red fluorescence in *bbs-7(n1606); klp-11(tm324)*. *n*=11-18 worms for each genotype.

All comparisons are between mutant and wild-type worms except where indicated.

* $p < 0.05$ and  *** $p < 0.01$ by t-test.  Errors bars indicate Standard Error of the Mean.

**Figure 4-4**
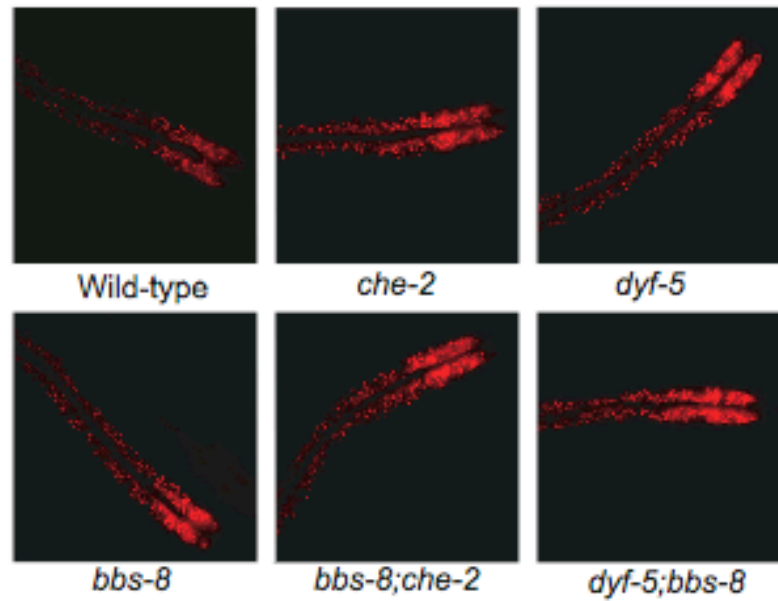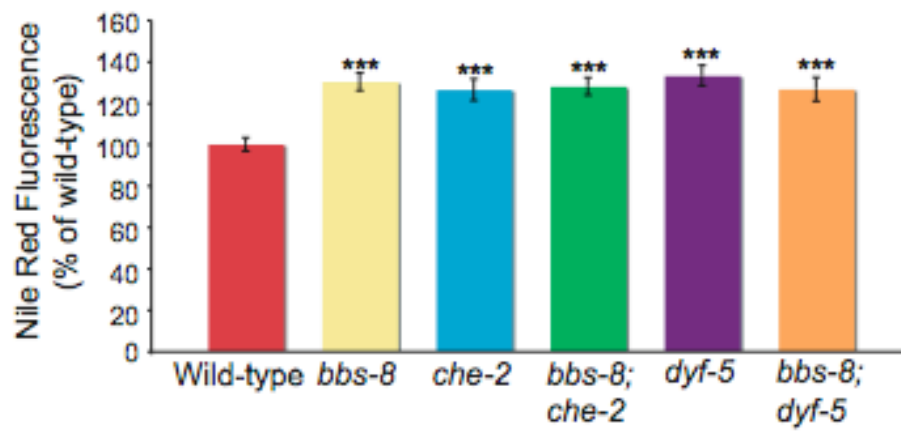
**Figure 4-4.** *bbs* **mutations acts in the same pathway as other cilia mutations that increase fat storage.**

(A) Fat content of *che-2(e1033)*; *bbs-8(nx77)* is similar to *che-2(e1033)* and *bbs-8(nx77)* single mutants.  Also, *dyf-5(mn400)*; *bbs-8(nx77)* mutants have comparable fat stores to single mutants. In addition, these mutants are extremely small.

(B) Quantitation of Nile Red in *che-2(e1033)*; *bbs-8(nx77)* and *dyf-5(mn400)*; *bbs-8(nx77)* mutants. *n*=12-19 worms for each genotype.

All comparisons are between mutant and wild-type worms.

\* p<0.05 and  \*\*\* p<0.01 by t-test.  Errors bars indicate Standard Error of the Mean.

**Figure 4-5**
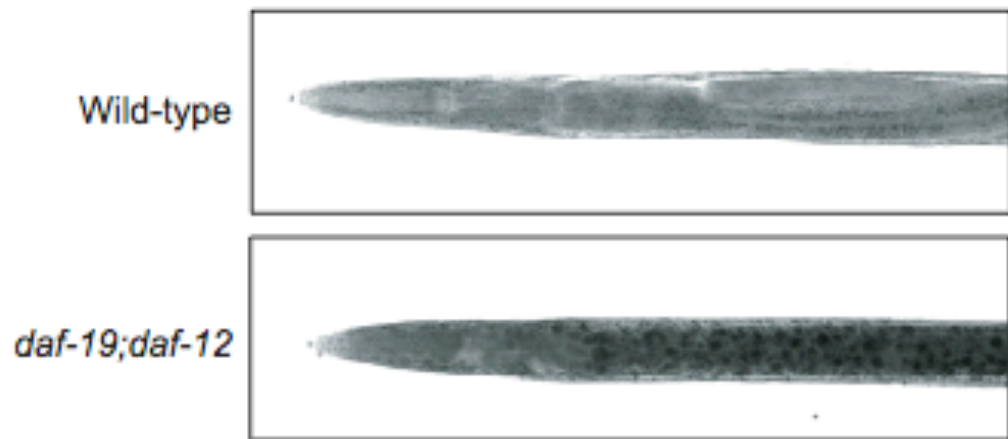
**Figure 4-5. Mutants lacking cilia have increased fat content.**

*daf-19* mutants completely lack all cilia. The fat content of *daf-19(m86); daf-12(sa204)* is increased compared to wild-type worms. Staining was performed on fixed worms using Sudan Black B under conditions to minimize staining variability. Lipid droplets are stained blue-black.

# Figure 4-6



**Single mutant phenotypes**

Legend (A):
- High fat
- Mild/variable increase in fat
- Low fat
- Wild-type fat
- Difficult to determine
- Unexamined

**Double mutant phenotypes**

Legend (B):
- High fat
- Low fat
- Unexamined
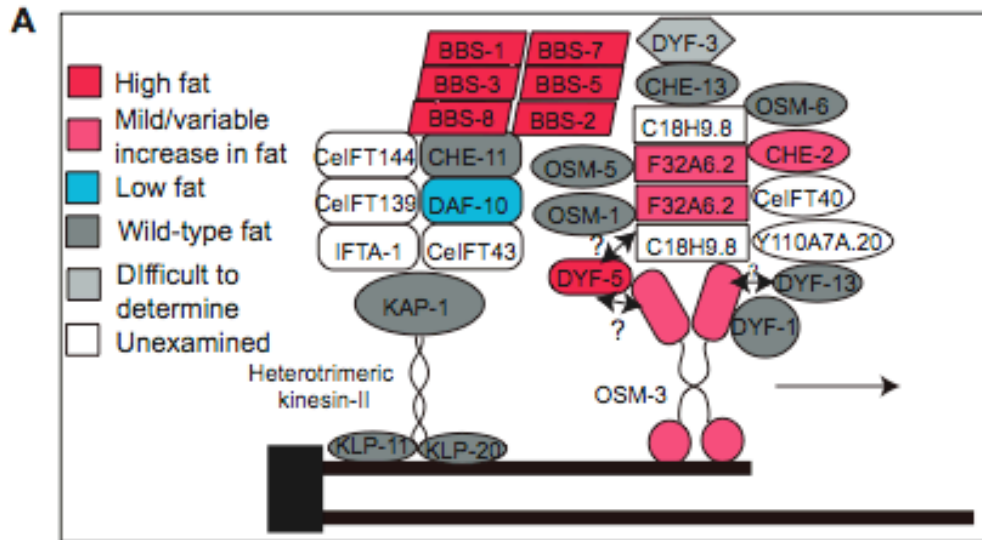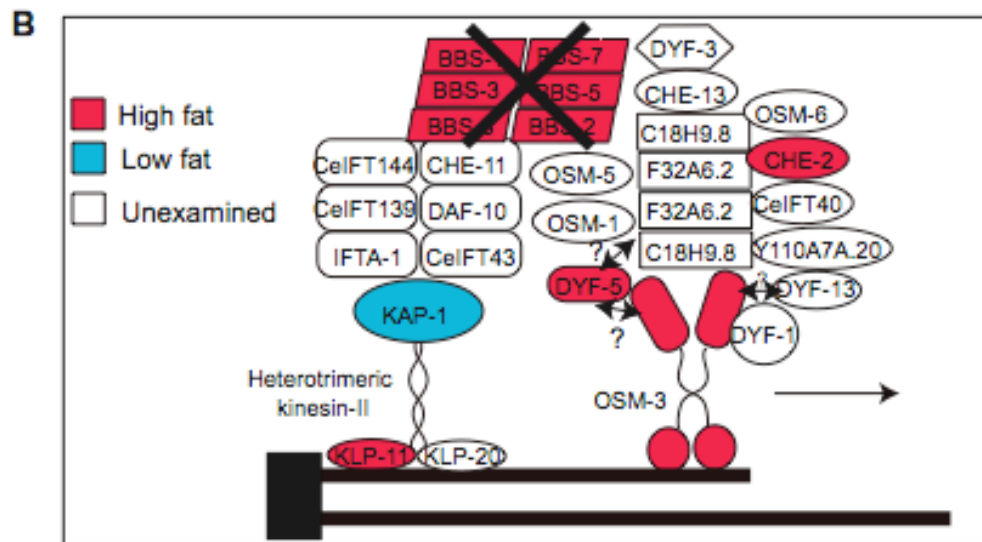
C

| Genotype | Fat phenotype | Genotype | Fat phenotype |
|---|---|---|---|
| Wild-type | 0 | | |
| bbs-7/bbs-8 | ++ | | |
| osm-3 | + | osm-3;bbs-8 | ++ |
| che-2 | + | che-2;bbs-8 | ++ |
| dyf-5 | ++ | dyf-5;bbs-8 | ++ |
| klp-11 | 0 | klp-11;bbs-7 | ++ |
| kap-1 | 0 | kap-1;bbs-8 | --- |

**Figure 4-6.  Summary of genetic analyses of *bbs* and IFT genes.**

(A) Schematic of the IFT components and their single mutant fat phenotypes. *che-2*, *osm-3*, and F32A6.2 mutants have mild or variable increases in lipid content.  *bbs* and *dyf-5* mutants display consistent, moderate increases in fat content.  *daf-10* mutants store less fat than wild-type worms. The phenotype of *dyf-3* was difficult to determine because of a severe developmental delay. Adapted from (Ou et al., 2007).

(B) Schematic of the IFT components and their double mutant phenotypes with *bbs*.  The color of the component represents its double mutant phenotype with *bbs*.

(C) Chart illustrating the phenotypes of IFT double mutants. 0 = Wild-type fat content; + = mild/variable increase in fat content (0-30%); ++ = moderate fat increase (30-50%); --- = decreased fat content (20-30%)

**Chapter Five**


**Investigating molecular mechanisms of increased fat storage caused by**

**mutations in Bardet-Biedl Syndrome genes**

**Conserved neuronal pathways regulate metabolism**

The regulation of metabolism is complex, involving coordination between several organ systems. An organism must integrate signals from the gut and adipose tissue indicating satiety and energy levels with sensory cues about food quality and availability. For example, during starvation, an animal stops reproduction and growth, increases foraging behavior, and decreases its metabolic rate to conserve energy. Coordination by the central nervous system is essential in producing the appropriate behavioral and metabolic responses to maintain metabolic homeostasis. Multiple, redundant pathways facilitate communication between several areas of the brain and the periphery to direct these responses.

In mammals, coordination between several nuclei of the hypothalamus, in particular, is important in maintaining energy homeostasis. Briefly, the arcuate nucleus of the hypothalamus comprises two subtypes of neurons, the pro-opiomelanocortin/ cocaine- and amphetamine-regulated transcript (POMC/CART) and Neuropeptide Y/Agouti-related Peptide (NPY/AgRP) containing neurons, which have opposing roles in the regulation of energy (Kalra et al., 1991; Schwartz et al., 2000; Zarjevski et al., 1993). Their afferents terminate in other hypothalamic nuclei, including the paraventricular nucleus (PVN), and the lateral hypothalamic nucleus (LHA; Elmquist et al., 1999; Elmquist et al., 1998; Sainsbury et al., 2002). The PVN and LHA integrate signals from the arcuate with input from other regions, such as the nucleus accumbens, an area involved in motivation and reward, and also send inputs to motor circuits that control feeding behavior (Arora and Anubhuti, 2006; Morton et al., 2006; Sainsbury et al., 2002). Although an obvious correlate to the hypothalamus or other brain regions has not been

identified in *C. elegans*, many of the neural pathways that regulate energy metabolism in mammals are conserved in *C. elegans.*

An example of such conserved signaling molecules are insulin and other peptide hormones. In mammals, the periphery and the CNS utilize insulin and peptide hormones as long-range metabolic messengers, communicating information about the metabolic state of the organism. Released in response to meals, insulin activates the POMC/CART neurons and inhibits NPY/AgRP neurons of the arcuate nucleus to decrease food intake and increase energy expenditure (Morton et al., 2006; Schwartz et al., 2000; Sipols et al., 1995; Woods et al., 1998). Leptin, a peptide produced by adipocytes, is an appetite-suppressing hormone that mediates its effects through receptors expressed in several parts of the brain including the arcuate nucleus (Elmquist et al., 1999; Friedman and Halaas, 1998). Additional appetite-suppressing signals produced by the gut include cholecystokinin and Peptide YY (Arora and Anubhuti, 2006; Batterham et al., 2006; Chaudhri et al., 2006), while other peptides such as ghrelin robustly stimulate food intake (Arora and Anubhuti, 2006; Williams and Cummings, 2005).

Insulin and other neuropeptides also regulate metabolism in *C. elegans*. Deficient insulin signaling due to mutations in the *daf-2* insulin receptor increases fat content, which is suppressible by mutations in the *daf-16* FOXO transcription factor (Ashrafi et al., 2003; Kimura et al., 1997; Ogg et al., 1997). Although worms do not produce obvious orthologs of the same peptides as mammals, preliminary evidence in the worm suggests that peptides are also needed for maintaining energy balance. Fat storage is markedly decreased by mutations in the proprotein convertase *egl-3*, needed for processing and production of all neuropeptides (Husson et al., 2007). Identifying the

effects of individual peptides is complicated by the fact that worms have approximately 28 FMRFamide-like, 42 neuropeptide-like and 38 insulin-like peptide genes (Husson et al., 2005; Kim and Li, 2004; Li, 2005; Li et al., 1999a; Li et al., 1999b; Li et al., 2003; McVeigh et al., 2005; Nathoo et al., 2001; Pierce et al., 2001). At least one peptide— *ins-11*—has been implicated in fat storage (Kawano et al., 2006). Thus, insulin and perhaps additional peptides are important for energy regulation in *C. elegans*.

Both mammals and *C. elegans* utilize neurotransmitters, such as serotonin, to communicate information about the energy state of the organism. In mammals, the central serotonergic system inhibits food intake and decreases body weight (Heisler et al., 2003); a major site of regulation is the $5HT_{2C}$ receptor expressed in the POMC neurons of the hypothalamus (Heisler et al., 2003). In worms, serotonin also coordinates energy intake and storage: application of exogenous serotonin causes a decrease in fat storage in the worms and an increase in pumping rate (S. Srinivasan and K. Ashrafi, unpublished data). Conversely, mutations in tryptophan hydroxylase (*tph-1*), resulting in a loss of an animal's ability to produce serotonin, cause an increase in fat storage in *C. elegans* (Ashrafi et al., 2003; Sze et al., 2000). At least three classes of neurons produce serotonin, including the ciliated amphid neuron ADF (Chase and Koelle, 2007; Sze et al., 2000). Which of these neurons regulates fat content is still unknown.

The transforming growth factor β (TGF-β) pathway is also an important metabolic modulator in mammals and *C. elegans*. In mammals, TGF-β1 levels are elevated in obese individuals and mice (Fain et al., 2005; Samad et al., 1997; Scaglione et al., 2003). TGF-β also regulates the differentiation of mesenchymal cells into adipocytes (Choy and Derynck, 2003; Clouthier et al., 1997). In worms, loss of function of *daf-7*,

the TGF-β ligand, or *daf-1* or *daf-4*, the TGF-β receptor, causes increased fat retention, which can be suppressed by mutations in *daf-3*, a SMAD transcription factor (Ashrafi et al., 2003; Kimura et al., 1997; Ogg et al., 1997).

In addition, several conserved mammalian obesity genes regulate fat content in *C. elegans*, including BBS, as discussed in Chapter Four, and Tubby. Mutations in mammalian *Tub* cause phenotypes reminiscent of Bardet-Biedl Syndrome, including hearing loss, vision loss due to retinal degeneration (Coleman and Eicher, 1990; Noben-Trauth et al., 1996; North et al., 1997; Ohlemiller et al., 1997; Stubdal et al., 2000) and age-dependent obesity (Coleman and Eicher, 1990; Stubdal et al., 2000). Tub is widely expressed in the brain (Beales et al., 2000; Kleyn et al., 1996; Noben-Trauth et al., 1996; North et al., 1997) and enriched in the hypothalamus (Kleyn et al., 1996; Noben-Trauth et al., 1996). Studies of the worm homolog *tub-1* have provided insight into the function of Tubby. *tub-1* is expressed in a ciliated sensory neurons and undergoes IFT within the cilium (Mak et al., 2006; Mukhopadhyay et al., 2005). Similar to mammals, TUB-1 negatively regulates fat storage; *tub-1* effects on fat storage are independent of insulin (Mukhopadhyay et al., 2005). RNAi of the Rab-GTPase activating protein RBG-3 suppresses increased fat storage in *tub-1* mutants; RBG-3 promotes the activity of RAB-7, which participates in vesicular packaging pathways (Mukhopadhyay et al., 2005; Mukhopadhyay et al., 2007a). This finding together with the observation of intraciliary movement of *tub-1* led to the hypothesis that *tub-1* functions in vesicle transport (Mukhopadhyay et al., 2005; Mukhopadhyay et al., 2007a). However, direct evidence for this hypothesis and whether these findings are relevant for mammalian tubby are yet to be determined.

The expression of *tub-1* and *bbs* in ciliated sensory neurons points to the significance of these neurons in regulating metabolism. Through their contact with the environment and the pseudocoelemic fluid of the worm, the ciliated sensory neurons are a likely site of coordination of responses to signals from the environment as well as information about the metabolic state of the organism. For example, food availability and population density modulate the expression of the TGF-β ligand DAF-7, expressed solely in ciliated sensory neuron ASI, which regulates fat content and feeding rate (Ashrafi et al., 2003; Kimura et al., 1997; Ogg et al., 1997; Savage-Dunn, 2005; Schackwitz et al., 1996). In addition to DAF-7, several other genes have been identified in ciliated sensory neurons that regulate fat storage in the worm (Ashrafi et al., 2003; Mak et al., 2006; Mukhopadhyay et al., 2005).

In sum, several conserved pathways regulate fat storage in *C. elegans* and mammals. I am interested in identifying genes and pathways that interact with *bbs* to regulate fat storage. In the following experiments, I explore the interaction between *bbs* and some of these conserved fat regulatory pathways. In addition, I discuss several screens to identify potential genes that act in the *bbs* pathway. Of the pathways examined, no novel pathways or genes emerged as candidates to explain the *bbs* phenotype.

**Results**

***bbs-7* acts independently of the serotonergic pathway to regulate fat content**

The effect of exogenous serotonin on fat storage as well as the production of serotonin by the ciliated neuron ADF suggests that the serotonergic pathway may interact with the *bbs* pathway. I hypothesized that if the effects of *bbs* on fat are mediated by

serotonin, the normal function of *bbs* may be to increase the production of serotonin, which would inhibit fat storage.   I examined the expression of a key serotonin biosynthetic enzyme, *tph-1* in *bbs-7(n1606)* mutants. Unexpectedly, I found that expression of a *GFP* reporter driven by the *tph-1* promoter increased in a *bbs-7(n1606)* background (Figure 5-1A).  Quantitation of the difference revealed expression was increased by 97% at the L2 larval stage and by 66% in L4 worms.

To further explore whether *bbs-7* affects fat storage through the serotonergic pathway, I examined a serotonergic receptor mutant that partially mediates the effect of serotonin on lipid storage.  Of the four serotonergic receptors that have been identified in *C. elegans* thus far, only mutations in the serotonin-gated chloride channel *mod-1* increase fat stores and partially suppress the decrease in fat caused by the addition of exogenous serotonin (S. Srinivasan & K. Ashrafi, unpublished data).  If *bbs* affects the storage of fat by its effect on the *mod-1* pathway, then a *bbs-7(n1606); mod-1 (ok103)* double mutant should have similar fat levels to a *bbs-7(n1606)*  or *mod-1(ok103)* mutant. However, the double mutant has increased fat content compared to either single mutant alone (Figure 5-1 B&C), thus suggesting that *bbs-7* and *mod-1* increase fat storage through independent pathways.

However, *mod-1* mutations only partially suppress the decrease in fat content caused by exogenous serotonin, suggesting that serotonin also regulates fat storage through an unidentified receptor.  Therefore, *bbs* may regulate fat through a *mod-1*-independent serotonergic pathway.  I examined whether *bbs-7(n1606)* mutants suppress the decrease in fat caused by serotonin.  *bbs-7(n1606)* worms were supplemented with serotonin or vehicle (HCl).  In wild-type worms, the addition of exogenous serotonin

results in a decrease in fat storage to about 55 % of wild-type levels. Serotonin similarly decreases fat in *bbs-7(n1606)* mutants, thus indicating that *bbs-7* is not a suppressor of the serotonergic fat phenotype (Figure 5-1D & E). Similar results were obtained with *bbs-1(ok1111)* (S. Srinivasan and K. Ashrafi, unpublished data).

Taken together, these experiments suggest that *bbs* does not regulate fat storage through its direct affects on serotonin, although indirect effects cannot be ruled out. Interestingly, defects in *bbs* cause increased expression of a *tph-1::GFP* reporter .

## *bbs-7* act independently of the insulin pathway to regulate fat content

The insulin pathway also regulates stress resistance, dauer formation, lifespan, and metabolism. Activation of the DAF-2 insulin receptor results in phosphorylation of the DAF-16 FOXO transcription factor, thus inactivating DAF-16 and sequestering it in the cytoplasm (Baumeister et al., 2006). Thus, all *daf-2* phenotypes can be suppressed by *daf-16*. Defects in the insulin pathway, such as mutations in *daf-2*, cause increased fat storage, which can be suppressed by *daf-16* mutations (Ashrafi et al., 2003; Kimura et al., 1997; Ogg et al., 1997). To determine whether *bbs* regulates fat storage through the insulin pathway, I examined *bbs-7(n1606); daf-16(mu86)* double mutants. The *bbs-7; daf-16* mutant is similar in fat content to the *bbs-7(n1606)* mutant (Figure 5-2), which suggests that the *bbs* complex acts independently of the insulin pathway to affect fat.

## *bbs-7* acts independently of the TGF-β pathway to regulate fat content

The TGF-β pathway controls diverse functions such as body size, dauer formation, egg-laying and metabolism. Reduction of activity of the TGF-β pathway causes increased fat storage (Ashrafi et al., 2003; Kimura et al., 1997; Ogg et al., 1997). The TGF-β ligand DAF-7 is expressed solely in the ciliated amphid neuron ASI; animals

with mutations in *daf-7* have increased fat content. DAF-3, a SMAD transcription factor downstream of DAF-7, suppresses all of the phenotypes associated with *daf-7* mutations, including increased fat storage (Kimura et al., 1997; Ogg et al., 1997; Savage-Dunn, 2005; Schackwitz et al., 1996). *bbs* may positively regulate *daf-7* in ASI, such that defects in *bbs* reduce DAF-7 causing an increase in fat. In this scenario, then increased fat content in *bbs* mutants should be suppressible by mutations in the DAF-3, the SMAD transcription factor downstream of DAF-7. However, fat levels of the double mutant *bbs-7(n1606); daf-3(mgDf90)* are increased similar to that of *bbs-7(n1606)* mutants (Figure 5-3). Therefore, *bbs* controls fat storage independently of the TGF-β pathway.

**Interactions between *bbs* and fat regulatory genes expressed in ciliated sensory neurons**

I am interested in identifying other candidate genes that are expressed in ciliated neurons and might interact with *bbs* genes to affect fat. *tub-1,* the homolog of the mammalian obesity gene Tubby, is one such candidate. *tub-1* is expressed in ciliated neurons (Mak et al., 2006; Mukhopadhyay et al., 2005), and *tub-1* mutations increase fat stores to approximately 15% greater than wild-type (Figure 5-4 A&B). As reported by Mak and colleagues, I found that *tub-1; bbs-7* mutants increased fat content similar to either mutant alone, suggesting that *tub-1* and *bbs-7* work in the same pathway (Mak et al., 2006).

Several of the genes identified in a genome-wide RNA interference (RNAi) screen for genes that affect fat are known to be expressed in ciliated neurons, which makes them excellent candidates for genes that interact with *bbs* to affect fat (Ashrafi et al., 2003). Some are expressed solely in ciliated neurons, while others are expressed in

both ciliated neurons as well as other tissues.  Therefore, I looked for interactions between *bbs* and these genes.

One example of a fat regulatory gene specific to ciliated neurons is the kinase Y11D7A.8, which is expressed in four ciliated sensory neurons.  Inactivation of Y11D7A.8 increases intestinal fat storage.  Thus, based on its expression pattern and its fat phenotype, Y11D7A.8 is an interesting candidate gene that may act in the *bbs* pathway to increase fat.  If Y11D7A.8 work in the *bbs* pathway to affect lipid storage, then reducing Y11D7A.8 function in a *bbs* mutant background should fail to increase fat stores compared to *bbs* mutants alone.  However, if Y11D7A.8 works in a different pathway to control lipid accumulation, then RNAi of Y11D7A.8 in *bbs-7* mutants should cause an additional increase in fat in comparison to *bbs-7*.  Indeed, reduction of Y11D7A.8 in a *bbs-7* mutant caused a roughly additive increase in fat suggesting that the two genes operate in separate pathway to affect fat (Figure 5-4 C & D).

Several other candidate ciliated neuron fat genes were similarly examined for interactions with *bbs-7*.  I was interested in gene inactivations that normally reduced fat in a wild-type background, but failed to decrease lipid content in *bbs*-7 mutants, thus suggesting that the candidate gene requires *bbs*-7 for its activity.  I was also interested in gene inactivations that increase fat storage in a wild-type worm, but failed to increase fat in *bbs-7* mutant worms, again suggesting that *bbs-7* is downstream of the candidate gene. However, no such interactions with *bbs-7* mutations were found (Figure 5-4E). Therefore, aside from *tub-1*, no other gene expressed in ciliated neurons has been found yet to interact with *bbs* to affect fat.

**Screening for candidate interactions between *bbs* and other genes that have a role in fat storage**

To gain insight into the *bbs* fat phenotype, I expanded my search to look for interactions between *bbs* and approximately four hundred genes identified in a genome-wide RNAi screen for genes that affect fat (Ashrafi et al., 2003). Many of these genes are conserved and function as metabolic enzymes or lipid-interacting proteins. Other candidates that emerged in the screen include receptors, channels and transporters, vesicle transport components, cytoskeletal elements, and transcription factors as well as many novel genes (Ashrafi et al., 2003). In an effort to find genes that interact with the *bbs* pathway to affect fat, I screened for genetic interactions between these four hundred genes and *bbs*.

Of the four hundred genes, approximately one hundred RNAi clones were identified that increased fat (Ashrafi et al., 2003). If any of these genes act within the *bbs* pathway to regulate fat depots, then inactivation of that gene should cause no further enhancement of fat in *bbs* mutants. Another interesting result is a synergistic increase in fat levels caused by inactivation of the candidate gene in a *bbs* mutant background. Such a result may suggest that the *bbs* pathway and the fat-increasing gene negatively co-regulate each other to preserve metabolic homeostasis; alternatively, it may suggest that *bbs* and the fat-increasing gene participate in compensatory mechanisms to maintain homeostasis. In fact, a prior screen revealed such an interaction between *bbs* and the intestinal 3-ketoacyl-coA-thiolase *kat-1*, involved in the final steps of β-oxidation. Loss of function of *kat-1* in a *bbs-1*, *tub-1*, or any of a number of cilia mutants causes an exacerbated enhancement of fat stores (Appendix Figure 2-3; Mak et al., 2006). Mak

and colleagues explained this result by suggesting that the reduction of the *bbs* pathway

causes increased lipid storage and a concurrent increase in *kat-1* expression to metabolize

the excess lipid; the loss of this homeostatic mechanism by inactivating *kat*-1 in a bbs

mutant background causes the synergistic enhancement of fat content (Mak et al., 2006).

In attempt to find genes that similarly interact with *bbs,* I used RNAi to inactivate each of

the 100 fat-increasing genes (Ashrafi et al., 2003) in *bbs-7(n1606)* and *bbs-8(nx77)*

mutants, and analyzed their fat phenotypes by Nile Red.  Beyond *kat-1*, I failed to find

any RNAi clones that caused a synergistic enhancement of fat.  In addition, I failed to

find clones that function in the same pathway (i.e. clones that increase fat in wild-type

worms but fail to increase lipids in *bbs-7* mutants).

Inactivation of the other three hundred genes in a wild-type background causes a

decrease in fat (Ashrafi et al., 2003).  If a gene is dependent upon *bbs* for its effects on

fat, then mutations in *bbs-7* should suppress the effects of inactivation of the gene.

Therefore, I looked for RNAi clones that failed to decrease fat in a *bbs-7(n1606)*

background.  No such genes were identified, which implies that all identified fat-

decreasing genes function downstream or independently of *bbs*.  Thus, I found no

obvious interaction between *bbs* mutations and other candidate fat regulatory genes.

Given that *bbs* regulates fat storage, core components of metabolic pathways are

likely to interact with the *bbs* pathway to regulate fat.  Such interactions with metabolic

genes may emerge by reducing their function in a *bbs-7(n1606)* mutant background.

Using RNAi, I screened ninety-six genes that correspond to components of beta-

oxidation, fatty acid synthesis, fatty acid elongation and binding (See Appendix Table 2-2

for gene identities).  I was interested in identifying genes that increased or decreased lipid

stores when inactivated in a wild-type background but failed to do so in a *bbs-7* mutant background; such an interaction would suggest that *bbs* is required for the gene's activity. I was also interested in finding RNAi clones that caused a synergistic enhancement in fat content in a *bbs-7* mutant background. Again, mutations in *bbs-7(n1606)* failed to suppress any of the fat phenotypes nor aggravate fat storage phenotypes caused by inactivation of these metabolic genes.

Finally, I screened for interactions between *bbs-7(n1606)* and a panel of twenty RNAi clones corresponding to eleven genes identified as human diabetes candidates (See Appendix Table 2-3 for gene identities; Saxena et al., 2007). Again, I found no interactions between *bbs-7* and these candidate genes.

**Discussion**

In this chapter of my dissertation, I attempted to identify pathways that may interact with *bbs* to regulate intestinal lipid stores. *bbs* genes do not regulate intestinal fat through interactions with other systems already known to regulate fat in the worm, including the serotonergic pathway, insulin pathway, and the TGF pathway (Figure 5-5). In addition, screens failed to identify other genes that may interact with *bbs* to control fat storage. The genes examined act either independently or downstream of the *bbs* pathway.

Several other pathways that may participate in metabolic regulation by *bbs* warrant further study. These include both dopaminergic and glutamatergic pathways as well as neuropeptides. Mutagenesis or more expansive RNAi screens may also reveal novel genes that act within the *bbs* pathway. For example, genomics and proteomic studies have identified hundreds of cilia candidate genes (e.g. Blacque et al., 2005; Keller

et al., 2005; Pazour et al., 2005). Screening these genes in a sensitized wild-type background may reveal novel cilia genes that participate in the metabolic homeostasis. Moreover, screening these genes by RNAi in a *bbs* mutant background may reveal genes that interact with *bbs* to regulate intestinal lipid. Additionally, microarrays of *bbs* mutants worms may uncover unexpected targets of altered signaling in *bbs* mutants.

The increased expression of a *tph-1* reporter in a *bbs-7* background is intriguing and suggests that the serotonergic system may be upregulated to compensate for the increased fat storage in *bbs* mutants. Confirmation that an increase in *tph-1* expression corresponds to an increase in production of serotonin can be accomplished by immunostaining for serotonin in *bbs* mutants. Furthermore, eliminating serotonin production by mutating *tph-1* in *bbs* mutants should result in an enhancement of lipid accumulation. However, because the fat content of *tph-1* mutants can only be examined by Sudan Black B staining[4] (Ashrafi lab, unpublished data) and because only robust differences in fat can be detected by this method, such an experiment may be technically difficult.

The genetic interaction between *tub-1* and *bbs* is also promising (Figure 5-4; Mak et al., 2006), but many questions remain. Does BBS regulate fat content by affecting trafficking of TUB-1? If so, how is the role of BBS in TUB-1 trafficking different than that of other cilia components, such as OSM-6? Do *tubby* and *bbs* coordinately regulate

---

[4] Fat storage cannot be assayed by Nile Red in many constitutive (or partial constitutive) dauer mutants *daf-2*, *daf-7*, and *tph-1* mutants, likely due to an uptake defect of the Nile Red dye (Ashrafi, 2007). Instead, fat storage can be assayed by a method involving fixation and staining with the fat-soluble dye Sudan Black, which stains lipids blue-black.

fat in mammals?  Identification of other molecules that cooperate with *tub-1*; *bbs* to regulate fat levels is also of interest.

Furthermore, as previously reported (Mak et al., 2006), I found that inactivation of *kat-1* thiolase, in a *bbs*, *tub-1*, or cilia mutant background causes a synergistic enhancement of fat (Appendix Figure 2-3; Figure 5-5).  Mak and colleagues propose that the alterations in signals from ciliated neurons causes increased lipid accumulation and a compensatory upregulation of *kat-1* thiolase, a key enzyme involved in the breakdown of fats.  Loss of this compensatory mechanism causes an aggravated accumulation of lipid (Mak et al., 2006).

In sum, *bbs* acts via a novel pathway, independently of some of the major pathways that regulate fat in the worm, including the serotonergic, insulin and TGF-β pathways.  These studies focus our understanding of how BBS participates in metabolic homeostasis.  Further analyses may reveal pathways downstream of *bbs* and shed light on how *bbs* alters metabolism in *C. elegans* and possibly mammals as well.

# Figure 5-1



A

| | L2 larvae | | L4 larvae | |
|---|---|---|---|---|
| | Fluorescence (% of wild-type) | n | Fluorescence (% of wild-type) | n |
| Wild-type | 100±-4.5% | 39 | 100 ± 3.4% | 46 |
| bbs-7(n1606) | 197 ±10.5% | 37 | 167 ± 8.5% | 34 |

B



Wild-type    mod-1

bbs-7    bbs-7;mod-1

C



D    HCl    5HT



Wild-type

bbs-7

E
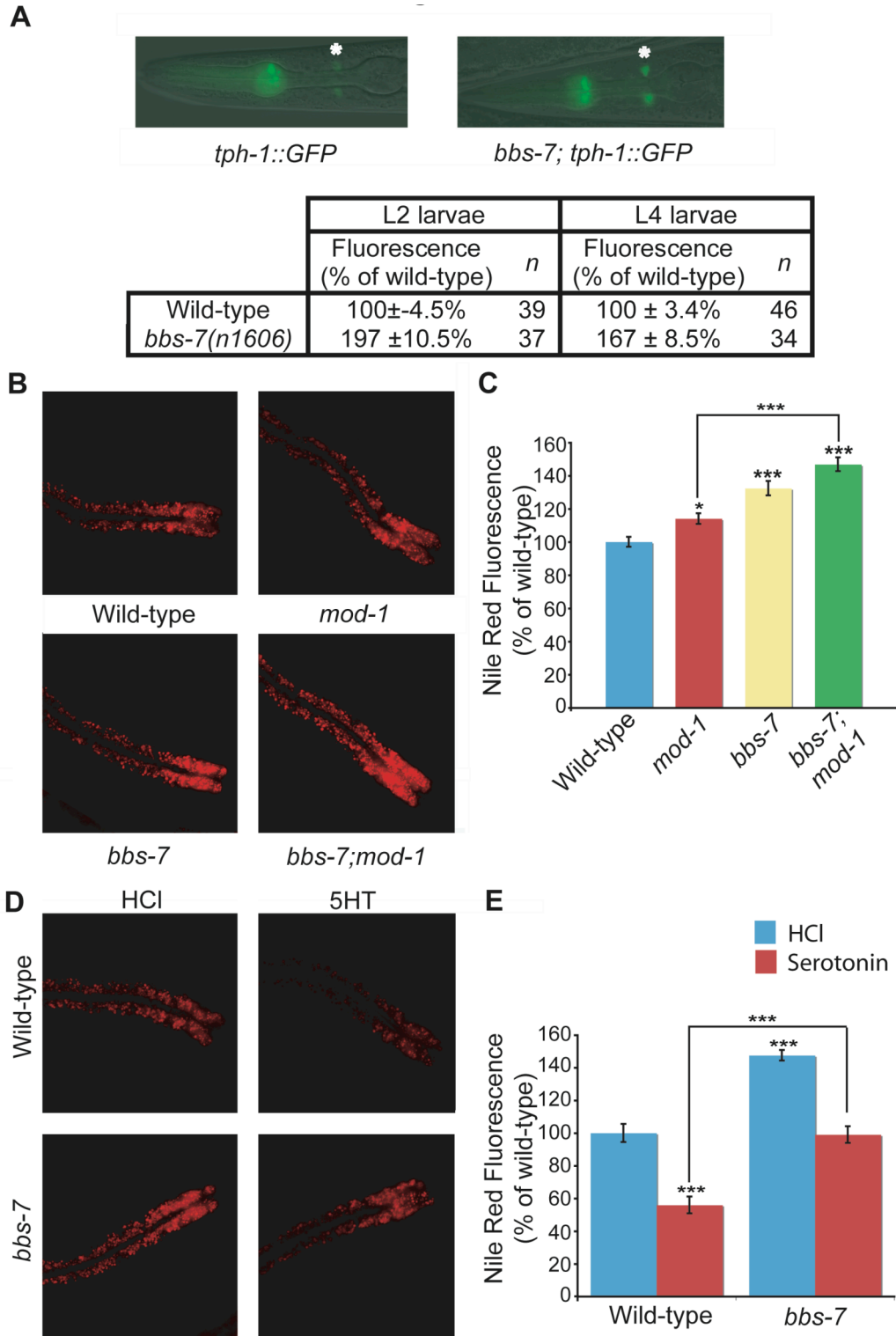
**Figure 5-1.** *bbs-7* **acts independently of the serotonergic pathways to regulate fat content.**

(A) Mutations in *bbs-7* cause increased *tph-1::GFP* expression in ADF. Images are of wild-type and *bbs-7(n1606)* mutant L4 worms expressing the *tph-1::GFP* reporter. Quantitation of changes in fluorescence at L2 and L4 stages is shown in the table. Changes in fluorescence were significant ($p < 0.001$). * indicates ADF.

(B) *bbs-7* and the serotonergic receptor *mod-1* act in different pathways to affect fat. *bbs-7(n1606);mod-1(ok103)* mutants have greater fat stores than either of the single mutants, *bbs-7(n1606)* or *mod-1(ok103)*.

(C) Quantitation of fat in *bbs-7(n1606); mod-1(ok103)* mutants. Nile Red fluorescence in *bbs-7(n1606);mod-1(ok103)* double mutants is 147% of wild-type worms compared to 132% for *bbs-7(n1606)* mutants and 114% in *mod-1(ok103)* mutants. *n*=13-17 worms per genotype.

(D) *bbs-7(n1606)* fails to suppress the decrease in fat caused by the addition of serotonin. Control worms were treated with the vehicle HCl.

(E) Quantitation of Nile Red fluorescence in serotonin-supplemented worms. Serotonin decreases fat by 44% compared to wild-type worms and 48% in *bbs-7(n1606)* worms. *n*=8-10 worms per genotype and condition.

All comparisons are between mutant and wild-type worms unless otherwise indicated. * $p < 0.05$ and *** $p < 0.01$ by t-test. Errors bars indicate Standard Error of the Mean.

# Figure 5-2

**A**
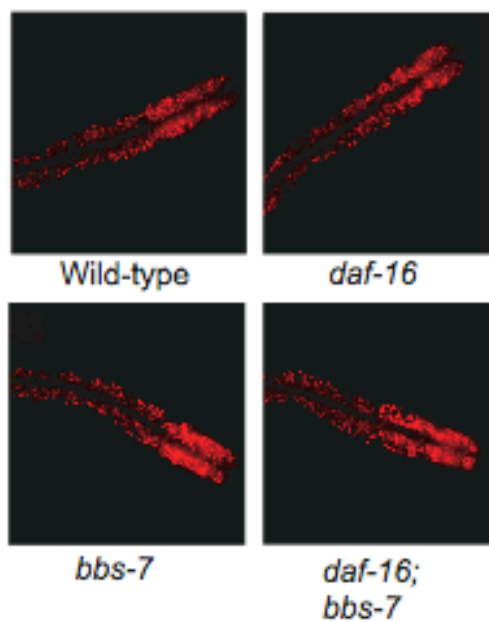


**B**
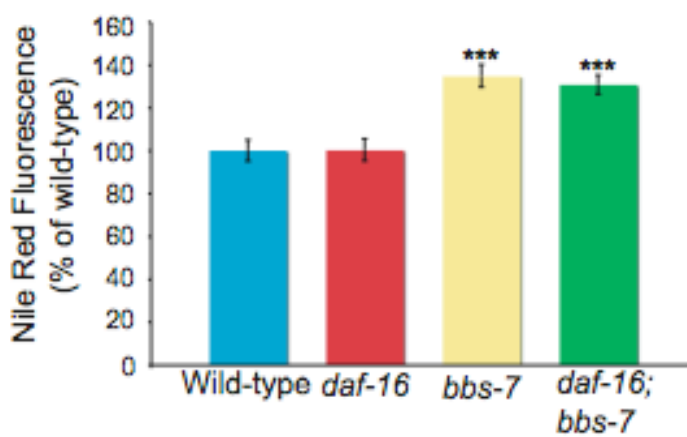
**Figure 5-2. *bbs-7* acts independently of the insulin pathway to regulate fat content.**

The insulin pathway regulates lipid content in *C. elegans*. Mutations in the insulin

receptor *daf-2* cause an increase in fat storage. The downstream *daf-16* FOXO

transcription factor suppresses the increased lipid content of *daf-2* mutant worms.

(A) *daf-16(mu86)* mutants have wild-type fat content. Double mutant *daf-16(mu86);*

*bbs-7(n1606)* show a similar increase in fat content to *bbs-7(n1606),* suggesting that

*bbs-7* functions independently of the insulin pathway to regulate fat content.

(B) Quantitation of Nile Red fluorescence in *daf-16(mu86); bbs-7(n1606)* double

mutants. *n*=11-13 worms per genotype.

\*\*\* p<0.001 by t-test. Errors bars indicate Standard Error of the Mean.

# Figure 5-3

**A**



Wild-type      *daf-3*

*bbs-7*      *bbs-7;daf-3*
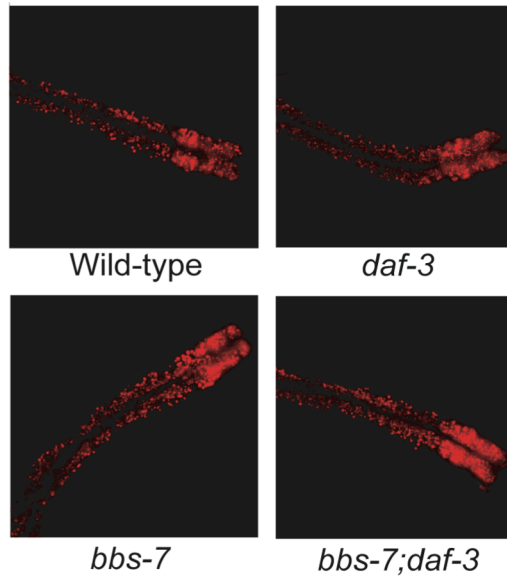
**B**
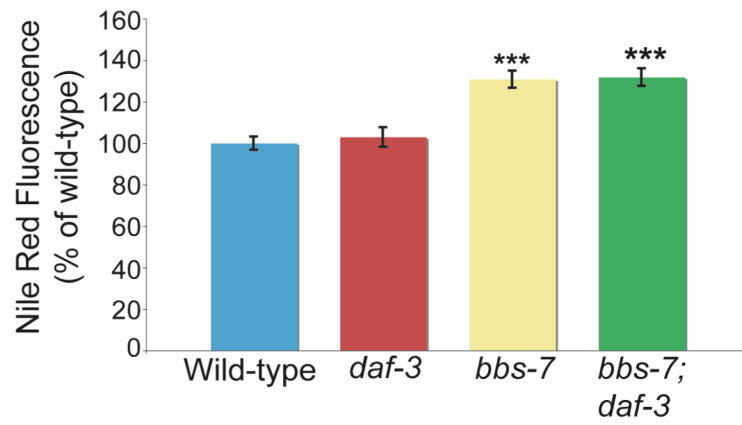
**Figure 5-3. *bbs-7* acts independently of the TGF-β pathway to regulate fat content.**

The TGF-β pathway regulates lipid storage in the worm. Mutations in the TGF-β ligand *daf-7* cause an increase in fat stores, which can be suppressed by mutations in a downstream SMAD transcription factor *daf-3*.

(A) *daf-3(mgDf90)* mutants display wild-type lipid levels. *daf-3(mgDf90)*; *bbs-7(n1606)* double mutants are similar in fat content to *bbs-7(n1606)* mutants, indicating that *bbs-7* acts independently of the TGF-β pathway to regulate fat content.

(B) Quantitation Nile Red fluorescence in *daf-3(mgDf90)*; *bbs-7(n1606)* double mutants. *n*=10-13 worms per genotype.

*** p<0.001 by t-test.  Errors bars indicate Standard Error of the Mean.

**Figure 5-4**



| Gene ID | Description | Expression | Fat phenotype | |
|---------|-------------|------------|---------------|---|
| | | | Wild-type | *bbs-7(n1606)* |
| F56B6.5 | Somatostatin receptor 2 | One CSN pair and other neurons | 0 | 0 |
| Y44A6B.2 | *srxa-15*; serpentine class receptor | CSN and other neurons | — | — |
| F53A9.4 | Amyotrophic lateral sclerosis protein | 7 pairs of amphids, labials, phasmids | 0 | 0 |
| C30F12.1 | Uncharacterized novel protein | CSN, nervous system & many other tissues | — — | — — |
| E04A4.6 | tectonic | unknown | 0 | 0 |
| F58G4.2 | *str-90*; 7TM receptor | CSN and other neurons | 0 | 0 |
| T04A11.8 | *sru-19*; serpentine class receptor | CSN and other neurons | — | — |

**Figure 5-4. Searching for candidate interactions between *bbs-7* and other fat regulatory genes expressed in ciliated neurons.**

(A) *tub-1* and *bbs-7* are in the same genetic pathway with respect to fat. *tub-1(nr2004); bbs-7(n1606)* double mutants demonstrate a similar increase in fat compared to wild-type worms.

(B) Quantitation of Nile Red fluorescence in *tub-1(nr2004); bbs-7(n1606)* double mutants. *n*=8-10 worms per genotype.

(C) *bbs-7* and Y11D7A.8, a fat regulatory gene expressed in four ciliated sensory neurons, affect fat through independent pathways.  Inactivation of Y11D7A.8 by RNAi increases fat in both wild-type and *bbs-7(n1606)* worms.

(D) Quantitation of Nile Red fluorescence in wild-type and *bbs-7(n1606)* worms fed Y11D7A.8 RNAi bacteria or L4440 control bacteria. *n*=14-16 worms per genotype. All comparisons are between mutant and wild-type worms unless otherwise indicated. * $p<0.05$ and  *** $p<0.01$ by t-test.  Errors bars indicate Standard Error of the Mean.

(E) Examining interactions between *bbs-7(n1606)* and other genes expressed in ciliated sensory neurons.  Genes were chosen for analysis based on their previously published expression patterns in ciliated sensory neurons and their fat phenotypes (Ashrafi et al., 2003).  Fat phenotypes were examined by RNAi.  " 0" = wild-type fat content; "—" = reduced fat content.

**Figure 5-5**
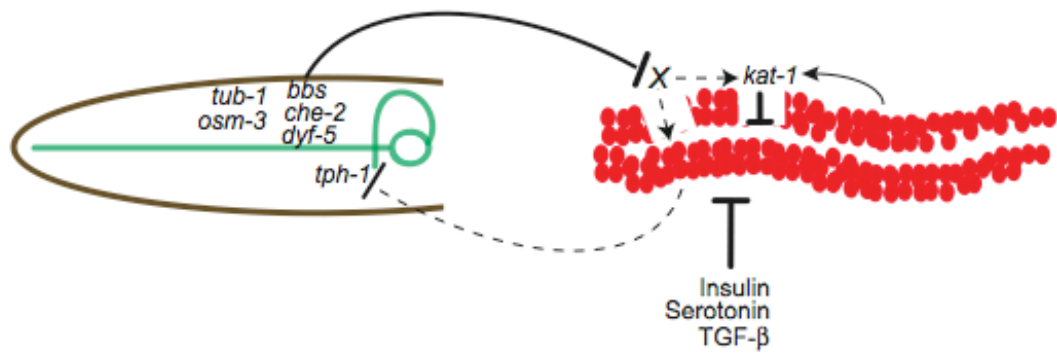
**Figure 5-5.** *bbs* **and other IFT components define a genetic pathway that regulates fat storage.**

*bbs*, *tub-1*, *dyf-5, che-2*, and *osm-3* define a cilia-localized pathway that regulates fat content.  Double mutations in *bbs* and any of these genes result in an increase in intestinal lipid accumulation comparable to single mutations in *bbs*. This pathway inhibits lipid accumulation through an unidentified signaling pathway independent of the serotonergic, TGF-β and insulin pathways.  Defects in the cilia pathway cause an upregulation of *kat-1,* an intestinal thiolase that breaks down fat, to maintain metabolic homeostasis.  The consequence of inactivating *kat-1* in a *bbs-7* mutant is a loss of this compensatory mechanism, resulting in synergistic enhancement of intestinal lipid.  Similarly, inactivation of *kat-1* in other cilia mutant backgrounds also results in an aggravated increase of lipids (Appendix Figure 2-3; Mak et al., 2006).

# Materials and Methods

## Strains

Strains were maintained as described by Brenner on plates of Nematode Growth Medium (NGM) at 20° or 15° (Brenner, 1974). A culture of OP50 *E. coli* was provided as a food source. The wild type strain is N2 Bristol. All mutant strains were obtained from the *Caenorhabditis* Genetic Center with the exception of *odr-8(ky31) IV* and *odr-8(ky28) IV*, kindly provided by the Bargmann lab, and the *bbs-1(ok1111) I; bbs-7(n1606) III;bbs-8(nx77) V* triple mutant, kindly provided by the Leroux lab.

## Nile Red staining

Nile Red staining of intestinal fat was carried out as reported in (Ashrafi et al., 2003). Nile Red powder (N-1142; Invitrogen, Carlsbad, CA, USA) was dissolved in acetone at 500 μg/ml, diluted in 1x phosphate buffered saline (PBS) and added on top of 6cm NGM plates with OP50 bacteria to a final concentration of 0.05 μg/ml. To synchronize worms as L1s, gravid adults were treated with hypochlorite to release the eggs, which were allowed to hatch and starve out overnight in S-Basal buffer. Worms were placed on Nile Red plates as starved, synchronized L1s. Worms were grown in uncrowded, well-fed conditions at 20°. To adjust for a slight developmental delay in *bbs-1*, *bbs-7*, *bbs-8*, *che-2*, *dyf-5*, single, double and triple mutants were grown at room temperature (22°) for the first 12-16 hours and then shifted to 20°. Their Nile Red phenotypes were assayed as adults at 72 -76 hours after plating L1s, corresponding to the first day of adulthood.

## RNAi experiments

RNAi clones (J. Ahringer and M. Vidal libraries), grown overnight in Luria Broth and ampicillin, were plated on plates supplemented with IPTG and allowed to grow for an

additional day at 37° to induce the RNAi and to increase thickness of the bacterial lawn.

Nile Red was then added to the plates as described above. Synchronized L1s were plated

the following day, and their Nile Red phenotype was assayed at 72hrs. The control

vector was L4440 in HT1115 bacteria.

**Sudan Black**

Sudan Black B staining was carried out as described previously (Kimura et al., 1997). To

minimize staining variability, control worms labeled with FITC and mutant worms were

stained in the same tube. Worms were washed off plates at early L4 stage and fixed in

0.5% paraformaldehyde. The worm slurry was subjected to three cycles of freeze-thaw,

washed three times in cold 1x PBS, and then dehydrated in an ethanol series. The worms

were stained overnight in a 50% saturated solution of Sudan Black B (Sigma 199664, St.

Louis, MO) in 70% ethanol and photographed.

**Microscopy and quantification**

Fluorescence images and Nomarski Differential Interference Contrast (DIC) were

captured by a Hamamatsu ORCA-ER cooled CCD camera attached to a Zeiss Axioplan 2

upright microscope using Openlab software (Improvision, England). Images were

acquired of worms at 16x at an exposure that was below saturation (2-5ms).

Image J software was used for analysis (U.S. National Institutes of Health, Bethesda,

MD, USA; http://rsb.info.nih.gov/ij/) with Stack Builder and Spot Tracker plugins (Sage

et al., 2005). The Region of Interest (ROI) was defined as the first two intestinal cells. A

1.0 pixel Gaussian filter was applied to identify fluorescence corresponding to lipid

droplets and to reduce background. The "Analyze Particles" function was used to

generate a mask, which was applied to the original ROI to isolate fluorescent signal in the

lipid droplets. Nile Red Fluorescence is quantified as Intensity Density, or Area of ROI

multiplied by ROI Mean Fluorescence.

Fat phenotypes were observed in at least three independent biological replicates (trials).

Quantitation of fat represents the data obtained in one trial.

Quantitation of GFP fluorescence of the *tph-1::GFP* reporter was performed by selecting

the neuronal cell body as the Region of Interest, and then using the Measure function in

Openlab.

**Egg-Laying**

Synchronized L4 worms were placed on individual plates, allowed to lay eggs for 24

hours and then transferred to a new plate each day for five days. The number of eggs laid

each day was counted.

**Pumping**

Synchronized, starved L1 larvae, were prepared, and maintained in uncrowded, well-fed

conditions at 20°.  Pharyngeal contractions of synchronized L4s (48-54 hours after

plating) were counted for 15 second intervals. At least three trials for each genotype were

conducted on separate days (*n*=10-15/genotype).

**Quantitative Real-Time PCR**

Synchronized populations of ~ 80,000-100,000 worms were grown in 100mL S-Basal

Buffer with OP50 supplemented with MgCl, $CaCl_2$ and trace metals. Worms were

harvested at the appropriate stage, washed three times in S-Basal and frozen in liquid

nitrogen. For RNA preparation, the pellet was thawed at 65° for 5-10 min.

RNA and cDNA were prepared according to (Van Gilst et al., 2005a). RNA was

extracted using Trizol.  Isolated total RNA was further purified using RNAeasy (Qiagen,

Valencia, California, USA) and treated with DNase. To make cDNA, 5ug of total RNA

was used in a 100ul reaction using the Protoscript cDNA kit (New England Biolabs,

Beverly, Massachusetts, USA). For quantitative RT-PCR, 30 μl PCR reactions consisted

of 1x Reaction Buffer (20mM Tris pH 8.4, 50 mM KCl), 1.5 mM MgCl, 125 μM dNTPs,

0.3 μM primers, cDNA (corresponding to cDNA derived from 8ng of RNA), *Taq*DNA

Polymerase (Promega or Invitrogen) and Sybr Green (Molecular Probes, Eugene,

Oregon, USA) for detection of the double-stranded DNA product. Quantitative RT-PCR

reactions were performed and analyzed on a Stratagene Mx3005P Machine using

MxPRO software (Stratagene, La Jolla, CA). Ct values for mutant and wild-type worms

were compared at a threshold of 1000.

**Serotonin treatment**

6cm NGM plates were supplemented with 250 μls of 0.2M serotonin hydrochloride

(Sigma, H9523) in a 0.1 M HCl solution to a final concentration of 5mM serotonin.

Plates were allowed to dry overnight, and then Nile Red was added. Worms were plated

on the serotonin-supplemented plates as synchronized L1s, and fat was assayed as in all

other Nile Red experiments.

# References

Albert, P.S., S.J. Brown, and D.L. Riddle. 1981. Sensory control of dauer larva formation in Caenorhabditis elegans. *J Comp Neurol*. 198:435-51.

Alcedo, J., and C. Kenyon. 2004. Regulation of C. elegans longevity by specific gustatory and olfactory neurons. *Neuron*. 41:45-55.

Ansley, S.J., J.L. Badano, O.E. Blacque, J. Hill, B.E. Hoskins, C.C. Leitch, J.C. Kim, A.J. Ross, E.R. Eichers, T.M. Teslovich, A.K. Mah, R.C. Johnsen, J.C. Cavender, R.A. Lewis, M.R. Leroux, P.L. Beales, and N. Katsanis. 2003. Basal body dysfunction is a likely cause of pleiotropic Bardet-Biedl syndrome. *Nature*. 425:628-33.

Apfeld, J., and C. Kenyon. 1999. Regulation of lifespan by sensory perception in Caenorhabditis elegans. *Nature*. 402:804-9.

Arora, S., and Anubhuti. 2006. Role of neuropeptides in appetite regulation and obesity--a review. *Neuropeptides*. 40:375-401.

Ashrafi, K. 2007. Obesity and the regulation of fat metabolism. *In WormBook*. T.C.e.R. Community, editor. WormBook.

Ashrafi, K., F.Y. Chang, J.L. Watts, A.G. Fraser, R.S. Kamath, J. Ahringer, and G. Ruvkun. 2003. Genome-wide RNAi analysis of Caenorhabditis elegans fat regulatory genes. *Nature*. 421:268-72.

Avery, L., and H.R. Horvitz. 1990. Effects of starvation and neuroactive drugs on feeding in Caenorhabditis elegans. *J Exp Zool*. 253:263-70.

Avidor-Reiss, T., A.M. Maer, E. Koundakjian, A. Polyanovsky, T. Keil, S. Subramaniam, and C.S. Zuker. 2004. Decoding cilia function: defining specialized genes required for compartmentalized cilia biogenesis. *Cell*. 117:527-39.

Badano, J.L., S.J. Ansley, C.C. Leitch, R.A. Lewis, J.R. Lupski, and N. Katsanis. 2003. Identification of a novel Bardet-Biedl syndrome protein, BBS7, that shares structural features with BBS1 and BBS2. *Am J Hum Genet*. 72:650-8.

Badano, J.L., N. Mitsuma, P.L. Beales, and N. Katsanis. 2006. The Ciliopathies: An Emerging Class of Human Genetic Disorders. *Annu Rev Genomics Hum Genet*. 7:125-148.

Bargmann, C.I. 2006. Chemosensation in *C. elegans*. *In WormBook*. T.C.e.R. Community, editor. WormBook.

Bargmann, C.I., E. Hartwieg, and H.R. Horvitz. 1993. Odorant-selective genes and neurons mediate olfaction in C. elegans. *Cell*. 74:515-27.

Bargmann, C.I., and H.R. Horvitz. 1991a. Chemosensory neurons with overlapping functions direct chemotaxis to multiple chemicals in C. elegans. *Neuron*. 7:729-42.

Bargmann, C.I., and H.R. Horvitz. 1991b. Control of larval development by chemosensory neurons in Caenorhabditis elegans. *Science*. 251:1243-6.

Bargmann, C.I.a.M. 1997. Chemotaxis and Thermotaxis.

Barr, M.M., J. DeModena, D. Braun, C.Q. Nguyen, D.H. Hall, and P.W. Sternberg. 2001. The Caenorhabditis elegans autosomal dominant polycystic kidney disease gene homologs lov-1 and pkd-2 act in the same pathway. *Curr Biol*. 11:1341-6.

Barr, M.M., and P.W. Sternberg. 1999. A polycystic kidney-disease gene homologue required for male mating behaviour in C. elegans. *Nature*. 401:386-9.

Batterham, R.L., H. Heffron, S. Kapoor, J.E. Chivers, K. Chandarana, H. Herzog, C.W. Le Roux, E.L. Thomas, J.D. Bell, and D.J. Withers. 2006. Critical role for peptide YY in protein-mediated satiation and body-weight regulation. *Cell Metab*. 4:223-33.

Baumeister, R., E. Schaffitzel, and M. Hertweck. 2006. Endocrine signaling in Caenorhabditis elegans controls stress response and longevity. *J Endocrinol*. 190:191-202.

Beales, P.L. 2005. Lifting the lid on Pandora's box: the Bardet-Biedl syndrome. *Curr Opin Genet Dev*. 15:315-23.

Beales, P.L., J.L. Badano, A.J. Ross, S.J. Ansley, B.E. Hoskins, B. Kirsten, C.A. Mein, P. Froguel, P.J. Scambler, R.A. Lewis, J.R. Lupski, and N. Katsanis. 2003. Genetic interaction of BBS1 mutations with alleles at other BBS loci can result in non-Mendelian Bardet-Biedl syndrome. *Am J Hum Genet*. 72:1187-99.

Beales, P.L., N. Elcioglu, A.S. Woolf, D. Parker, and F.A. Flinter. 1999. New criteria for improved diagnosis of Bardet-Biedl syndrome: results of a population survey. *J Med Genet*. 36:437-46.

Beales, P.L., H.A. Reid, M.H. Griffiths, E.R. Maher, F.A. Flinter, and A.S. Woolf. 2000. Renal cancer and malformations in relatives of patients with Bardet-Biedl syndrome. *Nephrol Dial Transplant*. 15:1977-85.

Beales, P.L., A.M. Warner, G.A. Hitman, R. Thakker, and F.A. Flinter. 1997. Bardet-Biedl syndrome: a molecular and phenotypic study of 18 families. *J Med Genet*. 34:92-8.

Bell, L.R., S. Stone, J. Yochem, J.E. Shaw, and R.K. Herman. 2006. The molecular identities of the Caenorhabditis elegans intraflagellar transport genes dyf-6, daf-10 and osm-1. *Genetics*. 173:1275-86.

Blacque, O.E., and M.R. Leroux. 2006. Bardet-Biedl syndrome: an emerging pathomechanism of intracellular transport. *Cell Mol Life Sci*. 63:2145-61.

Blacque, O.E., C. Li, P.N. Inglis, M.A. Esmail, G. Ou, A.K. Mah, D.L. Baillie, J.M. Scholey, and M.R. Leroux. 2006. The WD repeat-containing protein IFTA-1 is required for retrograde intraflagellar transport. *Mol Biol Cell*. 17:5053-62.

Blacque, O.E., E.A. Perens, K.A. Boroevich, P.N. Inglis, C. Li, A. Warner, J. Khattra, R.A. Holt, G. Ou, A.K. Mah, S.J. McKay, P. Huang, P. Swoboda, S.J. Jones, M.A. Marra, D.L. Baillie, D.G. Moerman, S. Shaham, and M.R. Leroux. 2005. Functional genomics of the cilium, a sensory organelle. *Curr Biol*. 15:935-41.

Blacque, O.E., M.J. Reardon, C. Li, J. McCarthy, M.R. Mahjoub, S.J. Ansley, J.L. Badano, A.K. Mah, P.L. Beales, W.S. Davidson, R.C. Johnsen, M. Audeh, R.H. Plasterk, D.L. Baillie, N. Katsanis, L.M. Quarmby, S.R. Wicks, and M.R. Leroux. 2004. Loss of C. elegans BBS-7 and BBS-8 protein function results in cilia defects and compromised intraflagellar transport. *Genes Dev*. 18:1630-42.

Brenner, S. 1974. The genetics of Caenorhabditis elegans. *Genetics*. 77:71-94.

Burghoorn, J., M.P. Dekkers, S. Rademakers, T. de Jong, R. Willemsen, and G. Jansen. 2007. Mutation of the MAP kinase DYF-5 affects docking and undocking of kinesin-2 motors and reduces their speed in the cilia of Caenorhabditis elegans. *Proc Natl Acad Sci U S A*. 104:7157-62.

Chalfie, M., and J. Sulston. 1981. Developmental genetics of the mechanosensory neurons of Caenorhabditis elegans. *Dev Biol*. 82:358-70.

Chase, D.L., and M.R. Koelle. 2007. Biogenic amine neurotransmitters in *C. elegans*. *In WormBook*. T.C.e.R. Community, editor. WormBook.

Chaudhri, O., C. Small, and S. Bloom. 2006. Gastrointestinal hormones regulating appetite. *Philos Trans R Soc Lond B Biol Sci*. 361:1187-209.

Chen, N., A. Mah, O.E. Blacque, J. Chu, K. Phgora, M.W. Bakhoum, C.R. Newbury, J. Khattra, S. Chan, A. Go, E. Efimenko, R. Johnsen, P. Phirke, P. Swoboda, M. Marra, D.G. Moerman, M.R. Leroux, D.L. Baillie, and L.D. Stein. 2006. Identification of ciliary and ciliopathy genes in Caenorhabditis elegans through comparative genomics. *Genome Biol*. 7:R126.

Chiang, A.P., J.S. Beck, H.J. Yen, M.K. Tayeh, T.E. Scheetz, R.E. Swiderski, D.Y. Nishimura, T.A. Braun, K.Y. Kim, J. Huang, K. Elbedour, R. Carmi, D.C. Slusarski, T.L. Casavant, E.M. Stone, and V.C. Sheffield. 2006. Homozygosity mapping with SNP arrays identifies TRIM32, an E3 ubiquitin ligase, as a Bardet-Biedl syndrome gene (BBS11). *Proc Natl Acad Sci U S A*. 103:6287-92.

Chiang, A.P., D. Nishimura, C. Searby, K. Elbedour, R. Carmi, A.L. Ferguson, J. Secrist, T. Braun, T. Casavant, E.M. Stone, and V.C. Sheffield. 2004. Comparative genomic analysis identifies an ADP-ribosylation factor-like gene as the cause of Bardet-Biedl syndrome (BBS3). *Am J Hum Genet*. 75:475-84.

Choy, L., and R. Derynck. 2003. Transforming growth factor-beta inhibits adipocyte differentiation by Smad3 interacting with CCAAT/enhancer-binding protein (C/EBP) and repressing C/EBP transactivation function. *J Biol Chem*. 278:9609-19.

Clouthier, D.E., S.A. Comerford, and R.E. Hammer. 1997. Hepatic fibrosis, glomerulosclerosis, and a lipodystrophy-like syndrome in PEPCK-TGF-beta1 transgenic mice. *J Clin Invest*. 100:2697-713.

Cole, D.G., D.R. Diener, A.L. Himelblau, P.L. Beech, J.C. Fuster, and J.L. Rosenbaum. 1998. Chlamydomonas kinesin-II-dependent intraflagellar transport (IFT): IFT particles contain proteins required for ciliary assembly in Caenorhabditis elegans sensory neurons. *J Cell Biol*. 141:993-1008.

Coleman, D.L., and E.M. Eicher. 1990. Fat (fat) and tubby (tub): two autosomal recessive mutations causing obesity syndromes in the mouse. *J Hered*. 81:424-7.

Collet, J., C.A. Spike, E.A. Lundquist, J.E. Shaw, and R.K. Herman. 1998. Analysis of osm-6, a gene that affects sensory cilium structure and sensory neuron function in Caenorhabditis elegans. *Genetics*. 148:187-200.

Colosimo, M.E., A. Brown, S. Mukhopadhyay, C. Gabel, A.E. Lanjuin, A.D. Samuel, and P. Sengupta. 2004. Identification of thermosensory and olfactory neuron-specific genes via expression profiling of single neuron types. *Curr Biol*. 14:2245-51.

Croft, J.B., D. Morrell, C.L. Chase, and M. Swift. 1995. Obesity in heterozygous carriers of the gene for the Bardet-Biedl syndrome. *Am J Med Genet*. 55:12-5.

Culotti, J.G., and R.L. Russell. 1978. Osmotic avoidance defective mutants of the nematode Caenorhabditis elegans. *Genetics*. 90:243-56.

Davenport, J.R., and B.K. Yoder. 2005. An incredible decade for the primary cilium: a look at a once-forgotten organelle. *Am J Physiol Renal Physiol*. 289:F1159-69.

Deane, J.A., D.G. Cole, E.S. Seeley, D.R. Diener, and J.L. Rosenbaum. 2001. Localization of intraflagellar transport protein IFT52 identifies basal body transitional fibers as the docking site for IFT particles. *Curr Biol*. 11:1586-90.

Dusenbery, D.B. 1974. Analysis of chemotaxis in the nematode Caenorhabditis elegans by countercurrent separation. *J Exp Zool*. 188:41-7.

Dusenbery, D.B., R.E. Sheridan, and R.L. Russell. 1975. Chemotaxis-defective mutants of the nematode Caenorhabditis elegans. *Genetics*. 80:297-309.

Dwyer, N.D., E.R. Troemel, P. Sengupta, and C.I. Bargmann. 1998. Odorant receptor localization to olfactory cilia is mediated by ODR-4, a novel membrane-associated protein. *Cell*. 93:455-66.

Efimenko, E., O.E. Blacque, G. Ou, C.J. Haycraft, B.K. Yoder, J.M. Scholey, M.R. Leroux, and P. Swoboda. 2006. Caenorhabditis elegans DYF-2, an orthologue of human WDR19, is a component of the intraflagellar transport machinery in sensory cilia. *Mol Biol Cell*. 17:4801-11.

Efimenko, E., K. Bubb, H.Y. Mak, T. Holzman, M.R. Leroux, G. Ruvkun, J.H. Thomas, and P. Swoboda. 2005. Analysis of xbx genes in C. elegans. *Development*. 132:1923-34.

Elmquist, J.K., C.F. Elias, and C.B. Saper. 1999. From lesions to leptin: hypothalamic control of food intake and body weight. *Neuron*. 22:221-32.

Elmquist, J.K., E. Maratos-Flier, C.B. Saper, and J.S. Flier. 1998. Unraveling the central nervous system pathways underlying responses to leptin. *Nat Neurosci*. 1:445-50.

Evans, J.E., J.J. Snow, A.L. Gunnarson, G. Ou, H. Stahlberg, K.L. McDonald, and J.M. Scholey. 2006. Functional modulation of IFT kinesins extends the sensory repertoire of ciliated neurons in Caenorhabditis elegans. *J Cell Biol*. 172:663-9.

Fain, J.N., D.S. Tichansky, and A.K. Madan. 2005. Transforming growth factor beta1 release by human adipose tissue is enhanced in obesity. *Metabolism*. 54:1546-51.

Fan, Y., M.A. Esmail, S.J. Ansley, O.E. Blacque, K. Boroevich, A.J. Ross, S.J. Moore, J.L. Badano, H. May-Simera, D.S. Compton, J.S. Green, R.A. Lewis, M.M. van Haelst, P.S. Parfrey, D.L. Baillie, P.L. Beales, N. Katsanis, W.S. Davidson, and M.R. Leroux. 2004. Mutations in a member of the Ras superfamily of small GTP-binding proteins causes Bardet-Biedl syndrome. *Nat Genet*. 36:989-93.

Farag, T.I., and A.S. Teebi. 1988. Bardet-Biedl and Laurence-Moon syndromes in a mixed Arab population. *Clin Genet*. 33:78-82.

Farag, T.I., and A.S. Teebi. 1989. High incidence of Bardet Biedl syndrome among the Bedouin. *Clin Genet*. 36:463-4.

Fath, M.A., R.F. Mullins, C. Searby, D.Y. Nishimura, J. Wei, K. Rahmouni, R.E. Davis, M.K. Tayeh, M. Andrews, B. Yang, C.D. Sigmund, E.M. Stone, and V.C. Sheffield. 2005. Mkks-null mice have a phenotype resembling Bardet-Biedl syndrome. *Hum Mol Genet*. 14:1109-18.

Fliegauf, M., J. Horvath, C. von Schnakenburg, H. Olbrich, D. Muller, J. Thumfart, B. Schermer, G.J. Pazour, H.P. Neumann, H. Zentgraf, T. Benzing, and H. Omran. 2006. Nephrocystin specifically localizes to the transition zone of renal and respiratory cilia and photoreceptor connecting cilia. *J Am Soc Nephrol*. 17:2424-33.

Friedman, J.M., and J.L. Halaas. 1998. Leptin and the regulation of body weight in mammals. *Nature*. 395:763-70.

Fujiwara, M., T. Ishihara, and I. Katsura. 1999. A novel WD40 protein, CHE-2, acts cell-autonomously in the formation of C. elegans sensory cilia. *Development*. 126:4839-48.

Gahmon, G.a.S., P. 2006. We would really like to know what all those isoforms of the DAF19 Transcription Factor are doing in all those Neurons. *In C. elegans* Neuroscience Meeting, University of Wisconsin-Madison.

Grace, C., P. Beales, C. Summerbell, S.A. Jebb, A. Wright, D. Parker, and P. Kopelman. 2003. Energy metabolism in Bardet-Biedl syndrome. *Int J Obes Relat Metab Disord*. 27:1319-24.

Gray, J.M., D.S. Karow, H. Lu, A.J. Chang, J.S. Chang, R.E. Ellis, M.A. Marletta, and C.I. Bargmann. 2004. Oxygen sensation and social feeding mediated by a C. elegans guanylate cyclase homologue. *Nature*. 430:317-22.

Guichard, C., M.C. Harricane, J.J. Lafitte, P. Godard, M. Zaegel, V. Tack, G. Lalau, and P. Bouvagnet. 2001. Axonemal dynein intermediate-chain gene (DNAI1) mutations result in situs inversus and primary ciliary dyskinesia (Kartagener syndrome). *Am J Hum Genet*. 68:1030-5.

Hall, D.H., and R.L. Russell. 1991. The posterior nervous system of the nematode Caenorhabditis elegans: serial reconstruction of identified neurons and complete pattern of synaptic interactions. *J Neurosci*. 11:1-22.

Hart, A.C., S. Sims, and J.M. Kaplan. 1995. Synaptic code for sensory modalities revealed by C. elegans GLR-1 glutamate receptor. *Nature*. 378:82-5.

Haycraft, C.J., J.C. Schafer, Q. Zhang, P.D. Taulman, and B.K. Yoder. 2003. Identification of CHE-13, a novel intraflagellar transport protein required for cilia formation. *Exp Cell Res*. 284:251-63.

Haycraft, C.J., P. Swoboda, P.D. Taulman, J.H. Thomas, and B.K. Yoder. 2001. The C. elegans homolog of the murine cystic kidney disease gene Tg737 functions in a ciliogenic pathway and is disrupted in osm-5 mutant worms. *Development*. 128:1493-505.

Hedgecock, E.M., and R.L. Russell. 1975. Normal and mutant thermotaxis in the nematode Caenorhabditis elegans. *Proc Natl Acad Sci U S A*. 72:4061-5.

Heisler, L.K., M.A. Cowley, T. Kishi, L.H. Tecott, W. Fan, M.J. Low, J.L. Smart, M. Rubinstein, J.B. Tatro, J.M. Zigman, R.D. Cone, and J.K. Elmquist. 2003. Central serotonin and melanocortin pathways regulating energy homeostasis. *Ann N Y Acad Sci*. 994:169-74.

Hu, J., and M.M. Barr. 2005. ATP-2 interacts with the PLAT domain of LOV-1 and is involved in Caenorhabditis elegans polycystin signaling. *Mol Biol Cell*. 16:458-69.

Husson, S.J., E. Clynen, G. Baggerman, A. De Loof, and L. Schoofs. 2005. Discovering neuropeptides in Caenorhabditis elegans by two dimensional liquid chromatography and mass spectrometry. *Biochem Biophys Res Commun*. 335:76-86.

Husson, S.J., T. Janssen, G. Baggerman, B. Bogert, A.H. Kahn-Kirby, K. Ashrafi, and L. Schoofs. 2007. Impaired processing of FLP and NLP peptides in carboxypeptidase E (EGL-21)-deficient Caenorhabditis elegans as analyzed by mass spectrometry. *J Neurochem*. 102:246-60.

Imanishi, M., N.F. Endres, A. Gennerich, and R.D. Vale. 2006. Autoinhibition regulates the motility of the C. elegans intraflagellar transport motor OSM-3. *J Cell Biol*. 174:931-7.

Inglis, P.N., K.A. Boroevich, and M.R. Leroux. 2006. Piecing together a ciliome. *Trends Genet*. 22:491-500.

Inglis, P.N., Ou, G., Leroux, M. R., Scholey, J. M. 2006. The sensory cilia of *Caenorhabditis elegans*. *In WormBook*. T.C.e.R. Community, editor. WormBook.

Iomini, C., V. Babaev-Khaimov, M. Sassaroli, and G. Piperno. 2001. Protein particles in Chlamydomonas flagella undergo a transport cycle consisting of four phases. *J Cell Biol*. 153:13-24.

Kalra, S.P., M.G. Dube, A. Sahu, C.P. Phelps, and P.S. Kalra. 1991. Neuropeptide Y secretion increases in the paraventricular nucleus in association with increased appetite for food. *Proc Natl Acad Sci U S A*. 88:10931-5.

Kaplan, J.M., and H.R. Horvitz. 1993. A dual mechanosensory and chemosensory neuron in Caenorhabditis elegans. *Proc Natl Acad Sci U S A*. 90:2227-31.

Katsanis, N., S.J. Ansley, J.L. Badano, E.R. Eichers, R.A. Lewis, B.E. Hoskins, P.J. Scambler, W.S. Davidson, P.L. Beales, and J.R. Lupski. 2001. Triallelic inheritance in Bardet-Biedl syndrome, a Mendelian recessive disorder. *Science*. 293:2256-9.

Katsanis, N., P.L. Beales, M.O. Woods, R.A. Lewis, J.S. Green, P.S. Parfrey, S.J. Ansley, W.S. Davidson, and J.R. Lupski. 2000. Mutations in MKKS cause obesity, retinal dystrophy and renal malformations associated with Bardet-Biedl syndrome. *Nat Genet*. 26:67-70.

Kawano, T., R. Nagatomo, Y. Kimura, K. Gengyo-Ando, and S. Mitani. 2006. Disruption of ins-11, a Caenorhabditis elegans insulin-like gene, and phenotypic analyses of the gene-disrupted animal. *Biosci Biotechnol Biochem*. 70:3084-7.

Keller, L.C., E.P. Romijn, I. Zamora, J.R. Yates, 3rd, and W.F. Marshall. 2005. Proteomic analysis of isolated chlamydomonas centrioles reveals orthologs of ciliary-disease genes. *Curr Biol*. 15:1090-8.

Kim, J.C., J.L. Badano, S. Sibold, M.A. Esmail, J. Hill, B.E. Hoskins, C.C. Leitch, K. Venner, S.J. Ansley, A.J. Ross, M.R. Leroux, N. Katsanis, and P.L. Beales. 2004. The Bardet-Biedl protein BBS4 targets cargo to the pericentriolar region and is required for microtubule anchoring and cell cycle progression. *Nat Genet*. 36:462-70.

Kim, J.C., Y.Y. Ou, J.L. Badano, M.A. Esmail, C.C. Leitch, E. Fiedrich, P.L. Beales, J.M. Archibald, N. Katsanis, J.B. Rattner, and M.R. Leroux. 2005. MKKS/BBS6, a divergent chaperonin-like protein linked to the obesity disorder Bardet-Biedl syndrome, is a novel centrosomal component required for cytokinesis. *J Cell Sci*. 118:1007-20.

Kim, K., and C. Li. 2004. Expression and regulation of an FMRFamide-related neuropeptide gene family in Caenorhabditis elegans. *J Comp Neurol*. 475:540-50.

Kimura, K.D., H.A. Tissenbaum, Y. Liu, and G. Ruvkun. 1997. daf-2, an insulin receptor-like gene that regulates longevity and diapause in Caenorhabditis elegans. *Science*. 277:942-6.

Kleyn, P.W., W. Fan, S.G. Kovats, J.J. Lee, J.C. Pulido, Y. Wu, L.R. Berkemeier, D.J. Misumi, L. Holmgren, O. Charlat, E.A. Woolf, O. Tayber, T. Brody, P. Shu, F.

Hawkins, B. Kennedy, L. Baldini, C. Ebeling, G.D. Alperin, J. Deeds, N.D. Lakey, J. Culpepper, H. Chen, M.A. Glucksmann-Kuis, G.A. Carlson, G.M. Duyk, and K.J. Moore. 1996. Identification and characterization of the mouse obesity gene tubby: a member of a novel gene family. *Cell*. 85:281-90.

Kobayashi, T., K. Gengyo-Ando, T. Ishihara, I. Katsura, and S. Mitani. 2007. IFT-81 and IFT-74 are required for intraflagellar transport in C. elegans. *Genes Cells*. 12:593-602.

Kozminski, K.G., K.A. Johnson, P. Forscher, and J.L. Rosenbaum. 1993. A motility in the eukaryotic flagellum unrelated to flagellar beating. *Proc Natl Acad Sci U S A*. 90:5519-23.

Kubo, A., and S. Tsukita. 2003. Non-membranous granular organelle consisting of PCM-1: subcellular distribution and cell-cycle-dependent assembly/disassembly. *J Cell Sci*. 116:919-28.

Kulaga, H.M., C.C. Leitch, E.R. Eichers, J.L. Badano, A. Lesemann, B.E. Hoskins, J.R. Lupski, P.L. Beales, R.R. Reed, and N. Katsanis. 2004. Loss of BBS proteins causes anosmia in humans and defects in olfactory cilia structure and function in the mouse. *Nat Genet*. 36:994-8.

Kunitomo, H., H. Uesugi, Y. Kohara, and Y. Iino. 2005. Identification of ciliated sensory neuron-expressed genes in Caenorhabditis elegans using targeted pull-down of poly(A) tails. *Genome Biol*. 6:R17.

Kyttala, M., J. Tallila, R. Salonen, O. Kopra, N. Kohlschmidt, P. Paavola-Sakki, L. Peltonen, and M. Kestila. 2006. MKS1, encoding a component of the flagellar apparatus basal body proteome, is mutated in Meckel syndrome. *Nat Genet*. 38:155-7.

Leroux, M.R. 2007. Taking vesicular transport to the cilium. *Cell*. 129:1041-3.

Lewis, J.A., and J.A. Hodgkin. 1977. Specific neuroanatomical changes in chemosensory mutants of the nematode Caenorhabditis elegans. *J Comp Neurol*. 172:489-510.

Li, C. 2005. The ever-expanding neuropeptide gene families in the nematode Caenorhabditis elegans. *Parasitology*. 131 Suppl:S109-27.

Li, C., K. Kim, and L.S. Nelson. 1999a. FMRFamide-related neuropeptide gene family in Caenorhabditis elegans. *Brain Res*. 848:26-34.

Li, C., L.S. Nelson, K. Kim, A. Nathoo, and A.C. Hart. 1999b. Neuropeptide gene families in the nematode Caenorhabditis elegans. *Ann N Y Acad Sci*. 897:239-52.

Li, J.B., J.M. Gerdes, C.J. Haycraft, Y. Fan, T.M. Teslovich, H. May-Simera, H. Li, O.E. Blacque, L. Li, C.C. Leitch, R.A. Lewis, J.S. Green, P.S. Parfrey, M.R. Leroux, W.S. Davidson, P.L. Beales, L.M. Guay-Woodford, B.K. Yoder, G.D. Stormo, N. Katsanis, and S.K. Dutcher. 2004a. Comparative genomics identifies a flagellar and basal body proteome that includes the BBS5 human disease gene. *Cell*. 117:541-52.

Li, S., C.M. Armstrong, N. Bertin, H. Ge, S. Milstein, M. Boxem, P.O. Vidalain, J.D. Han, A. Chesneau, T. Hao, D.S. Goldberg, N. Li, M. Martinez, J.F. Rual, P. Lamesch, L. Xu, M. Tewari, S.L. Wong, L.V. Zhang, G.F. Berriz, L. Jacotot, P. Vaglio, J. Reboul, T. Hirozane-Kishikawa, Q. Li, H.W. Gabel, A. Elewa, B. Baumgartner, D.J. Rose, H. Yu, S. Bosak, R. Sequerra, A. Fraser, S.E. Mango, W.M. Saxton, S. Strome, S. Van Den Heuvel, F. Piano, J. Vandenhaute, C. Sardet, M. Gerstein, L. Doucette-Stamm, K.C. Gunsalus, J.W. Harper, M.E.

Cusick, F.P. Roth, D.E. Hill, and M. Vidal. 2004b. A map of the interactome network of the metazoan C. elegans. *Science*. 303:540-3.

Li, W., S.G. Kennedy, and G. Ruvkun. 2003. daf-28 encodes a C. elegans insulin superfamily member that is regulated by environmental cues and acts in the DAF-2 signaling pathway. *Genes Dev*. 17:844-58.

Lin, F., T. Hiesberger, K. Cordes, A.M. Sinclair, L.S. Goldstein, S. Somlo, and P. Igarashi. 2003. Kidney-specific inactivation of the KIF3A subunit of kinesin-II inhibits renal ciliogenesis and produces polycystic kidney disease. *Proc Natl Acad Sci U S A*. 100:5286-91.

Lucker, B.F., R.H. Behal, H. Qin, L.C. Siron, W.D. Taggart, J.L. Rosenbaum, and D.G. Cole. 2005. Characterization of the intraflagellar transport complex B core: direct interaction of the IFT81 and IFT74/72 subunits. *J Biol Chem*. 280:27688-96.

Mak, H.Y., L.S. Nelson, M. Basson, C.D. Johnson, and G. Ruvkun. 2006. Polygenic control of Caenorhabditis elegans fat storage. *Nat Genet*. 38:363-8.

Marszalek, J.R., X. Liu, E.A. Roberts, D. Chui, J.D. Marth, D.S. Williams, and L.S. Goldstein. 2000. Genetic evidence for selective transport of opsin and arrestin by kinesin-II in mammalian photoreceptors. *Cell*. 102:175-87.

McVeigh, P., S. Leech, G.R. Mair, N.J. Marks, T.G. Geary, and A.G. Maule. 2005. Analysis of FMRFamide-like peptide (FLP) diversity in phylum Nematoda. *Int J Parasitol*. 35:1043-60.

Michaud, E.J., and B.K. Yoder. 2006. The primary cilium in cell signaling and cancer. *Cancer Res*. 66:6463-7.

Mollet, G., F. Silbermann, M. Delous, R. Salomon, C. Antignac, and S. Saunier. 2005. Characterization of the nephrocystin/nephrocystin-4 complex and subcellular localization of nephrocystin-4 to primary cilia and centrosomes. *Hum Mol Genet*. 14:645-56.

Mori, I. 1999. Genetics of chemotaxis and thermotaxis in the nematode Caenorhabditis elegans. *Annu Rev Genet*. 33:399-422.

Morton, G.J., D.E. Cummings, D.G. Baskin, G.S. Barsh, and M.W. Schwartz. 2006. Central nervous system control of food intake and body weight. *Nature*. 443:289-95.

Moyer, J.H., M.J. Lee-Tischler, H.Y. Kwon, J.J. Schrick, E.D. Avner, W.E. Sweeney, V.L. Godfrey, N.L. Cacheiro, J.E. Wilkinson, and R.P. Woychik. 1994. Candidate gene associated with a mutation causing recessive polycystic kidney disease in mice. *Science*. 264:1329-33.

Mukhopadhyay, A., B. Deplancke, A.J. Walhout, and H.A. Tissenbaum. 2005. C. elegans tubby regulates life span and fat storage by two independent mechanisms. *Cell Metab*. 2:35-42.

Mukhopadhyay, A., X. Pan, D.G. Lambright, and H.A. Tissenbaum. 2007a. An endocytic pathway as a target of tubby for regulation of fat storage. *EMBO Rep*.

Mukhopadhyay, S., Y. Lu, H. Qin, A. Lanjuin, S. Shaham, and P. Sengupta. 2007b. Distinct IFT mechanisms contribute to the generation of ciliary structural diversity in C. elegans. *Embo J*. 26:2966-80.

Murayama, T., Y. Toh, Y. Ohshima, and M. Koga. 2005. The dyf-3 gene encodes a novel protein required for sensory cilium formation in Caenorhabditis elegans. *J Mol Biol*. 346:677-87.

Murcia, N.S., W.G. Richards, B.K. Yoder, M.L. Mucenski, J.R. Dunlap, and R.P. Woychik. 2000. The Oak Ridge Polycystic Kidney (orpk) disease gene is required for left-right axis determination. *Development*. 127:2347-55.

Mykytyn, K., T. Braun, R. Carmi, N.B. Haider, C.C. Searby, M. Shastri, G. Beck, A.F. Wright, A. Iannaccone, K. Elbedour, R. Riise, A. Baldi, A. Raas-Rothschild, S.W. Gorman, D.M. Duhl, S.G. Jacobson, T. Casavant, E.M. Stone, and V.C. Sheffield. 2001. Identification of the gene that, when mutated, causes the human obesity syndrome BBS4. *Nat Genet*. 28:188-91.

Mykytyn, K., R.F. Mullins, M. Andrews, A.P. Chiang, R.E. Swiderski, B. Yang, T. Braun, T. Casavant, E.M. Stone, and V.C. Sheffield. 2004. Bardet-Biedl syndrome type 4 (BBS4)-null mice implicate Bbs4 in flagella formation but not global cilia assembly. *Proc Natl Acad Sci U S A*. 101:8664-9.

Mykytyn, K., D.Y. Nishimura, C.C. Searby, G. Beck, K. Bugge, H.L. Haines, A.S. Cornier, G.F. Cox, A.B. Fulton, R. Carmi, A. Iannaccone, S.G. Jacobson, R.G. Weleber, A.F. Wright, R. Riise, R.C. Hennekam, G. Luleci, S. Berker-Karauzum, L.G. Biesecker, E.M. Stone, and V.C. Sheffield. 2003. Evaluation of complex inheritance involving the most common Bardet-Biedl syndrome locus (BBS1). *Am J Hum Genet*. 72:429-37.

Mykytyn, K., D.Y. Nishimura, C.C. Searby, M. Shastri, H.J. Yen, J.S. Beck, T. Braun, L.M. Streb, A.S. Cornier, G.F. Cox, A.B. Fulton, R. Carmi, G. Luleci, S.C. Chandrasekharappa, F.S. Collins, S.G. Jacobson, J.R. Heckenlively, R.G. Weleber, E.M. Stone, and V.C. Sheffield. 2002. Identification of the gene (BBS1) most commonly involved in Bardet-Biedl syndrome, a complex human obesity syndrome. *Nat Genet*. 31:435-8.

Nachury, M.V., A.V. Loktev, Q. Zhang, C.J. Westlake, J. Peranen, A. Merdes, D.C. Slusarski, R.H. Scheller, J.F. Bazan, V.C. Sheffield, and P.K. Jackson. 2007. A core complex of BBS proteins cooperates with the GTPase Rab8 to promote ciliary membrane biogenesis. *Cell*. 129:1201-13.

Nathoo, A.N., R.A. Moeller, B.A. Westlund, and A.C. Hart. 2001. Identification of neuropeptide-like protein gene families in Caenorhabditiselegans and other species. *Proc Natl Acad Sci U S A*. 98:14000-5.

Nauli, S.M., F.J. Alenghat, Y. Luo, E. Williams, P. Vassilev, X. Li, A.E. Elia, W. Lu, E.M. Brown, S.J. Quinn, D.E. Ingber, and J. Zhou. 2003. Polycystins 1 and 2 mediate mechanosensation in the primary cilium of kidney cells. *Nat Genet*. 33:129-37.

Nishimura, D.Y., M. Fath, R.F. Mullins, C. Searby, M. Andrews, R. Davis, J.L. Andorf, K. Mykytyn, R.E. Swiderski, B. Yang, R. Carmi, E.M. Stone, and V.C. Sheffield. 2004. Bbs2-null mice have neurosensory deficits, a defect in social dominance, and retinopathy associated with mislocalization of rhodopsin. *Proc Natl Acad Sci U S A*. 101:16588-93.

Nishimura, D.Y., C.C. Searby, R. Carmi, K. Elbedour, L. Van Maldergem, A.B. Fulton, B.L. Lam, B.R. Powell, R.E. Swiderski, K.E. Bugge, N.B. Haider, A.E. Kwitek-Black, L. Ying, D.M. Duhl, S.W. Gorman, E. Heon, A. Iannaccone, D. Bonneau, L.G. Biesecker, S.G. Jacobson, E.M. Stone, and V.C. Sheffield. 2001. Positional cloning of a novel gene on chromosome 16q causing Bardet-Biedl syndrome (BBS2). *Hum Mol Genet*. 10:865-74.

Nishimura, D.Y., R.E. Swiderski, C.C. Searby, E.M. Berg, A.L. Ferguson, R. Hennekam, S. Merin, R.G. Weleber, L.G. Biesecker, E.M. Stone, and V.C. Sheffield. 2005. Comparative genomics and gene expression analysis identifies BBS9, a new Bardet-Biedl syndrome gene. *Am J Hum Genet*. 77:1021-33.

Noben-Trauth, K., J.K. Naggert, M.A. North, and P.M. Nishina. 1996. A candidate gene for the mouse mutation tubby. *Nature*. 380:534-8.

North, M.A., J.K. Naggert, Y. Yan, K. Noben-Trauth, and P.M. Nishina. 1997. Molecular characterization of TUB, TULP1, and TULP2, members of the novel tubby gene family and their possible relation to ocular diseases. *Proc Natl Acad Sci U S A*. 94:3128-33.

Ogg, S., S. Paradis, S. Gottlieb, G.I. Patterson, L. Lee, H.A. Tissenbaum, and G. Ruvkun. 1997. The Fork head transcription factor DAF-16 transduces insulin-like metabolic and longevity signals in C. elegans. *Nature*. 389:994-9.

Ohlemiller, K.K., R.M. Hughes, J.M. Lett, J.M. Ogilvie, J.D. Speck, J.S. Wright, and B.T. Faddis. 1997. Progression of cochlear and retinal degeneration in the tubby (rd5) mouse. *Audiol Neurootol*. 2:175-85.

Olbrich, H., K. Haffner, A. Kispert, A. Volkel, A. Volz, G. Sasmaz, R. Reinhardt, S. Hennig, H. Lehrach, N. Konietzko, M. Zariwala, P.G. Noone, M. Knowles, H.M. Mitchison, M. Meeks, E.M. Chung, F. Hildebrandt, R. Sudbrak, and H. Omran. 2002. Mutations in DNAH5 cause primary ciliary dyskinesia and randomization of left-right asymmetry. *Nat Genet*. 30:143-4.

Ostrowski, L.E., K. Blackburn, K.M. Radde, M.B. Moyer, D.M. Schlatzer, A. Moseley, and R.C. Boucher. 2002. A proteomic analysis of human cilia: identification of novel components. *Mol Cell Proteomics*. 1:451-65.

Ou, G., O.E. Blacque, J.J. Snow, M.R. Leroux, and J.M. Scholey. 2005. Functional coordination of intraflagellar transport motors. *Nature*. 436:583-7.

Ou, G., M. Koga, O.E. Blacque, T. Murayama, Y. Ohshima, J.C. Schafer, C. Li, B.K. Yoder, M.R. Leroux, and J.M. Scholey. 2007. Sensory ciliogenesis in Caenorhabditis elegans: assignment of IFT components into distinct modules based on transport and phenotypic profiles. *Mol Biol Cell*. 18:1554-69.

Pan, X., G. Ou, G. Civelekoglu-Scholey, O.E. Blacque, N.F. Endres, L. Tao, A. Mogilner, M.R. Leroux, R.D. Vale, and J.M. Scholey. 2006. Mechanism of transport of IFT particles in C. elegans cilia by the concerted action of kinesin-II and OSM-3 motors. *J Cell Biol*. 174:1035-45.

Pazour, G.J., N. Agrin, J. Leszyk, and G.B. Witman. 2005. Proteomic analysis of a eukaryotic cilium. *J Cell Biol*. 170:103-13.

Pazour, G.J., B.L. Dickert, Y. Vucica, E.S. Seeley, J.L. Rosenbaum, G.B. Witman, and D.G. Cole. 2000. Chlamydomonas IFT88 and its mouse homologue, polycystic kidney disease gene tg737, are required for assembly of cilia and flagella. *J Cell Biol*. 151:709-18.

Pazour, G.J., and J.L. Rosenbaum. 2002. Intraflagellar transport and cilia-dependent diseases. *Trends Cell Biol*. 12:551-5.

Pazour, G.J., C.G. Wilkerson, and G.B. Witman. 1998. A dynein light chain is essential for the retrograde particle movement of intraflagellar transport (IFT). *J Cell Biol*. 141:979-92.

Peden, E.M., and M.M. Barr. 2005. The KLP-6 kinesin is required for male mating behaviors and polycystin localization in Caenorhabditis elegans. *Curr Biol*. 15:394-404.

Pedersen, L.B., S. Geimer, and J.L. Rosenbaum. 2006. Dissecting the molecular mechanisms of intraflagellar transport in chlamydomonas. *Curr Biol*. 16:450-9.

Pedersen, L.B., M.S. Miller, S. Geimer, J.M. Leitch, J.L. Rosenbaum, and D.G. Cole. 2005. Chlamydomonas IFT172 is encoded by FLA11, interacts with CrEB1, and regulates IFT at the flagellar tip. *Curr Biol*. 15:262-6.

Pennarun, G., C. Chapelin, E. Escudier, A.M. Bridoux, F. Dastot, V. Cacheux, M. Goossens, S. Amselem, and B. Duriez. 2000. The human dynein intermediate chain 2 gene (DNAI2): cloning, mapping, expression pattern, and evaluation as a candidate for primary ciliary dyskinesia. *Hum Genet*. 107:642-9.

Perez, C.L., and Van Gilst, M. 2007. Using Metabolic Tracers to Quantify Fatty Acid Synthesis, Absorption, and Expenditure in *C. elegans*. *In* 16th International *C. elegans* Meetin, University of California, Los Angeles.

Perkins, L.A., E.M. Hedgecock, J.N. Thomson, and J.G. Culotti. 1986. Mutant sensory cilia in the nematode Caenorhabditis elegans. *Dev Biol*. 117:456-87.

Pierce, S.B., M. Costa, R. Wisotzkey, S. Devadhar, S.A. Homburger, A.R. Buchman, K.C. Ferguson, J. Heller, D.M. Platt, A.A. Pasquinelli, L.X. Liu, S.K. Doberstein, and G. Ruvkun. 2001. Regulation of DAF-2 receptor signaling by human insulin and ins-1, a member of the unusually large and diverse C. elegans insulin gene family. *Genes Dev*. 15:672-86.

Piperno, G., E. Siuda, S. Henderson, M. Segil, H. Vaananen, and M. Sassaroli. 1998. Distinct mutants of retrograde intraflagellar transport (IFT) share similar morphological and molecular defects. *J Cell Biol*. 143:1591-601.

Porter, M.E., R. Bower, J.A. Knott, P. Byrd, and W. Dentler. 1999. Cytoplasmic dynein heavy chain 1b is required for flagellar assembly in Chlamydomonas. *Mol Biol Cell*. 10:693-712.

Qamar, S., M. Vadivelu, and R. Sandford. 2007. TRP channels and kidney disease: lessons from polycystic kidney disease. *Biochem Soc Trans*. 35:124-8.

Qin, H., J.L. Rosenbaum, and M.M. Barr. 2001. An autosomal recessive polycystic kidney disease gene homolog is involved in intraflagellar transport in C. elegans ciliated sensory neurons. *Curr Biol*. 11:457-61.

Qin, H., Z. Wang, D. Diener, and J. Rosenbaum. 2007. Intraflagellar transport protein 27 is a small G protein involved in cell-cycle control. *Curr Biol*. 17:193-202.

Quarmby, L.M., and J.D. Parker. 2005. Cilia and the cell cycle? *J Cell Biol*. 169:707-10.

Robert, A., G. Margall-Ducos, J.E. Guidotti, O. Bregerie, C. Celati, C. Brechot, and C. Desdouets. 2007. The intraflagellar transport component IFT88/polaris is a centrosomal protein regulating G1-S transition in non-ciliated cells. *J Cell Sci*. 120:628-37.

Rosenbaum, J. 2002. Intraflagellar transport. *Curr Biol*. 12:R125.

Rosenbaum, J.L., and G.B. Witman. 2002. Intraflagellar transport. *Nat Rev Mol Cell Biol*. 3:813-25.

Ross, A.J., H. May-Simera, E.R. Eichers, M. Kai, J. Hill, D.J. Jagger, C.C. Leitch, J.P. Chapple, P.M. Munro, S. Fisher, P.L. Tan, H.M. Phillips, M.R. Leroux, D.J. Henderson, J.N. Murdoch, A.J. Copp, M.M. Eliot, J.R. Lupski, D.T. Kemp, H.

Dollfus, M. Tada, N. Katsanis, A. Forge, and P.L. Beales. 2005. Disruption of Bardet-Biedl syndrome ciliary proteins perturbs planar cell polarity in vertebrates. *Nat Genet*. 37:1135-40.

Sage, D., F.R. Neumann, F. Hediger, S.M. Gasser, and M. Unser. 2005. Automatic tracking of individual fluorescence particles: application to the study of chromosome dynamics. *IEEE Trans Image Process*. 14:1372-83.

Sainsbury, A., G.J. Cooney, and H. Herzog. 2002. Hypothalamic regulation of energy homeostasis. *Best Pract Res Clin Endocrinol Metab*. 16:623-37.

Samad, F., K. Yamamoto, M. Pandey, and D.J. Loskutoff. 1997. Elevated expression of transforming growth factor-beta in adipose tissue from obese mice. *Mol Med*. 3:37-48.

Savage-Dunn, C. 2005. TGF-β signaling. *In WormBook*. T.C.e.R. Community, editor. WormBook.

Sawin, E.R., R. Ranganathan, and H.R. Horvitz. 2000. C. elegans locomotory rate is modulated by the environment through a dopaminergic pathway and by experience through a serotonergic pathway. *Neuron*. 26:619-31.

Saxena, R., B.F. Voight, V. Lyssenko, N.P. Burtt, P.I. de Bakker, H. Chen, J.J. Roix, S. Kathiresan, J.N. Hirschhorn, M.J. Daly, T.E. Hughes, L. Groop, D. Altshuler, P. Almgren, J.C. Florez, J. Meyer, K. Ardlie, K. Bengtsson Bostrom, B. Isomaa, G. Lettre, U. Lindblad, H.N. Lyon, O. Melander, C. Newton-Cheh, P. Nilsson, M. Orho-Melander, L. Rastam, E.K. Speliotes, M.R. Taskinen, T. Tuomi, C. Guiducci, A. Berglund, J. Carlson, L. Gianniny, R. Hackett, L. Hall, J. Holmkvist, E. Laurila, M. Sjogren, M. Sterner, A. Surti, M. Svensson, M. Svensson, R. Tewhey, B. Blumenstiel, M. Parkin, M. Defelice, R. Barry, W. Brodeur, J. Camarata, N. Chia, M. Fava, J. Gibbons, B. Handsaker, C. Healy, K. Nguyen, C. Gates, C. Sougnez, D. Gage, M. Nizzari, S.B. Gabriel, G.W. Chirn, Q. Ma, H. Parikh, D. Richardson, D. Ricke, and S. Purcell. 2007. Genome-wide association analysis identifies loci for type 2 diabetes and triglyceride levels. *Science*. 316:1331-6.

Scaglione, R., C. Argano, T. di Chiara, D. Colomba, G. Parrinello, S. Corrao, G. Avellone, and G. Licata. 2003. Central obesity and hypertensive renal disease: association between higher levels of BMI, circulating transforming growth factor beta1 and urinary albumin excretion. *Blood Press*. 12:269-76.

Schackwitz, W.S., T. Inoue, and J.H. Thomas. 1996. Chemosensory neurons function in parallel to mediate a pheromone response in C. elegans. *Neuron*. 17:719-28.

Schafer, J.C., C.J. Haycraft, J.H. Thomas, B.K. Yoder, and P. Swoboda. 2003. XBX-1 encodes a dynein light intermediate chain required for retrograde intraflagellar transport and cilia assembly in Caenorhabditis elegans. *Mol Biol Cell*. 14:2057-70.

Schafer, W.R. 2005. Egg-laying. *In WormBook*. T.C.e.R. Community, editor. WormBook.

Scholey, J.M. 2003. Intraflagellar transport. *Annu Rev Cell Dev Biol*. 19:423-43.

Scholey, J.M., G. Ou, J. Snow, and A. Gunnarson. 2004. Intraflagellar transport motors in Caenorhabditis elegans neurons. *Biochem Soc Trans*. 32:682-4.

Schwartz, M.W., S.C. Woods, D. Porte, Jr., R.J. Seeley, and D.G. Baskin. 2000. Central nervous system control of food intake. *Nature*. 404:661-71.

Shakir, M.A., T. Fukushige, H. Yasuda, J. Miwa, and S.S. Siddiqui. 1993. C. elegans osm-3 gene mediating osmotic avoidance behaviour encodes a kinesin-like protein. *Neuroreport*. 4:891-4.

Signor, D., K.P. Wedaman, J.T. Orozco, N.D. Dwyer, C.I. Bargmann, L.S. Rose, and J.M. Scholey. 1999a. Role of a class DHC1b dynein in retrograde transport of IFT motors and IFT raft particles along cilia, but not dendrites, in chemosensory neurons of living Caenorhabditis elegans. *J Cell Biol*. 147:519-30.

Signor, D., K.P. Wedaman, L.S. Rose, and J.M. Scholey. 1999b. Two heteromeric kinesin complexes in chemosensory neurons and sensory cilia of Caenorhabditis elegans. *Mol Biol Cell*. 10:345-60.

Simon, J.M., and P.W. Sternberg. 2002. Evidence of a mate-finding cue in the hermaphrodite nematode Caenorhabditis elegans. *Proc Natl Acad Sci U S A*. 99:1598-603.

Sipols, A.J., D.G. Baskin, and M.W. Schwartz. 1995. Effect of intracerebroventricular insulin infusion on diabetic hyperphagia and hypothalamic neuropeptide gene expression. *Diabetes*. 44:147-51.

Slavotinek, A.M., E.M. Stone, K. Mykytyn, J.R. Heckenlively, J.S. Green, E. Heon, M.A. Musarella, P.S. Parfrey, V.C. Sheffield, and L.G. Biesecker. 2000. Mutations in MKKS cause Bardet-Biedl syndrome. *Nat Genet*. 26:15-6.

Smith, J.C., J.G. Northey, J. Garg, R.E. Pearlman, and K.W. Siu. 2005. Robust method for proteome analysis by MS/MS using an entire translated genome: demonstration on the ciliome of Tetrahymena thermophila. *J Proteome Res*. 4:909-19.

Smith, U.M., M. Consugar, L.J. Tee, B.M. McKee, E.N. Maina, S. Whelan, N.V. Morgan, E. Goranson, P. Gissen, S. Lilliquist, I.A. Aligianis, C.J. Ward, S. Pasha, R. Punyashthiti, S. Malik Sharif, P.A. Batman, C.P. Bennett, C.G. Woods, C. McKeown, M. Bucourt, C.A. Miller, P. Cox, L. Algazali, R.C. Trembath, V.E. Torres, T. Attie-Bitach, D.A. Kelly, E.R. Maher, V.H. Gattone, 2nd, P.C. Harris, and C.A. Johnson. 2006. The transmembrane protein meckelin (MKS3) is mutated in Meckel-Gruber syndrome and the wpk rat. *Nat Genet*. 38:191-6.

Snow, J.J., G. Ou, A.L. Gunnarson, M.R. Walker, H.M. Zhou, I. Brust-Mascher, and J.M. Scholey. 2004. Two anterograde intraflagellar transport motors cooperate to build sensory cilia on C. elegans neurons. *Nat Cell Biol*. 6:1109-13.

Starich, T.A., R.K. Herman, C.K. Kari, W.H. Yeh, W.S. Schackwitz, M.W. Schuyler, J. Collet, J.H. Thomas, and D.L. Riddle. 1995. Mutations affecting the chemosensory neurons of Caenorhabditis elegans. *Genetics*. 139:171-88.

Stoetzel, C., V. Laurier, E.E. Davis, J. Muller, S. Rix, J.L. Badano, C.C. Leitch, N. Salem, E. Chouery, S. Corbani, N. Jalk, S. Vicaire, P. Sarda, C. Hamel, D. Lacombe, M. Holder, S. Odent, S. Holder, A.S. Brooks, N.H. Elcioglu, E.D. Silva, B. Rossillion, S. Sigaudy, T.J. de Ravel, R.A. Lewis, B. Leheup, A. Verloes, P. Amati-Bonneau, A. Megarbane, O. Poch, D. Bonneau, P.L. Beales, J.L. Mandel, N. Katsanis, and H. Dollfus. 2006. BBS10 encodes a vertebrate-specific chaperonin-like protein and is a major BBS locus. *Nat Genet*. 38:521-4.

Stoetzel, C., J. Muller, V. Laurier, E.E. Davis, N.A. Zaghloul, S. Vicaire, C. Jacquelin, F. Plewniak, C.C. Leitch, P. Sarda, C. Hamel, T.J. de Ravel, R.A. Lewis, E. Friederich, C. Thibault, J.M. Danse, A. Verloes, D. Bonneau, N. Katsanis, O.

Poch, J.L. Mandel, and H. Dollfus. 2007. Identification of a novel BBS gene (BBS12) highlights the major role of a vertebrate-specific branch of chaperonin-related proteins in Bardet-Biedl syndrome. *Am J Hum Genet*. 80:1-11.

Stolc, V., M.P. Samanta, W. Tongprasit, and W.F. Marshall. 2005. Genome-wide transcriptional analysis of flagellar regeneration in Chlamydomonas reinhardtii identifies orthologs of ciliary disease genes. *Proc Natl Acad Sci U S A*. 102:3703-7.

Stubdal, H., C.A. Lynch, A. Moriarty, Q. Fang, T. Chickering, J.D. Deeds, V. Fairchild-Huntress, O. Charlat, J.H. Dunmore, P. Kleyn, D. Huszar, and R. Kapeller. 2000. Targeted deletion of the tub mouse obesity gene reveals that tubby is a loss-of-function mutation. *Mol Cell Biol*. 20:878-82.

Sulston, J., M. Dew, and S. Brenner. 1975. Dopaminergic neurons in the nematode Caenorhabditis elegans. *J Comp Neurol*. 163:215-26.

Sulston, J.E., D.G. Albertson, and J.N. Thomson. 1980. The Caenorhabditis elegans male: postembryonic development of nongonadal structures. *Dev Biol*. 78:542-76.

Swoboda, P., H.T. Adler, and J.H. Thomas. 2000. The RFX-type transcription factor DAF-19 regulates sensory neuron cilium formation in C. elegans. *Mol Cell*. 5:411-21.

Sze, J.Y., M. Victor, C. Loer, Y. Shi, and G. Ruvkun. 2000. Food and metabolic signalling defects in a Caenorhabditis elegans serotonin-synthesis mutant. *Nature*. 403:560-4.

Tabish, M., Z.K. Siddiqui, K. Nishikawa, and S.S. Siddiqui. 1995. Exclusive expression of C. elegans osm-3 kinesin gene in chemosensory neurons open to the external environment. *J Mol Biol*. 247:377-89.

Takai, Y., T. Sasaki, and T. Matozaki. 2001. Small GTP-binding proteins. *Physiol Rev*. 81:153-208.

Tobin, D., D. Madsen, A. Kahn-Kirby, E. Peckol, G. Moulder, R. Barstead, A. Maricq, and C. Bargmann. 2002. Combinatorial expression of TRPV channel proteins defines their sensory functions and subcellular localization in C. elegans neurons. *Neuron*. 35:307-18.

Tobin, J.L., and P.L. Beales. 2007. Bardet-Biedl syndrome: beyond the cilium. *Pediatr Nephrol*. 22:926-36.

Troemel, E.R., B.E. Kimmel, and C.I. Bargmann. 1997. Reprogramming chemotaxis responses: sensory neurons define olfactory preferences in C. elegans. *Cell*. 91:161-9.

Van Gilst, M.R., H. Hadjivassiliou, A. Jolly, and K.R. Yamamoto. 2005a. Nuclear hormone receptor NHR-49 controls fat consumption and fatty acid composition in C. elegans. *PLoS Biol*. 3:e53.

Van Gilst, M.R., H. Hadjivassiliou, and K.R. Yamamoto. 2005b. A Caenorhabditis elegans nutrient response system partially dependent on nuclear receptor NHR-49. *Proc Natl Acad Sci U S A*. 102:13496-501.

Wang, Q., J. Pan, and W.J. Snell. 2006. Intraflagellar transport particles participate directly in cilium-generated signaling in Chlamydomonas. *Cell*. 125:549-62.

Ward, S. 1973. Chemotaxis by the nematode Caenorhabditis elegans: identification of attractants and analysis of the response by use of mutants. *Proc Natl Acad Sci U S A*. 70:817-21.

Ward, S., N. Thomson, J.G. White, and S. Brenner. 1975. Electron microscopical reconstruction of the anterior sensory anatomy of the nematode Caenorhabditis elegans.?2UU. *J Comp Neurol*. 160:313-37.

Ware, R.W., Clark, D., Crossland, K., and Russell, R. L. 1975. The nerve ring of the nematode *Caenorhabditis elegans*: sensory input and motor output. *Journal of Comparative Neurology*. 162:71-110.

White, J.G., Southgate E., Thomson, J.N., and Brenner, S. 1986. The structure of hte nervous system of the nematode *Caenorhabditis Elegans*. *Philos Trans R Soc Lond B Biol Sci*. 314:1-340.

Williams, D.L., and D.E. Cummings. 2005. Regulation of ghrelin in physiologic and pathophysiologic states. *J Nutr*. 135:1320-5.

Winkelbauer, M.E., J.C. Schafer, C.J. Haycraft, P. Swoboda, and B.K. Yoder. 2005. The C. elegans homologs of nephrocystin-1 and nephrocystin-4 are cilia transition zone proteins involved in chemosensory perception. *J Cell Sci*. 118:5575-87.

Woods, S.C., R.J. Seeley, D. Porte, Jr., and M.W. Schwartz. 1998. Signals that regulate food intake and energy homeostasis. *Science*. 280:1378-83.

Yen, H.J., M.K. Tayeh, R.F. Mullins, E.M. Stone, V.C. Sheffield, and D.C. Slusarski. 2006. Bardet-Biedl syndrome genes are important in retrograde intracellular trafficking and Kupffer's vesicle cilia function. *Hum Mol Genet*. 15:667-77.

Zarjevski, N., I. Cusin, R. Vettor, F. Rohner-Jeanrenaud, and B. Jeanrenaud. 1993. Chronic intracerebroventricular neuropeptide-Y administration to normal rats mimics hormonal and metabolic changes of obesity. *Endocrinology*. 133:1753-8.

# Conclusion

The coordination of behavior and physiology in a multicellular organism is complex, requiring integration of diverse inputs from both the external environment and the internal milieu. The nervous system is required for the detection of stimuli and the interpretation of information to coordinate the appropriate behaviors and physiological responses.  For example, if a starving animal smells food and also sees a potential predator nearby, it must decide whether pursuing the food is too risky.  As in this example, sensory neurons are crucial for the detection of external stimuli, such as odors and visual cues, that provide important information about an animal's surroundings. These inputs are relayed to interneurons and/or higher brain centers, and the incredibly complex task of the brain is to compile and sort through these signals to produce an appropriate response.  In this example, the brain must coordinate the decision to either quickly retrieve the food or to flee in the opposite direction.  Intact function and connectivity of the nervous system is dependent on the proper development of neuronal processes.  If the neuronal structures that gather inputs from the external environment, including cilia and dendrites, fail to grow or elaborate properly, or if the appropriate receptors and signaling pathway components are not localized properly to these structures, the information that the brain receives will be compromised.  In this thesis, I use two invertebrate models to explore molecules that affect the development of sensory neuron dendrites and sensory neuron cilia and to examine physiological changes caused by inappropriate functioning of these neurons.

Elaborating complex and diverse dendritic arbors, the multidendritic (MD) neurons of the PNS in *Drosophila* larvae are sensory neurons required for nociception, thermosensation and proprioception. In Chapter Two, I explore the role of Ago1 and Ago2, two essential components of the microRNA and RNAi pathways, respectively, in dendritic patterning. Preliminary analyses revealed that these two genes have minimal or no effect on dendritic branching in PNS neurons. However, Ago2, in cooperation with DFMR, regulates levels of *ppk1* mRNA, a DEG/ENAC channel that controls larval crawling behavior. Elucidating the mechanism by which Ago2 regulates *ppk1* mRNA is of great interest. Additionally, the behavioral implications of Ago2 regulation of *ppk1* mRNA remains to be determined. As *ppk1* controls larval locomotion, it would be interesting to test whether Ago2 also participates in larval locomotion.

Additionally, in Chapter Two, I find that *lola*, a BTB-POZ domain transcription factor that produces at least twenty isoforms, also regulates dendritic outgrowth. Lola expression is required for dendrite elaboration and growth in several DA neurons with diverse dendritic morphologies. Further exploration of Lola may reveal isoform-specific effects on dendritic branching. Additionally, in a yeast-two-hybrid screen, Lola interacts with another BTB-POZ domain, Abrupt, which restricts dendrite branching in simple class I DA neurons. If this interaction is recapitulated in vivo, examining the nature of the interaction and how the two genes cooperate to control dendrite arborization will enhance our understanding of a transcriptional program that regulates dendritogenesis of the DA sensory neurons.

Sensory neurons also have an essential function in an organism's physiology. In Chapters Four and Five, I use *C. elegans* as a model organism to explore how mutations

that compromise intraflagellar transport (IFT) within ciliated sensory neurons affect metabolic homeostasis. I focus on the worm orthologs of eight genes that cause the human disease Bardet-Biedl syndrome, characterized by obesity. I find that, similar to their human counterparts, *bbs* mutant worms display increased Nile Red fat storage. Changes in fat storage cannot be attributed to changes in pumping rate, an indicator of food intake, or egg-laying, a major energetic investment.

Unexpectedly, generally interfering with cilia signaling does not cause altered lipid accumulation. In a comprehensive exploration of *C. elegans* cilia mutants with defects in IFT motors, core IFT components, and cilia structure, only a few displayed altered fat content. Alterations in OSM-3 kinesin, the IFT-B component CHE-2, and DYF-5 kinase increase fat stores whereas defects in the IFT-A component DAF-10 decrease lipid accumulation. Genetic experiments revealed that these cilia components participate in the same pathway as *bbs* to regulate fat content. Intriguingly, *kap-1* functions downstream of *bbs*; this interaction may provide a clue to how *bbs* works through IFT to control metabolic homeostasis.

In Chapter Five, I use candidate gene approaches and RNAi screens to seek an understanding of how *bbs* genes control fat stores. I examine interactions between *bbs* and the insulin, serotonergic and TGF-β pathways, all of which have been shown to regulate fat storage in worms. Interestingly, *bbs* acts independently of these well-known pathways that regulate fat storage, thus suggesting that *bbs* functions through a novel pathway to regulate lipid content. Additionally, I search for interactions between *bbs* and approximately four hundred genes previously found to affect fat. Although I fail to find

any interaction that would help explain the *bbs* fat phenotype, many candidate pathways remain to be examined, including other neurotransmitters and neuropeptides.

Taken together, this thesis presents an exploration of sensory neurons and their formation and function in physiology and behavior. As an animal's windows to the external world, cilia and dendrites of sensory neurons must develop and signal properly to relay information that is critical to the organism's survival. An understanding of the factors that affect the integrity of these essential neuronal structures ultimately leads to a broader comprehension of the function of sensory neurons in physiology and behavior.

# Appendix One

# Quantitation of Nile Red Fluorescence

A major challenge in the Ashrafi lab was quantitating Nile Red fluorescence reliably and accurately. While this issue did not pose a problem in investigating mutants with substantial differences in Nile Red fat staining, it presented difficulties in studying mutants with more subtle phenotypes. Because the mutants I was interested in had a more moderate fat phenotype, I worked on finding a method to reliably quantitate fat. The method in use when I started in the lab failed to correctly quantitate the difference in Nile Red staining of mutants that clearly had a phenotype by eye. Therefore, I tested different methods of quantitation using both fluorescence and confocal microscopes as well as different imaging analysis software.

## Quantitation of 16x images using Openlab

*Image Acquisition*

The quantitation protocol initially followed in the Ashrafi lab used Openlab software (Improvision, Lexington, MA, USA) for image acquisition and analysis. Images at 16x magnification were photographed using a Hamamatsu ORCA-ER cooled CCD camera attached to a Zeiss Axioplan 2 upright microscope with a 2-5 ms exposure at highest fluorescence setting for the rear fluorescence shutter or 50-100 ms exposure at the lowest fluorescence setting. If any part of the image was saturated (4095 intensity units), then the exposure was adjusted appropriately. At 16x magnification, approximately two-thirds of the worm's body can be captured in the field of view; however, a common issue is the difficulty of keeping the entire intestine in focus. Therefore, I usually focused on the

anterior end of the worm, and the image was discarded if the entire first two intestinal cells were not in focus.

*Selection of Region of Interest (ROI) and Quantitation*

The two most anterior intestinal cells were outlined using the Freehand tool on Nomarski Differential Interference Contrast (DIC) images, and the corresponding fluorescence images were quantitated using the Openlab "Measure" function. Nile Red fluorescence was quantitated as Area of ROI multiplied by Mean Fluorescence of ROI.

*Results*

Using this method I analyzed *bbs-7(n1606)*, *bbs-7(ok1351),* and *bbs-8(nx77)* mutants, which have a clear, increased fat phenotype (Appendix Figure 1-1A). Quantitation of *bbs-7(n1606)* and *bbs-7(ok1351)* failed to demonstrate a clear increase in fat (Appendix Figure 1-1B). Others in the lab reported similar variability in their measurements and lack of consistency between their measurements and the phenotypes observed by eye (e.g. S. Srinivasan). Therefore, this method was unreliable for measuring Nile Red fluorescence.

**Quantitation of 5x images using Openlab**

*Image Acquisition*

I experimented with methods that would quantitate fat in the entire body of the worm. Images acquired at 5x capture the full length of several worms although they are much lower resolution. The images taken with 5x are similar to what is seen by eye on dissecting fluorescence microscopes. Using Openlab and the Zeiss Axioplan 2 microscope, I acquired 5x images at 100ms exposure with the full rear fluorescence setting.

*Selection of Region of Interest and Quantitation*

For the most accurate selection of the entire intestine of the worm, drawing the ROI around the worm by the freehand tool is optimal, but tedious. I was interested in finding a higher throughput method to quickly outline and measure worms' intestinal fluorescence to achieve a higher *n*. Using the lasso tool set to a threshold range of 6-8 for 5x images, I was able to select the intestine of wild-type worms with reasonable accuracy. One major difficulty with this method was that the threshold had to be adjusted occasionally from worm to worm within genotypes and between genotypes. Another problem with this method is that a small amount out-of-focus light was also often unintentionally selected.

I used the Openlab "Measure" function for quantitation of total intestinal fluorescence. To eliminate background, I drew a circle around a blank region without a worm, and subtracted the Mean Fluorescence of Background from Mean Fluorescence of each worm. This difference represented the total mean fluorescence of each worm.

*Results*

Using this method, I was able to quantitate differences in Nile Red staining for strains with increased fat content—*bbs-7(n1606)* and *tub-1(nr2004)*—and a strain with decreased fat storage—*flp-1(yn2)* (Appendix Figure 1-2). However, this method was unsatisfactory due to difficulties in selection, low resolution, and inclusion of out-of-focus light.

**16x z-stacks acquired with Openlab and quantitated with Volocity**

*Image Acquisition*

I acquired z-stacks at 16x at 100ms with the rear fluorescence filter at lowest setting using Openlab and the Zeiss Axioplan 2. I imported images into Volocity (Improvision, Lexington, MA, USA) as a library and converted the stack of 2-dimensional slices through the worm into a 3-dimensional volume.

*Selection of Region of Interest and Quantitation*

Using the Freehand tool, I manually selected the ROI, including the anterior half of the worm from the pharynx to the vulva, according to the DIC image. I used two different measures of fluorescence, including ROI mean fluorescence across the entire volume and ROI mean fluorescence of a collapsed Z-stack. To collapse the Z-stack, I used the Volocity "Capture Snapshot" function. Nile Red Fluorescence was quantitated as Mean Fluorescence multiplied by Area of ROI.

*Results*

Quantitation of either the entire volume or the collapsed z-stack demonstrated a significant difference between wild-type N2 and *bbs-7(n1606)* worms (Appendix Figure 1-3). At the expense of losing resolution and some accuracy, quantitation of the collapsed z-stack was significantly faster.

A major disadvantage to this method was the amount of time needed to acquire a z-stack of one worm. The time needed for acquiring images was so lengthy that it precludes acquiring more than three or four genotypes in a single experiment. In addition, as with all images acquired with the Zeiss Axioplan 2 microscope, out-of-focus light is also a concern.

**Quantitation of z-stacks acquired with swept-field confocal**

(this work was done together with Amanda Kahn-Kirby, Nico Stuurman, and Kurt Thorn)

*Image Acquisition*

To achieve higher quality images, with less scatter from out-of-focus light, we captured images with a Photometrics Cascade camera attached to a Nikon Live-Scan swept-field confocal TE2000U inverted microscope.

Images were acquired as z-series of 1μm slices at 40x with an exposure time of 500ms and camera gain of 3600, which was adjusted if images reached saturation.

*Selection of Region of Interest and Quantitation*

For analysis, Image J software (U.S. National Institutes of Health, Bethesda, MD, USA; http://rsb.info.nih.gov/ij/) with Stack Builder and Spot Tracker plugins (Sage et al., 2005) was used.  As part of a collaboration with the Schoofs' lab, the first experiment was to quantitate *egl-3,* a mutant with severely reduced fat stores and an enlarged lumen (Husson et al., 2005).  We quantitated *egl-3* and wild-type worms using fluorescence images representing a maximum intensity projection of seven 1μm slices corresponding to the midsection of the animal.  In a separate experiment quantifying *dyf-5,* I used a maximum intensity projection representing the entire animal. For both experiments, the ROI was defined as the first two intestinal cells.  A 1.0 pixel Gaussian filter was applied to identify fluorescence corresponding to lipid droplets and to reduce background.  The "Analyze Particles" function generated a mask, which was applied to the original ROI to extract fluorescent signal in the lipid droplets.  We quantitated Nile Red Fluorescence as Intensity Density, or Area of ROI multiplied by ROI Mean Fluorescence.

*Results*

Using this method, we found that the intestinal fat stores of *egl-3(gk238)* mutants were decreased to approximately 45% of wild-type (Appendix Figure 4A&B; Husson et

al., 2005).  I found that quantitation of *dyf-5* using this method also accurately identified an increase in lipid droplet fluorescence.  This method had several advantages, including eliminating out-of-focus light and background, and using high resolution. In addition, the swept-field confocal is much faster than the Zeiss Axioplan for z-stack acquisition.

**Quantitation of 16x Openlab images using ImageJ**

*Image Acquisition*

Images were acquired as 16x Openlab images on the Zeiss Axioplan 2 microscope, as detailed in the first section, and saved as tiff files.

*Selection of Region of Interest and Quantitation*

The first two cells were outlined using the polygon tool and duplicated. Quantitation was performed using Image J as outlined above.  Nile Red fluorescence was again reported as Intensity Density.

*Results*

I first tested this method to accurately quantify an epistasis experiment reported in my dissertation.   Reflecting the Nile Red phenotypes seen by eye, the quantitation demonstrated that *bbs-7; klp-11*  has similar levels of Nile Red fluorescence to the single mutant *bbs-7* and that both mutants have significantly higher Nile Red fluorescence than wild-type or *klp-11* worms (Figure 4-3C&D).  This method was used for all experiments involving quantitation of Nile Red fluorescence reported in my thesis.  In addition, S. Srinivasan used this method to perform a series of mutant and epistasis analyses.  Our analyses have consistently revealed that quantitation using this method mirrors the differences in Nile Red staining observed by eye.  A disadvantage in using the Zeiss Axioplan 2 microscope is that the resolution is lower than that of the swept-field confocal
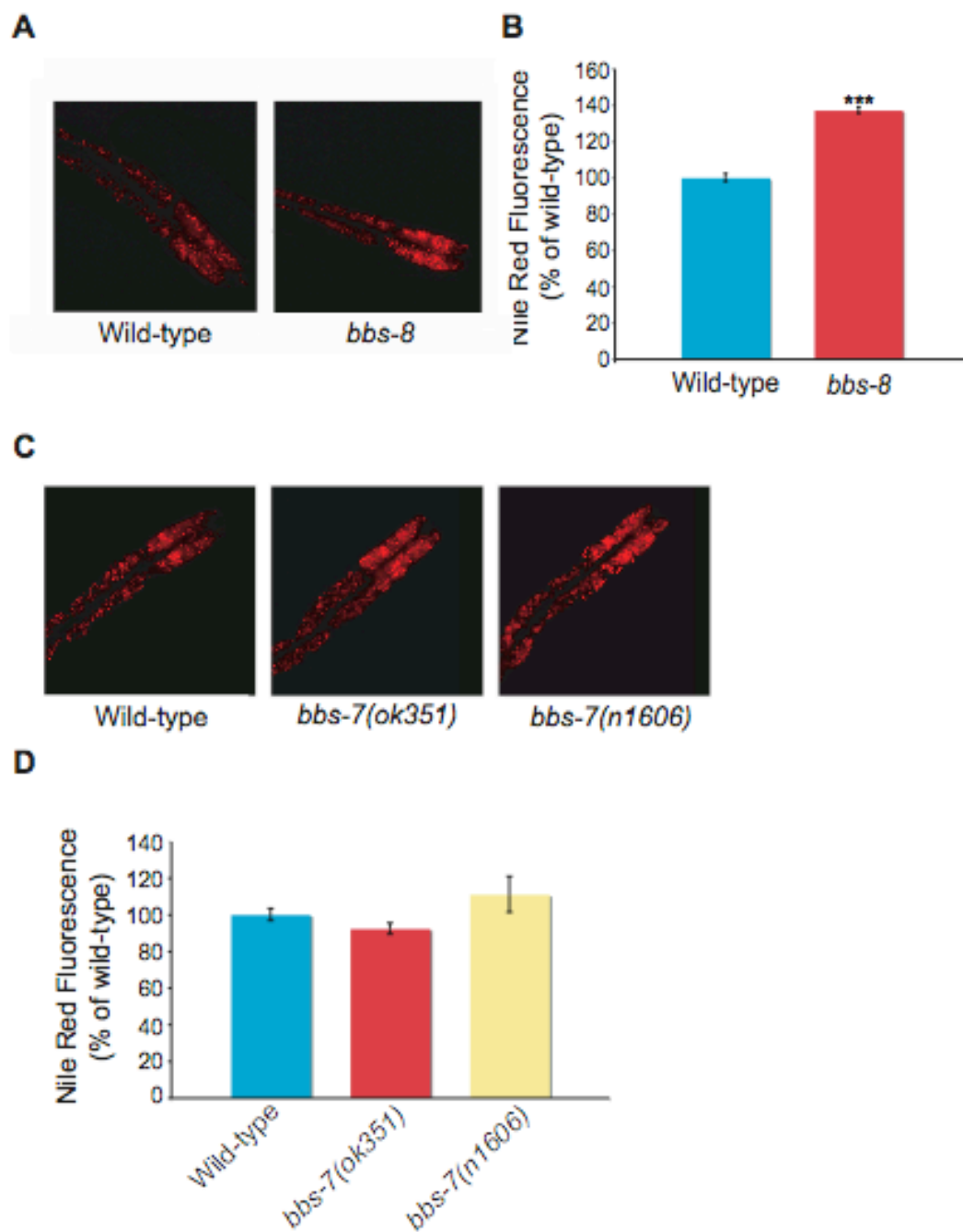
and some out-of-focus light is included.  However, the benefits of this method outweigh this disadvantage.  Because of the ease of use and the relative efficiency with which the images can be acquired, multiple genotypes can be analyzed within an experiment. Therefore, this method has proved a reliable and valid method of quantitating Nile Red fluorescence.

In sum, Image J can be successfully used to quantitate of images of Nile Red fluorescence acquired with either the swept-field confocal or the Zeiss Axioplan 2. Images can be acquired relatively quickly with the confocal and the Axioplan 2.  While images acquired on the confocal have a higher resolution, acquiring images on the Zeiss Axioplan 2 is slightly faster.  In addition, because lower magnification images can be acquired on the Zeiss Axioplan 2, a greater proportion of the worm's intestine can be included in quantitation.

# Appendix Figure 1-1



A

Wild-type    *bbs-8*

B

Nile Red Fluorescence (% of wild-type)

***

Wild-type    *bbs-8*

C

Wild-type    *bbs-7(ok351)*    *bbs-7(n1606)*

D

Nile Red Fluorescence (% of wild-type)

Wild-type    *bbs-7(ok351)*    *bbs-7(n1606)*

**Appendix Figure 1-1. Acquiring 16x images and quantitating Nile Red fluorescence using Openlab fails to accurately quantify fat content.**

(A) Images of *bbs-8(nx77)*, a mutant with increased fat depots, and wild-type worms.

(B) Quantification of Nile Red fluorescence of *bbs-8(nx77)* shows a difference between *bbs-8* ($n$=10) and wild-type ($n$=13) worms.

(C) Images of *bbs-7(ok1351)* and *bbs-7(n1606)*, two mutants with increased fat content, and wild-type worms.

(D) Quantification of Nile Red fluorescence of *bbs-7(ok1351)* ($n$=14) and *bbs-7(n1606)* ($n$=9) fails to show a difference between mutant and wild-type ($n$=11) worms.

Images were acquired at 16x magnification and quantitated using Openlab. The Region of Interest (ROI)—the first two intestinal cells—was manually selected based on the Differential Interference Contrast images.

***$p<0.001$ by t-test.

**Appendix Figure 1-2**



A

Wild-type      *bbs-7*

B

*Nile Red Fluorescence (% of wild-type)* — bar graph showing Wild-type at 100 and *bbs-7* at ~125 (***)

C

Wild-type      *tub-1*      *flp-1*

D

*Nile Red Fluorescence (% of wild-type)* — bar graph showing Wild-type at 100, *tub-1* at ~150 (***), *flp-1* at ~68 (***)
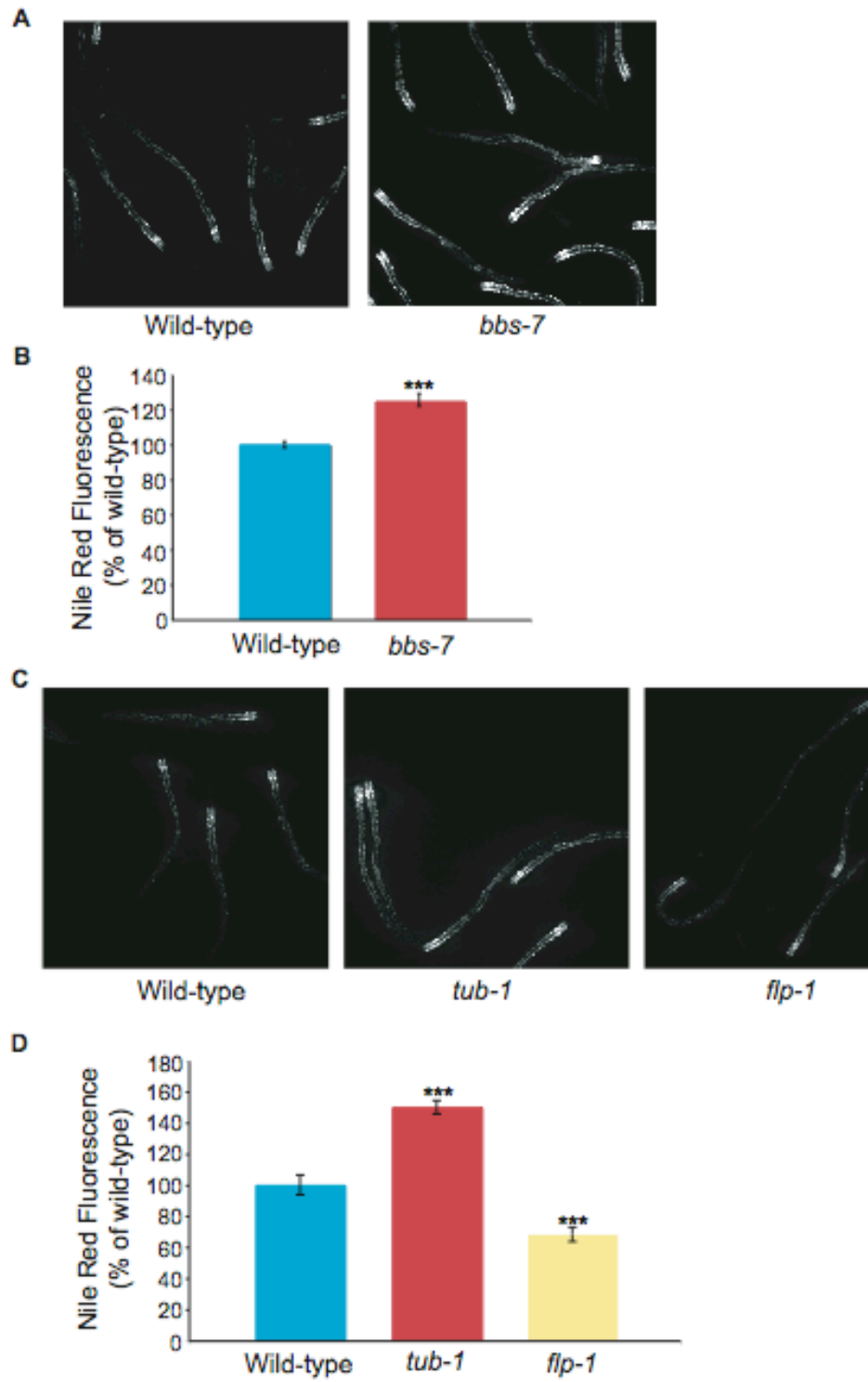
**Appendix Figure 1- 2. Acquiring 5x images and quantifying Nile Red fluorescence using Openlab.**

(A) Images of the *bbs-7(n1606)*, a mutant with excessive fat levels, and wild-type worms.

(B) Quantification of Nile Red fluorescence of *bbs-7(n1606)* demonstrates an increase in Nile Red fluorescence in *bbs-7(n1606)* mutants compared to wild-type worms. ($n$=20 worms per genotype).

(C) Images of *tub-1(nr2004)*, a mutant with increased fat stores, and *flp-1(yn2)*, a mutant with decreased fat levels, and wild-type worms.
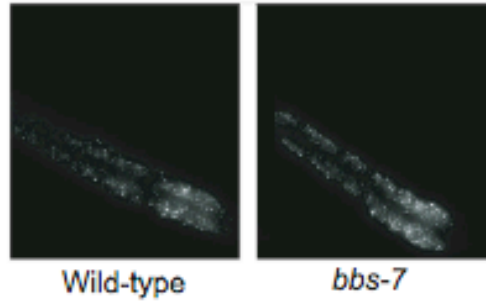
(D) Quantification of Nile Red fluorescence of *tub-1(nr2004)* ($n$=10) and *flp-1(yn2)* ($n$=9) demonstrates a difference between mutant and wild-type worms ($n$=10). Images acquired at 5x magnification and quantitated using Openlab. The entire worm was selected as the Region of Interest (ROI).
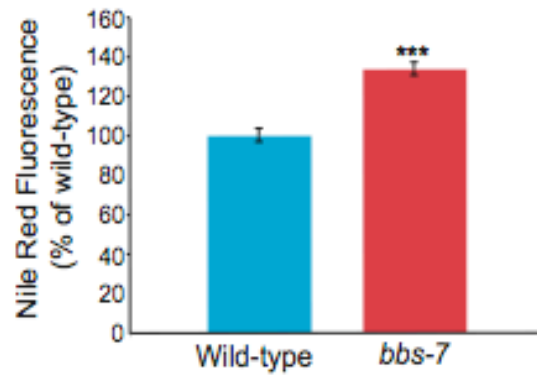
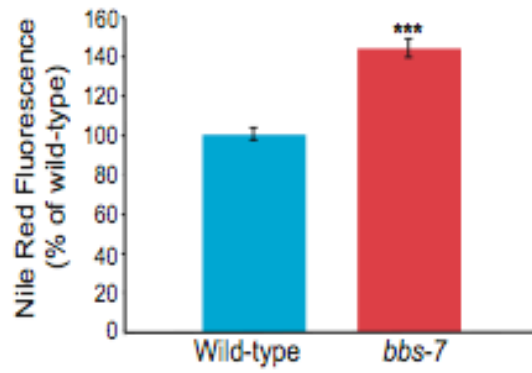***$p$<0.001 by t-test

**Appendix Figure 1-3**

**Appendix Figure 1-3. Acquiring 16x z-stacks and quantitating Nile Red fluorescence using Volocity demonstrates a difference between mutant and wild-type worms.**

(A) Images of *bbs-7(n1606)*, containing increased fat levels, and wild-type worms. Images represent a maximum intensity projection of 1μm slices through the worm.

(B) Quantification of a volume of slices shows a significant increase in Nile Red lipid droplets in *bbs-7(n1606)* mutant worms ($n$=10) compared to wild-type worms ($n$=8).

(C) Z-stack volumes in (B) were collapsed into single plane images. Quantification of the compressed z-stacks revealed a significant increase in Nile Red fluorescent staining in *bbs-7(n1606)* ($n$=10) relative to wild-type worms ($n$=8).

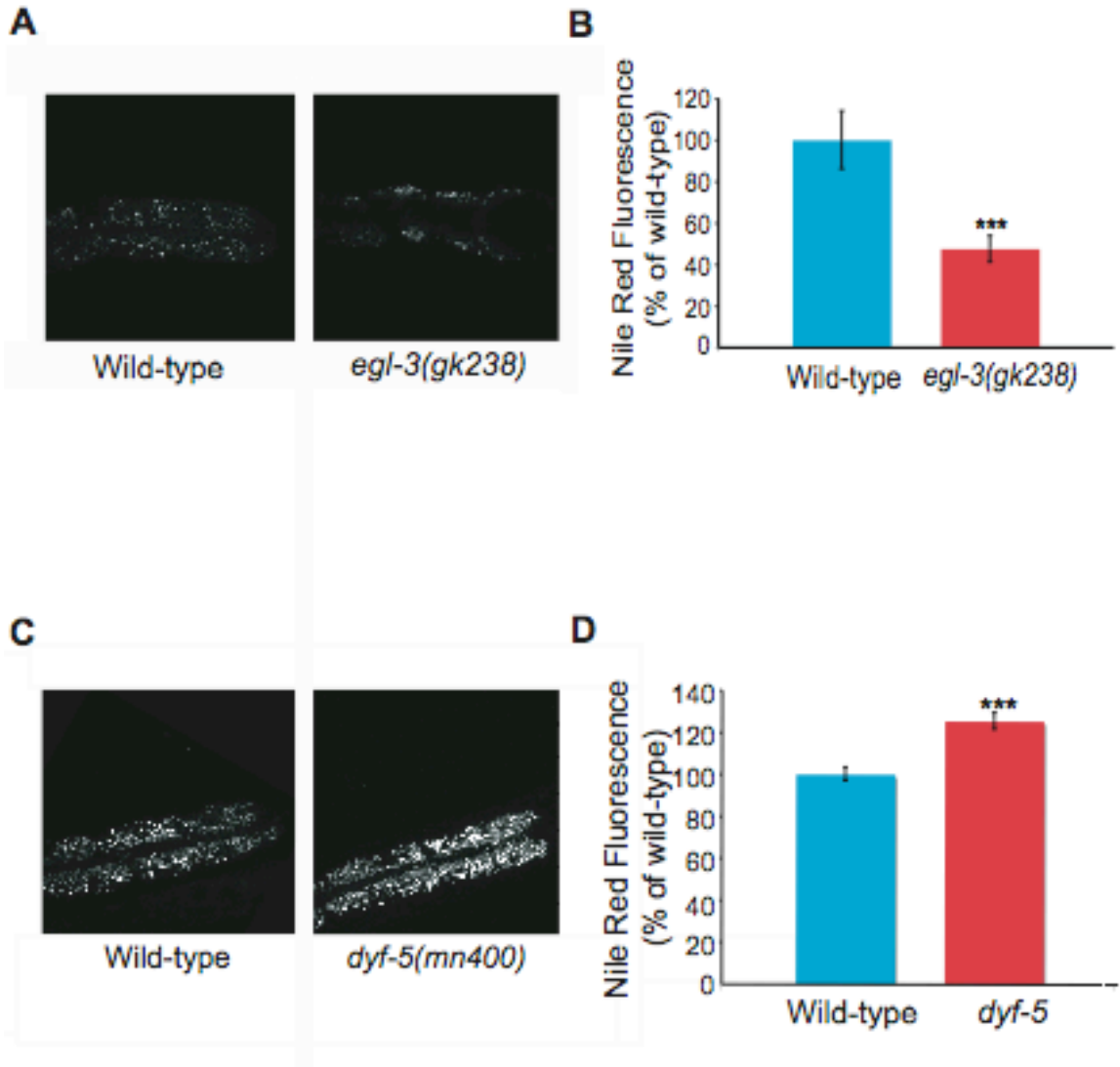Z-stacks were acquired at 16x magnification using Openlab and quantitated using Volocity. The Region of Interest (ROI)—the anterior half of the worm from the pharynx to the vulva—was manually selected based on the Differential Interference Contrast images.

***$p < 0.01$ by t-test

**Appendix Figure 1-4**

**Appendix Figure 1-4. Acquiring 40x images using the swept-field confocal and quantitating Nile Red fluorescence using ImageJ reveals a differences in Nile Red.**

(A) Images of *egl-3(gk238)* and wild-type worms. Images represent a maximum intensity projection of seven 1 μm slices corresponding to the mid-section of the worm. Note the severe reduction in fat content and broadening of the intestinal lumen. Arrow indicates lumen. Anterior is to the right.

(B) Quantification of Nile Red fluorescence of *egl-3(gk238)*($n$=11) and wild-type worms ($n$=7).

(C) Images of *dyf-5(mn400)* mutants, containing excessive Nile Red-stained lipids, and wild-type worms. Images represent a maximum intensity projection of 1 μm slices corresponding to the entire body of the worm. Anterior is to the right.

(D) Quantification of Nile Red fluorescence of *dyf-5(mn400)* ($n$=8) shows a significant increase in Nile Red fluorescence in *dyf-5* mutants relatively to wild-type worms ($n$=8). Images were acquired at 40x magnification with the swept-field confocal and quantitated using ImageJ. The Region of Interest (ROI)—the first two intestinal cells—was manually selected.

\*\*\*p<0.01 by t-test

# Appendix Two

# Additional Figures and Tables

## Appendix Figure 2-1
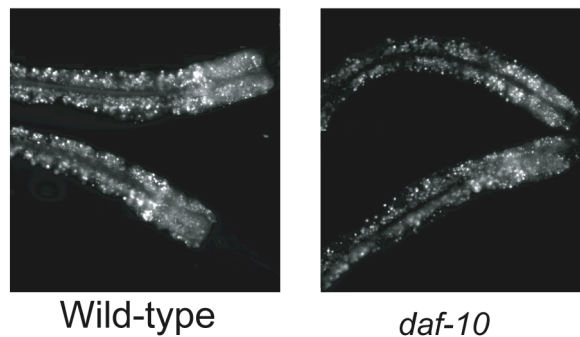


Wild-type            *daf-10*

**Appendix Figure 2-1.** *daf-10* **mutants have reduced lipid content.**

DAF-10/IFT22 is a component of the IFT-A complex.  Loss of function mutations in

*daf-10* cause a reduction in lipid storage, as seen in the images above. Images of

*daf-10(p821)* and wild-type worms stained with Nile Red were acquired using Openlab

and a Zeiss Axioplan 2 microscope.  Images were taken at 16x.

# Appendix Figure 2-2
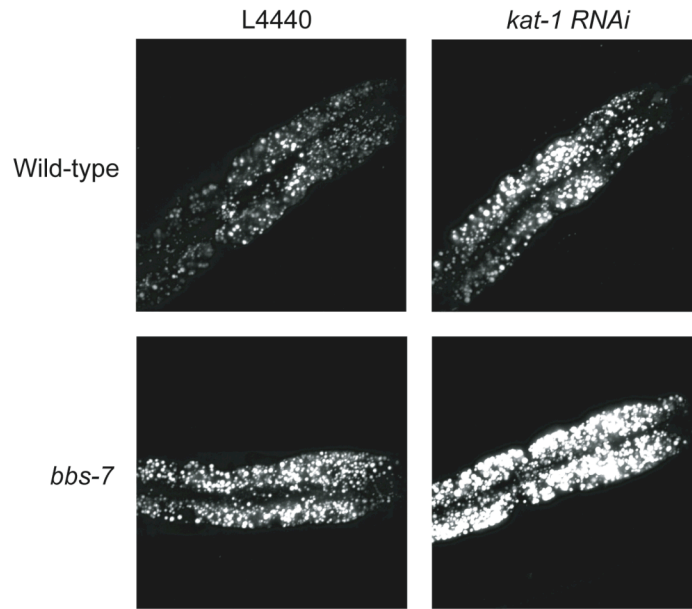


**Appendix Figure 2-2. Inactivation of *kat-1* synergistically enhances fat content in cilia mutants.** Inactivation of *kat-1* by RNAi modestly increases Nile Red lipid content in wild-type worms.  Loss of *kat-1* in a *bbs-7(n1606)* mutant background causes a synergistic increase in fat content.  Similar results were seen for all cilia mutants examined, including the following: *bbs-1(ok1111)*, *bbs-8(nx77)*, *osm-3(p802)*, *kap-1(ok676)*, *klp-11(tm324)*, *xbx-1(ok279)*, *che-2(e1033)*, *osm-1(p808)*, *osm-6(p811)*, *dyf-5(mn400)*, *mec-8(e398)*, *tub-1(nr2004)*.  Worms were fed vector control (L4440) or *kat-1* RNAi bacteria and their fat content was assay at 72 hours.  Images were acquired at 40x using a Photometrics Cascade camera attached to a Nikon Live-Scan swept-field confocal TE2000U inverted microscope.  Confocal imaging was performed at the Nikon Imaging Center at UCSF.  Similar results were reported in (Mak et al., 2006)

**Appendix Table 2-1. Identities of metabolic genes tested by real-time PCR**

Marc van Gilst (Van Gilst et al., 2005a; Van Gilst et al., 2005b) developed a real-time PCR assay to analyze expression levels of approximately150 genes that correspond to well-known components of metabolism.  I examined expression of these genes in *bbs-7(n1606)*, *bbs-8(nx77)* single and *bbs-1(ok1111); bbs-7(n1606); bbs-8(nx77)* triple mutants at the L4 stage and *glp-4(bn2); bbs-7(n1606)* mutants at the adult stage (80 hours).  No expression changes above a threshold of two were observed.  This suggests that *bbs* mutations do not cause large transcriptional changes in metabolic genes.  The identities of the genes examined are listed below.

| Gene ID | Gene Name | Gene ID | Gene Name |
|---------|-----------|---------|-----------|
| C46F4.2 | Acyl-CoA Synthetase | VZK822L.1 | Fat-6 |
| F37C12.7 | Acyl-CoA Synthetase | Y54E5A.1 | Omega-3 Desaturase |
| F46E10.1 | Acyl-CoA Synthetase | F33D4.4 | Desaturase |
| F28F8.2 | Acyl-CoA Synthetase | W09B6.1 | Acetyl-CoA Carboxylase |
| F47G6.2 | Acyl-CoA Synthetase | F32H2.5 | Fatty Acid Synthase |
| R07C3.4 | Acyl-CoA Synthetase | F10G8.9 | Beta Keto-Acyl Synthetase |
| R09E10.3 | Acyl-CoA Synthetase | W02D3.5 | lbp-6 |
| R09E10.4 | Acyl-CoA Synthetase | W02D3.7 | lbp-5 |
| T01B8.6 | Acyl-CoA Synthetase | F40F4.2 | lbp-2 |
| Y65B4BL.5 | Acyl-CoA Synthetase | F40F4.4 | lbp-3 |
| Y76A2B.3 | Acyl-CoA Synthetase | ZK742.5 | lbp-6 |
| F38H4.8 | Enoyl-CoA Hydratase | T22G5.2 | lbp-7 |
| F43H9.1 | Enoyl-CoA Hydratase | T22G5.6 | lbp-8 |
| R06F6.9 | Enoyl-CoA Hydratase | F40F4.3 | lbp-1 |
| F56B3.5 | Enoyl-CoA Hydratase | EEED8.2 | Fatty Acid Binding Protein |
| T05G5.6 | Enoyl-CoA Hydratase | EEED8.3 | Fatty Acid Binding Protein |
| Y105E8A.4 | Enoyl-CoA Hydratase | Y40B10A.1 | Fatty Acid Binding Protein |
| F01G10.2 | Enoyl-CoA Hydratase | ctl-2 | Catalase-2 |
| F01G10.3 | Enoyl-CoA Hydratase | ctl-1 | Catalase-1 |
| C29F3.1 | Enoyl-CoA Hydratase | ctl-3 | Catalase-3 |
| F09E10.3 | Short-chain Dehydrogenase | C03H5.4 | Phospholipase |
| K05F1.3 | Acyl-CoA Dehydrogenase | C07E3.9 | Phospholipase A2 |
| F01G4.2 | 3OH-Acyl CoA Dehydrogenase | C42D8.5 | Angiotensin Conv Enzy |
| F54C8.1 | 3OH-Acyl CoA Dehydrogenase | C44B7.8 | ATP Binding Protein |
| T25G12.5 | 3OH-Acyl CoA Dehydrogenase | C25A1.5 | Fatty-Acid Hydroxylase |
| B0272.3 | 3OH-Acyl CoA Dehydrogenase | C44B7.9 | Peroxisomal Membrane |

| Gene ID | Gene Name | Gene ID | Gene Name |
|---|---|---|---|
| R09B5.6 | 3OH-Acyl CoA Dehydrogenase | Y56A3A.19 | Acyl Carrier Protein |
| C48B4.1 | Acyl-CoA Oxidase-1 | T02G5.7 | Acetyl-CoA Acetyltransferase |
| F08A8.1 | Acyl-CoA Oxidase-1 | T02G5.8 | Acetyl-CoA Acetyltransferase |
| F08A8.2 | Acyl-CoA Oxidase-1 | F47F2.1 | Protein Kinase C |
| F08A8.3 | Acyl-CoA Oxidase | K04F1.15 | Aldehyde Dehydrogenase |
| F08A8.4 | Acyl-CoA Oxidase | C50D2.7 | GlucoKinase |
| F25C8.1 | Acyl-CoA Oxidase-1 | F13D12.9 | Lipid Biosynthesis |
| F59F4.1 | Acyl-CoA Oxidase-1 | F28D1.9 | Fatty Acid Transport Protein |
| C46C11.1 | Hormone Sensitive Lipase | F56H11.4 | elo-1 |
| T02G5.4 | Acetyl-CoA Thiolase | T08G2.3 | Acyl-CoA Dehydrogenase |
| B0303.3 | KetoAcyl-CoA Thiolase | T25G12.5 | Acyl-CoA Dehydrogenase |
| Y46G5A.17 | Carnitine Palmitoyl Transferase I | K06A5.6 | Acyl-CoA Dehydrogenase |
| R07H5.2 | Carnitine Palmitoyl Transferase II | C55B7.4A | Acyl-CoA Dehydrogenase |
| F28A10.6 | Acyl-CoA Dehydrogenase | R09B5.11 | Sugar Transporter |
| C02B10.1 | Acyl-CoA Dehydrogenase | K10B3.7 | Glyceraldehyde-3 Phosphate Dehydrogenase |
| E04F6.5 | Acyl-CoA Dehydrogenase | K10B3.8 | Glyceraldehyde-3 Phosphate Dehydrogenase |
| C17C3.12A | Acyl-CoA Dehydrogenase | T09F3.3 | Glyceraldehyde-3 Phosphate Dehydrogenase |
| F54D5.7 | Acyl-CoA Dehydrogenase | F33H1.2 | Glyceraldehyde-3 Phosphate Dehydrogenase |
| F41C3.3 | Acyl-CoA Synthase | R11A5.4a/b | PEPCK (a and b spliceforms) |
| T20B3.1 | Carnitine Palmitoyl Transferase | R11A5.4a/c/d | PEPCK (a, c and d isoforms) |
| F09F3.9 | Carnitine Palmitoyl Transferase | W05G11.6a/d | PEPCK (a and d spliceforms) |
| K11D12.4 | Carnitine Palmitoyl Transferase | W05G11.6a/b/d | PEPCK (a,b and d spliceforms) |
| Y48G9A.10 | Carnitine Palmitoyl Transferase | W05G11.6a/b/c | PEPCK (a,b and c spliceforms) |
| W01A11.5 | Carnitine Palmitoyl Transferase | F25H5.3b | Pyruvate Kinase (b spliceform) |
| F41E7.6 | Carnitine Palmitoyl Transferase | F25H5.3a/b | Pyruvate Kinase (a and b spliceforms) |
| D2024.3 | ELO-3 | Y110A7A.6a | Phosphofructokinase (a isoform) |
| ELO-4 | ELO-4 | H17B01.1b | Sugar Transporter (b isoform) |
| ELO-5 | ELO-5 | K07A3.1 | fructose, 1,6 bisphosphatase |
| ELO-6 | ELO-6 | F54H12.1a/b | aconitase (a and b spliceforms) |
| ELO-7 | ELO-7 | F54H12.1a/b/c | aconitase (a, b and c spliceforms) |
| ELO-8 | ELO-8 | ZK455.1 | aconitase |

| Gene ID | Gene Name | Gene ID | Gene Name |
|---------|-----------|---------|-----------|
| ELO-9 | ELO-9 | F46E10.10a/c | lactate/malate dehydrogenase (a and c) |
| Y57A10C.6 | Thiolase (kat-1) | F46E10.10a/b | lactate/malate dehydrogenase (a and b) |
| BO395.3 | Carnitine Palmitoyl Transferase | C05E4.9.a | Isocitrate lyase family/Malate synthase |
| C05C10.3 | Succinyl-CoA;3-ketoacid CoA Transferase | C05E4.9.b | Isocitrate lyase family/Malate synthase |
| F25B4.6 | HMG-CoA Synthase | F14B4.2 | Hexokinase |
| Y71G12B.10 | HMG-CoA Lyase | H25P06.1 | Hexokinase |
| Y71H10A.1 | 6-Phosphofructokinase (both spliceforms) | F20H11.3 | malate dehydrogenase |
| C50F4.2 | 6-phosphofructokinase | C34B2.7 | succinate dehydrogenase |
| R11A5.4 | PEPCK (all spliceforms) | R11F4.1 | glycerol kinase |
| W05G11.6 | PEPCK (all spliceforms) | F47G4.3 | NAD- GAPDH |
| F25H5.3 | Pyruvate Kinase (all spliceforms) | Y71H10A.1a | 6-phosphofructokinase (a spliceform) |
| ZK593.1 | Pyruvate Kinase | Y110A7A.6 | Phosphofructokinase (both spliceforms) |
| F48E8.3 | succinate dehydrogenase | K02B2.1 | Phosphofructokinase |
| C03G5.1 | succinate dehydrogenase | H17B01.1 | Sugar Transporter (both spliceforms) |

**Appendix Table 2-2. Identities of metabolic genes tested by RNAi**

Increased fat storage in *bbs* mutants may be a consequence of changes in metabolic gene expression or activity. Interactions between the *bbs* pathway and metabolic pathways may be revealed by inactivating various metabolic genes in *bbs* mutant backgrounds. Using RNAi, I inactivated each of 96 metabolic genes in *bbs-7(n1606)* and *bbs-8(nx77)* mutant backgrounds and compared their phenotypes to the effects of reducing the gene's function in wild-type background. I was interested in identifying gene inactivations that caused an aggravated enhancement of fat storage in *bbs* mutants. In addition, I was interested in identifying gene inactivations that decrease or increase fat content in wild-type worms but failed to have the same effect in *bbs* mutants. I failed to find candidate genes in any of these categories. The identities of the genes examined are listed below.

| Gene ID | Gene Name | Gene ID | Gene Name |
|---------|-----------|---------|-----------|
| F53A2.7 | Thiolase | Y48G9A.10 | Carnitine Palmitoyl Transferase |
| F40F4.3 | lbp-1 | C07E3.9 | Phospholipase A2 |
| ZK742.5 | lbp-6 | EEED8.3 | Fatty Acid Binding Protein |
| EEED8.2 | Fatty Acid Binding Protein | Y53F4B.2 | ELO-9 |
| F01G4.2 | 3OH-Acyl CoA Dehydrogenase | K05F1.3 | Acyl-CoA Dehydrogenase |
| F56H11.4 | elo-1 | R07C3.4 | Acyl-CoA Synthetase |
| B0272.3 | 3OH-Acyl CoA Dehydrogenase | T02G5.8 | Acetyl-CoA Acetyltransferase |
| C25A1.5 | Fatty-Acid Hydroxylase | F28A10.6 | Acyl-CoA Dehydrogenase |
| W02A2.1 | Fat-2 D12 Desaturase | C44B7.9 | Peroxisomal Membrane |
| F13D12.9 | Lipid Biosynthesis | C44B7.8 | ATP Binding Protein |
| T02G5.7 | Acetyl-CoA Acetyltransferase | R06F6.9 | Enoyl-CoA Hydratase |
| F54D5.7 | Acyl-CoA Dehydrogenase | W09B6.1 | Acetyl-CoA Carboxylase |
| T13F2.1 | Fat-4 D5 Desaturase | F56H11.3 | ELO-7 |
| T20B3.1 | Carnitine Palmitoyl Transferase | F33D4.4 | Desaturase |
| R07H5.2 | Carnitine Palmitoyl Transferase II | F01G10.3 | Enoyl-CoA Hydratase |
| W08D2.4 | Fat-3 D6 Desaturase | F01G10.2 | Enoyl-CoA Hydratase |
| Y57A10C.6 | Thiolase | D2024.3 | ELO-3 |

| Gene ID | Gene Name | Gene ID | Gene Name |
|---------|-----------|---------|-----------|
| W06D12.3 | Fat-5 | F38H4.8 | Enoyl-CoA Hydratase |
| K06A5.6 | Acyl-CoA Dehydrogenase | F41H10.8 | ELO-6 |
| C40H1.4 | ELO-4 | R09E10.3 | Acyl-CoA Synthetase |
| Y56A3A.19 | Acyl Carrier Protein | F28D1.9 | Fatty Acid Transport Protein |
| T05G5.6 | Enoyl-CoA Hydratase | Y54E5A.1 | Omega-3 Desaturase |
| C05C10.3 | Succinyl-CoA;3-ketoacid CoA Transferase | T22G5.2 | lbp-7 |
| E04F6.5 | Acyl-CoA Dehydrogenase | F43H9.1 | Enoyl-CoA Hydratase |
| B0303.3 | KetoAcyl-CoA Thiolase | F10D2.9 | Fat-7 Desaturase |
| F37C12.7 | Acyl-CoA Synthetase | R09B5.6 | 3OH-Acyl CoA Dehydrogenase |
| C48B4.1 | Acyl-CoA Oxidase-1 | F28F8.2 | Acyl-CoA Synthetase |
| F54C8.1 | 3OH-Acyl CoA Dehydrogenase | F25B4.6 | HMG-CoA Synthase |
| W02D3.7 | lbp-5 | W01A11.5 | Carnitine Palmitoyl Transferase |
| W02D3.5 | lbp-6 | T02G5.4 | Acetyl-CoA Thiolase |
| F10G8.9 | Beta Keto-Acyl Synthetase | Y40B10A.1 | Fatty Acid Binding Protein |
| F47G6.2 | Acyl-CoA Synthetase | F40F4.4 | lbp-3 |
| Y65B4BL.5 | Acyl-CoA Synthetase | F32H2.5 | Fatty Acid Synthase |
| F25C8.1 | Acyl-CoA Oxidase-1 | F08A8.1 | Acyl-CoA Oxidase-1 |
| F09F3.9 | Carnitine Palmitoyl Transferase | F08A8.2 | Acyl-CoA Oxidase-1 |
| Y76A2B.3 | Acyl-CoA Synthetase | F08A8.3 | Acyl-CoA Oxidase |
| C29F3.1 | Enoyl-CoA Hydratase | F08A8.4 | Acyl-CoA Oxidase |
| F40F4.2 | lbp-2 | C50D2.7 | GlucoKinase |
| F09E10.3 | Short-chain Dehydrogenase | F41C3.3 | Acyl-CoA Synthase |
| T08G2.3 | Acyl-CoA Dehydrogenase | C02B10.1 | Acyl-CoA Dehydrogenase |
| T25G12.5 | 3OH-Acyl CoA Dehydrogenase | F41H10.7 | ELO-5 |
| T25G12.5 | Acyl-CoA Dehydrogenase | VZK822L.1 | Fat-6 |
| C46F4.2 | Acyl-CoA Synthetase | Y67H2A.8 | Fat-1 w3 Desaturase |
| F59F4.1 | Acyl-CoA Oxidase-1 | F11E6.5 | elo-2 Palmitic Acid Elongase |
| C42D8.5 | Angiotensin Conv Enzy | K04F1.15 | Aldehyde Dehydrogenase |
| C03H5.4 | Phospholipase | F46E10.1 | Acyl-CoA Synthetase |
| R09E10.4 | Acyl-CoA Synthetase | T22G5.6 | lbp-8 |
| C46C11.1 | Hormone Sensitive Lipase | F41E7.6 | Carnitine Palmitoyl Transferase |

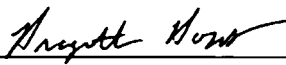**Appendix Table 2-3. Identities of human diabetes homologs tested by RNAi**

Several novel human diabetes genes were recently identified (Saxena et al., 2007). I looked for interactions between the worm homologs of these genes and *bbs* mutations. Using RNAi, I inactivated each of these metabolic genes in *bbs-7(n1606)* mutants and compared their phenotypes to the effects of reducing the gene's function in wild-type background. I was interested in identifying gene inactivations that caused an aggravated enhancement of fat storage in *bbs* mutants. In addition, I was interested in identifying gene inactivations that decrease or increase fat content in wild-type worms but failed to have the same effect in *bbs* mutants. I failed to find candidate genes in any of these categories. The identities of the genes examined are listed below.

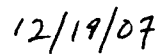| Gene ID | Gene Name/Description |
|---------|----------------------|
| Y39E4A.2b | $Zn^{2+}$ transporter |
| T18D3.3 | $Zn^{2+}$ transporter |
| M88.5 | IMP2(Insulin-like growth factor-II mRNA-binding protein |
| K12C11.4 | dapk/kinase |
| D2021.8 | Ankyrin repeat &DHHC-type Zn-finger domain containing protein |
| W10C8.2 | pop-1/transcription factor |
| F46F6.2 | serine/threonin protein kinase |
| M6.3 | pha-2/homeodomain protein HEX |
| M02A10.2 | irk-2/inward rectifier K+ channel |
| R03E9.4 | irk-1/inward rectifier K+ channel |
| T01D3.2 | bHLH-PAS transcription factor/SIM1 |

# Publishing Agreement

It is the policy of the University to encourage the distribution of all theses and dissertations. Copies of all UCSF theses and dissertations will be routed to the library via the Graduate Division. The library will make all theses and dissertations accessible to the public and will preserve these to the best of their abilities, in perpetuity.

Please sign the following statement: I hereby grant permission to the Graduate Division of the University of California, San Francisco to release copies of my thesis or dissertation to the Campus Library to provide access and preservation, in whole or in part, in perpetuity.

_____          12/19/07
Author Signature                              Date

214